Introduction to Biomolecular Electron Paramagnetic Resonance Theory

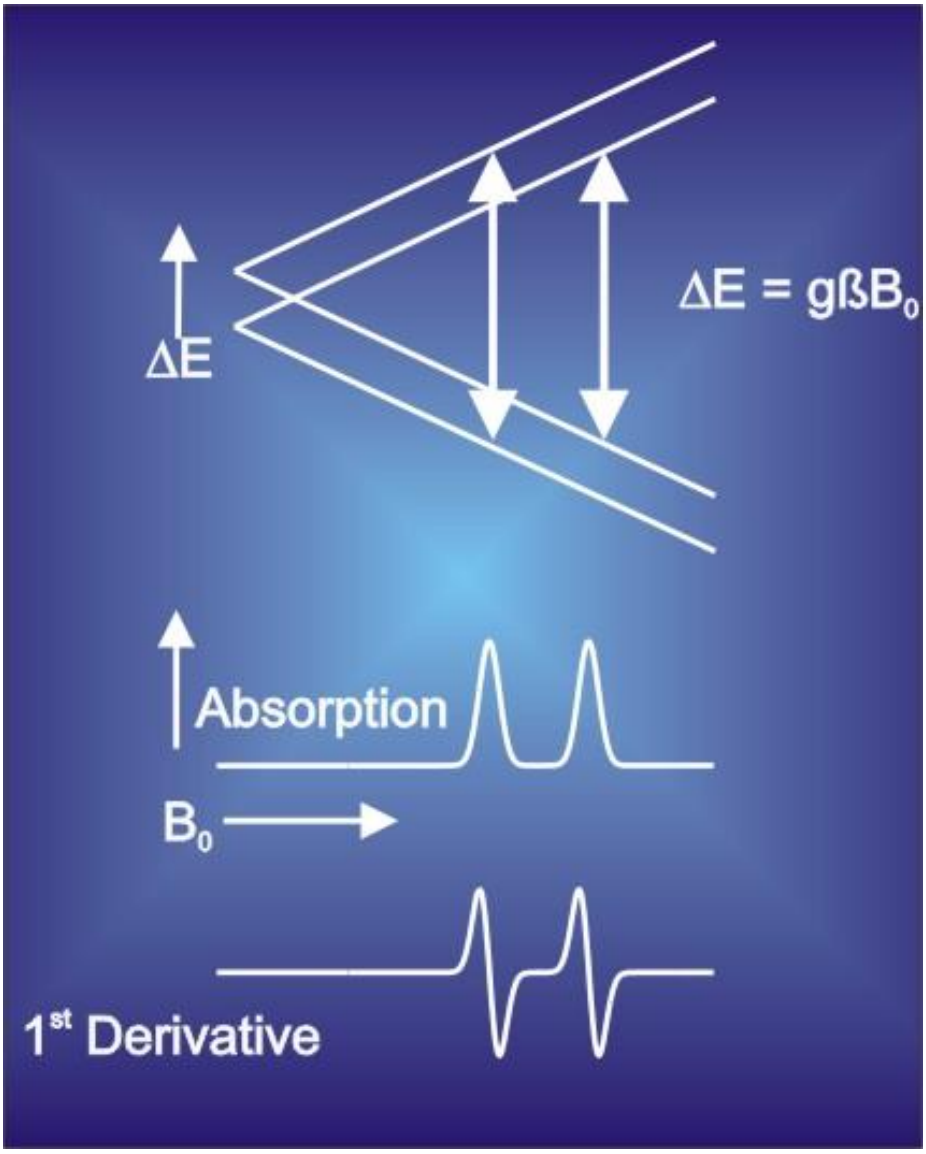

E. C. Duin

Content

Chapter 1 - Basic EPR Theory

Chapter 2 - Practical Aspects

Chapter 3 - Simulations of EPR Spectra

Chapter 4: Selected samples

1. Basic EPR Theory

1.1 Introduction

This course manual will provide the reader with a basic understanding needed to be able to get useful information using the technique of electron paramagnetic resonance (EPR) spectroscopy. In this course we will mainly focus on biological systems, but the general theory is applicable to any paramagnetic system.

EPR spectroscopy is similar to any other technique that depends on the absorption of electromagnetic radiation. A molecule or atom has discrete (or separate) states, each with a corresponding energy. Spectroscopy is the measurement and interpretation of the energy differences between the atomic or molecular states. With knowledge of these energy differences, you gain insight into the identity, structure, and dynamics of the sample under study.

We can measure these energy differences, ΔE, because of an important relationship between ΔE and the absorption of electromagnetic radiation. According to Planck's law, electromagnetic radiation will be absorbed if:

$$\Delta E = h\nu, \tag{1}$$

where h is Planck's constant and ν is the frequency of the radiation. The absorption of energy causes a transition from a lower energy state to a higher energy state. In conventional spectroscopy, ν is varied or swept and the frequencies at which absorption occurs correspond to the energy differences of the states. (We shall see later that EPR differs slightly.) Typically, the frequencies vary from the megahertz range for NMR (Nuclear Magnetic Resonance) (AM, FM, and TV transmissions use electromagnetic radiation at these frequencies), through visible light, to ultraviolet light. Radiation in the gigahertz range (GHz) with a wavelength of a few cm (ca. 3 cm) is used for EPR experiments. Such radiation lies far outside the visible region: it is *microwave radiation* used in ordinary radar equipment and microwave ovens.

1.2 The Zeeman Effect

An isolated electron, all alone in space without any outside forces, still has an intrinsic angular momentum called "spin", $\bar{S}$. Because an electron is charged, the angular motion of this charged particle generates a magnetic field. In other words, the electron due to its charge and angular momentum, acts like a little bar magnet, or magnetic dipole, with a magnetic moment, $\bar{\mu}$.

Fig. 1: Free, unpaired electron in space: electron spin – magnetic moment

The energy differences studied in EPR spectroscopy are predominately due to the interaction of ***unpaired*** electrons in the sample with a magnetic field produced by a magnet in the laboratory. This effect is called the ***Zeeman Effect***. The magnetic field, B_0, produces two energy levels for the magnetic moment, $\bar{\mu}$, of the electron. In the classic description one can say that the unpaired electron will have a state of lowest energy when the moment of the electron is aligned with the magnetic field and a stage of highest energy when $\bar{\mu}$ is aligned against the magnetic field.

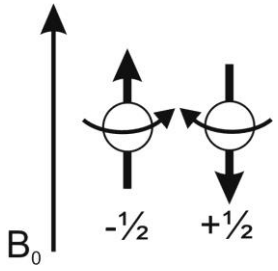

Fig. 2: Minimum and maximum energy orientations of $\bar{\mu}$ with respect to the magnetic field B_0

The two states are labeled by the projection of the electron spin, m_s, on the direction of the magnetic field. Because the electron is a spin ½ particle, the parallel state is designated as $m_s = -½$ and the antiparallel state is $m_s = +½$ (Fig. 2). The energy of each orientation is the product of μ and B_0. For an electron $\mu = m_s g_e \beta$, where β is a conversion constant called the Bohr magneton and g_e is the spectroscopic *g*-factor of the free electron and equals 2.0023192778 (≈ 2.00). Therefore, the energies for an electron with $m_s = +½$ and $m_s = -½$ are, respectively

$$E_{1/2} = ½\, g_e \beta B_0 \quad \text{and} \tag{2}$$

$$E_{-1/2} = -½\, g_e \beta B_0 \tag{3}$$

As a result there are two energy levels for the electron in a magnetic field (Fig. 3).

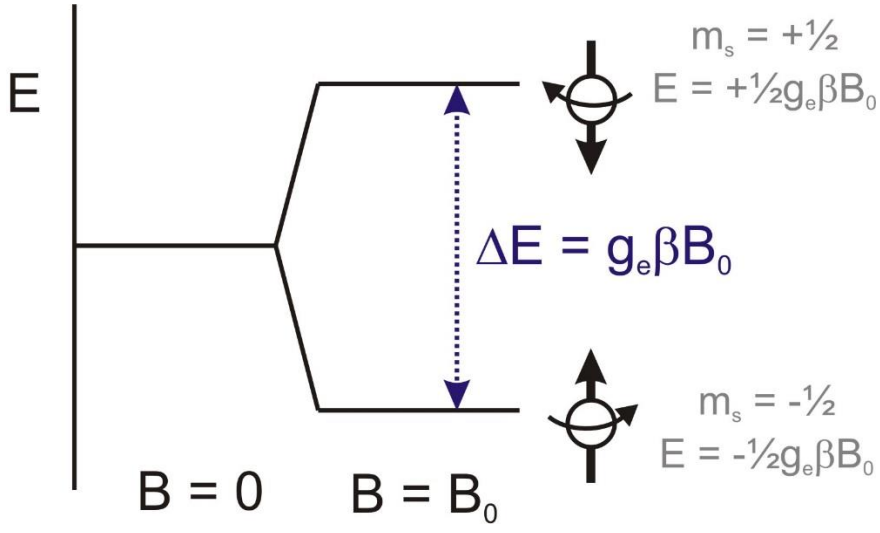

Fig. 3: Induction of the spin state energies as a function of the magnetic field B_0.

1.3 Spin-Orbit Interaction

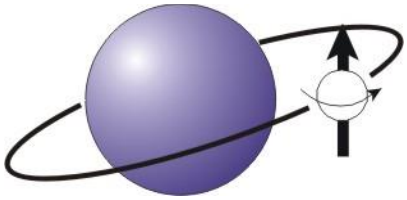

Fig. 4

When we take an electron in space with no outside forces on it and place it on to a molecule, its total angular momentum changes because, in addition to the intrinsic spin angular momentum ($\bar{S}$), it now also possesses some orbital angular momentum ($\bar{L}$). An electron with orbital angular momentum is in effect a circulating current, and so there is also a magnetic moment arising from the orbital angular momentum. These two magnetic moments interact, and the energy of this spin-orbit interaction depends on their relative orientations.

Electron in space

$$\bar{\mu} \propto g_e \bar{S} \tag{4}$$

Electron in a molecule

$$\bar{\mu} \propto g_e \bar{S} + \bar{L} \tag{5}$$

In general, the orbital angular momentum is approximately zero for an electron in the ground state (*s* electron). Interaction between the ground state and excited states, however, admixes small amounts of orbital angular momentum to the ground state: ***spin-orbit coupling contribution***.

$$\bar{\mu} \propto g_e \bar{S} + spin\text{-}orbit\ coupling\ contribution \tag{6}$$

It is common practice to assume that the spin-orbit coupling term is proportional to $\bar{S}$ which means we can simply combine both terms on the right and just change the value of g_e to g, or

$$\bar{\mu} \propto g \bar{S} \tag{7}$$

and

$$\Delta E = g \beta B_0 \tag{8}$$

The magnitude of the spin-orbit coupling contribution depends on the size of the nucleus containing the unpaired electron. Therefore, organic free radicals, with only H, O, C and N atoms, will have a small contribution from spin-orbit coupling, producing *g*-factors very close to g_e while the *g*-factors of much larger elements, such as metals, may be significantly different from g_e.

A simpler alternative way of thinking about the spin-orbit coupling is that a virtual observer on the electron would experience the nucleus (nuclei) as an orbiting positive charge producing a second magnetic field, δB, at the electron.

$$h\nu = g_e \beta (B_e + \delta B) \tag{9}$$

Since only the spectrometer value of B is known we can rewrite this as:

$$h\nu = (g_e + \delta g)\beta B = g\beta B \tag{10}$$

The quantity '$g_e + \delta g$' or 'g' contains the chemical information on the nature of the bond between the electron and the molecule, the electronic structure of the molecule.

The value of g can be taken as a fingerprint of the molecule.

1.4 *g*-Factor

From the above discussion we can see that one parameter whose value we may wish to know is *g*. In an EPR spectrometer, a paramagnetic sample is placed in a large uniform magnetic field which, as shown above, splits the energy levels of the ground state by an amount ΔE where

$$\Delta E = g\beta B_0 = h\nu \tag{11}$$

Since β is a constant and the magnitude of B_0 can be measured, all we have to do to calculate *g* is determine the value of ΔE, the energy between the two spin levels. This is done by irradiating the sample with microwaves with a set frequency and sweeping the magnetic field (Fig. 5).

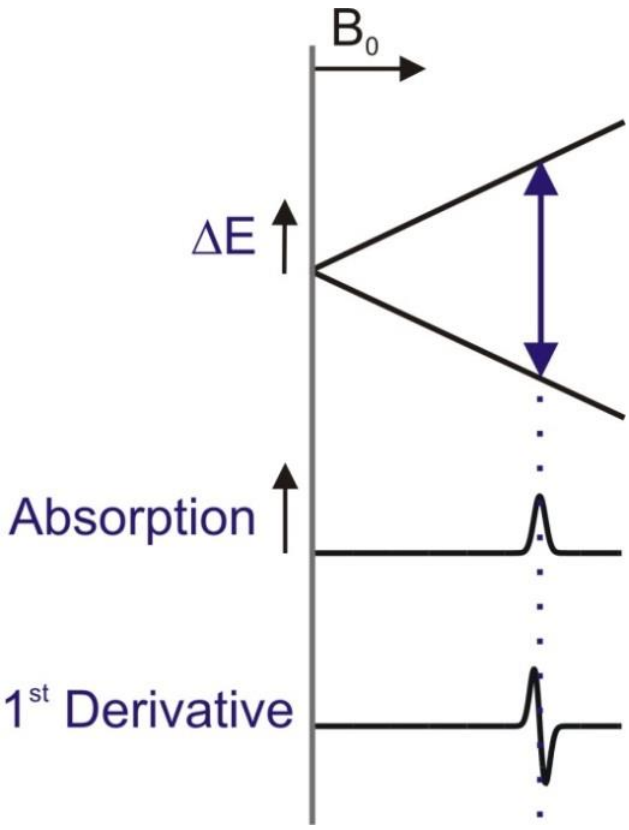

Fig. 5: The EPR experiment

Absorption of energies will occur when the condition in (11) is satisfied. The value of *g* can then be calculated from *v* (in GHz) and B_0 (in gauss) using,

$$g = \frac{h\nu}{\beta B_0} \tag{12}$$

or

$$g = 0.7145 \frac{\nu\ (MHz)}{B_0\ (Gauss)} \tag{13}$$

($h = 6.626 \cdot 10^{-34}$ J·s; $\beta = 9.274 \cdot 10^{-28}$ J·G^{-1})

Two facts are apparent from equations 2 and 3, equation 11 and the graph in Figure 5. Firstly, the two spin states have the same energy in the absence of a magnetic field. Secondly, the energies of the spin states diverge linearly as the magnetic field increases. These two facts have important consequences for spectroscopy:

1) Without a magnetic field, there is no energy difference to measure.
2) The measured energy difference depends linearly on the magnetic field

Because we can change the energy differences between the two spin states by varying the magnetic field strength, we have an alternative means to obtain spectra. We could apply a constant magnetic field and scan the frequency of the electromagnetic radiation as in conventional spectroscopy. Alternatively, we could keep the electromagnetic radiation frequency constant and scan the magnetic field. A peak in the absorption will occur when the magnetic field "tunes" to the two spin states so that their energy difference matches the energy of the radiation. This field is called the "field of resonance". A radiation source for radar waves produces only a very limited spectral region. In EPR such a source is called a klystron. A so-called X-band klystron has a spectral band width of about 8.8-9.6 GHz. This makes it impossible to continuously vary the wavelength similarly to optical spectroscopy. It is therefore necessary to vary the magnetic field, until the quantum of the radar waves fits between the field-induced energy levels.

1.5 Line Shape

In the above described EPR experiment we only looked at one molecule in one orientation in a magnetic field. The deviation of the measured *g*-factor from that of the free electron arises from spin-orbit coupling between the ground state and excited states. Because orbitals are oriented in the molecule, the magnitude of this mixing is direction dependent, or ***anisotropic***. In a low-viscosity solution, all of this anisotropy is averaged out. However, this is not the situation when all the paramagnetic molecules are in a fixed orientation, as in a single crystal. You would find that the *g*-factor of the EPR spectrum of a single crystal would change as you rotated the crystal in the spectrometer, due to *g*-factor anisotropy. For every paramagnetic molecule, there exists a unique axis system called the ***principal axis system***. The *g*-factors measured along these axes are called the principal *g*-factors and are labeled g_x, g_y and g_z.

Figure 6, shows as an example a molecule where the paramagnetic metal is coordinated by two equal ligands in the *z*-direction and four different but equal ligands in both the *x*- and *y*-directions. As a result the resulting *g*-factor will be different for the situations where the field B_0 is parallel to the *z*-axis or parallel to either the *x*- or *y*-axes.

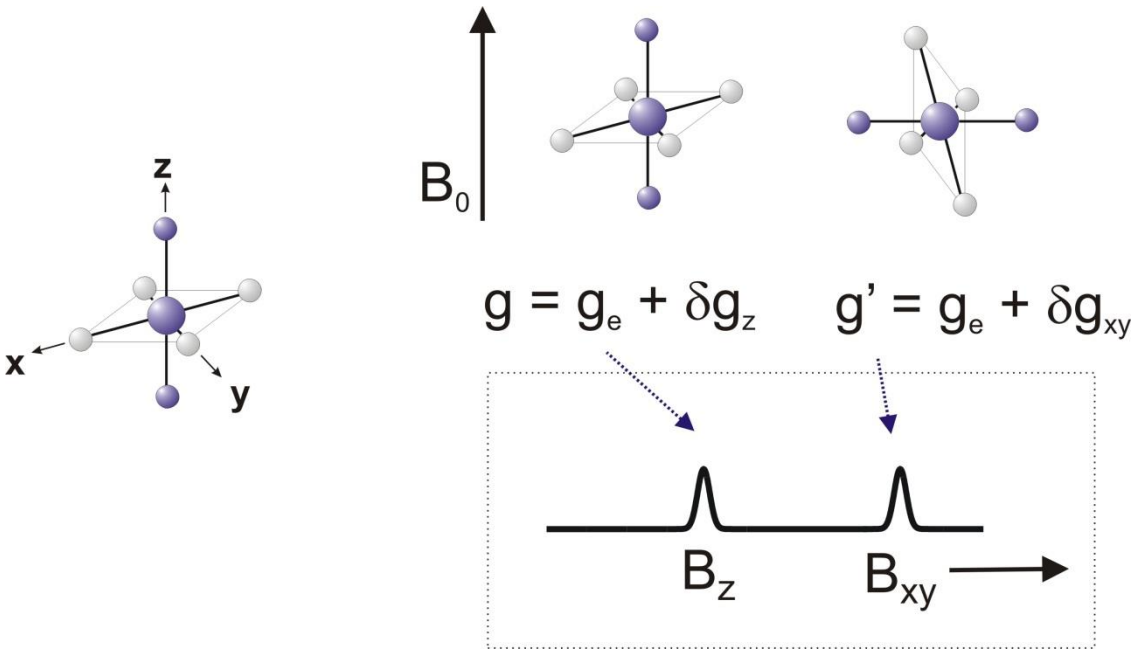

Fig. 6: Dependency of the *g*-value on the oritentation of the molecules in the magnetic field.

Most EPR spectra of biological transition metals are recorded on frozen solution samples. In these samples, the paramagnets are neither aligned in a set direction, as in an oriented single crystal, nor are they rapidly rotating, as in a low-viscosity solution. The act of freezing fixes the molecules in all possible orientations. Therefore the spectrum of a frozen sample represents the summation of all possible orientations and is called a ***powder spectrum***. Note that to get the complete powder spectrum of a single crystal you would have to measure a spectrum for the crystal in all possible *x-, y-* and *z*-directions. Alternatively you could ground up the single crystal into an actual powder.

There is only one step left to understand the shape of spectra, measured with a frozen enzyme solution. It has to do with one of the ***selection rules*** in EPR, namely that only the magnetic moments from the sample in the direction of the external field (to be more precise: ***perpendicular*** to the direction of the magnetic field created by the microwaves) are detected. Imagine that a metal ion has a total symmetric environment, i.e. the electrons in the different *d*-orbitals have equal interactions in all directions: the orbital moment then is equal in all directions, so also the total magnetic moment is the same in all directions ($\mu_x = \mu_y = \mu_z$ so also $g_x = g_y = g_z$). Now if you put such an ion in an external field, it does not matter at all how you put it in: the magnitude of the total magnetic momentum in the direction of the external field will always be the same. This means that there is only one *g*-value and only one value of the external field where resonance occurs: $h\nu = g\beta B$. There will only be one absorption line (Fig. 8a).

Now suppose there is axial symmetry, such that the total magnetic moment in the *z*-direction is rather large. If you place such an ion in the external field, it does matter how you position it as shown in Figures 6 and 7. If you place it such that the *z*-direction is parallel to the external field *B*, the energy difference between the two energy levels for the electron will be $2\mu_z B$. Since we have assumed a large value of μ_z, we only need a small external field (B_z) to get resonance (Fig. 6). If we put our ion in the magnet with either the *x*-axis or the *y*-axis (or any other direction within the *xy*-plane) parallel to the external field, then the energy difference is $2\mu_{x,y}B$, As we have made $\mu_{x,y}$ small, we need a large field ($B_{x,y}$) for resonance (Fig. 6). If we rotate our ion from the 'z$\mathcal{2}$*B*' to the position 'z⊥*B*' (x,y-plane$\mathcal{2}$*B*), the total magnetic moment in the direction of the external field will decrease from μ_z to $\mu_{x,y}$. The one and only absorption line in the spectrum then moves from B_z to $B_{x,y}$.

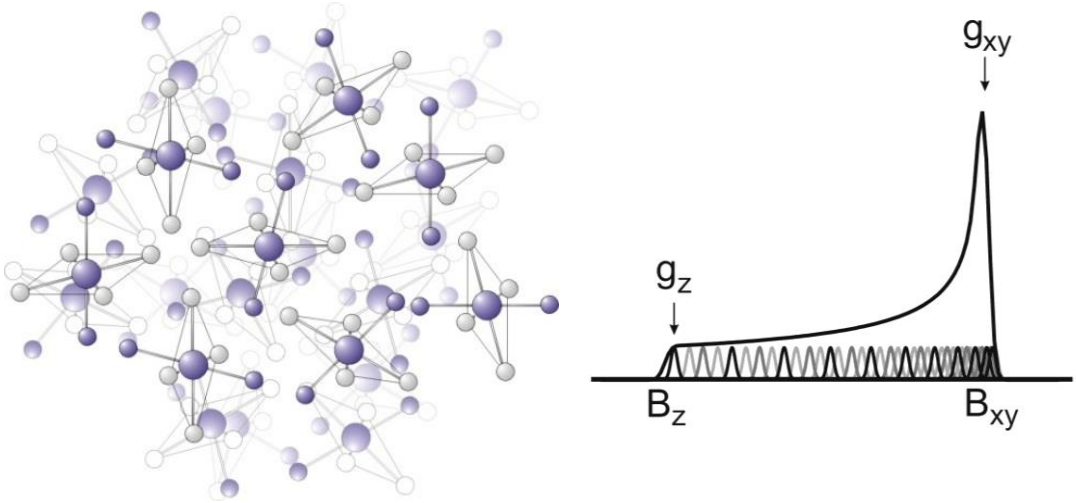

Fig. 7: A power spectrum is the sum of the spectra for all possible ortientations of the molecule

In a frozen sample all orientations occur and consequently there are a large number of overlapping absorption lines starting at B_z and ending at $B_{x,y}$ (Fig. 7). What is detected is the sum of all these lines. It is simply a matter of statistics that our ion with its *x*- or *y*-direction parallel to *B* occurs much more frequently than one with its *z*-axis parallel to B. This is the reason that the total absorption in the *x,y*-direction is much larger than in the *z*-direction. This usually enables us to recognize those directions in a spectrum.

Fig. 8 shows the absorption and first-derivative spectra for three different classes of anisotropy. In the first class, called **isotropic**, all of the principal *g*-factors are the same (Fig. 8a). In the second class, called **axial**, there is a unique axis that differs from the other two ($g_x = g_y \neq g_z$) (Fig. 8b and c). This would have been the powder spectrum for our molecule shown in Figure 6. The *g*-factor along the unique axis is said to be parallel with it, $g_z = g_{\parallel}$ while the remaining two axes are perpendicular to it, $g_{x,y} = g_{\perp}$. The last class, called **rhombic**, occurs when all the *g*-factors differ (Fig. 8d).

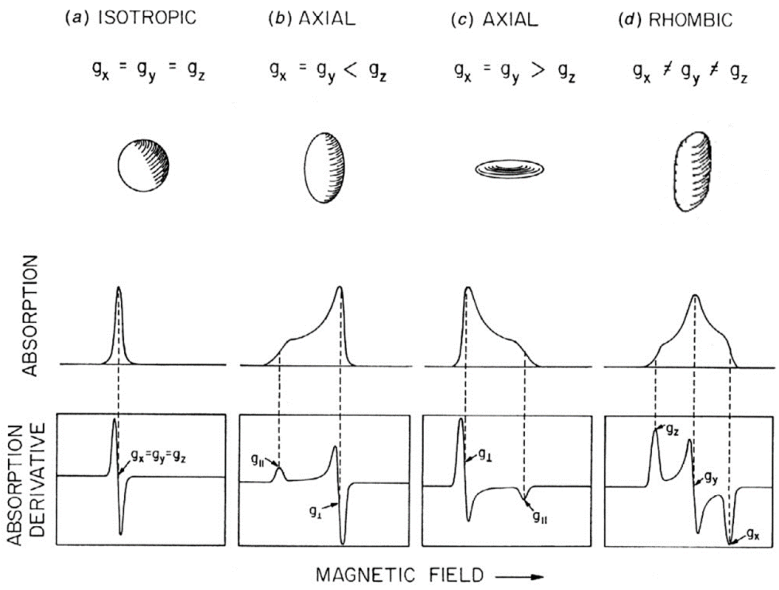

Fig. 8: Schematic representation of *g*-tensor and the consequential EPR spectra. The upper solid bodies show the shapes associated with isotropic (a), axial (b, c) and rhombic (d) magnetic moments. Underneath are shown the absorption curves. The corresponding EPR derivative curves are shown on the bottom. (Adapted from Palmer (2000) Electron paramagnetic resonance of metalloproteins, In: Physical Methods in Bioinorganic Chemistry, Ed. Que, Jr., University Science Books, Sausalito, CA, pp 121-186)

A more thorough way of describing the effect shown in Figure 6, is to define the angular dependency of the *g*-value. For this we first have to define the orientation of the magnetic field (a vector) with respect to the coordinates of the molecule (and vice versa). This can be done by defining two polar angles, θ and ϕ, where θ is the angle between the vector *B* and the molecular *z*-axis, and ϕ is the angle between the projection of *B* onto the *xy*-plane and the *x*-axis (Fig. 9).

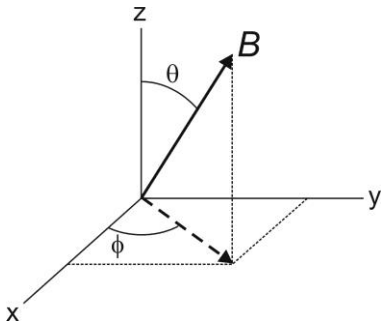

Fig. 9: Orientation of the magnetic field *B* with respect to the coordinates of the molecule.

Inclusion of the angular terms into Equation 11 gives:

$$h\nu = g(\theta,\phi)\beta B_0 \tag{14}$$

A spin Hamiltonian that considers any arbitrary orientation of *B* relative to *g* is given by:

$$\hat{H} = \beta B^T \cdot g \cdot \hat{S} \tag{15}$$

With $\hat{S}$ being the Pauli spin operator vector with individual components $\hat{S}_x$, $\hat{S}_y$, and $\hat{S}_z$. *B* can be aligned along any of the principle *g* tensor axes and the individual components of *B* are defined in terms of the polar angles (θ, ϕ).

$$B_x = B\sin\theta\cos\varphi$$
$$B_y = B\sin\theta\sin\varphi$$
$$B_z = B\cos\theta$$

Filling in these values provides a more detailed matrix representation of the spin Hamiltonian equation:

$$\hat{H} = \beta \cdot \begin{bmatrix} B_x & B_y & B_z \end{bmatrix} \cdot \begin{bmatrix} g_{xx} & 0 & 0 \\ 0 & g_{yy} & 0 \\ 0 & 0 & g_{zz} \end{bmatrix} \cdot \begin{bmatrix} \hat{S}_x \\ \hat{S}_y \\ \hat{S}_z \end{bmatrix} \tag{16}$$

Combination with the polar angles equations for the individual components of B gives:

$$\hat{H} = \beta(Bsin\theta cos\phi \cdot g_{xx} \cdot \hat{S}_x + Bsin\theta sin\phi \cdot g_{yy} \cdot \hat{S}_y + Bcos\theta \cdot g_{zz} \cdot \hat{S}_z) \tag{17}$$

The effect of the $\hat{S}_x, \hat{S}_y, \hat{S}_z$ operators can be represented by the 2 × 2 Pauli spin matrices quantized in units of $\hbar$ as:

$$\hat{S}_x = \frac{1}{2}\begin{bmatrix} 0 & 1 \\ 1 & 0 \end{bmatrix}, \qquad \hat{S}_y = \frac{1}{2}\begin{bmatrix} 0 & -i \\ -i & 0 \end{bmatrix}, \qquad \hat{S}_z = \frac{1}{2}\begin{bmatrix} 1 & 0 \\ 0 & -1 \end{bmatrix} \tag{18}$$

In order to find the solutions to eqn 17, the term given in eqn 18 have to be considered. The matrix of the Hamiltonian then has the form:

$$\hat{H} = \beta\frac{1}{2}B\begin{bmatrix} g_{zz}cos\theta & g_{xx}sin\theta cos\phi + ig_{yy}sin\theta sin\phi \\ g_{xx}sin\theta cos\phi - ig_{yy}sin\theta sin\phi & -g_{zz}cos\theta \end{bmatrix} \tag{19}$$

The two resulting eigenvalues are:

$$E_1 = -\frac{1}{2}\beta B\sqrt{g_{xx}^2 sin^2\theta cos^2\phi + g_{yy}^2 sin^2\theta sin^2\phi + g_{zz}^2 cos^2\theta} \tag{20a}$$

$$E_2 = \frac{1}{2}\beta B\sqrt{g_{xx}^2 sin^2\theta cos^2\phi + g_{yy}^2 sin^2\theta sin^2\phi + g_{zz}^2 cos^2\theta} \tag{20b}$$

For resonance absorption to occur:

$$E_1 - E_2 = h\nu = g(\theta, \phi)\beta B_0 \tag{21}$$

As a result the value of $g(\theta, \phi)$ now becomes:

$$g(\theta, \phi) = \sqrt{g_{xx}^2 sin^2\theta cos^2\phi + g_{yy}^2 sin^2\theta sin^2\phi + g_{zz}^2 cos^2\theta} \tag{22}$$

Equation 22 gives the effective anisotropic g value for any orientation (θ, ϕ) with respect to the applied magnetic field B.

Going back to our example of an axial S = ½ spin system, eqn 22 can be simplified:

$$g_{ax}(\theta) = \sqrt{g_{xy}^2 sin^2\theta + g_z^2 cos^2\theta} \tag{23}$$

In which $g_\perp \equiv g_x \equiv g_y$, and $g_{//} \equiv g_z$. In this case the variation in the g values is solely dependent on the value of θ (the vector orientation of B with respect to the z-axis). Figure 10 shows the plot of θ and $g_{ax}(\theta)$ as a function of the resonance field B_{res}. Note that resonance will only occur in between $g_\perp$ and $g_{//}$. When θ = 0 resonance absorption will occur only for those paramagnetic centers in which their z-axis is aligned directly along the B direction. In creasing the value of θ from 0 to 90° causes the peak position to move from the g_2 position to the $g_\perp$ position. In this example $g_{//}$ = 2.050 and $g_\perp$ = 2.002.

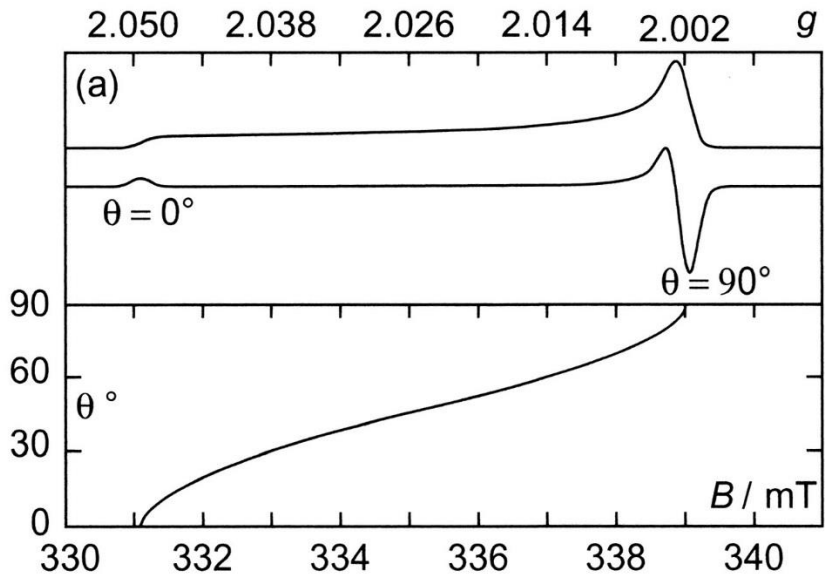

Fig. 10: Angular dependency of axial g-value. The angle θ between B_0 and the molecular z-axis and the axial g-value are plotted versus the resonance field for an axial S = ½ species with g_2 = 2.050 and $g_\perp$ = 2.002: ν = 9500 MHz (Taken from Chechik (2016) Electron Paramagentic Resonance, Oxford University Press, Oxford, UK).

Note that the resonance field B_{res} is relatively insensitive to change in orientation (here, in θ) for orientations of B near the molecular axes (here θ = 0 or 90°). As a result of this insensitivity, clear so-called turning-point features appear in the powder spectrum that closely correspond with the position of the g-values. Therefore the g-values can be read from the absorption-type spectra. For practical reasons (see chapter 2), the first derivative instead of the true absorption is recorded. In these types of spectra the g-values are very easy to recognize. This is not the reason, however, that the first derivative is recorded. To improve the sensitivity of the EPR spectrometer, magnetic field modulation is used. In field modulation, the amplitude of the external field, B_0, is made to change by a small amount (~0.1-20 G) at a frequency of 100 kHz (other frequencies can also be used). Because the spectrometer is tuned to only detect signals that change amplitude as the field changes, the resultant signal appears as a first derivative (i.e., ΔSignal amplitude/ΔMagnetic field). The derivative spectra are characterized by those places where the first derivative of the absorption spectrum has its extreme values. In EPR spectra of simple S = ½ systems there are maximally 3 such places which correspond with the g-factors. The position of these 'lines' can be expressed in field units (Gauss, or Tesla (1 T = 10^4 G)), but it is better to use the so-called g-value. The field for resonance is not a unique "fingerprint" for identification of a compound because spectra can be acquired at several different frequencies using different klystrons. The g-factor, being independent of the microwave frequency, is much better for that purpose. Notice that high values of a g occur at low magnetic fields and vice versa. A list of fields for resonance for a g = 2 signal at microwave frequencies commonly available in EPR spectrometers is presented in Table 1.1.

Table 1.1: Field for resonance B_{res} for a g = 2 signal at selected microwave frequencies

Microwave Band	Frequency (GHz)	B_{res} (G)
L	1.1	392
S	3.0	1070
X	9.5	3389
Q	35	12485
W	90	32152
J	270	96458

An advantage of derivative spectroscopy is that it emphasizes rapidly-changing features of the spectrum, thus enhancing resolution. Note, however, that a slowly changing part of the spectrum has near zero slope, so in the derivative display there is "no intensity". This can be detected in the examples of the two types of axial spectra shown in Figure 8 (b and c). While the absorption spectrum clearly shows intensity between the $g_{//}$ and $g_{\perp}$ values, the derivative spectrum is pretty much flat in between the peaks indicating the $g_{//}$ and $g_{\perp}$ positions. This makes it sometimes difficult to estimate the concentration of EPR samples since a large part of the signal appears to be hidden. A typical mistake is too assign a larger intensity to an isotropic signal ($g_x = g_y = g_z$) while a broad axial or rhombic signal is viewed as having less intensity. An isotropic signal has all the signal intensity spread over a very small field region causing the signal to have a very large signal amplitude, while a broad axial or rhombic signal is spread over a larger field region causing the observed amplitude to decrease significantly.

1.6 Quantum Mechanical Description

A full quantum mechanical description of the spectroscopic EPR event is not possible due to the complexity of the systems under study. In particular the lack of symmetry in biological samples excludes the use of this aspect in simplifying the mathematical equations. Instead in Biomolecular EPR the concept of the ***spin Hamiltonian*** is used. This describes a system with an extremely simplified form of the ***Schrödinger wave equation*** that is a valid description *only* of the lowest electronic state of the molecule *plus* magnetic interactions. In this description the simplified operator, H_s, is the spin Hamiltonian, the simplified wave function, ψ_s, are the spin functions, and the eigenvalues E are the energy values of the ground state spin manifold.

$$H_s\psi_s = E\psi_s \tag{24}$$

For an isolated system with a single unpaired electron and no hyperfine interaction the only relevant interaction is the electronic Zeeman term, so the spin Hamiltonian is

$$\hat{H}_s = \beta B\beta(sin\theta cos\phi \cdot g_{xx} \cdot \hat{S}_x + sin\theta sin\phi \cdot g_{yy} \cdot \hat{S}_y + cos\theta \cdot g_{zz} \cdot \hat{S}_z) \tag{25}$$

A shorter way of writing this is

$$H_s = \beta B \bullet g \bullet S \tag{26}$$

Solving this we get the equation we saw earlier for the angular dependency of the g-value

$$g(\theta,\phi) = \sqrt{g_{xx}^2 sin^2\theta cos^2\phi + g_{yy}^2 sin^2\theta sin^2\phi + g_{zz}^2 cos^2\theta} \tag{27}$$

More terms can be added to the Hamiltonian when needed as for example described in the next section where the effect of nuclear spin is introduced. The emphasis of this text (and the associated EPR course) is to get a practical understanding of EPR spectroscopy. A full quantum mechanical description is outside the scope of this text. However, later on, and in the following chapters, several handy tools and simulation software will be introduced for the interpretation of EPR data. These tools are based on the simplified operator H_s. It is important to realize that a majority of the EPR spectra you will encounter in biological systems can be described accurately by this simplified operator, but not all. Therefore we will discuss the different forms of the spin Hamiltonian at the appropriate places and include the conditions under which it gives an accurate description of the EPR data and the conditions under which it will not.

1.7 Hyperfine and Superhyperfine Interaction, the Effect of Nuclear Spin

The magnetic moment of the electron can be represented as a classical bar magnet. From basic physics, we know that a bar magnet will align itself in an external magnetic field (Zeeman interaction). Physics also tells us that the energy of a bar magnet can be influenced by interaction with a neighboring bar magnet. In this latter case, the magnitude of the interaction depends on the distance of separation and the relative alignment of the two magnets.

In EPR there are three types of interaction that can occur. The first two types are due to the interaction between an unpaired electron and a magnetic nucleus. Interaction of an unpaired electron with a nuclear magnetic moment is termed ***nuclear hyperfine interaction***. Usually called ***hyperfine*** if it results from the nucleus where the unpaired electron originates (Fig. 11A) and ***superhyperfine*** if it is from a neighboring nucleus (Fig. 11B). The third type is the interaction between two unpaired electrons on different atoms normally within a molecule, which is termed ***spin-spin interaction*** (Fig. 11C). Table 1.2, lists the nuclei that are important in biology. Indicated are which isotopes are present (natural abundance), which of these have a nuclear spin, and the respective spin.

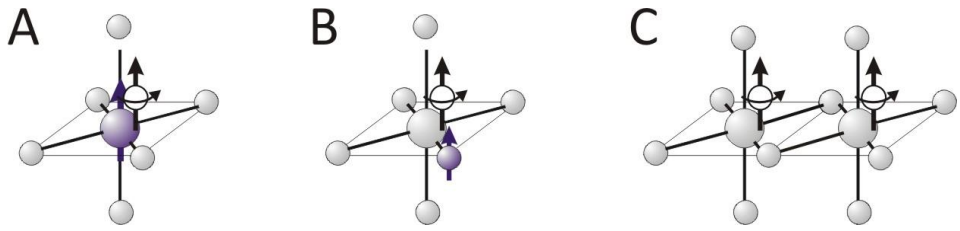

Fig. 11: Three types of magnetic interaction that can occur in EPR: Hyperfine interaction (A), superhyperfine interaction (B), and spin-spin interaction (C).

Here we will first consider systems with an electron spin and a nuclear spin. The first thing we assume is that the Zeeman interaction is much larger, two orders of magnitude or more, than the hyperfine interaction (this is known as the *high field approximation*). Now the hyperfine interaction can be treated as a ***perturbation*** of the larger Zeeman interaction

$$H_s = \beta B \bullet g \bullet S + S \bullet A \bullet I \qquad (28)$$

Where *A* is the anisotropic hyperfine tensor. Just like the Zeeman interaction, the hyperfine interaction will be anisotropic and it is assumed that *g* and *A* are collinear.

The resonance condition becomes

$$h\nu = g\beta B_0 + hAm_I \qquad (29)$$

where *A* is called the ***Hyperfine Coupling Constant*** (Note that *A* is in magnetic-field units of gauss, while sometimes *A'* is used, which is an energy in units of cm^{-1}) and m_I is the magnetic quantum number for the nucleus. Since there are $2I + 1$ possible values of m_I ($m_I = I, I\text{-}1, \ldots, 0, \ldots, -I\text{+}1, -I$), the hyperfine interaction terms splits the Zeeman transition into $2I + 1$ lines of equal intensity. For

Table 1.2: Nuclear spin of some nuclei that are important in biology. The isotope with a nuclear spin are indicated in blue and italics. The amount of spin and the relative abundance are indicated in the third column.

Atom	Isotope	Spin (abundance)
H	***1***, ***2***	^{1}H, $^{1}/_{2}$ (99.985); ^{2}H, 1 (0.015)
C	12, ***13***	$^{1}/_{2}$ (1.07)
N	***14***, ***15***	^{14}N, 1 (99.632); ^{15}N, $^{1}/_{2}$ (0.368)
O	16, ***17***, 18	$^{5}/_{2}$ (0.038)
F	***19***	$^{1}/_{2}$
P	***31***	$^{1}/_{2}$
S	32, ***33***, 34	$^{3}/_{2}$ (0.76)
Cl	***35***, ***37***	^{35}Cl, $^{3}/_{2}$ (75.78); ^{37}Cl, $^{3}/_{2}$ (24.22)
As	***75***	$^{3}/_{2}$
Se	76, ***77***, 78, 80, 82	$^{1}/_{2}$ (7.63)
Br	***79***, ***81***	^{79}Br, $^{3}/_{2}$ (50.69); ^{81}Br, $^{3}/_{2}$ (49.31)
I	***127***	$^{5}/_{2}$
V	***50***, ***51***	^{50}V, 6 (0.25); ^{51}V, $^{7}/_{2}$ (99.75)
Mn	***55***	$^{5}/_{2}$
Fe	54, 56, ***57***, 58	$^{1}/_{2}$ (2.119)
Co	***59***	$^{7}/_{2}$
Ni	58, 60, ***61***, 62	$^{3}/_{2}$ (1.14)
Cu	***63***, ***65***	^{63}Cu, $^{3}/_{2}$ (69.17); ^{65}Cu, $^{3}/_{2}$ (30.83)
Mo	92, 94, ***95***, 96, ***97***, 98, 100	^{95}Mo, $^{5}/_{2}$ (15.92); ^{97}Mo, $^{5}/_{2}$ (9.55)
W	180, 182, ***183***, 184, 186	$^{1}/_{2}$ (14.3)

example, interaction of the electron with a nucleus with I = ½ (for example a proton) will yield an EPR spectrum containing two lines. The local field of the nucleus either adds or subtracts from the applied B_0 field. As a result the ground-state and excited-state energy levels are split in two (Fig. 12).

In a system that has $2I + 1$ energy levels there are now $2I + 1$ allowed EPR transitions between these levels. This is the result of selection rules where only electron spin flips ($\Delta m_s = \pm 1$) but not the nuclear spin ($\Delta m_I = 0$). As a result of this the EPR spectrum of a radical that experiences hyperfine interaction with a spin I nucleus shows $2I + 1$ lines. In the example EPR experiment with I = ½ we detect now two lines instead of one (Fig. 13).

Organic Radicals

To fully understand the effect of hyperfine interactions on the shape of an EPR signal we will first consider the line shape of organic radicals. The shape of the EPR signals of these species is purely isotropic. This is the result of measuring samples in solution. Fast tumbling motions of the molecules averages the axial anisotropy of the *g*-factors resulting in the detection of only a narrow isotropic EPR signal with a single *g*-value, 'g_{iso}'.

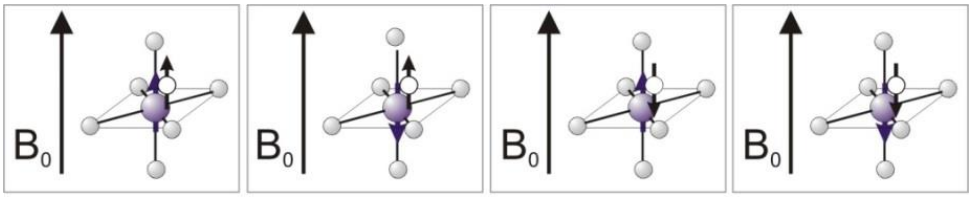

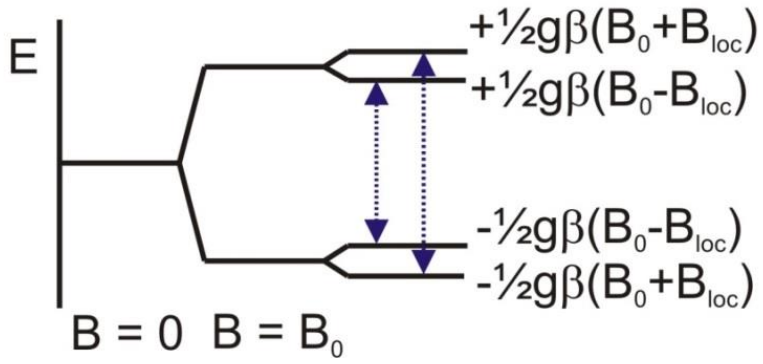

Fig. 12: Permanent local fields arising from the magnetic moments of magnetic nuclei

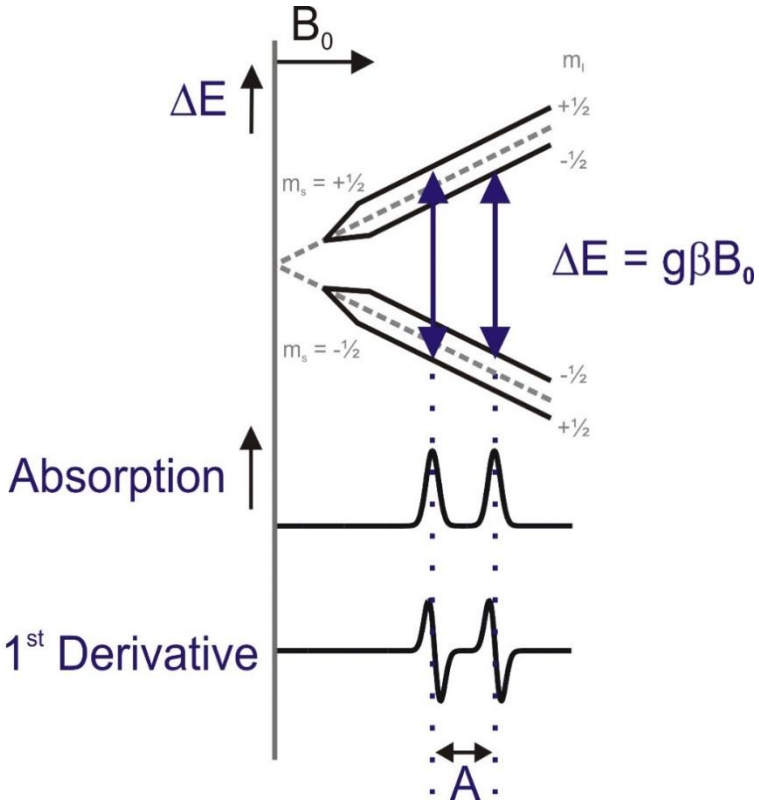

Fig. 13: EPR experiment for a single electron interacting with a magnetic nucleus with nuclear spin I = ½.

When hyperfine structure is introduced to this isotropic signal a highly symmetric line pattern is generated. In the high field approximation, the EPR transitions are characterized by very similar energy gaps and the probabilities of these transitions are very similar. All the hyperfine lines in the spectrum will therefore have equal intensity. Since the m_I levels are evenly spaced the distances between the $2I + 1$ lines are equivalent and are all separated by the same value, A (Fig. 13).

The hyperfine interaction can make an EPR spectrum look very complex. Figure 14 gives examples of how hyperfine interactions can influence spectra using an isotropic EPR signal. Figure 14A, shows the interaction of the unpaired electron with different magnetic nuclei. The 'original' signal is split in two or more signals with equal intensity. Note, however, that in an actual measurement the total intensity of the signal would now be spread out over more than one peak and therefore the signal amplitude would become smaller and smaller. Figure 14B, shows how the line shape is affected by interaction with more than one magnetic nucleus. In this example, the hyperfine splitting pattern is shown for interaction of the unpaired electron with one, two, three, or four identical nuclei with m_I = ½. The splitting pattern is becoming more complex due to the fact that some of the split lines occupy the same field position and therefore some of the resulting lines have different intensities. Included in the figure is a stick diagram or Pascal's triangle that shows how the relative intensities of the different lines can be calculated. Also note that the actual *g*-value of the signal is the position of the 'original' non-split signal. In the case where there is interaction with an odd amount of nuclei there is not an actual line occupying this central part of the spectrum. Figure 14C, shows what the resulting spectrum looks like of a species that has interaction with up to four nuclei with *I* = 1. The result of the interaction with four nuclei is a spectrum consisting of nine lines with a relative intensity of 1:4:10:16:19:16:10:4:1. Note that the lines on the outside have a very low relative intensity. Measurement of such signals can be come complicated if the sample has a low concentration and these peaks with the lowest relative intensity get overlooked in the noise. In such a case, simulation of the spectra can be very helpful since it will not be possible to get a good match of the relative intensities indicating that something is not correct with the interpretation of the splitting pattern.

In the examples used in parts B and C the interactions are with nuclei that are identical. The patterns will become much more complex and at first sight much less informative when the electron is interacting with different nuclei with different nuclear spins and coupling constants. Note that regardless of the number of hyperfine lines the EPR spectrum is always centered about the Zeeman transition. In other words, *g* can be determined from the value of the magnetic field at the middle of the spectrum even if there is no actual line present at that position.

The size of the hyperfine constant is dependent on several factors. First of all we can discern between two types of radicals. The first types are ***localized radicals*** where the unpaired electron density or spin density is close to unity on one particular atom in the molecule. An example would be the ethanol radical $HOCH_2CH_2\bullet$ (Fig. 15). The unpaired electron will not interact to a significant amount for nuclei further than two bonds away from the atom with the unpaired electron. For this ethanol radical you would only expect to see splittings from the protons of the two CH_2 groups. These protons are termed α- and β-protons, counting from the atom with the unpaired electron. Protons that are further away (e.g., the OH proton) will be expected to give a negligible hyperfine coupling constant. Note that due to the fact that the OH proton is exchangeable there is no interaction observed. However, since only the α- and β-protons are contributing virtually the same spectrum is generated by making a n-propyl radical ($CH_3CH_2CH_2\bullet$) or a n-butanyl radical ($CH_3CH_2CH_2CH_2\bullet$). The EPR spectrum of the ethanol radical shows a triplet of triplets (Fig. 15). The two β-protons split the signal in three (1:2:1 ratio). Each resulting peak is split in three due to the action of the two α-protons (1:2:1 ratio). Note that due to

orbital overlap between the orbital of the unpaired electron and the orbital of the C-H bond at the adjacent carbon atom, the β-hyperfine constants are actually larger than the α-hyperfine constants. This of course is not always the case and it would be expected that nuclei that are further away should induce splitting with smaller coupling constants.

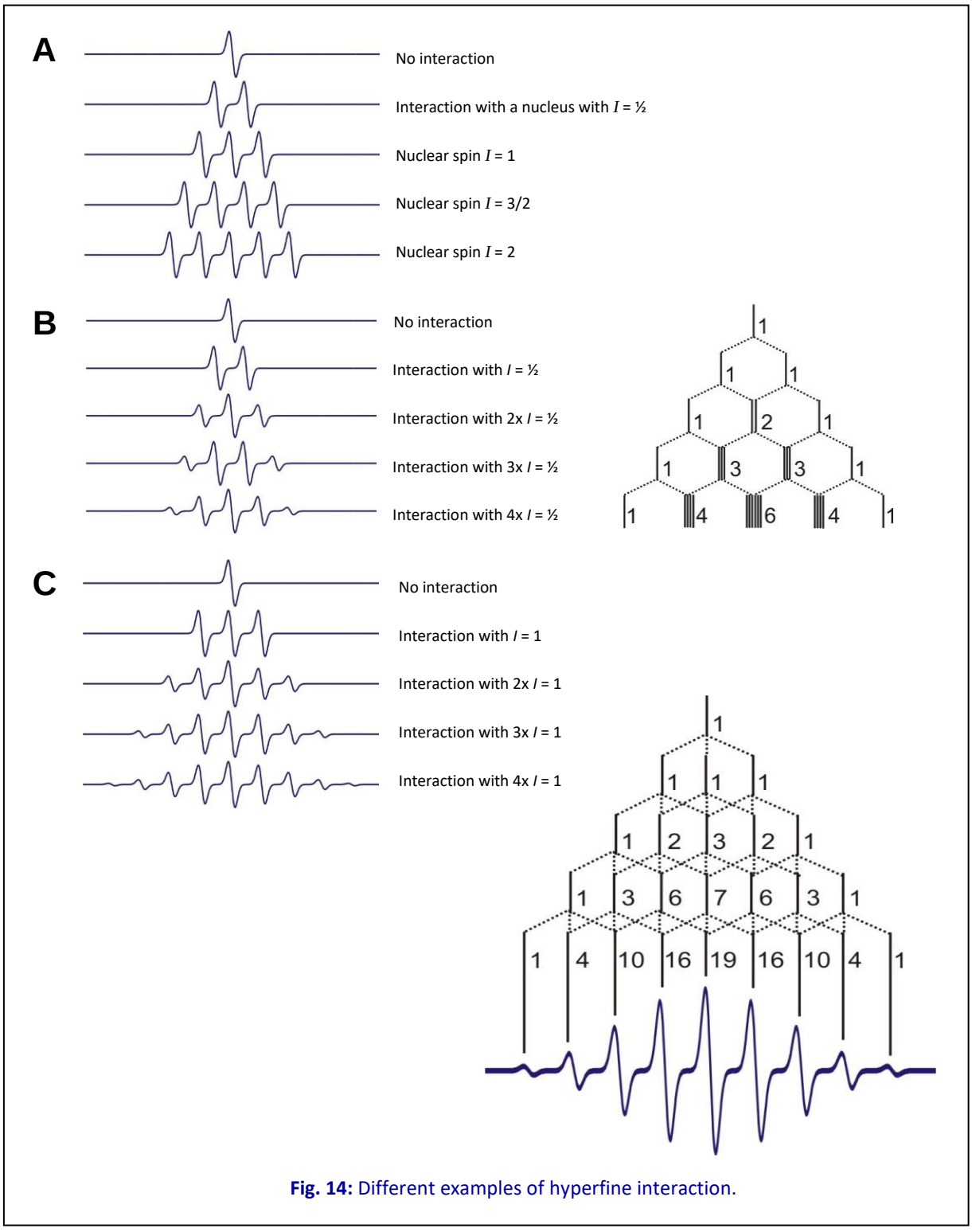

Fig. 14: Different examples of hyperfine interaction.

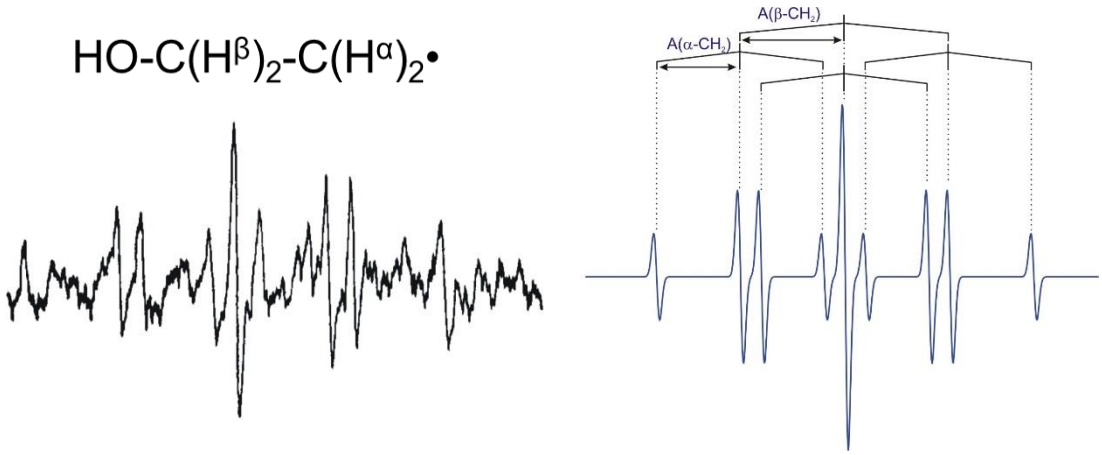

Fig. 15: EPR spectrum and splitting diagram for the ethanol radical $HOCH_2CH_2$•.
(Spectrum taken from Shiga (1966) J. Phys. Chem., 69, 3805)

The second types of radicals, ***delocalized radicals***, have their unpaired electron in an orbital that can be delocalized over the whole molecule or a large section. An example for this is the benzene radical anion. Due to the delocalization, the spin density is spread around the whole molecule and all the protons interact with the unpaired electron. In delocalized radicals, hyperfine interaction affects spin-active nuclei attached to atoms in the α- and β-position with respect to the unpaired electron. Nuclei in identical chemical environments are equivalent. In the benzene anion radical all six hydrogen atoms are equivalent and they will cause a split of the EPR signal into a septet.

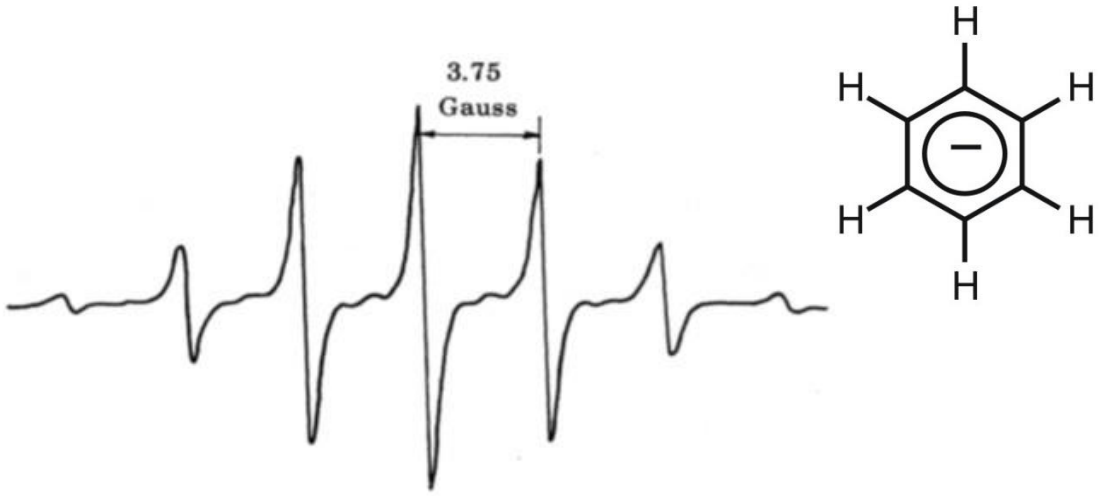

Fig. 16: EPR spectrum for the benzyl radical.

So the distance of the nuclei plays and important role in the size of hyperfine interaction. However, even if different nuclei would be at identical distances the hyperfine constants are still different since they are proportional to the nuclear *g*-factor (g_N) of the respective nuclei. For example, it is possible to prove that a specific interaction is due to a hydrogen atom by replacing it by a deuterium atom. Deuterium has a nuclear spin I = 1 but the g_N factor for hydrogen is 5.5854 and that of deuterium is 0.8574. That means that the hyperfine constant for deuterium will always be about a factor 6.5

smaller resulting in a narrower overall EPR signal. The relative orientations of the respective *g*-tensors for the unpaired electron and the paramagnetic nuclei will also have an effect on the interaction.

As discussed before when measuring protein samples this is done on frozen samples. There are several reasons for this. A particular protein might be inherently unstable or oxygen sensitivity. The Curie behavior of the paramagnetic species (see chapter 2) might require the use of measuring temperatures in the liquid nitrogen or liquid helium range. In frozen samples the spectra will be basically powder spectra and are generally anisotropic. It is possible to measure a protein sample in aqueous solution at room temperature. For this purpose a so-called flat cells has to be used to minimize absorption of the microwaves by the water present in the sample (see discussion in section 2.3). Due to their large size, however, the protein tumbling in solution is too slow to average the anisotropic interactions and even at those conditions an isotropic spectrum is obtained in most cases.

Amino-acid-based radical species.

Whether a signal looks isotropic and anisotropic is actually highly dependent on the frequency used for the measurements. In section 1.12 there will be a more in-depth discussion on the benefits and drawbacks of using different (higher) frequencies. The most common type of EPR spectroscopy uses X-band frequency (~9.4-9.6 GHz). Generally we define radicals as species that display an isotropic signal in either solution or frozen samples when measured at X-band. Most radical species, however, do display some anisotropy. The *g*-factors, however, can only be determined by using an EPR spectrometer that runs at a much higher frequency (and magnetic field). Typically 90 GHz (W-band) or higher is used. Common radical species that can be detected in proteins are glycyl and tyrosyl radicals. Spectra for both species are shown in Figure 17. The spectra of a tyrosyl and a glycyl radical look somewhat similar at X-band but differ significantly at 285 GHz. At X-band the shape of the glycyl radical is dominated by the isotropic hyperfine coupling interaction of the spin with the remaining hydrogen atom on the glycine backbone C_α (amino acid numbering!), giving rise to a doublet at g_{iso} = 2.0033-2.0037 in several different proteins. Under these measuring conditions, the *g*-anisotropy of the radical is very small and cannot be determined. At high frequency, the anisotropy of the *g*-tensor now dominates the spectrum, which display a rhombic Zeeman powder pattern without the resolved hyperfine coupling observed at lower frequency (Why the hyperfine is lost at higher frequencies is explained in section 1.12). The *g*-values are g_1 = 2.0042, g_2 = 2.0033, and g_3 = 2.0023. Note that g_1, g_2, and g_3 are used when it is not clear which direction is the g_z factor.

The spectra obtained for the tyrosyl radical of the ribonucleotide reductase enzyme from Epstein-Barr virus is shown on the right in Figure 17. In this case one can expect contributions to the hyperfine pattern from all the hydrogen atoms in the benzene ring, but these are actually very small. The largest contribution comes from one of the hydrogen atoms, $H_{\beta 1}$, attached to the C_β-atom (tyrosine numbering!) giving the spectrum the shape of a doublet. The contribution from $H_{\beta 2}$ is much smaller as a result on how the ring is positioned in the protein structure. Again at this frequency the anisotropic *g*-tensor components are poorly resolved while these are clearly shown at 285 GHz with values at g_1 = 2.0080, g_2 = 2.0043, and g_3 = 2.0021. A comparison of different tyrosyl radicals generated in different types of proteins will show differences in the EPR signals. This is because the EPR signal line shape and resonance features depend on the rotational configuration of the tyrosyl ring. In addition, hydrogen bonding and other close by groups will have an effect of the overall shape of the EPR signal.

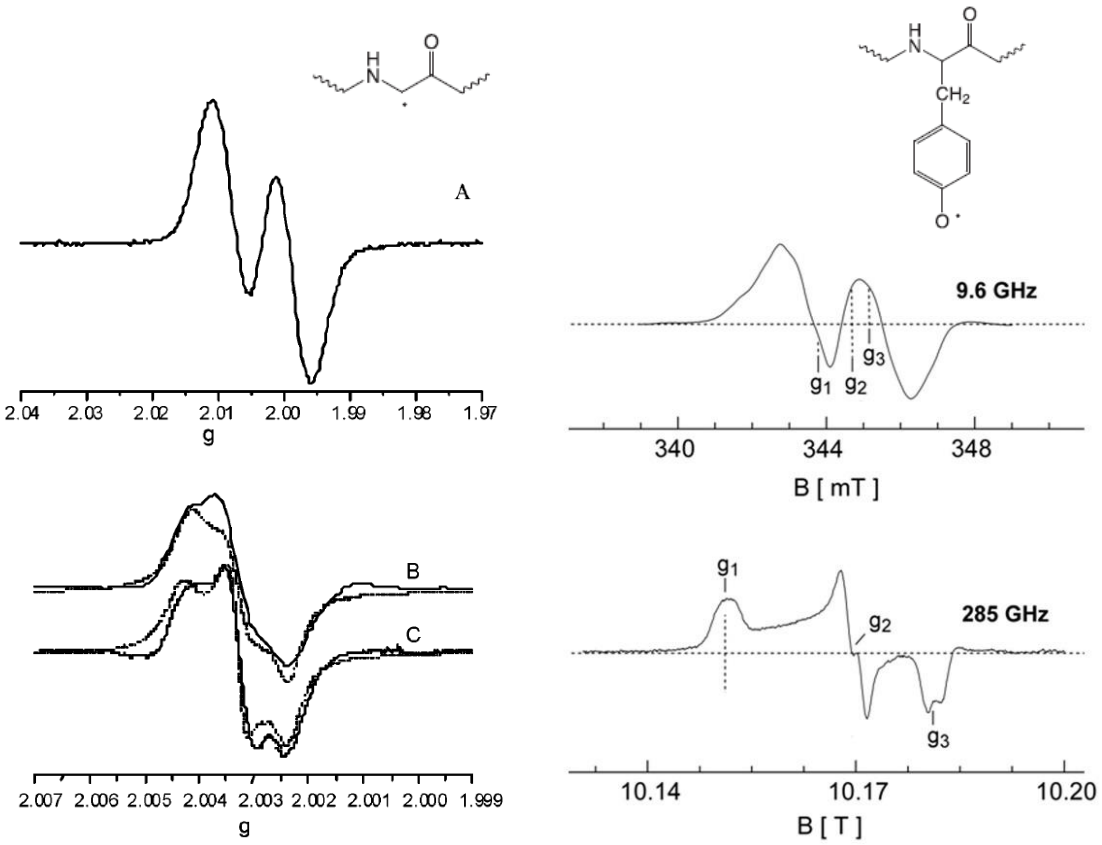

Fig. 17: Left: EPR spectra of glycyl radical of anaerobic ribonucleotide reductase at X-band (A) and high-field (285 GHz) at 2 and at 10.2 T (B and C) (Taken from Duboc-Toia et al. (2003) J. Am. Chem. Soc., 125, 38-39). Right: EPR spectra of the tyrosyl radical of Ribonucleotide Reductase from Epstein-Barr virus. The upper spectrum shows the 9.6 GHz (X-band) resonance spectrum. The lower spectrum shows the 285 GHz spectrum (Adapted from Tomter et al. (2011) PLOS ONE 6(9): e25022).

The radical species are only one type of paramagnetic species detected in proteins. The more common signals that we will discuss here are the signals due to the wide variety of metal ions present in proteins and these will display highly anisotropic spectra at X-band frequency and in several cases hyperfine splitting will be present. The hyperfine splitting pattern will be the same for each of the principle *g*-factors but due to the anisotropy of *A* this is not the case for the magnitude of the splitting, which can differ significantly. In some cases the patterns on the different *g*-factors can even overlap partly or completely making it much more difficult to analyze these patterns. Below follow a couple of example spectra to show this.

Cu^{2+} in $Cu(ClO_4)$

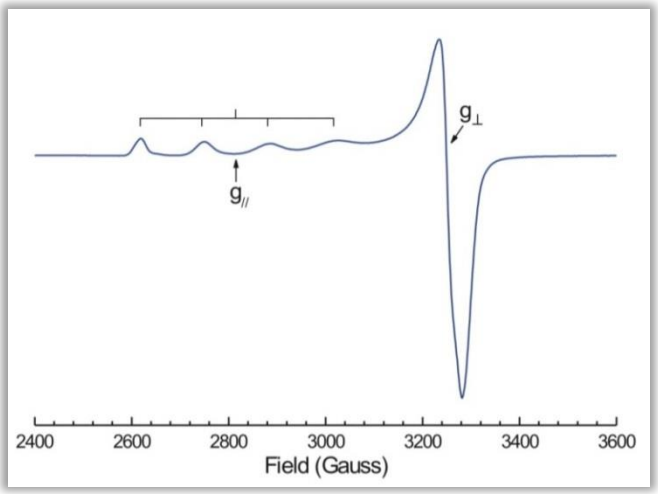

Fig. 18: EPR spectrum of $Cu(ClO_4)_2$

Cu^{2+} typically yields an axial EPR spectrum. The two principal isotopes of copper, ^{63}Cu and ^{65}Cu, both have nuclear spins of 3/2 so that the Zeeman line will be split into four lines (m_I = 3/2, 1/2, -1/2, -3/2). Since the magnetic moments of these two isotopes are very similar, the hyperfine couplings are nearly coincident. The direct consequence of the anisotropy in the central hyperfine splitting is that it is frequently much better resolved in one direction that is along a particular molecular axis than along the other two directions. The hyperfine coupling along $g_{//}$ for Cu^{2+} is always much greater than that along $g_{\perp}$, resulting in a large splitting of the $g_{//}$-line with only minor (often unobservable) splitting of $g_{\perp}$. An example of a powder spectrum of Cu^{2+} (d^9) is shown in Figure 18.

Ni^{1+} in methyl-coenzyme-M reductase

In methyl-coenzyme M reductase, four nitrogen atoms from the tetrapyrrole F_{430} coordinate the nickel (Fig. 19). Now we have a case of superhyperfine interaction. The paramagnetic Ni^{1+} (d^9) is coordinated by four nitrogen atoms of which the nuclei have a nuclear spin 1. Figure 19 shows two spectra. The top spectrum shows the spectra obtained of methyl-coenzyme M in the so-called red1 state. The superhyperfine lines due to the four nitrogen ligands can clearly be detected on the $g_{\perp}$-peak. The resolution of the hyperfine structure on the $g_{//}$-peak is less but still detectable. In an effort to prove that the signals that were detected in this enzyme were due to nickel, the enzyme was enriched in ^{61}Ni, which has a nuclear spin 3/2. The bottom spectrum in Figure 19 shows the resulting spectrum. In addition to the superhyperfine structure from nitrogen we also detect hyperfine structure due to the nickel isotope. The $g_{//}$-peak is now split into four lines. The splitting on the $g_{\perp}$-peak is only detectable as a line broadening since the hyperfine splitting is less than the line width of the peak. Note that this spectrum is very similar to that of Cu^{2+} in Figure 15. In both cases we have d^9 systems.

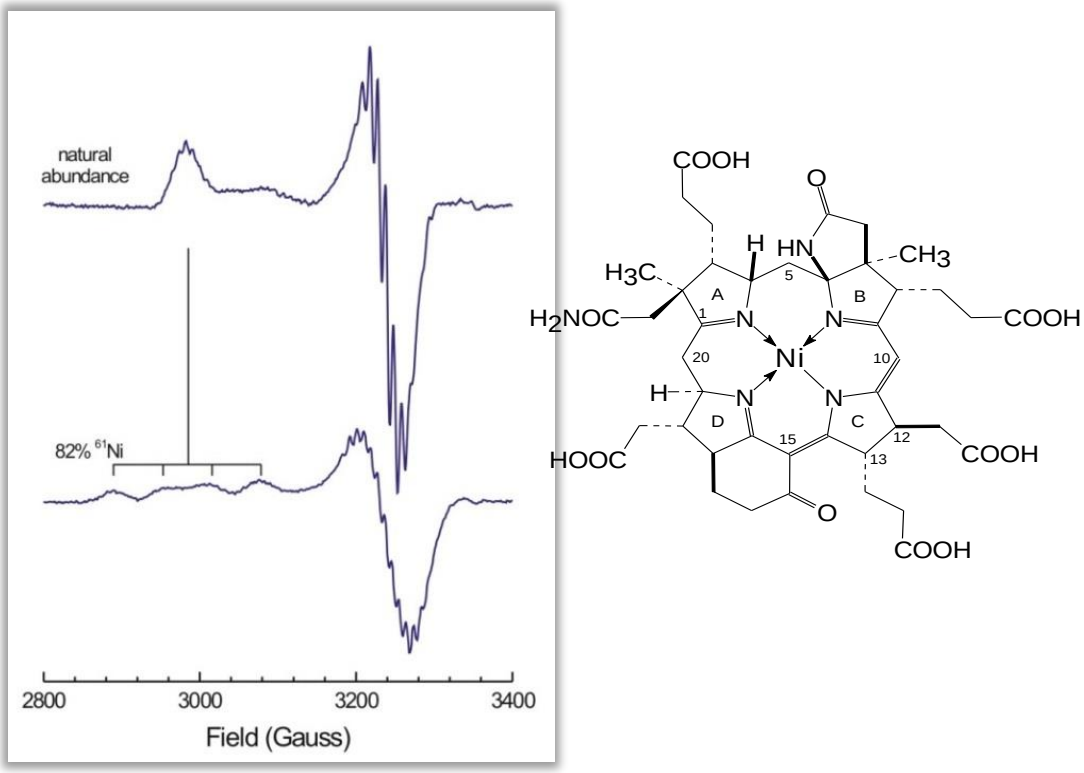

Fig. 19 EPR spectra of methyl-coenzyme M from *Methanothermobacter marburgensis* in the red1 state. The top spectrum shows the spectrum obtained after growing cells with natural abundance nickel isotopes. The bottom spectrum shows the spectrum obtained after growing cells on ^{61}Ni (I = 3/2). The structure of cofactor 430 (F_{430}) is shown on the right.

V^{4+} in chloroperoxidase

In the reduced form of the enzyme, the spectrum of V^{4+} (d^1) can be observed (Fig. 20). Because vanadium has axial symmetry, its powder spectrum consists of two major peaks ($g_\perp$ = 1.95 and $g_{/\!/}$ = 1.98). Vanadium possesses one stable isotope ^{51}V with I = 7/2. Therefore each peak will be further split into eight ($2I$ + 1) lines. Due to overlap, not all lines are observed. On top of that the Hyperfine Coupling Constant A is very large, causing the hyperfine lines of $g_\perp$ to pass the $g_{/\!/}$-peak, causing an effect termed ***overshoot***. The lines of the $g_\perp$-peak will have a different orientation when they are present on the site of the $g_{/\!/}$-peak opposite to that of the position of the $g_\perp$-peak. The same is true for the hyperfine lines of the $g_{/\!/}$-peak.

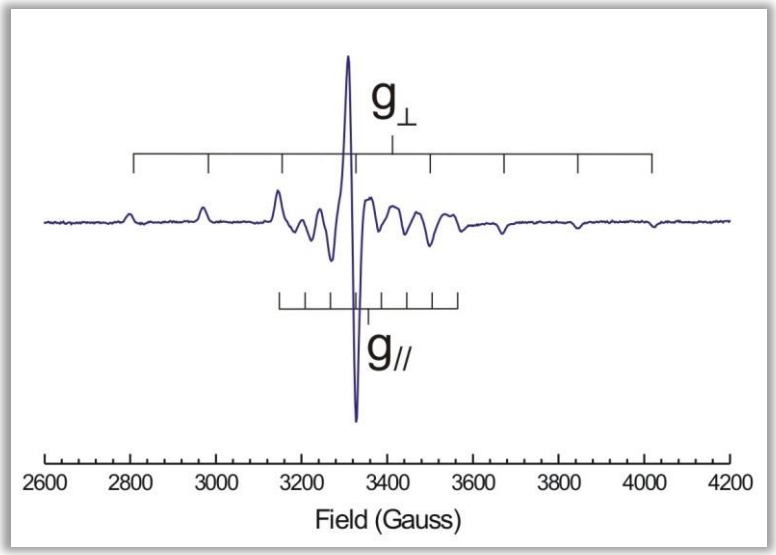

Fig. 20: Vanadium-containing chloroperoxidase from the fungus *Curvularia inaqualis*.

Second-Order and Low-Symmetry Effects

The assumption that the nuclear hyperfine interaction is only a perturbation of the Zeeman interaction is generally true in biochemical systems measured at X-band frequency. For some transition ions, however, the central hyperfine splittings are too large to be called perturbations. The typical effect, also called second-order effect, is an unequal splitting between the hyperfine lines. In this case a second-order correction is needed to be able to get a good description of the EPR data. These types of effects are typically observed for copper spectra where A_z-values are in the range of 30-200 gauss. Note that when the two interactions become equal in magnitude none of the resonance expressions in this handout will be valid and the analysis requires a numerical approach.

Another effect that is also commonly observed for copper spectra is the low-symmetry effect. In low-symmetry systems the axis system that defines the anisotropy in the *g*-value need not necessarily be the same axis system that defines the anisotropy of a central hyperfine system. Thus also referred to as ***tensor noncolinearity***. As a result the EPR spectrum becomes more complex and additional asymmetric peaks can be detected in addition to the main peaks, which might make one believe the sample under study is inhomogeneous. To be able to describe and/or simulate the EPR data knowledge is needed about the rotations needed to correlate the two axis systems. This means an additional set of parameters and an increase in spectral simulation time.

1.8 Spin Multiplicity and Kramers' Systems

A system with *n* unpaired electrons has a spin equal to *S* = *n*/2. Such a system has a spin multiplicity:

$$m_s = 2S + 1 \tag{30}$$

And this value is equal to the number of spin energy levels. All the spin levels together are called the ***spin multiplet***. An essential difference between *S* = ½ systems and high-spin or *S* ≥ 1 systems is that the latter are subject to an extra magnetic interaction namely between the individual unpaired electrons. Unlike the electronic Zeeman interaction this interaction is always present and is independent of any external field. Another name for this interaction therefore is ***zero-field interaction***. In biological transition-ion complexes this zero-field interaction is usually significantly stronger than the Zeeman interaction produced by an X-band spectrometer.

The spin Hamiltonian becomes

$$H_s = \beta B \bullet g \bullet S + S \bullet D \bullet S \tag{31}$$

In the further discussion it is important to make the distinction between ***half-integer systems*** or ***Kramers' systems*** with *S* = *n*/2 (3/2, 5/3, etc.), and ***integer systems*** or ***non-Kramers' systems*** with S = *n* (1, 2, etc.). Solving the wave equations, it can be shown that in zero field the sub levels of a half-integer spin multiplet group in pairs (***Kramer pairs***) and these pairs are separated by energy spacings significantly greater than the X-band microwave energy *hv*. These spacing are also called ***zero-field splittings***, or ZFS. As an example let's look at the high-spin Fe^{3+} ion which has five unpaired electrons. This type of ion can either be found coordinated by four Cys residues in rubredoxins or within a tetrapyrrole structure forming a heme group. Figure 21 shows the energy diagram for the high-spin Fe^{3+} ion in these systems.

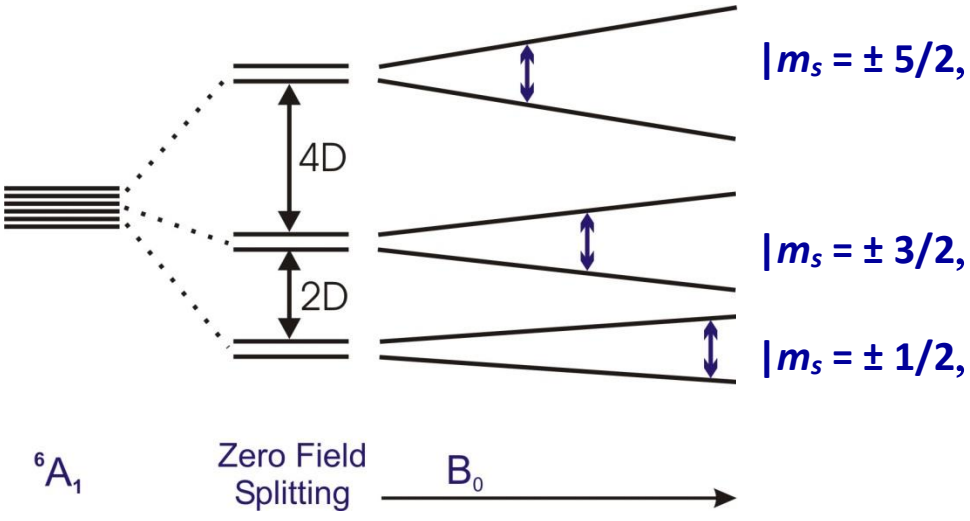

Fig. 21: Zero-field splitting effects in S = 5/2 systems with a zero field splitting parameter (D) that is large compared to the microwave frequency.

The important aspect here is that the *S* = 5/2 multiplet forms three Kramers' doublets that are separated from the others by energies significantly larger than the ~0.3-cm^{-1} microwave quantum (X-

band). Note that the doublets are labeled with the quantum number m_s. The doublets, however, are linear combinations of the different levels but the EPR selection rule $|\Delta m_s| = 1$ still applies.

The degeneracy between the pairs is lifted in an external field. Since the zero field splitting is very large the external field-induced splitting allows for the occurrence of EPR transitions within each (split) pair of levels. There is no crossing over and mixing of the energy levels. For Kramers' systems each Kramer's pair can give rise to its own resonance. Each of these can be described in terms of an effective $S = ½$ spectrum with three effective g-values.

$$h\nu = g^{eff}\beta B \tag{32}$$

g^{eff} encompasses the real g-values plus the effect of the zero-field interaction. Just like the g-value and A-values also the zero-field interaction parameter can be anisotropic and have three values, D_x, D_y, and D_z. In contrast to g and A, however, the three D_i's are not independent because $D_x^2 + D_y^2 + D_z^2 = 0$, and so they can be reduced to two independent parameters by redefinition:

$$D = \frac{3D_z}{2} \tag{33}$$

$$E = \frac{D_x - D_y}{2} \tag{34}$$

We can also define a rhombicity

$$\eta = {}^{E}/_{D} \text{ with } 0 \leq \eta \leq {}^{1}/_{3} \tag{35}$$

From the complete energy matrix it can be derived that under the so-called weak-field limit (Zeeman interaction << zero-field interaction) the three elements of the real g-tensor, g_x, g_y, and g_z, can be fixed at 2.00 and that the shape of the EPR spectra, the effective g-values, is a function of the rhombicity E/D. The relationship of the effective g-values versus the rhombicity can be plotted in two-dimensional graphs, so-called ***rhombograms***. The rhombogram for an $S = 5/2$ system is shown in Figure 22.

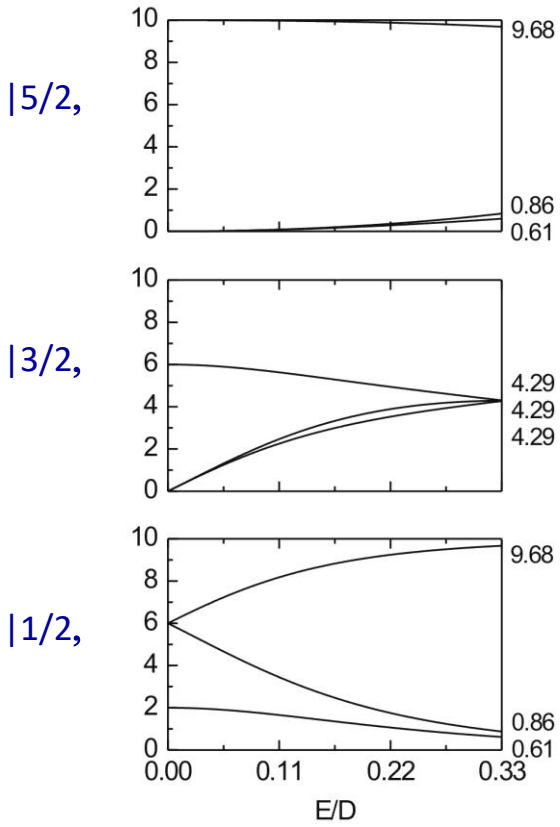

Fig. 22: Rhombogram for an S = 5/2 system.

All possible *g*-values for the subspectrum from a particular Kramers' doublet are represented by the three curves in the individual panels. Spectral analysis means now simply placing a ruler parallel to the vertical axes of Figure 22 and moving it along the horizontal axes to a rhombicity that produces all the experimental observed effective *g*-values. (The *g*-values can also be calculated with the program Visual Rhombo in the BioEPR package, see chapter 3). In practice not all *g*-values will be observable. Most X-band magnets go up to 1 T, precluding the detection of anything below $g = 0.6$. In addition, the highly anisotropic spectra will have very low intensity just because of the wide spread in *g*-values. An infinitely wide spectrum has infinitely low intensity. Visa versa the smaller the *g*-anisotropy, the higher the spectral intensity will be. Maximal intensity is reached when a doublet has three coinciding *g*-values. This is the case for the $|\pm 3/2\rangle$ doublet of the $S = 5/2$ system. An $E/D = 1/3$ gives rise to the well-known $g = 4.3$ line typical for Fe^{3+} ions.

Another complication is the fact that at different temperatures different doublets will be populated and therefore spectra have to be recorded at different temperatures to fully characterize the system. In most cases more than one doublet will be occupied, even at the lowest measuring temperature. Note that when the value of *D* is positive the $|\pm 1/2\rangle$ doublet is the lowest lying doublet, but when the value of *D* is negative this doublet will have the highest energy. Below are a couple of examples to familiarize the reader with some of the high-spin signals found in biological samples.

Fe^{3+} in rubredoxin

The main feature in this spectrum (Fig. 23), measured at 4.5 K, is the very isotropic-looking peak at *g* = 4.32. The blow-up shows there is also a low-intense peak at *g* = 9.63. Taking out our ruler (red, dashed line) we can see that the spectra are due, of course to an *S* = 5/2 system, with *E/D* = 0.315, and that the 9.63 peak is due to the $|\pm 1/2\rangle$ doublet (value smaller than 9.68), and the 4.32 peak is due to the $|\pm 3/2\rangle$ doublet. Note that the exact value of E/D was obtained with the Visual Rhombo program.

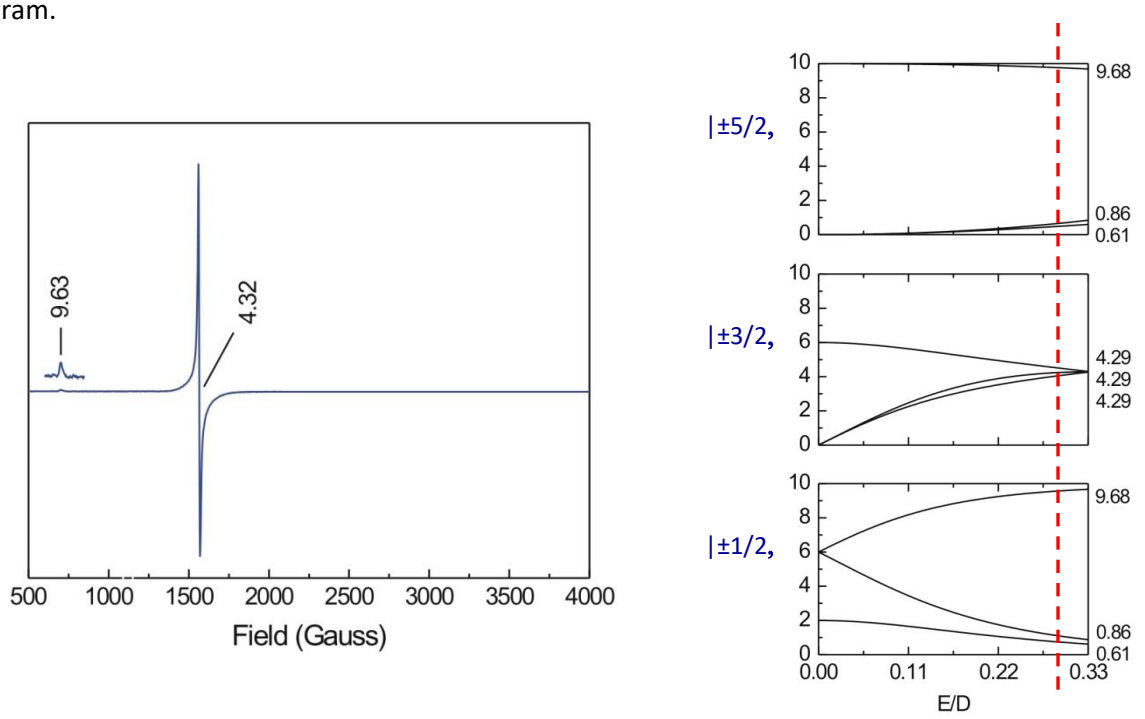

Fig. 23: EPR spectrum for Fe^{3+} in rubredoxin from *Guillardia theta* and the accompanying rhombogram indicating the effective *g*-values for a system with E/D = 0.315

Fe^{3+}-heme in katG

The heme group in the katG enzyme displays a very broad spectrum (Fig. 24) with the lowest *g*-value at 1.99 and the highest at 6.63. This example shows a typical problem you could run into where two species are present with different rhombicity. The top two spectra in the figure are the original data (black line) and a simulation (blue line). The simulation is built up from two different species that are shown separately below this simulation. Again the signal is due to an *S* = 5/2 species. The first component is an axial species with *E/D* = 0.00 and is due to the $|\pm 1/2\rangle$ doublet. The same is true for the second component, but now the spectrum is more rhombic, with *E/D* = 0.03. (In the actual publication the axial species was simulated with two slightly different *E/D* values to accommodate for the different peaks at around *g* = 2).

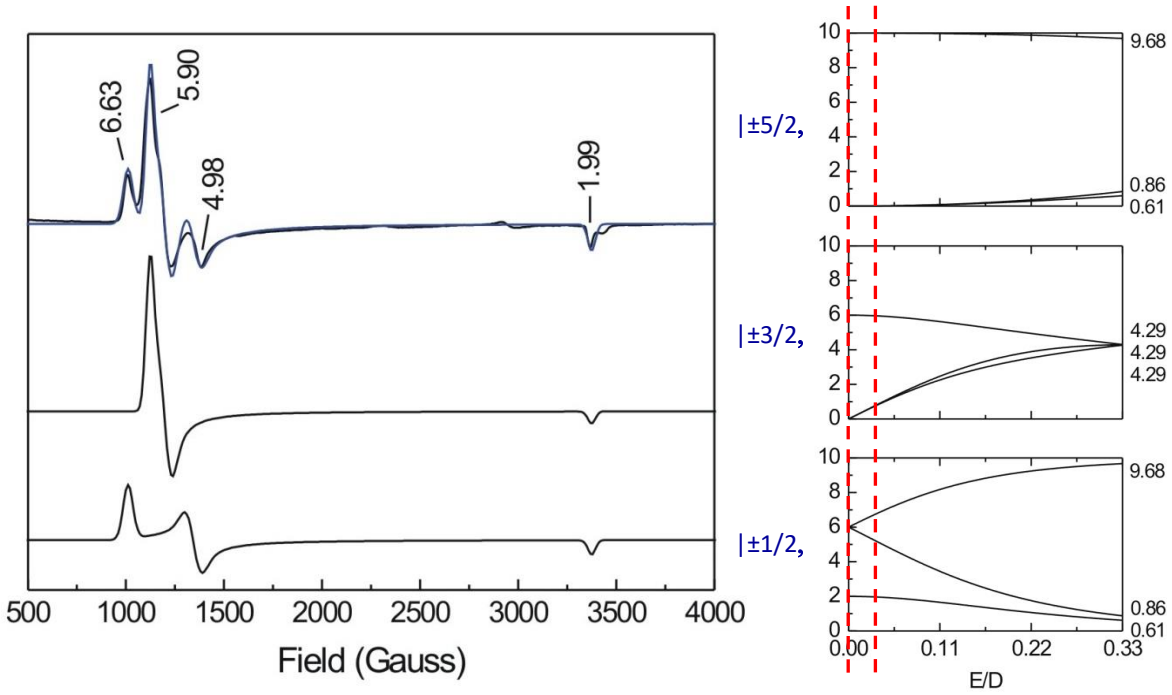

Fig. 24: EPR spectrum of Fe^{3+}-heme in katG. The top two spectra are the original data (black line) and a simulation (blue line). The two spectra below the original date are simulations of the different components with different E/D values, 0.00 and 0.03, as indicated in the accompanying rhombogram.

The rhombograms for all Kramers' systems can be found in Appendix A. Note that there is always a maximal value for *g* dependent on the spin system. For *S* = ½ systems the highest *g*-value is 4. For *S* = 3/2 systems the highest *g*-value is 6, for *S* = 5/2 the highest *g*-value is 10, for S= 7/2 the highest *g*-value is 14, and for *S* = 9/2 the highest *g*-value is 18.

$[2Fe\text{-}2S]^+$ in ferredoxin

The last example shows data obtained for a mutant 2Fe-ferredoxin from *Clostridium pasteurianum* (Fig. 25). This cluster has a spin *S* = 9/2. The figure shows the different spectra that can be obtained at different temperatures. The spectra are clearly different, showing that different doublets are occupied at different temperatures. The EPR spectra can be explained with an *E/D* value of 0.124 and a negative value of *D*. Note that both the $|\pm1/2\rangle$ and the $|\pm9/2\rangle$ doublet will have their highest *g*-value at around 17. The order of appearance/disappearance of the other peaks, particularly the 9.59 peak and the 8.53 peaks are in line with a negative value of *D*. Also note that even at the lowest temperature there are no signals detectable due to the $|\pm9/2\rangle$ doublet.

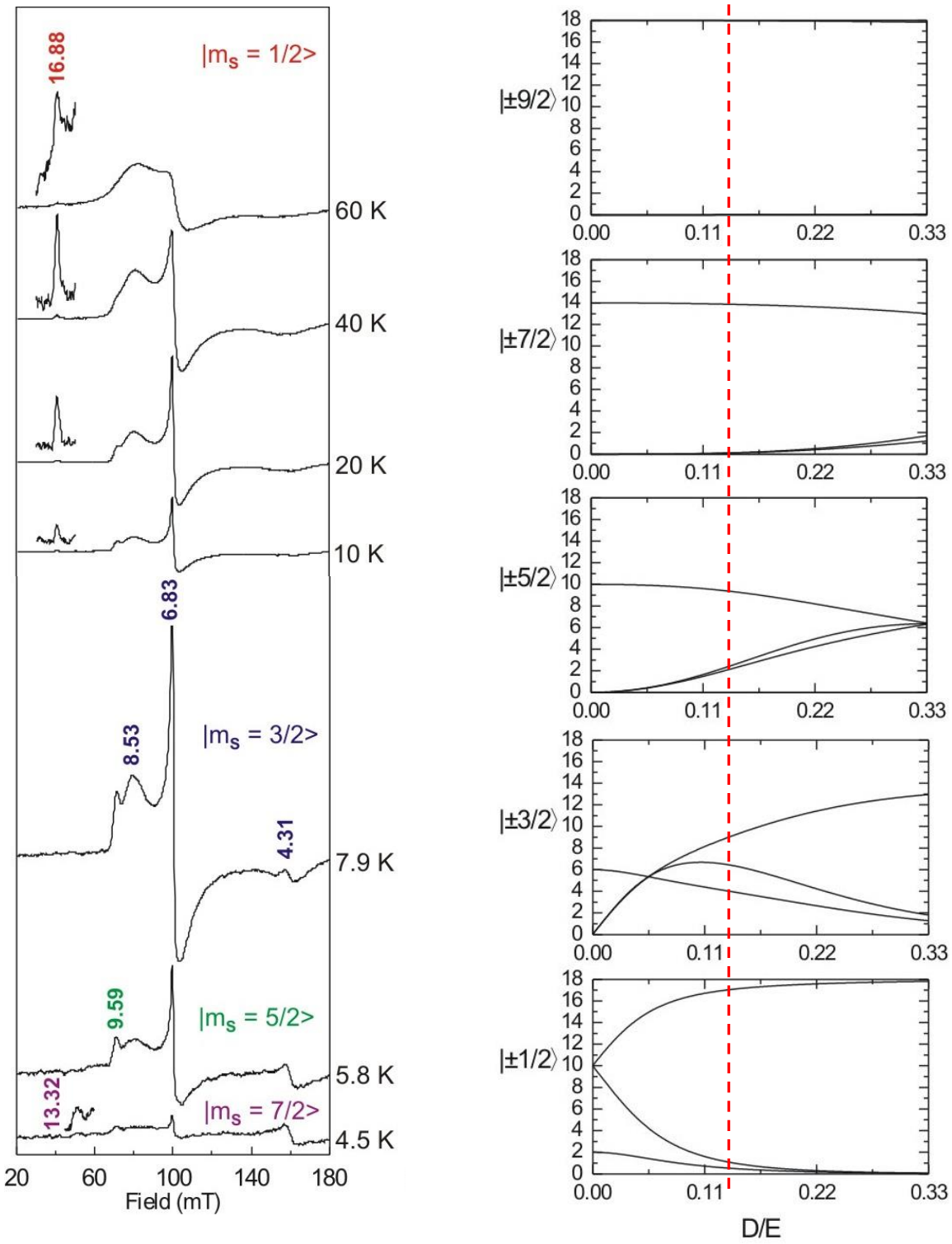

Fig. 25: EPR spectrum of the *S* = 9/2 [2Fe-2S] cluster in ferredoxin from *Clostridium pasteurianum*. The left panel shows the spectra obtained at different temperatures. The right panel shows the rhombogram for an *S* = 9/2 system. The red, dashed, line indicates the E/D value (0.124).

Mn^{2+}

The somewhat simplified description of the EPR spectra of the different Fe^{3+} systems and iron-sulfur-cluster containing proteins is possible due to the fact that they all fall within the weak-field limit (Zeeman interaction << zero-field interaction). It is also possible that the zero-field interaction is much weaker than the Zeeman interaction, and this "strong-field limit" holds for six-coordinate Mn^{2+}, which is not only biologically relevant as a site in some manganese proteins, but also because this is a very common contaminant of biological preparations.

The electronic spin state of Mn^{2+} is $S = 5/2$. Six energy states with the electron spin magnetic quantum number, $m_s = 5/2, 3/2, 1/2. -1/2, -3/2$, and $-5/2$ arise due to the Zeeman effect. To give an impression of the increased complexity of the energy level diagrams and the resulting EPR spectra let us consider a pure cubic (e.g., octahedral) situation. Although D and E are zero in this case and g is isotropic, because of the high spin a new zero-field energy term exists that produces EPR anisotropy. The zero-field splitting for $B \| z$ are shown in Figure 26. The double arrows indicate the 5 transitions that are allowed and contribute to the total EPR spectrum.

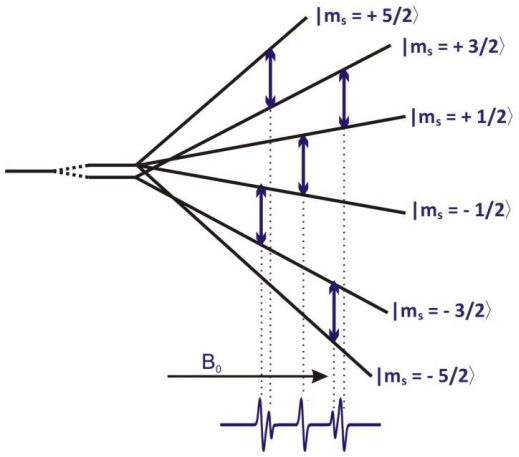

Fig. 26: Energy-level diagram for a d^5 ion in an octahedral crystal field and the allowed EPR spectrum. The diagram applies only for B parallel to a principle axis of the octahedron.

Due to the nuclear spin magnetic quantum number of Mn, all lines will be further split into six hyperfine lines, $m_I = 5/2, 3/2, 1/2. -1/2, -3/2$, and $-5/2$. Thus one expects a 30-line pattern. However, depending on the relative magnitudes of D and A (hyperfine coupling constant of manganese), these 30 lines appear as a separate bunch of 30 lines or 6 lines (if $D = 0$). The separation between the extreme set of resonance lines is approximately equal to 8D (first order). If D is very small compared to hyperfine coupling constant A, the 30 lines are so closely packed that one could see only six lines corresponding to -1/2 to +1/2 transitions. If $D = 0$, the system is perfectly octahedral. Deviation from axial symmetry leads to a term known as E in the spin-Hamiltonian. The value of E can be easily calculated from single crystal measurements. A non-zero value of E results in making the spectrum unsymmetrical about the central sextet.

The full energy level diagram is shown in Figure 27. Note that due to second-order effects the energy level splitting by the Zeeman effect is not linear. The energy level diagram predicts that the spectrum is dominated by the $m_s = +1/2 \leftrightarrow -1/2$ transition and shows the presence of six hyperfine lines each

split by a small anisotropy induced by the zero-field splitting. An actual spectrum (Fig. 28), however, shows additional features. In between the six hyperfine lines there are five pairs of weak lines from forbidden $\Delta m_I = \pm 1$ transitions with an order of magnitude lower intensity than the main lines. This whole $m_s = \pm 1/2$ spectrum is on top of a very broad, rather structureless feature that is the sum of all the other five $\Delta m_s = 1$ transitions (e.g., $m_s = -3/2 \leftarrow -5/2$). At higher microwave frequencies (~35 GHz and beyond) this complex situation dissolves and a simple, isotropic, six hyperfine line pattern remains.

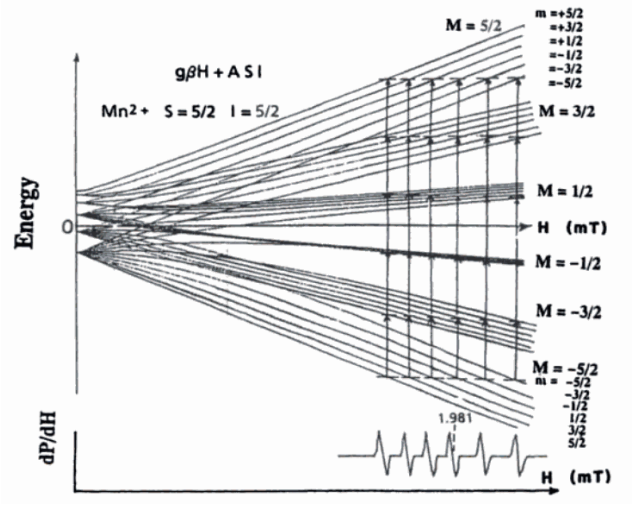

Fig. 27: The energy levels of Mn^{2+} as a function of the external magnetic field. Splitting into $2S + 1 = 6$ by the Zeeman effect for m_s (M in figure) and further into $2I + 1 = 6$ states for m_I (m in figure) by the hyperfine magnetic field. The resonance fields for allowed transitions ($\Delta m_s = \pm 1$, $\Delta m_I = 0$) are the same for different m_s values when $A/g\beta < H_0$. Fine structure splitting occurs for a large A value, which is part of the reason of the different linewidth of each hyperfine line. (Taken from M. Ikeya (1993) New Applications of Electron Spin Resonance, World Scientific Publishing, Singapore)

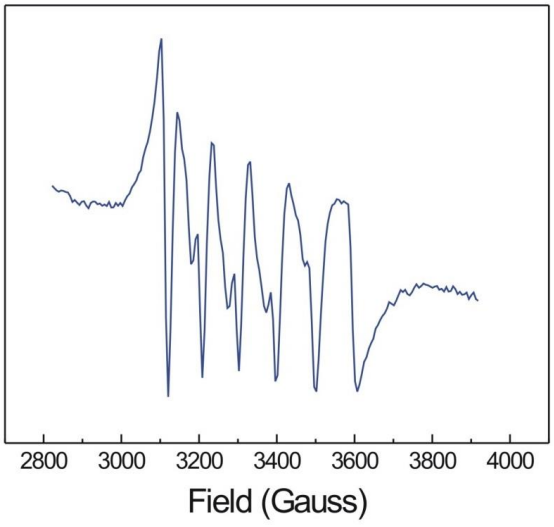

Fig. 28: Manganese as a common contaminant in protein EPR. This X-band spectrum is characteristic for high-spin Mn(II) specifically bound to proteins.

1.9 Non-Kramers' Systems

Non-Kramers' systems or integer systems are systems with S = 1, 2, 3, 4. These systems are very seldom observed in biological systems. One of the reasons is that just as in the Kramers' systems the energy levels are organized in doublets (and one singlet, $|0\rangle$). These doublets, however, are split even at zero fields and this splitting is generally greater than the energy of the X-band radiation. This means that in most cases the signals cannot be detected. In addition, the transitions between the doublets are forbidden because the spin has to change by more than ±1 and are very weak in the normal EPR spectrometer configurations where the static magnetic component of the microwave, B_1, is perpendicular to the static magnetic field, B_0. The transitions in integer spin systems, however, are enhanced when B_1 is put parallel to B_0. This requires a special experimental setup called ***parallel-mode EPR***. The Bruker ER411DM "dual mode" cavity is designed for these studies. It is called dual mode because it operates in one mode with $B_1 \perp B_0$ at about 9.8 GHz, and in another mode with $B_1 // B_0$ at ca. 9.3 GHz. The only reported cases for biological systems are from different types of iron-sulfur clusters and heme groups. The most common signal detected is the S = 2 state in $[3Fe\text{-}4S]^0$ clusters and Fe^{2+}-heme. Figure 29 shows the S = 2 signal detected for a $[3Fe\text{-}4S]^0$ cluster in the hydrogenase from *Allochromatium vinosum*. Although the transition is forbidden it can still be detected in perpendicular mode EPR. The full signal, however, is detected in parallel-mode EPR. Due to several mechanisms, the EPR signals are very broad and deformed and not much information can be obtained from the signals itself. The fact that the signals can be detected, however, can be a very important piece of evidence. The lack of a signal in parallel-mode EPR is often used to exclude the presence of $[3Fe\text{-}4S]^0$ clusters.

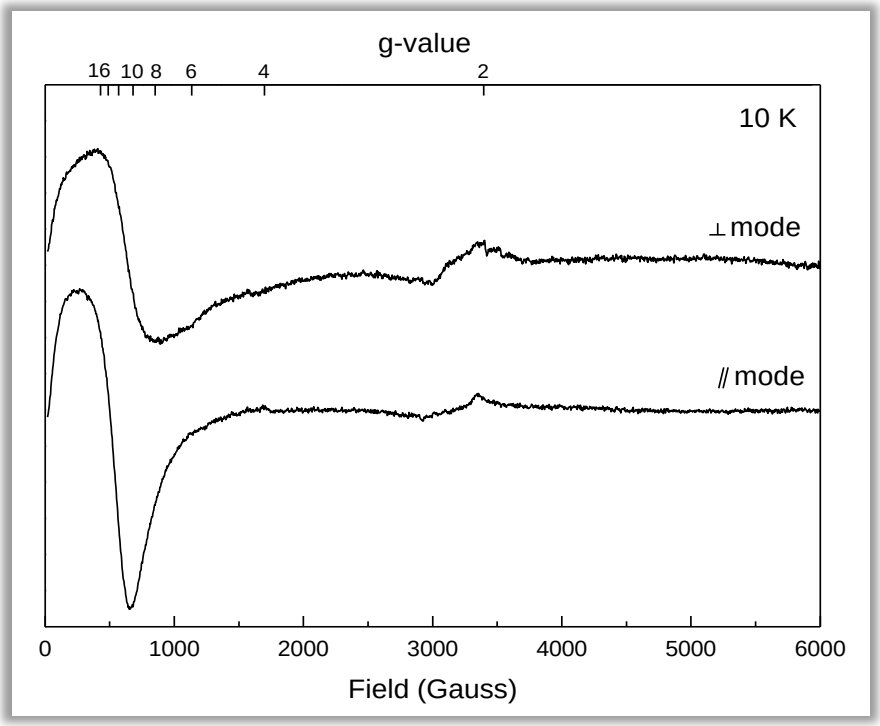

Fig. 29: EPR spectrum of the S = 2 $[3Fe\text{-}4S]^0$ cluster in hydrogenase of *Allochromatium vinosum*. The top spectrum was recorded in standard EPR spectroscopy. The bottom spectrum was recorded in parallel-mode EPR spectroscopy.

1.10 Characterization of Metalloproteins

EPR spectroscopy is one of the most important techniques for the characterization of metalloproteins. There are several things that can help with identifying the metal-ion that is present. First of all only the paramagnetic forms are detectable or as we say, are ***EPR active***. The properties of Fe, Ni, and Cu ions are shown in Table 1.3

Table 1.3: Electronic properties of metal ions

Metal Ion	Electron Configuration	Spin State
Fe^{2+}	d^6	S = 0 (ls) or S = 2 (hs)
Fe^{3+}	d^5	S = 5/2 (hs)
Ni^{1+}	d^9	S = ½
Ni^{2+}	d^8	S = 0 or S = 1
Ni^{3+}	d^7	S = ½
Cu^{1+}	d^{10}	S = 0
Cu^{2+}	d^9	S = ½

In the case of Fe, both redox states can potentially be EPR active, although the 2+ state is not when the ion is in the low-spin (ls) form which is commonly the case. With Ni the 1+ and 3+ states are EPR active. With Cu only the 2+ state is EPR active. Therefore, in EPR studies, samples are prepared of the enzyme preparation in different states: as such, reduced, and oxidized. As a reductant dithionite can be used. For an oxidant ferricyanide is commonly used. The fact that a signal can be detected in the reduced form, or the oxidized form, or both forms gives the first clue on what metal ion is present.

The next step is to look closer at the EPR signal. The position of the *g*-values will tell whether you are dealing with a high-spin system or not. Hyperfine splitting might be present that might give a clue about the origin of the metal ions itself. Most metals have a very unique nuclear spin. The hyperfine splitting can also indicate the presence of ligands with a nuclear spin.

From the position of the *g*-values we can also tell something about the type of metal ion. The spin–orbit coupling parameter is positive for S = ½ systems with less than half filled outer shells and negative for those with more than half filled shells, which means that the former have $g<g_e$ and the latter have $g>g_e$. The only exceptions to that rule are W- or Mo-containing systems.

Similar consideration can be made for more complex systems. As an example, Figure 30, shows the EPR spectra obtained for proteins containing different types of iron-sulfur clusters. There are three basic types of iron-sulfur clusters: [2Fe-2S] clusters, [3Fe-4S] clusters, and [4Fe-4S] clusters. All can be present in different oxidation states, some of which are EPR active. The 4Fe clusters come in two varieties: standard clusters that shuttle between the 1+ and 2+ oxidation states, and high-potential iron-sulfur (protein) (HiPIP) clusters that shuttle between 2+ and 3+ oxidation states.

In an oxidized protein sample that contains an Fe-S cluster you would only be able to detect a $[3Fe\text{-}4S]^{1+}$ cluster or a HiPIP $[4Fe\text{-}4S]^{3+}$ cluster. These signals are very different and easily discernable. In a reduced sample you would detect either $[2Fe\text{-}2S]^{+}$ or $[4Fe\text{-}4S]^{+}$ clusters. These signal are more similar

in shape, but as will be described later in more detail, have very different temperature behavior, with the optimal temperature for detection at around 10 K for the $[4Fe\text{-}4S]^{+}$ cluster and 20-70 K for the $[2Fe\text{-}2S]^{+}$ cluster.

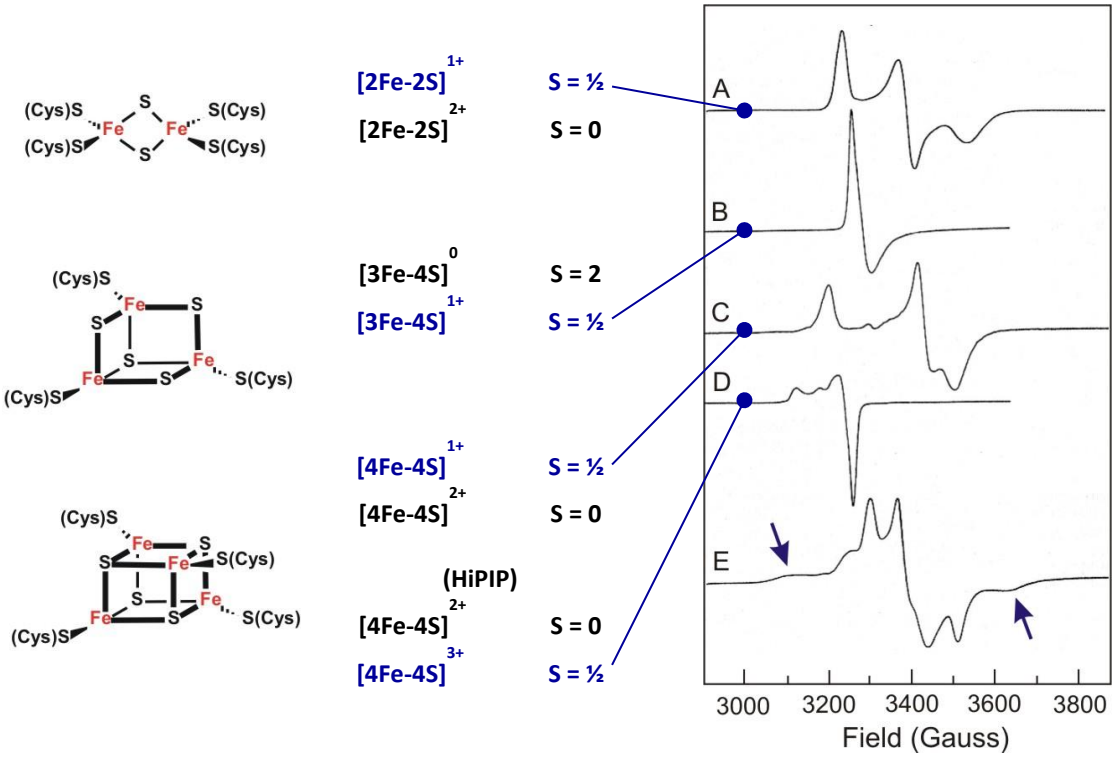

Fig. 30: EPR spectra of different types of iron-sulfur clusters. On the left, the basic structure of the cluster types is shown. In the middle, redox states and their respective spin states are indicated. The panel on the left show the EPR spectra of the iron-sulfur clusters in ferredoxins from *Mastigocladus laminosus* (A), *Desulfovibrio gigas* (B), *Bacillus stearothermophilus* (C), *Chromatium vinosum* high-potential iron-sulfur protein (HiPIP) (D), and *Clostridium pasteurianum* 8Fe ferredoxin (E). (Adapted from Cammack (1985) Biochem, Soc. Trans., 13, 572)

1.11 Spin-Spin Interaction

In chapter 3, the BioEPR software package for the simulation of EPR spectra will be introduced. This package is very user friendly and most types of EPR spectra that will be encountered in biological systems can be simulated with this software, ranging from simple radical species to complex hyperfine spectra, high-spin systems, and some of the integer spectra. Note, however, that the software can only be used under a certain set of conditions. When these conditions are not met, different or more advanced software is needed for spectral simulation. An important example of this is found in enzymes where 2 radical species are present in close proximity of each other. In Figure 30, trace E, a spectrum is shown that is detected in a so-called 8Fe ferredoxin. In this protein two $[4Fe\text{-}4S]^{+}$ clusters are present. For comparison, look at trace C in Figure 30 that shows the spectrum of a single $[4Fe\text{-}4S]^{+}$ cluster detected in another ferredoxin enzyme. If the two clusters would be far apart and not able to sense each other, the spectrum for the 8Fe Ferredoxin would be a simple summation of two single $[4Fe\text{-}4S]^{+}$ spectra. If you are lucky, both paramagnets could display somewhat different *g*-values and it should be possible to discern both signals in the spectrum. If the distance between the two paramagnets is 10-12 Å or less, however, the two paramagnets will interact with each other and both signals would split up similar to the effect seen with hyperfine interaction. However, this is not what is detectable in Figure 30, trace E. Broad wings are detectable in the EPR spectrum (indicated by the arrows). These are generally the first indication that there are two species that are spin coupled. Note how these wings reach far beyond the region where the *g*-values of both paramagnets would be in the absence of the spin-spin interaction. Unlike in hyperfine interaction where the *g*-tensor of the electron spin and the anisotropic hyperfine tensor *A* are assumed to be collinear, the individual *g*-tensors of the two interacting paramagnets in spin-spin interaction can have every possible orientation causing the resulting EPR signal to be very different in shape. Therefore in spin-spin interaction both the distance and the angle of the respective *g*-tensors of the paramagnetic species are of importance.

To further complicate the interpretation of these types of signals there will also be different types of interactions dependent on the distance between the two interacting paramagnets. The two magnetic interactions that operate between paramagnetic centers are the through-space dipole-dipole interaction and an exchange interaction that depends on orbital overlap and spin polarization effects. The former is an anisotropic interaction that follows a $1/r^3$ dependence on the spacing between the interacting centers. The latter is usually considered an isotropic interaction, which falls off approximately exponentially with the distance between the partners. At distances greater than approximately 9 Å, the exchange interaction creates a doublet splitting in the EPR spectrum of each partner. At closer distances, the exchange interaction mixes the two spin systems, such that their *g*-values become averaged and eventually converge to a triplet state at interspin separations of <7 Å.

To understand the shape of the interaction spectra, a second example is discussed here and is from a family of enzymes called adenosylcobalamin (coenzyme B_{12})-dependent isomerases. These enzymes catalyze skeletal rearrangements via a radical mechanism. The reaction starts with the generation of the 5'-deoxyadenosyl radical and cob(II)alamin from enzyme-bound adenosylcobalamin by homolysis of the coenzyme's cobalt-carbon σ-bond in the presence of a substrate molecule SH. Stereospecific hydrogen abstraction from the substrate molecule by the 5'-deoxyadenosyl radical gives 5'-deoxyadenosine and a substrate radical $S^{\bullet}$. At this point two paramagnetic species are present in the enzyme, the Co^{2+} species and the $S^{\bullet}$ radical species (Fig. 31).

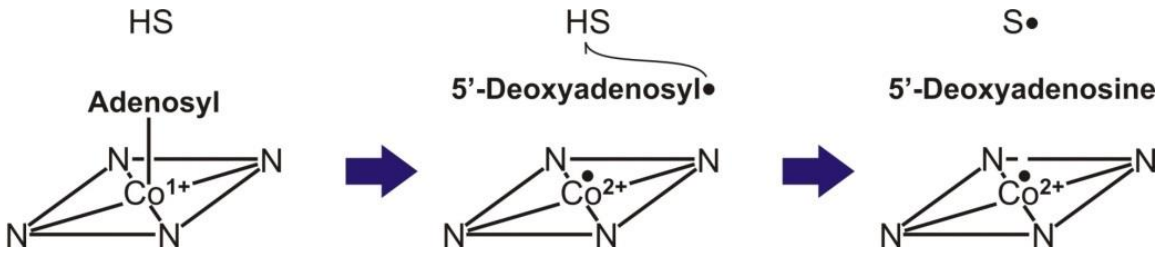

Fig. 31: Formation of the two paramagnetic species in adenosylcobalamin (coenzyme B_{12})-dependent isomerases.

To be able to understand the reaction mechanisms of these enzymes in detail, it is important to determine what radial species are present at different reaction times and where they are located in the enzyme active site. The distance between the Co^{2+} and the deoxyadenosyl or the substrate-based radicals can be obtained from simulation of the detected EPR spectra. For distances larger than 4-5 Å both paramagnets can be considered point dipoles. The dipole–dipole interaction lifts the degeneracy of the spin states in the absence of an external magnetic field and is a source of zero-field splitting. In the most general formulation, the zero-field splitting is described as a traceless tensor with an axial, *D*, and a rhombic, *E*, term. In the commonly used point-dipole approximation, $E \equiv 0$. The principal axis of the zero-field splitting normally contains the interspin vector. In simulations, Euler rotations (θ) are required to relate the axis system of the zero-field splitting tensor to a reference system, such as the *g*-axis of Co^{2+} (Fig. 32). The EPR spectra are normally interpreted with the aid of a spin Hamiltonian containing the *g*- and *A*-tensors of the individual radicals, as well as the exchange and dipole–dipole interaction terms of the spin–spin coupling. Good approximations for the *g*- and *A*-tensors of cob(II)alamin bound to the enzyme of interest are frequently available, such that the spin-spin interaction terms and Euler angles relating the interspin vector to an appropriate molecule fixed axis (e.g. the *g*-axis of Co^{2+}) are the major unknowns in the analysis.

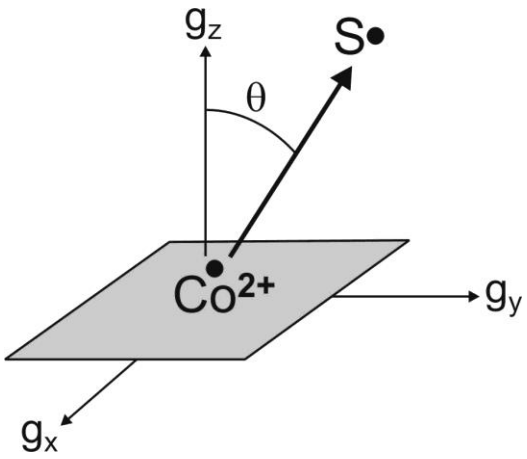

Fig. 32: Position of the substrate radical in respect to the position of the Co^{2+}

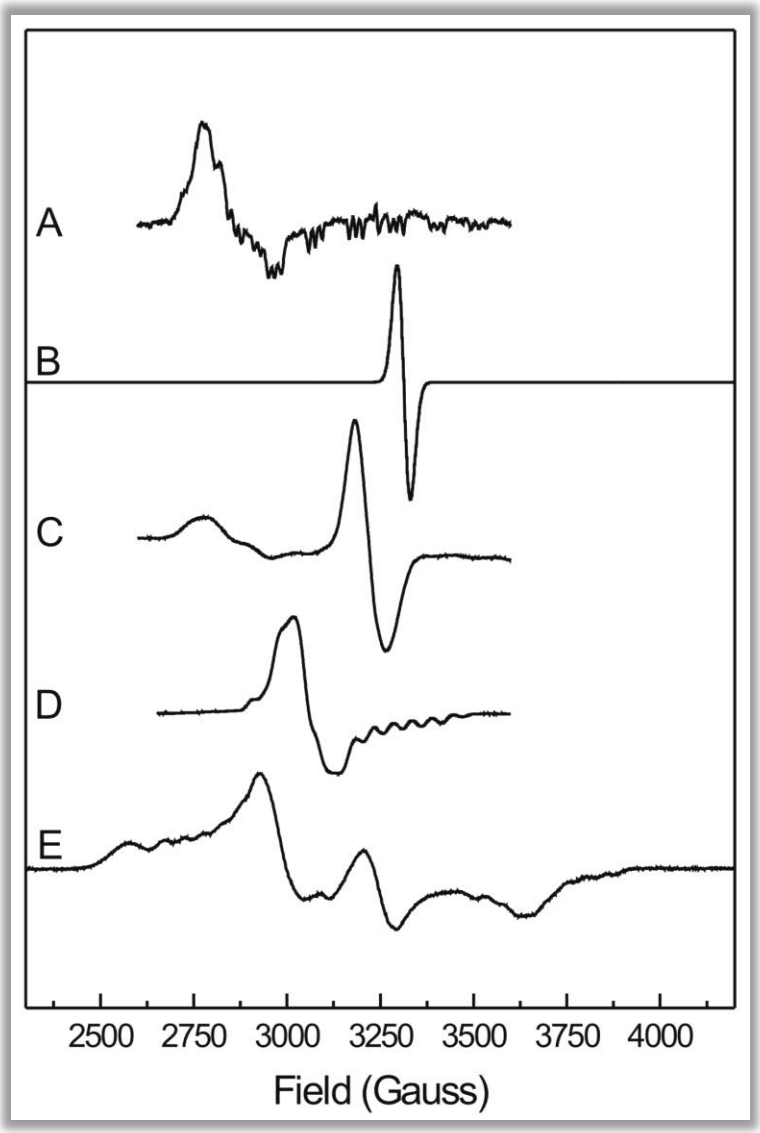

Fig. 33: (A) Co^{2+} signal detected in ethanolamine ammonia lyase obtained by reacting the enzyme with a suicide inactivator (e.g. methanol) that escapes from the active site after forming the substrate radical and becomes quenched. This leaves behind the isolated Co^{2+} signal. (B) Simulation of a radical species with g = 2.0023. (C) Signal of the coupled Co^{2+}/radical species in ethanolamine ammonia lyase after reacting with ethanolamine. The interspin distance is 8.7 Å and θ = 25° (D) Coupled Co^{2+}/radical species in lysine-5,6-aminomutase after reacting with 4-thialysine. The interspin distance is 7.0 Å and θ = 43°. (E) Coupled Co^{2+}/radical species in diol dehydratase after reacting with 5'-deoxy-3',4'-anhydroadenosylcobalamin. The interspin distance is 3.5 Å and θ = 75°.

Figure 33, shows a set of spectra from different adenosylcobalamin-dependent isomerases. The first spectrum (Fig. 33, trace A) is the Co^{2+} spectrum observed in ethanolamine lyase after quenching of the radical species. This is an example of the Co^{2+} spectrum when there is no interaction with a second paramagnet. The spectrum is axial, with the $g_{//}$ peak on the high-field site. The whole spectrum is split in 8 lines due to the nuclear spin of the cobalt ion (I = 7/2). On top of that there is interaction of the electron in the d_{z2} orbital with an axial nitrogen ligand which causes an additional 3-fold split of each

of the 8 lines. Note that the hyperfine splitting of the $g_{\perp}$ peak is not resolved. The $g_{//}$ peak, however, shows a large hyperfine coupling. Of the expected 8 lines, 6 can be easily recognized, including the additional 3-fold split. Two of the lines overlap with the $g_{\perp}$ peak and are more difficult to discern. In chapter 4 with examples of different types of spectra, a Co spectrum is shown recorded at higher frequency. In this case the lines of the g_2 peak do not overlap with the $g_{\perp}$ peak and the 8 lines can be easily recognized. (The effect of different frequencies on EPR signals will be discussed in section 1.12). Also shown in Figure 33, trace B, is a simulation of a radical species.

Weakly coupled spin systems

Shown in a separate figure (Fig. 34) is an example of a weakly coupled system. The suicide inactivation of ethanolamine ammonia-lyase by hydroxyethylhydrazine results in the formation of a hydrazine cation radical that is positioned 13 Å from Co^{2+} and approximately along the $g_{//}$-axis of the ion (i.e. directly above the plane of the corrin ring). The individual paramagnetic species can easily be recognized in the measured EPR spectrum (Fig. 34). The signals from the low-spin Co^{2+} and the partner radical were split by a combination of exchange and dipole-dipole coupling. This can be detected as the additional hyperfine splitting of the Co^{2+} signal (Compare with Figure 33, trace A).

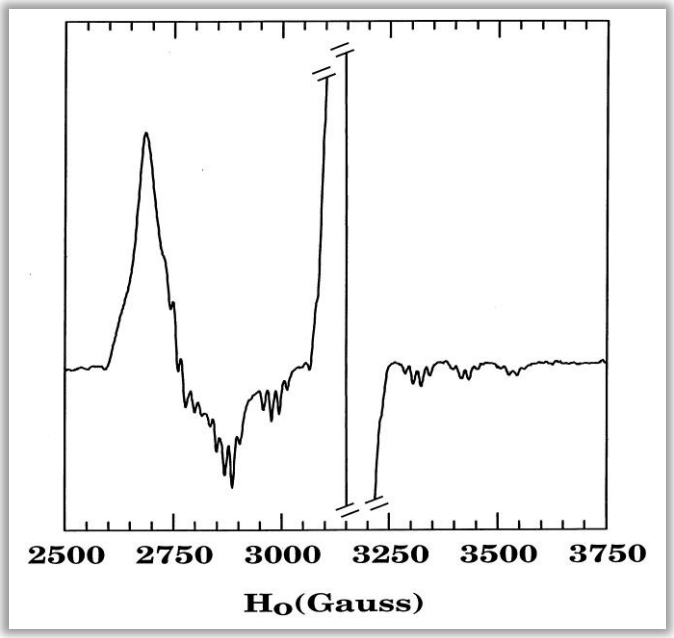

Fig. 34: X-Band EPR spectrum of hydroxyethylhydrazine-inactivated ethanolamine ammonia-lyase showing presence of features corresponding to B_{12r} and a companion radical species with absorption near g = 2.0. The amplitude of the signal of the radical centered at g = 2.0 is off scale. (Taken from Bandarian (1999) Biochemistry 38, 12394)

Strongly coupled spin systems

In Figure 33, traces C and D are representatives of cases where there is a strong coupling between the cobalt and the radical species. In trace C the spectra of the two paramagnets have moved closer towards each other and there are clear differences in the shapes of the signals. In trace D the EPR

spectra appears to be a hybrid of both the cobalt and the radical EPR signals and exhibit an average *g*-value of ≈ 2.1 that arises from coupling between a carbon centered radical (g = 2.0023) with cob(II)alamin (g_{av} ≈ 2.18). The signals are due to a 'hybrid' triplet spin system comprising both paramagnetic species. Trace C in Figure 33 is detected in ethanolamine ammonia lyase after reacting with ethanolamine. The interspin distance is 8.7 Å and θ = 25°. Trace D in Figure 33 is from lysine-5,6-aminomutase after reacting with 4-thialysine. The interspin distance is 7.0 Å and θ = 43°.

Very strongly coupled spin systems

The last example spectrum in Figure 33, trace E, is a signal detected in diol dehydratase after reacting with the analog 3',4'-anhydroadenosylcobalamin (anhydro-AdoCbl). This gives a more stable allylic radical upon hemolysis of the cobalt–carbon bond, creating a somewhat stable radical very close the Co^{2+}. The EPR spectrum (Fig. 33, trace E) does not resemble that of Co^{2+} or a radical species or the other spectra shown in Figure 33. However, it is still consistent with a rhombic triplet-state species. A prominent half-field transition at around g = 4 can be detected (not shown) which is a hallmark of strongly coupled triplet spin systems. Changes in the linewidths of transitions in the EPR spectra resulting from ^{13}C and ^{2}H isotopic substitutions in the anhydroribosyl moiety identified one of the triplet spin partners as the anhydroadenosyl radical. The presence of ^{59}Co hyperfine splitting, as well as the apparent *g*-values of the signals, identified low-spin Co^{2+} of cob(II)alamin as the other spin in the hybrid triplet system. Note that also in this case the EPR spectrum covers an area much wider than one would expect based on the *g*-values of the two individual paramagnets (Fig. 33, traces A and B). The spectrum can still be simulated using the point-dipole approximation, but to get a more accurate value for the distance and the Euler a higher level of treatment is required. The spectrum can be simulated using an interspin distance of 3.5 Å and a θ of 75°.

1.12 High-Frequency EPR Spectroscopy

Why would we use different frequencies in EPR spectroscopy? Going back to Figure 5, you can see that an increase in the strength of the magnetic field B_0 will result in a larger separation of the two energy levels. As a result there will be an increased population difference between the ground and excited state resulting in higher signal amplitude. To be able to meet the resonance conditions the frequency will also have to be increased according to $g = 0.7145\,\nu/B_0$. For both technical and fundamental reasons, however, it turned out that the optimum sensitivity in EPR is reached in the 8-12 GHz range and X-band is right there in the middle of that range. This is the reason that X-band EPR spectroscopy is the most common EPR technique. There are cases, however, that the information obtained at X-band frequencies is limited and a higher frequency is needed. EPR absorption lines can have a width that is independent of the used frequency and the corresponding resonance field. As a consequence, the resolution of two partially overlapping lines will increase with increasing frequency as illustrated in Figure 35. Note that there is a theoretical limit of maximal resolution enhancement by frequency increase. In practical cases the enhancement is usually less or in some cases there is no enhancement at all.

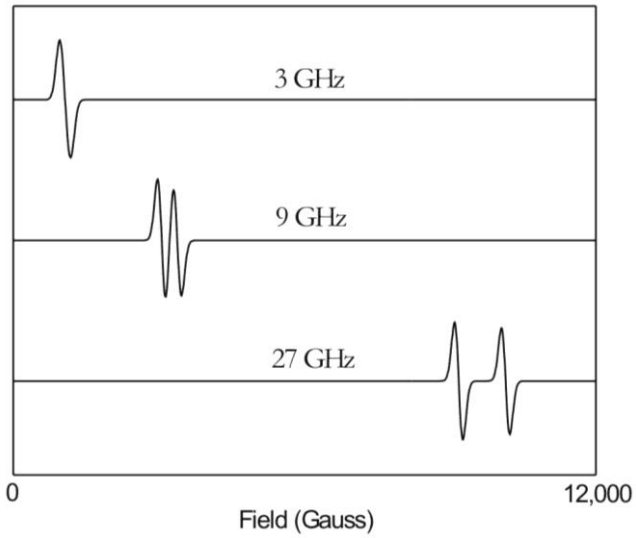

Fig. 35: Theoretical increase in resolution with increasing frequency. A two-line EPR spectrum is given at three different microwave frequencies.

Again using a practical example the extra information from using a higher frequency can be easily demonstrated. Let us go back to the Red1 signal detected in methyl-coenzyme M reductase (Figs. 19 and 36). The spectrum seems to be due to an axial species. When you count the amount of hyperfine lines on the $g_\perp$-peak, however, you will find 10 lines instead of the 9 lines you would expect for an interaction with four N nuclei (Fig. 36B, top). It turns out that the signal is slightly rhombic and the g_x and g_y have two different values. The difference is such that there is still a perfect match between the hyperfine lines, but one set is just shifted so that an additional peak can be detected.

When the same species is now measured at W-band (90 GHz) the signal looks much different. First of all the hyperfine structure is lost. This is due to the fact the hyperfine coupling constant A is not dependent on the frequency. The additional splitting of the energy levels is now negligible in comparison to the splitting due to B_0, and as a result is no longer detected. The line widths of the

signal did not change, but the peaks are now more spread apart. The peaks, however, can be matched by squeezing the W-band spectrum horizontally. Now to the eye it looks like the peaks have become much sharper and the g_y- and g_x-peaks are nicely resolved. Note that the best way to compare spectra at different frequencies is to use the only property that does not change, the *g*-value. The same plot can be obtained if both spectra are plotted using a *g*-scale. Note that the *g*-scale is a reciprocal scale and not a linear scale.

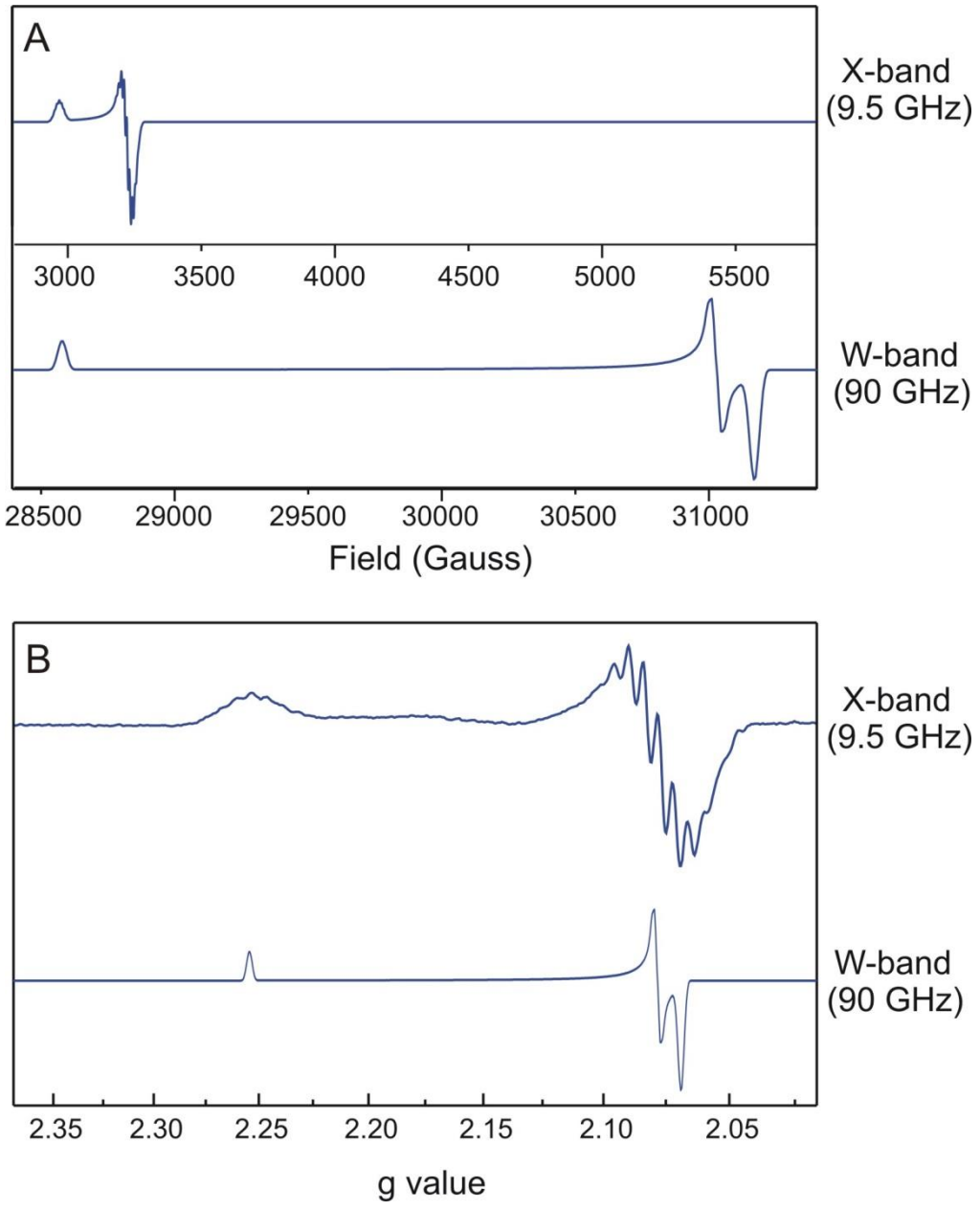

Fig. 36: EPR spectra of the Ni^{1+} signal (red1) detected in methyl-coenzyme M reductase measured at X-band (9.4 GHz) and W band (90 GHz). (**A**) Spectra shown with a linear field scale. (**B**) Spectra shown with a reciprocal *g*-scale.

1.13 *g*-Strain

We know from folding studies and from structural NMR and X-ray studies that samples of proteins come with a distribution of conformations. For EPR this means that the paramagnet in each molecule has a slightly different structural surrounding and thus a slightly different *g*-value. This structural inhomogeneity or ***g-strain*** is reflected in the spectroscopy in the form of an inhomogeneous line shape. This normally results in a change from a Lorentzian to Gaussian line shape. An important consequence of this *g*-value anisotropy is that the line width, *W*, is in general, also isotropic.

Most of the time we do not have to worry about this, but particularly in the EPR spectra of the iron-sulfur clusters *g*-strain can have a big effect on the shape of the EPR spectrum and therefore on the simulation and interpretation of the EPR data. The most noticeable difference is now that the linewidth, plotted on a *g*-scale does not change when the spectra are measured at higher frequency. This effect is shown in Figure 37 for the [4Fe-4S] cluster detected in spinach-leaf ferredoxin. The line width is very similar in the range of 35 to 3.3 GHz. At 1.1 GHz a broadening is detected due to unresolved hyperfine coupling.

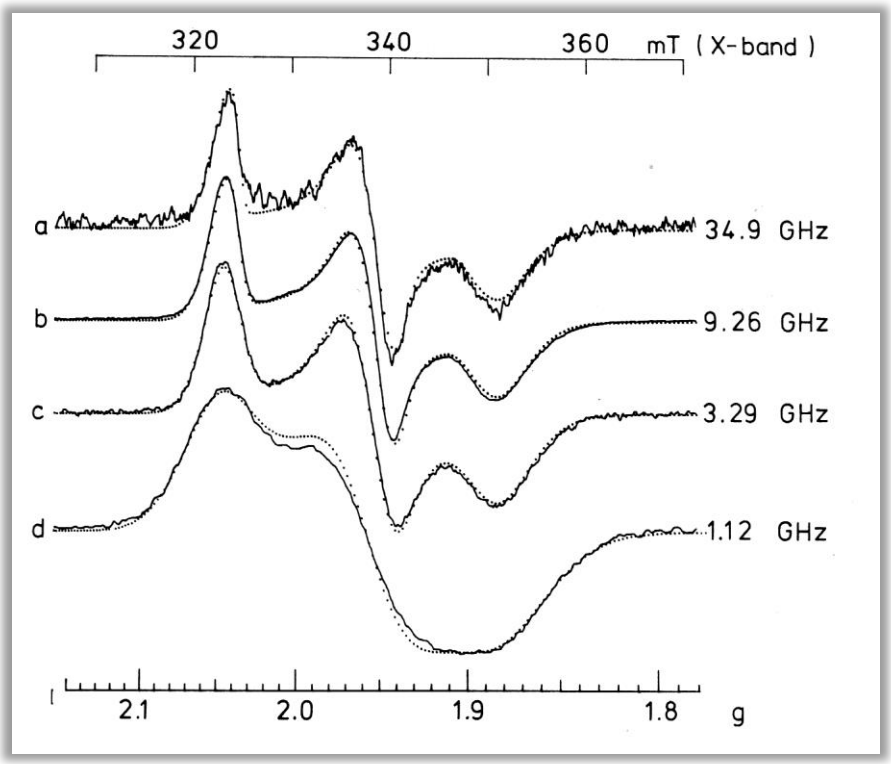

Fig. 37: Experimental and simulated spectrum of spinach-leaf ferredoxin at four microwave frequencies.

The example in Figure 36 for MCRred1-Ni(I), showed that in some cases the use of higher frequency can give additional essential information. The example in Figure 37, however, shows that this is not always the case.

1.14 ENDOR, ESEEM, and HYSCORE

In the examples we have seen up until now, the nuclear hyperfine splitting was always clearly detectable, at least in one of the peaks of the EPR signal. More often than not the hyperfine splitting is not resolved but is hidden in the EPR peaks, as in the example in Figure 37, where the spectrum contains unresolved hyperfine splitting. This interaction might be coming from a ligand or compound that is bound to the paramagnetic metal ion in the active site of an enzyme of interest. Since knowledge of this information could be important to gain more insight into the properties and function of the metal ion, techniques have been developed to detect these interactions. These are normally pulsed techniques also referred to as advanced techniques: ***E***lectron-***N***uclear ***DO***uble ***R***esonance (ENDOR), ***E***lectron ***S***pin ***E***cho ***E***nvelope ***M***odulation (ESEEM) and ***HY***perfine ***S***ublevel **COR**r***E***lation (HYSCORE) spectroscopies.

In transition metal complexes and metalloproteins, magnetic nuclei such as ^{1}H, ^{2}H, ^{13}C, ^{14}N, ^{15}N, ^{17}O, ^{31}P and ^{33}S, in the vicinity of the paramagnetic metal ion can be detected by these techniques. Not only do ENDOR and ESEEM enable one to identify the presence of a particular ligand nucleus but under favorable circumstances metal-ligand nuclei distances and angles can be obtained as well. Although both techniques give similar types of information about your enzyme, depending on the interaction parameters, the sensitivity of the two techniques can be drastically different. Sometimes only one of the techniques can be employed and there are situations where complementary results are obtained from ESEEM and Pulsed ENDOR. The sensitivity of ESEEM is highest at low hyperfine transition frequencies and decreases with increasing frequency due to the limited microwave field strength. The sensitivity of Pulsed ENDOR is approximately proportional to the hyperfine transition frequency. At zero frequency, the ENDOR sensitivity is zero. ENDOR is therefore extremely difficult at low transition frequencies whereas it has a high sensitivity for high frequencies.

Let us now consider the spin Hamiltonian relevant for these techniques. Equation 36 shows the spin Hamiltonian for the simplest system, with effective electron spin S = ½ and a single nucleus with I = ½

$$H_s = \beta_e B \bullet g_e \bullet S - \beta_n B \bullet g_n \bullet I + S \bullet A \bullet I \qquad (36)$$

Where β_e and β_n are electronic and nuclear magnetons, g and g_n are the electronic and nuclear g-tensors, and A is the anisotropic hyperfine tensor describing the interaction between the electronic and nuclear spins. In this equation, the first term is the electronic Zeeman interaction, the second is the nuclear Zeeman interaction, and the third is the hyperfine interaction.

The energies to first order are given by the expression

$$E(m_s m_I) = g_e \beta_e B m_s - g_n \beta_n B m_I + h A m_s m_I \qquad (37)$$

Figure 38 shows the energy level diagram calculated from equation 37 and illustrates the splitting of the spin states by the successively smaller interactions for a magnetic field of approximately 3300 G.

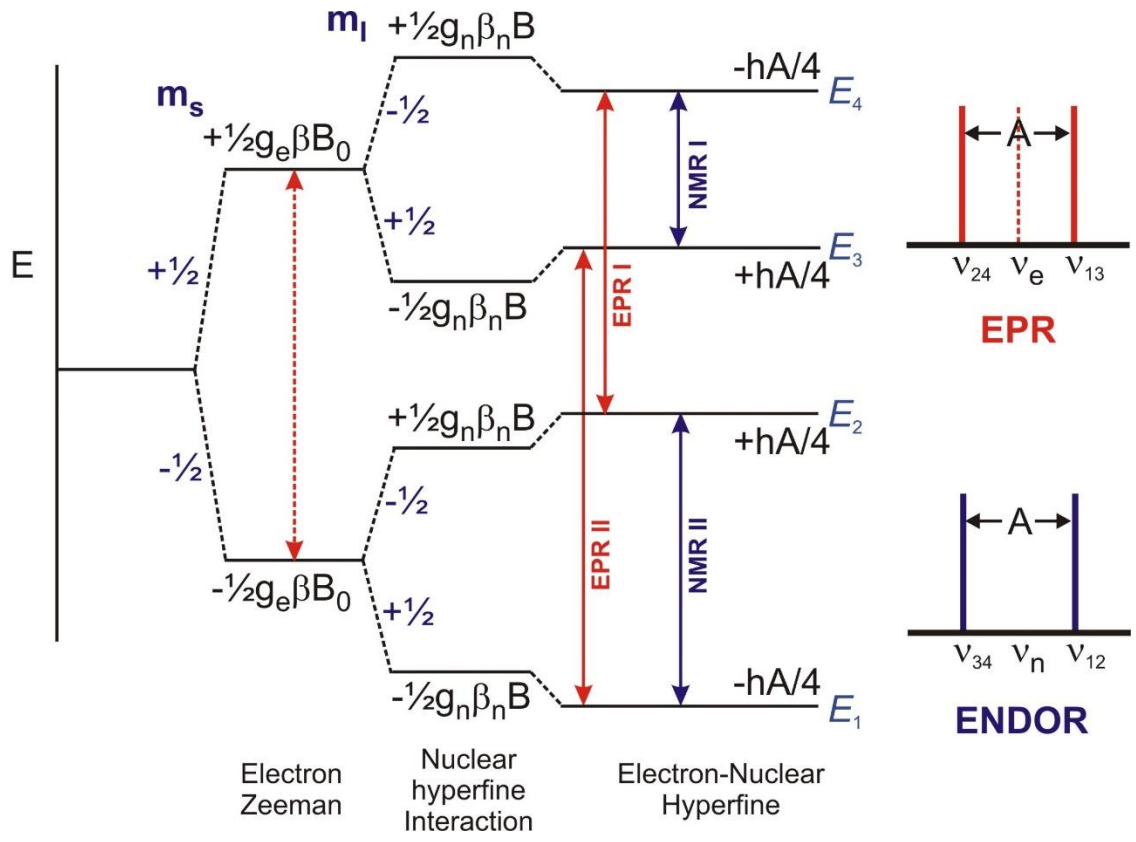

Fig. 38: Energy level diagram for an $S = ½$, $I = ½$ spin system. The g-value and hyperfine coupling are assumed to be isotropic. The red lines show the allowed EPR transitions and the stick EPR spectrum. The blue lines show the NMR (ENDOR) transitions and the stick ENDOR spectrum.

Two types of transitions are indicated in the figure. First are the usual EPR transitions occurring at frequencies ν_{13} and ν_{24} and indicated by red lines between levels E_1 and E_3 and between levels E_2 and E_4. These transitions obey the usual EPR selection rule $|\Delta m_s| = 1$, $|\Delta m_I| = 0$ where only electron spin flips but no nuclear spin flips are allowed. The second transitions, indicated by blue lines, are NMR transitions ($|\Delta m_s| = 0$, $|\Delta m_I| = 1$) and occur at the frequencies ν_{12} and ν_{34}. These frequencies are also known as the ENDOR or ESEEM frequencies. The little stick spectra on the right hand side/top show what the EPR spectrum would look like if the lines were resolved (ν_e is the position of the original, unsplit, EPR peak). The bottom stick spectrum shows what the ENDOR spectrum will look like. The splitting by the coupling constant A is indicated.

*E*lectron-*N*uclear *DO*uble *R*esonance (ENDOR) Spectroscopy

In ENDOR spectroscopy two irradiating frequencies (short microwave, MW, and radiofrequency, RF) of high power are simultaneously applied to the spin system. Electron and nuclear spin transitions are induced. This is why this is called a double resonance experiment. ENDOR can be performed in both CW and pulse mode. The ENDOR spectrometer essentially consists of a standard CW EPR spectrometer with an NMR RF source and an RF coil within the microwave cavity. This arrangement enables EPR and NMR experiments to be performed simultaneously on the sample. In CW ENDOR, the EPR signal at a given field is partially saturated by an increase of microwave power. When the radio frequency matches a nuclear frequency, in another word, when a nuclear transition is induced,

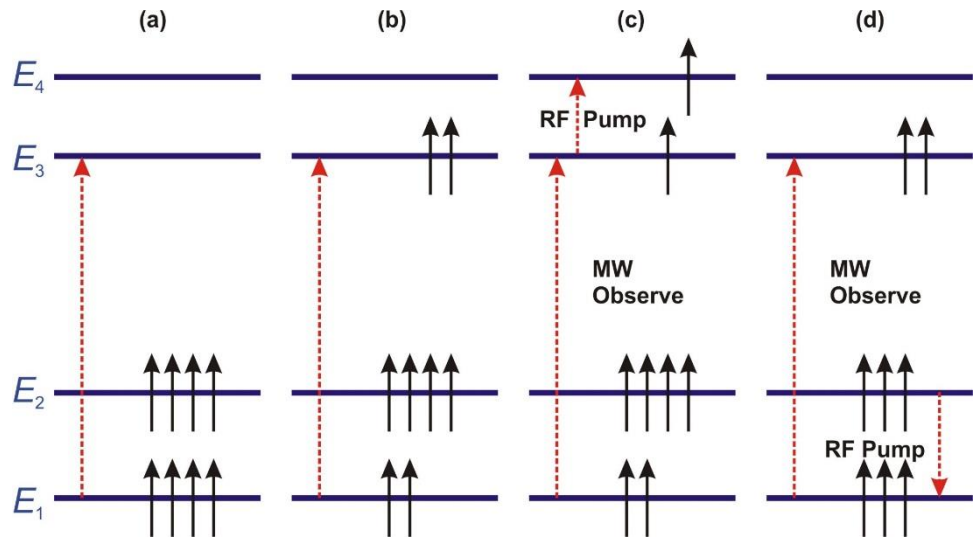

Fig. 39: Energy level diagram for the two-spin S = ½, I = ½ (shown in Fig. 38). Each panel illustrates the effect of the applied MW and RF powers. (**a**) Application of low MW power to induce transition EPR II, (**b**) saturating MW power, (**c**) saturating RF power to induce transition NMR I, and (**d**) saturating RF power to induce transition NMR II.

the population of the partially saturated EPR transition will be changed and the recovery of this signal will be realized by detecting net microwave absorption.

The energy levels for an $S = ½$, $I = ½$ spin system are shown again in Figure 39. Using low MW powers, resonance absorption occurs as, for example, the EPR II transition frequency $E_1 \leftrightarrow E_3$ is induced but rapid relaxation ensures that the excited spins return quickly to the ground state leading to an unsaturated EPR signal (Fig. 39a). Using higher MW power, the $E_1 \leftrightarrow E_3$ transition becomes saturated such that the spin population in both levels equalizes (Fig. 39b), a situation that should be avoided in regular CW EPR spectroscopy since the signal intensity will decrease to almost zero (see Chapter 2). To restore the EPR signal intensity, a population difference between the levels E_1 and E_3 needs to be created. There are two mechanisms to do this. One way is by 'pumping' the RF transition $E_3 \leftrightarrow E_4$ (NMR I) using a saturating RF field (Fig. 39c). An enhancement of the EPR absorption is detected if the irradiated RF frequency is resonant with this transition. This enhancement represents the first ENDOR signal. In an alternative way, the RF transition $E_1 \leftrightarrow E_2$ (NMR II) can be pumped (Fig. 39d). This also creates an enhancement and represents the second ENDOR resonance line.

The resonance lines are inherently narrower in ENDOR than in EPR spectroscopy and the chief use of ENDOR in the metalloprotein investigations is that it enables weaker hyperfine interactions to be resolved. In addition, nuclei can be unambiguously identified by their ***Larmor frequency***. The principle disadvantage of this technique is the greatly reduced sensitivity compared with EPR. This means that samples need to be more than 10 fold concentrated to yield acceptable ENDOR spectra.

Figure 41 shows the data obtained for a paramagnetic species detected in the enzyme (*E*)-4-hydroxy-3-methylbut-2-enyl diphosphate synthase (IspG). IspG converts 2-*C*-methyl-D-erythritol-2,4-cyclodiphosphate (MEcPP) into (*E*)-4-hydroxy-3-methyl-but-2-enyl diphosphate (HMBPP) in the penultimate step of the MEP pathway for isoprene biosynthesis. MEcPP is a cyclic compound and the reaction involves the opening of the ring and removal of the C3 hydroxyl group consuming the total of two electrons (Fig. 40).

Fig. 40: Reaction catalyzed by IspG

The enzyme contains a single [4Fe-4S] cluster in its active site. In kinetic studies where the enzyme was incubated with dithionite and the substrate MEcPP a paramagnetic species was detected that displayed a rhombic EPR signal with g_{xyz} = 2.000, 2.019, and 2.087 (Fig. 41, panel A. See also the freeze-quench section in chapter 2). The spread in *g*-values would argue against a radical-type species. In addition, labeling with ^{57}Fe caused extensive broadening of the EPR signal, indicating it is Fe-based and most likely represents a new form of the Fe-S cluster. Note that this species does not have any resemblance with the standard type iron-sulfur cluster signals shown in Figure 30. It was proposed that the substrate MEcPP binds to the cluster during the reaction mechanism, most likely via the –OH group that is removed in the reaction (Fig. 41, panel B). Figure 41, panel C, shows the ^{31}P-ENDOR measurements for this signal. At six different field positions an ENDOR spectrum was obtained. These

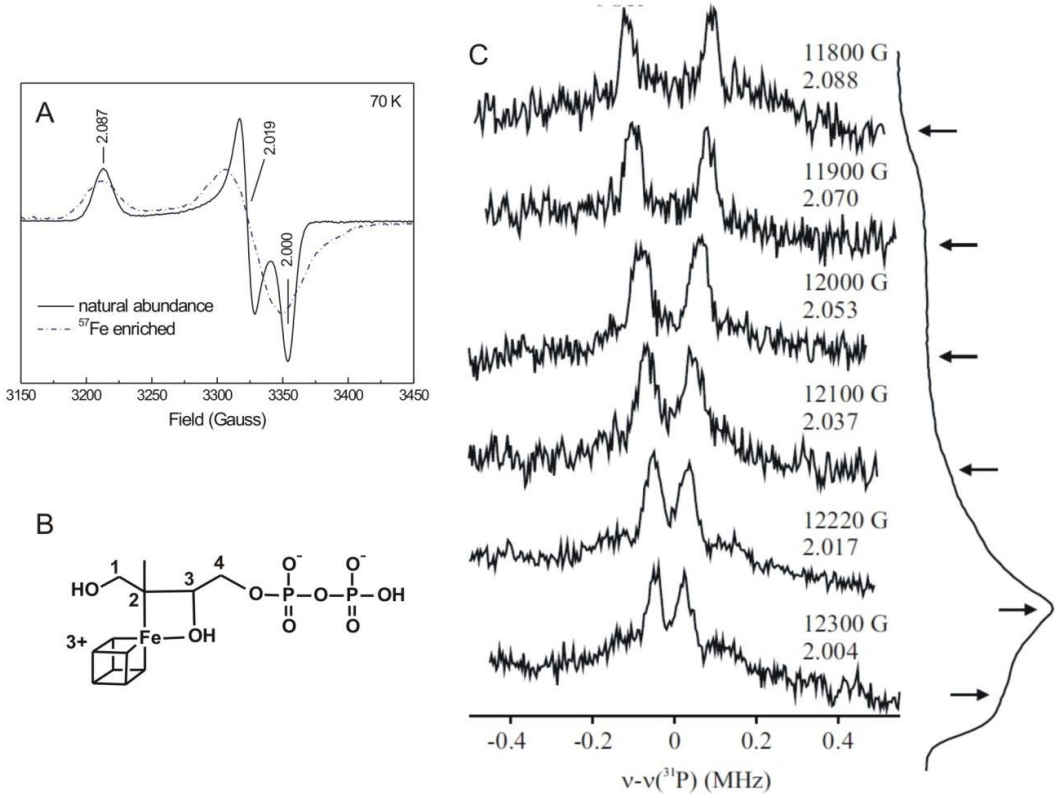

Fig. 41: (**A**) EPR spectrum obtained for IspG upon incubation with the substrate MEcPP and the reductant dithionite. (**B**) Proposed structure for the reaction intermediate. The [4Fe-4S] cluster is represented by the cube. (**C**) ^{13}P-ENDOR spectra. **35 GHz pulsed ^{31}P ENDOR spectra at 2 K.** Spectra were collected at the fields and *g*-values indicated, and are shown alongside the respective pulse-echo detected EPR spectra. ENDOR spectra are normalized to a fixed intensity for clarity.

are indicated on the absorption EPR signal (Under the saturation conditions used in ENDOR not the first derivative, but the 'regular' absorption-type signal is measured.) Note that the ENDOR was obtained at Q-band frequency (35 GHz) and therefore the field values do not match with those of panel A. The *g*-values are included for easy comparison. The EPR species showed a weak ^{31}P coupling which was detectable over the whole EPR envelope. From the coupling constant a distance of 5-6 Å could be estimated which is in line with binding of the substrate to the enzyme in close proximity of the active-site cluster. In a separate experiment (see below) using ^{17}O labeled MEcPP, a very short distance between the cluster and the ^{17}O atom was found.

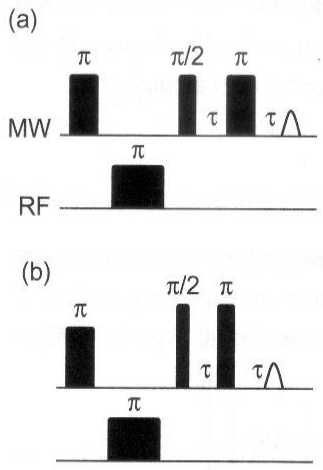

Fig. 42: The pulse sequences for echo detected Davies ENDOR using (a) selective, and (b) non-selective pulses.

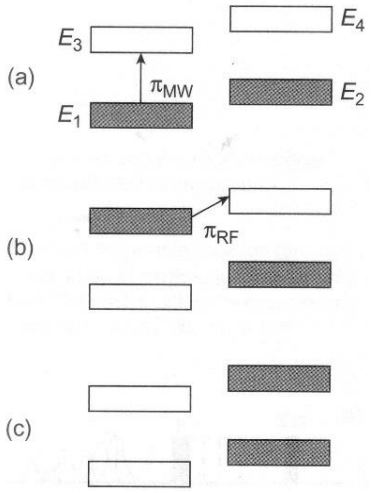

Fig. 43: (a) The π_{MW} pulse selectively inverts electron spin populations, (b) the π_{RF} pulse selectively inverts nuclear spin populations resulting in electron spin saturation (c).

CW ENDOR spectroscopy is an extremely powerful technique, however, a significant disadvantage is the requirement to meet saturation conditions for both the EPR and NMR transitions, which demands a critical balance between the rates of induced transitions and relaxation. Even under optimal conditions, the ENDOR signal accounts for only a small percentage of the change in EPR signal intensity. These shortcomings can be overcome using pulsed ENDOR methods. Typical pulse sequences are shown in Figure 42. The Davies ENDOR sequence (π_{MW}-π_{RF}-$\pi/2_{MW}$-τ-π_{MW}-τ-echo) is the pulsed equivalent of a CW ENDOR experiment. The effect of this sequence on the occupation of the energy levels for the two-spin system ($S = ½$, $I = ½$) is shown in Figure 43. The first selective π_{MW} pulse inverts the electron spin populations in the E_1 and E_3 manifolds (Fig. 43a) inducing the transition EPR II. This is followed by a π_{RF} pulse that inverts the nuclear spin populations upon resonance with an NMR transition (NMR I, Fig. 43b). The remaining sequence consists of either the selective (Fig. 42a) or non-selective (Fig. 42b) electron-spin echo detection pulses.

*E*lectron Spin *E*cho *E*nvelope *M*odulation (ESEEM) and *HY*perfine *S*ub-level *COR*r*E*lation (2D-HYSCORE) Spectroscopy

ENDOR spectroscopy experiments are performed directly in the frequency domain. ESEEM experiments are time-domain experiments (Fig. 44a/b). ESEEM is complementary to ENDOR and is particularly powerful for detecting low frequency coupling (<5 MHz). With ESEEM the NMR frequencies are observed indirectly through observation of the mixing of allowed and (formally) forbidden EPR transitions as modulations superimposed on a time-decaying spin-echo. Echo envelope modulation occurs when state mixing of hyperfine levels occurs. Fourier transformation of the modulated time trace results in spectra in the frequency domain containing the nuclear frequencies.

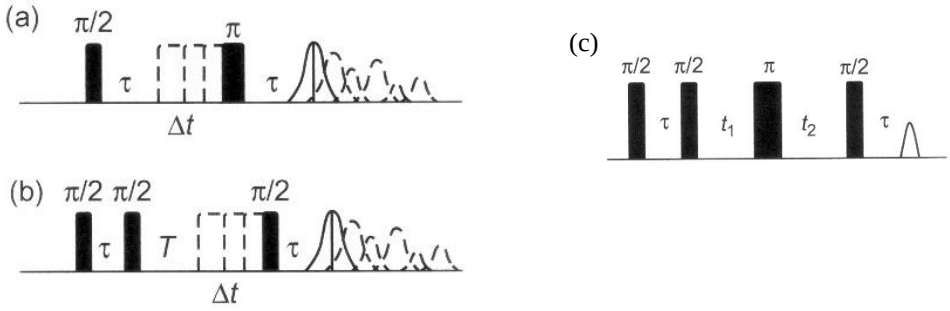

Fig. 44: (a) The two-pulse ESEEM sequence, in which the time interval τ is incremented by the dwell time Δt; a primary echo is observed at time τ after the second pulse. (b) The three-pulse ESEEM sequence, in which τ is kept constant and the time interval *T* is incremented. (c) The HYSCORE sequence, which has an additional π-pulse inserted into the three-pulse ESEEM experiment.

An extension of this technique is ***HY***perfine ***S***ub-level ***COR***r***E***lation (2D-HYSCORE). This technique is essentially a two dimensional ESEEM experiment in which correlation is transferred from one electron spin manifold to another. HYSCORE allows one to take a complicated ESEEM spectrum and extend the data into a second dimension. The HYSCORE pulse sequence is a four-pulse MW sequence in which an additional mixing π pulse is inserted between the second and third π/2 pulse of the three-pulse ESEEM Experiment (Fig. 44c). The two inter-pulse delays, t_1 and t_2, are varied independently to produce a two-dimensional (2D) time delay array. The nuclear coherence generated by the first two π/2 pulses undergoes free evolution during time t_1 with frequency ω_{12} (ω_{34}). The mixing π pulse then transfers populations in one m_s manifold to the other and similarly transfers the nuclear coherence between manifolds so that it evolves with frequency ω_{34} (ω_{12}) during time t_2. The modulated time decay data is subsequently Fourier transformed in both dimensions (i.e. t_1 and t_2) to produce a 2D frequency-domain spectrum (with axes ν_1 and ν_2). The nuclear frequencies from the different m_s manifolds are correlated and appear as cross-peaks at the frequencies (ν_1, ν_2), (ν_2, ν_1), and (ν_1, $-\nu_2$), (ν_2, $-\nu_1$) in the (+,+) and (+,-) quadrants of the 2D spectrum, respectively. As strong cross peaks can only be observed between NMR frequencies of the same nucleus, HYSCORE spectra can be significantly simplified compared to three-pulse ESEEM.

Another advantage of HYSCORE spectroscopy is that the frequencies from weakly-coupled nuclei ($|a_{iso}| < 2|\nu_L|$) appear as cross-peaks in the (+, +) quadrant, whereas strongly-coupled nuclei ($|a_{iso}| > 2|\nu_L|$) are observed in the (+,–) quadrant (Fig. 45a). This facilitates spectral interpretation for systems containing many interacting nuclei such as metalloenzymes or proteins. For disordered systems with

broad ESEEM features, the correlation peaks broaden into ridges, as illustrated for the two-spin system (S = ½, I = ½) with an axial hyperfine tensor (Fig. 45 b). The anisotropy of the dipolar hyperfine interaction, T, can be determined from the maximum curvature of the ridges away from the anti-diagonal, labelled ω_{max}, and the magnitude of a_{iso} can be found from the ridge end points or from simulation.

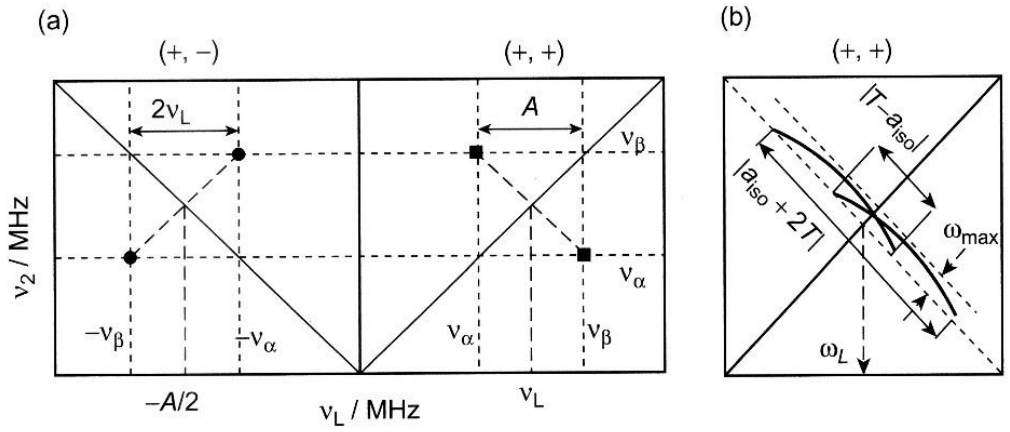

Fig. 45: (a) Two-dimensional HYSCORE spectrum where full squares ▪ represent cross peaks from weakly coupled nuclei in the (+,+) quadrant, and full circles • represent cross peaks from strongly coupled nuclei in the (+,–) quadrant. ν_L is the Larmor frequency for the nucleus of interest, A is the hyperfine coupling, ν_α (= ω_{12}) and ν_β (= ω_{34}); (b) (+,+) quadrant for the powder HYSCORE pattern for an S = ½, I = ½ spin system with an axial hyperfine tensor.

Peaks appearing in the upper right and lower left quadrants of the 2D spectra typically arise from nuclei in which the hyperfine coupling is less than the Larmor frequency. They appear at the Larmor frequency, separated by the hyperfine coupling. Peaks from nuclei in which the hyperfine interaction is greater than the Larmor frequency appear in the upper left and lower right quadrants of the spectra. Even with the complexity of the spectra, HYSCORE on systems with multiple nuclei can make ESEEM spectra that would be difficult or impossible to interpret much more manageable.

As an example, let us revisit the IspG enzyme. Figure 46, shows the data obtained using either ^{13}C-MECPP or ^{17}O-labelled HMBPP-epoxide (a substrate analog). The top panel (Panel A) shows the peaks observable due to natural abundance ^{13}C and ^{14}N in the protein sample. In an attempt to study how MEcPP is bound to the cluster, different positions in the MEcPP structure were labeled with either ^{13}C or ^{17}O. Figure 46, panel B, shows the data obtained when both the C3 and the C2 positions are labeled. Now additional peaks show up in the spectrum. The specific assignment is based on a whole set of labeling studies not all shown here. The last panel (panel C), shows the additional peaks observed when the epoxy oxygen of the HMBPP-epoxide is labeled with ^{17}O. The observed interactions are indicative for a short Fe-O bond. The different labeling studies and the obtained data resulted in the binding model shown in Figure 41B.

ENDOR, HYSCORE, and high-frequency EPR are less common techniques and are only available in selected laboratories that are specialized in doing these types of measurements. The technique available at Auburn University is CW X-band EPR spectroscopy. The next chapters will provide information on how to run this EPR spectrometer and how to find the correct instrumental settings

to get your EPR spectrum. The other techniques are available through collaborations with other laboratories. Through these it will be possible to do Q-band and W-band experiments and to obtain ENDOR or HYSCORE data on a particular sample.

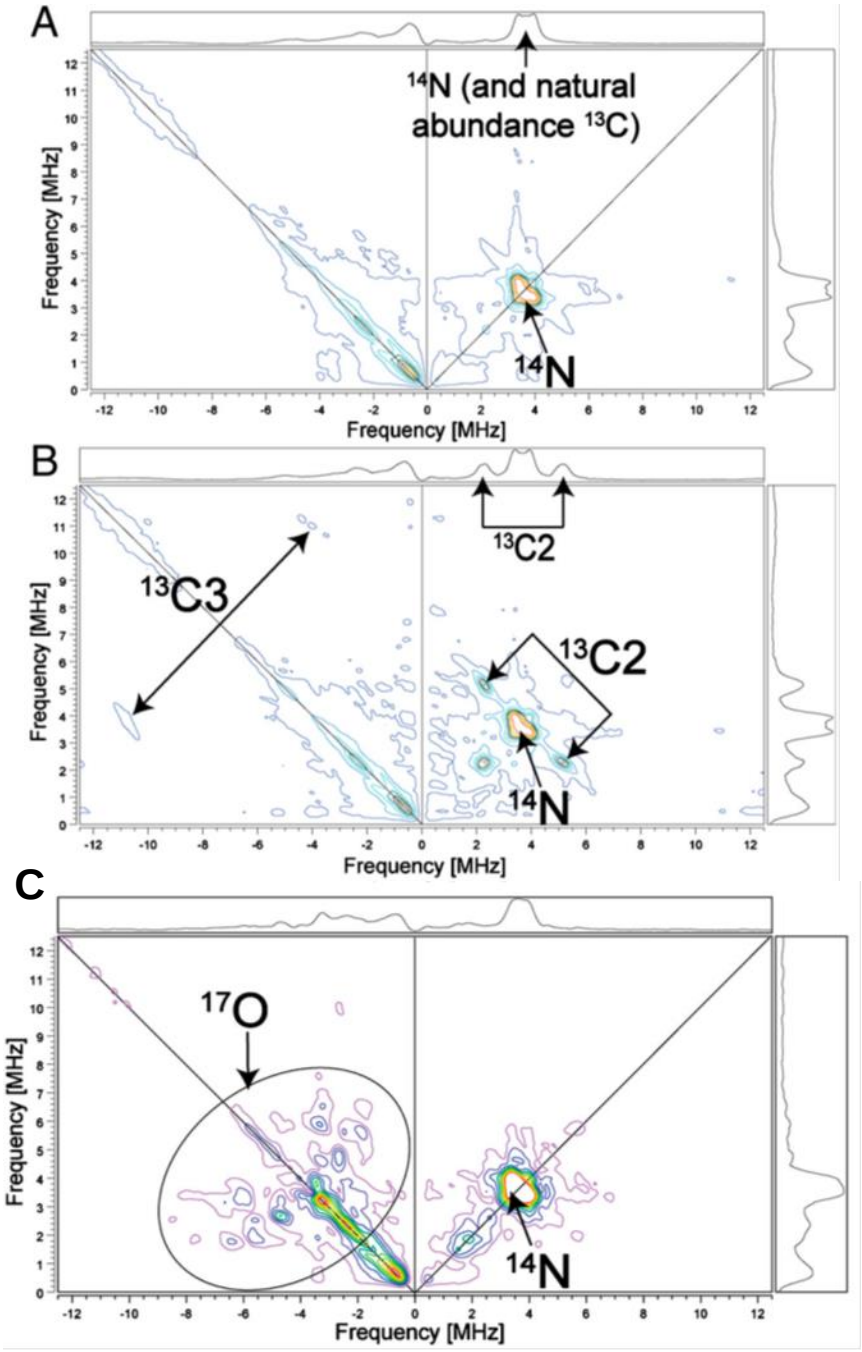

Fig. 46: HYSCORE spectra at g_2 (g = 2.019) of the signal shown in Figure 41A. (**A**) IspG incubated with unlabeled MEcPP. (**B**) As A, but with MEcPP enriched with (~30%) ^{13}C at C2 and/or C3. (**C**) IspG incubated with ½ 2;3-^{17}O-HMBPP epoxide (as substrate analog). Frequency = 9.64 GHz, spectra were collected at 18 K with τ ¼ 136 ns. (Adapted from Wang et al. PNAS 107(2010) 11189.)

1.15 Selected Reading

Text Books

1. ***Biomolecular EPR Spectroscopy*** **(2009) Hagen, W.R., CRC Press, Taylor & Francis Group, Boca Raton**

2. *Electron Paramagnetic Resonance: Elementary Theory and Practical Applications* (1994) Weil, J.A., Wertz, J.E. and Bolton, J.R., McGraw-Hill, John Wiley & Co, New York

3. *Principles and Applications of ESR spectroscopy* (2011) Lund, A., Shiotani, M., Shimida, S., Springer, New York

4. ***Electron Paramagnetic Resonance*** **(2016) Chechik, V., Carter, E., Murphy, D., Oxford Chemistry Primers, Oxford University Press, Oxford, UK.**

5. *Advanced EPR: Applications in Biology and Biochemistry* (1989) Hoff, A.J. (Ed.), Elsevier, Amsterdam

6. *Principles of Pulse Electron Paramagnetic Resonance* (2001) Schweiger, A., Jeschke, G., Oxford University Press, Oxford

7. *Quantitative EPR* (2010) Eaton, G.R., Eaton, S.S., Barr, D.P., Weber, R.T., Springer, New York

Introductory Articles

8. *Electron Paramagnetic Resonance* (1967) Palmer G., Meth. Enzymol., 10, 594-609

9. *Transition Metal Electron Paramagnetic Resonance Related to Proteins* (1978) Fee, J.A., Meth. Enzymol. 49, 512-528

10. *Electron Paramagnetic Resonance* (1993) Pilbrow, J.R., Hanson, G.R., Meth. Enzymol. 227, 330-353

11. *Electron Paramagnetic Resonance Spectroscopy* (1995) Brudvig, G.W., Meth. Enzymol. 246, 536-554

12. *Protein Structure and Mechanism Studied by Electron Nuclear Double Resonance Spectroscopy* (1995) DeRose, V.J., Hoffman, B.M., Meth. Enzymol. 246, 554-589

13. ***Electron Paramagnetic Resonance of Metalloproteins*** **(2000) Palmer, G., In: Physical Methods in Bioinorganic Chemistry, Que, L., Jr. (Ed.) University Science Books, Sausalito, pp. 121-185**

14. ***ESEEM and ENDOR Spectroscopy*** **(2000) Chasteen, N.D., Snetsinger, P.A., In: Physical Methods in Bioinorganic Chemistry, Que, L., Jr. (Ed.) University Science Books, Sausalito , pp. 187-231**

15. *EPR Spectroscopy as a Probe of Metal Centres in Biological Systems* (2006) Hagen, W.R., Dalton Trans. 4415–4434

Iron and Iron-Sulfur

16. *EPR Spectroscopy of Components of the Mitochondrial Electron-transfer system* (1978) Beinert, H., *Meth. Enzymol.*, 54, 133-150 (1978)

17. *Integer-spin Electron Paramagnetic Resonance of Iron Proteins* (1989) Hendrich, M.P., Debrunner, P.G., *Biophys. J.*, 56, 489-506

18. *EPR Spectroscopy of Iron-Sulfur Proteins* (1992) **Hagen, W.R., *Adv. Inorg. Chem.* 38, 164-222**

19. *Electron Paramagnetic Resonance Spectroscopy of Iron Complexes and Iron-Containing Proteins*, Cammack, R., Cooper, C.E. (1993) *Meth. Enzymol.*, 227, 353-384

20. *Application of EPR Spectroscopy to the Structural and Functional Study of Iron-sulfur Proteins*, Guigliarelli, B., Bertrand, P. (1999) *Adv. Inorg. Chem.*, 47, 421-497

21. Advanced paramagnetic resonance spectroscopies of iron–sulfur proteins: Electron nuclear double resonance (ENDOR) and electron spin echo envelope modulation (ESEEM), Cutsail III, G.E., Telser, J., Hoffman, B.M., Biochim. Biophys. Acta 1853 (2015) 1370–1394

B_{12}

22. *EPR of B_{12}-dependent Enzyme Reactions and Related Systems* (1982) Pilbrow, J.R., In: B_{12}, volume 1, Dolphin, D. (Ed.) John Wiley & Sons, New York, pp. 431-462

23. *EPR Spectroscopy of B_{12}-dependent Enzymes* (1999) Gerfen, G.J., In: Chemistry and Biochemistry of B_{12}, Banerjee R. (Ed.) John Wiley & Sons, New York, pp. 165-195

24. The positions of radical intermediates in the active sites of adenosylcobalamin-dependent enzymes, Reed, G.H., Mansoorabadi, S.O. (2003) *Curr. Opin. Struct. Biol.* 13, 716-721.

Other

25. *The Role of Microwave Frequency in EPR Spectroscopy of Copper Complexes* (1982) Hyde, J.S., Froncisz, W., *Ann. Rev. Biophys. Bioeng.* 11, 391-417

26. *Characterization and Reactivity of Surface-localized Inorganic Radicals and Radical Ions* (2010) Chiesa, M., Giamello, E., Che, M., Chem. Rev. 110, 1320-1347

2. Practical Aspects

2.1 The EPR Spectrometer

EPR spectrometers come in different sizes and models, dependent on the year they were produced and on the frequency and field they operate. The first EPR spectrometers functioned at very low frequencies. As with NMR spectroscopy, over the years the frequency was increased to improve resolution and to obtain higher sensitivity. Unlike NMR, however, an optimum sensitivity in EPR is reached in the 8-12 GHz range. It is not possible to produce frequency sources in this microwave frequency region that cover a wide range of frequencies in a continuous mode. Microwave frequencies can only be produced at particular small frequency windows called bands. The names of the bands originate in military communication partially dating back to World War II. The so-called X-band with a frequency window around 9.6 GHz, is right in the middle of the 8-12 GHz range. This is the reason that X-band EPR spectroscopy is the most common EPR technique and is therefore also the one available in our Department.

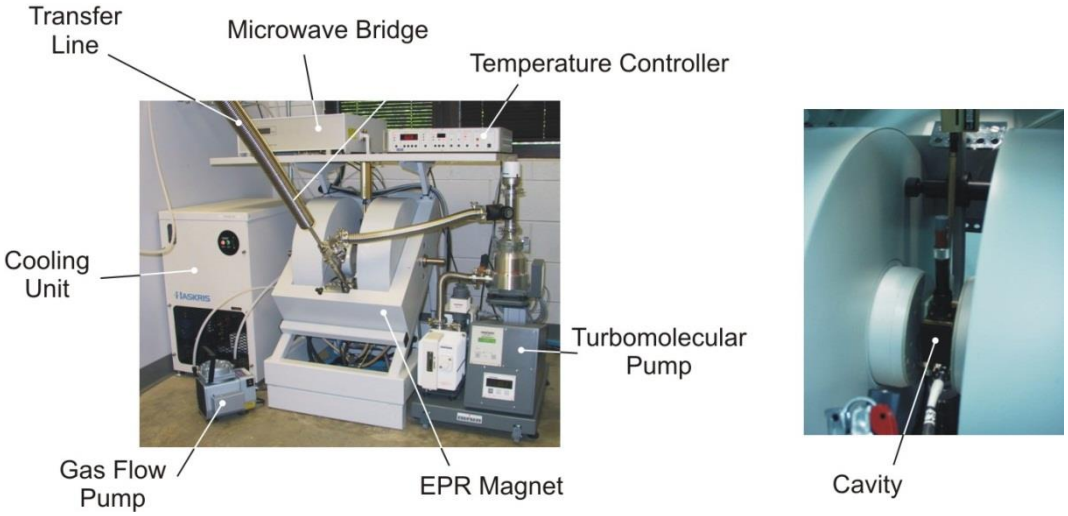

Fig. 1: Different parts of the EPR spectrometer in the Department of Chemistry and Biochemistry.

Important parts of the spectrometer are the ***microwave bridge*** and the ***EPR magnet***. The ***microwave bridge*** is where the X-band waves are generated. These are directed through a wave guide towards the ***cavity*** or ***resonator*** where the sample under study is situated. The ***cavity*** and the sample are subjected to a magnetic field during the EPR measurements generated by the ***EPR magnet***. In this case the coils of the magnet are water cooled, with the cold water coming from the ***cooling unit***. Samples can be measured at room temperature, but in most cases lower temperatures are needed, sometimes as low as 4.2 K. To be able to do that, the spectrometer can be fitted with a cryostat. Liquid and gaseous helium will flow through this system in response to the working of the ***gas flow pump***. The liquid helium comes from a large storage Dewar via a ***transfer line***. The cold helium is protected from the 'hot' environment by a high vacuum generated by the ***turbomolecular pump***.

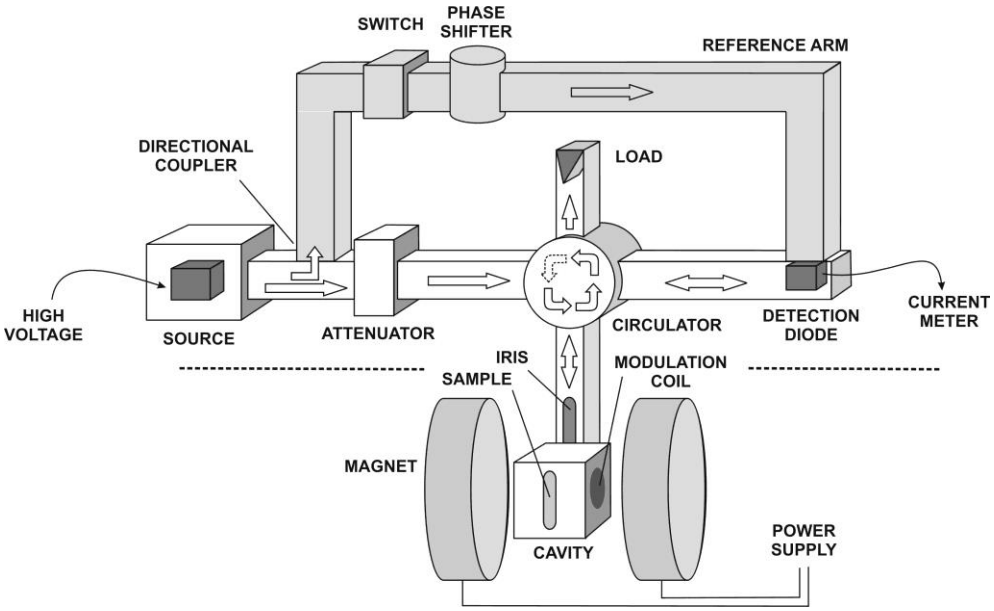

Fig. 2: Flow of the microwaves in the EPR spectrometer. (Adapted from Hagen, W.R. (2009) *Biomolecular EPR Spectroscopy.*)

Figure 2, shows the flow of the microwaves in the EPR spectrometer. The parts above the dashed lines are all hidden inside the Microwave Bridge box. On the left is a monochromatic ***source of microwaves*** of constant output (200 mW) and slightly (10%) tunable frequency. The produced radiation is transferred by means of a rectangular, hollow wave guide to an attenuator where the 200 mW can be reduced by a factor between 1 and 10^6. The output of the attenuator is transferred with a waveguide to a circulator that forces the wave into the resonator/cavity. The entrance of the cavity is marked by the ***iris***, a device to tune the amount of radiation reflected back out of the cavity. The reflected radiation returns to the circulator and is directed to the ***diode*** for the detection of microwave intensity. Any remaining radiation that reflects back from the detector is forced by the circulator into the upward waveguide that ends in a wedge to convert the radiation into heat. A small amount of the 200 mW source output is directed through the ***reference arm*** directly to the detector to produce a constant working current. The reference arm contains a port that can be closed and a device to shift the phase of the wave. These parts are important for the tuning of the cavity.

2.2 Tuning and Measurement Parameters

More detailed, step-by-step, instructions on how to operate the EPR spectrometer can be found in the separate manuals that each describe how to obtain spectra at *room temperature*, with a *liquid nitrogen finger Dewar*, or with the *liquid nitrogen* or *liquid helium flow system*. Here more background information is provided that explain the idiosyncrasies related to this measuring technique that the reader needs to understand to be able to tune the spectrometer and obtain useful data.

Most EPR spectrometers are reflection spectrometers. This means that they measure the changes (due to spectroscopic transitions) in the amount of radiation reflected back from the microwave cavity containing the sample. The detector should only detect the microwave radiation coming back from the cavity.

Simply put, a microwave cavity is a metal box with a rectangular or cylindrical shape which resonates with microwaves much as an organ pipe resonates with sound waves. The cavity or resonator is designed to set up a pattern of standing microwaves in its interior (Fig. 3). Standing electromagnetic waves have their electric and magnetic field components exactly out of phase - where the magnetic field is maximum, the electric field is minimum and vice versa. The place where the sample is situated has a minimum electric field and maximum magnetic field.

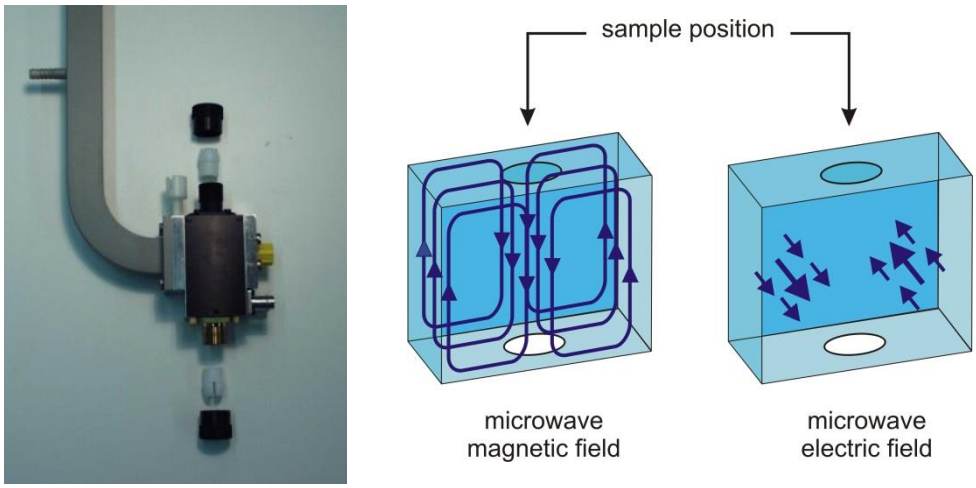

Fig. 3: Detail of the waveguide and the cavity. The diagrams on the right show the directions of the microwave magnetic field and the microwave electric field when the cavity is critically coupled.

Resonance means that the cavity stores the microwave energy; therefore, at the resonance frequency of the cavity, no microwaves will be reflected back, but will remain inside the cavity. Energy can be lost to the side walls of the cavity because the microwaves generate electrical currents in the side walls of the cavity which in turn generates heat.

Cavities are characterized by their Q or quality factor, which indicates how efficiently the cavity stores microwave energy. The *Q* factor is defined as:

$$Q = (\nu_{res})/(\Delta\nu) \quad (1)$$

where ν_{res} is the resonant frequency of the cavity and $\Delta\nu$ is the width at half height of the resonance.

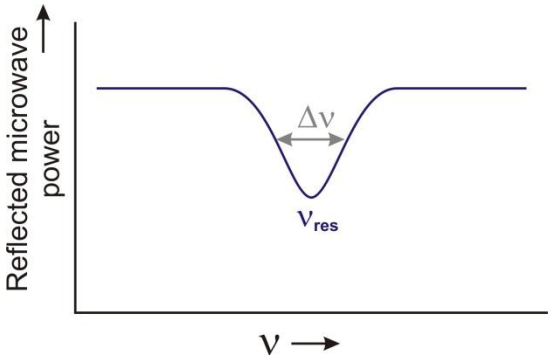

Fig. 4: Plot of the reflected microwave power vs. the frequency produced by the microwave source. The 'dip' is the result of the loss of reflected waves at the resonance frequency of the cavity.

In order for the microwaves to enter the cavity one of its end walls must have an opening: the iris. The size of the iris controls the amount of microwaves which will be reflected back from the cavity and how much will enter the cavity. Just before the iris is a small metal plate (attached to the iris screw). Moving this plate up or down changes the amount of coupling. Only for one unique position is the cavity critically coupled: all powers enter the cavity, and no radiation is reflected out.

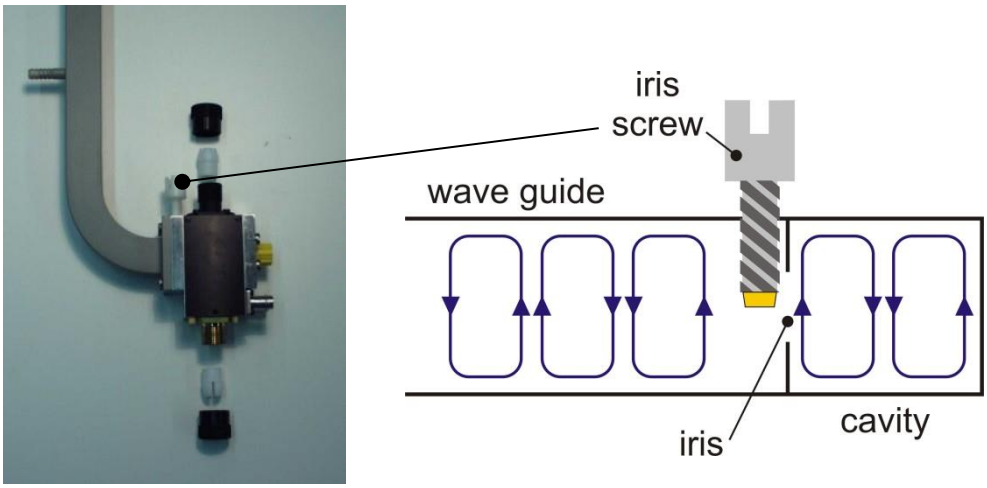

Fig. 5: Detail of the waveguide and the Cavity. The diagrams on the right show the positions of the iris and the iris screw. Turning the iris screw causes the iris to become larger and smaller. Only at one position is the cavity critically coupled. This position will be different, however, with different samples and different temperatures.

The actual EPR signal is the result of the EPR sample absorbing the microwave energy. At the beginning of a measurement, the system is tuned resulting in the cavity being critically coupled. During the measurement, when the sample absorbs the microwave energy, the Q is lowered because of the increased losses and the coupling changes. The cavity is therefore no longer critically coupled and microwaves will be reflected back to the bridge, resulting in an EPR signal.

Tuning the Microwave Cavity and Bridge

Figure 6, shows what the computer screen will look like when you are in the process of tuning the bridge. The window with the yellow curve on the black background is a display of the microwave power reflected from the cavity and the reference arm power as a function of the microwave frequency. The dip corresponds to the microwave power absorbed by the cavity and thus is not reflected back to the detector diode. By centering the dip on the display monitor, using the frequency slider, the microwave source is set to oscillate at the same frequency as the cavity resonant frequency.

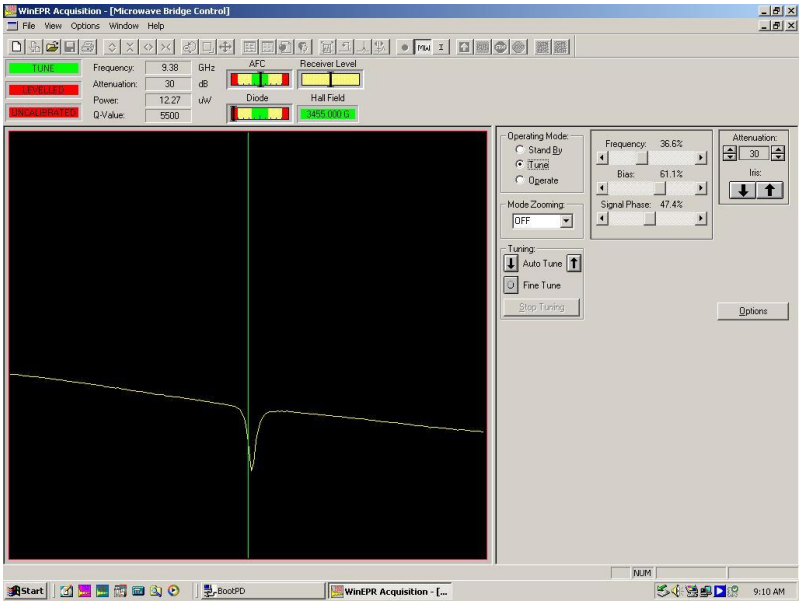

Fig. 6: Screen shot of the EPR computer during the tuning

Additional steps will be needed and include the adjustment of the signal reference phase. For quantitative signal intensity measurements as well as optimal sensitivity, the diode should operate in the linear region. The best results are attained with a detector current of approximately 200 microamperes. To insure that the detector operates at that level, the reference arm supplies the detector with some extra microwave power or “bias”. Some of the source power is tapped off into the reference arm, where a second attenuator controls the power level (and consequently the diode current) for optimal performance. There is also a phase shifter to insure that the reference arm microwaves are in phase with the reflected signal microwaves when the two signals combine at the detector diode. On the display this will result in the dip looking symmetric and having maximal depth.

For the critical coupling of the cavity, the power is increased step wise and the iris position is adjusted to keep the diode meter in the center. The size of the iris controls the amount of microwaves which will be reflected back from the cavity and how much will enter the cavity. The iris accomplishes this

by carefully matching or transforming the impedances (the resistance to the waves) of the cavity and the waveguide. Turning the iris adjusts the "matching". This adjustment can be visualized by noting that as the screw moves up and down, it effectively changes the size of the iris. When the iris screw properly matches the cavity impedance(also called critical coupling), no microwaves are reflected back from the cavity.

Microwave Bridge Parameters

Most of the parameters are just important for getting a signal somewhere in the middle of your computer screen during the measurement. The ***center field*** and ***sweep width*** determine what region of the field is measured. Our magnet covers the field region from 100 Gauss all the way up to 6000 Gauss. Ideally, you chose the center field value right in the middle of your EPR signal and the sweep width as wide as the width of the signal. These values will be different for each type of sample and will have to be determined for each new type of sample you run.

Another parameters related to the display of the spectrum is the ***gain***. The gain is adjusted to give the desired size of display and where possible should be increased to use the full range of the digitizer. The receiver gain must be high enough to show all details in the spectrum. Figure 7 shows the results of insufficient or excessive receiver gain. If the receiver gain is too low the effect of digitization will be evident in the spectrum (Fig. 7b), whereas at high gain the signals will be clipped due to an overload in the signal channel (Fig. 7c).

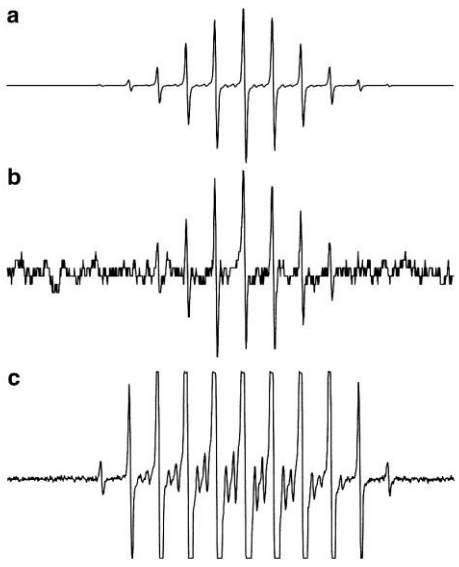

Fig. 7: Effect of using gain setting that are either (**a**) optimal, (**b**) too low, or (**c**) too high on an EPR spectrum.

Some of the other parameters, however, need a better understanding since the wrong setting might result in deformation and/or complete loss of the signal. Several of these are related to how the EPR signal is detected. The EPR spectrometer makes use of phase sensitive detection. This enhances the sensitivity of the spectrometer significantly and diminishes the noise from the detection diode and

baseline instabilities due to the drift in DC electronics. This is achieved by modulating the magnetic field at the site of the sample. The field is modulated (varied) sinusoidally at a set modulation frequency. If there is an EPR signal, the field modulation quickly sweeps through part of the signal and the microwaves reflected from the cavity are amplitude modulated at the same frequency (Fig. 8). Only the amplitude modulated signals are detected. Any signals which do not fulfill these requirements (i.e. noise and electrical interference) are suppressed. For an EPR signal which is approximately linear over an interval as wide as the modulation amplitude, the EPR signal is transformed into a sine wave with an amplitude proportional to the slope of the signal. As a result the ***first derivative*** of the signal is measured.

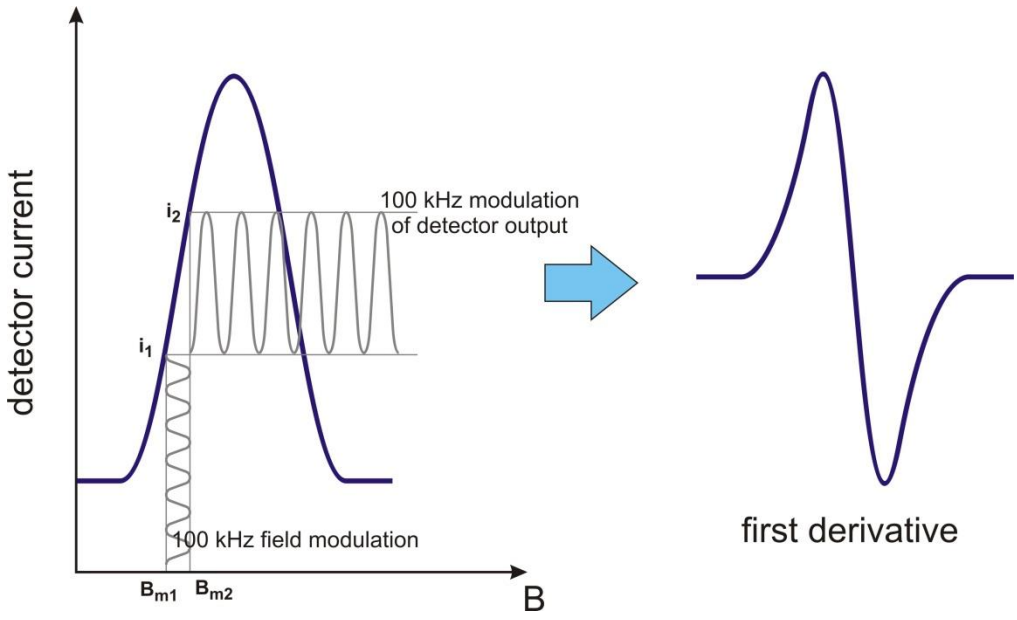

Fig. 8: Schematic representation of phase sensitive detection. As the main field is scanned slowly through the EPR line, a small additional oscillating magnetic field, B_m, is applied in the same direction as the main field B. B_m is commonly at 100 kHz. As B_m increases from the value B_{m1} to B_{m2}, the crystal detector output increases from i_1 to i_2. If the magnitude of B_m is small relative to line width, the detector current oscillating at 100 kHz has a peak-to-peak value that approximates the slope of the absorption curve. Consequently, the output of the 100 kHz phase-sensitive detector is the derivative of the absorption curve. (Adapted from Eaton, Eaton, Barr and Weber, 2010.)

There are two parameters associated with the phase sensitive detection: ***modulation amplitude***, and ***modulation frequency***. These parameters have to be chosen wisely. With more magnetic field modulation, the intensity of the detected EPR signals increases; however, if the modulation amplitude is too large (larger than the linewidths of the EPR signal), the detected EPR signal broadens and becomes distorted (Fig. 9). To get the most accurate information about signal line shape, the modulation amplitude should be less than 10% of the distance (in Gauss) between the positive and negative peaks in the derivative spectrum (of isotropic signals). This low modulation amplitude, however, can result in unacceptable poor signal-to-noise ratio for the signal. A good compromise between signal intensity and signal distortion occurs when the amplitude of the magnetic field modulation is equal to the width of the EPR signal. Figure 9, also shows that if a modulation amplitude is used greater than the splitting between two EPR signals, we can no longer resolve the two signals.

For measurements at X-band frequency, the modulation frequency is normally set to 100 kHz. This is a value that works well for the broader signals due to metals centers in proteins. The modulation amplitude has to be smaller than the line width of these types of signals. It is therefore important to start the first measurement with a small value (6 Gauss). The values can be increased for subsequent measurements if needed. When the signal is very intense there is no real need to do this, but very low intense signals might show a better signal-to-noise ratio if the value can be increased.

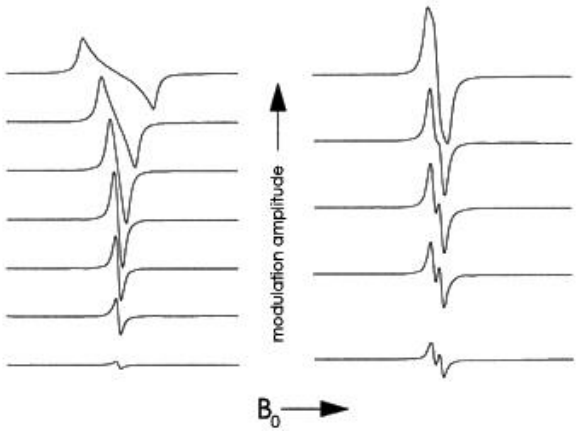

Fig. 9: Effect of increasing modulation amplitude on signal intensity and signal shape.

To further improve the sensitivity, a ***time constant*** is used to filter out more of the noise. Time constants filter out noise by slowing down the response time of the spectrometer. As the time constant is increased, the noise levels will drop. If we choose a time constant which is too long for the rate at which we scan the magnetic field, however, we can distort or even filter out the very signal which we are trying to extract from the noise (Fig. 10). Also, the apparent field for resonance will shift.

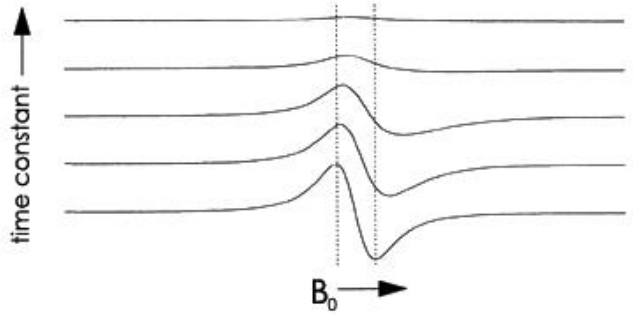

Fig. 10: Effect of increasing time constant on signal intensity and signal shape.

A parameter that is directly related to the time constant is ***conversion time***. A longer conversion time also improves the signal to noise ratio, but in a different way: The signal channel incorporates an integrating ADC (Analog to Digital Converter) to transfer the analog EPR spectra to the digital data acquisition system. An important side effect of using the integration method for the conversion is that it integrates the noise out of the signal. If the Time Constant is too large in comparison with the Conversion Time (the rate at which the field is scanned) the signals we want to detect will get distorted

or will even be filtered out. The actual values for the time constant and conversions time will depend on the type of signal being measured.

Very weak signals might get lost in the noise. You can increase your signal to noise ratio by ***signal averaging***. The resultant signal to noise is proportional to √N, where N is the number of scans. With a perfectly stable laboratory environment and spectrometer, signal averaging and acquiring a spectrum with a long scan time and a long time constant are equivalent. Unfortunately perfect stability is impossible to attain. For example, there is a delicate balance between the heat dissipated by the cavity and the air flow around it and slow variations will result in baseline drifts. For a slow scan (>15 min) the variations can cause broad features in the spectrum dependent on the sample concentration and the gain used. If you were to signal average the EPR signal with a scan time short compared to the variation time, these baseline features could be averaged out.

The one parameter left to discuss is the ***microwave power level***. The EPR signal intensity grows as the square root of the microwave power in the absence of saturation effects. When saturation sets in, the signals broaden and become weaker. Several microwave power levels should be tried to find the optimal microwave power. Since there is a more intricate relationship between sample temperature and saturation this will be discussed in the next section.

2.3 Sample Temperature and Microwave Power

There are several reasons why we need to do EPR measurements at lower temperatures than room temperature. One reason has to do with the fact that in biological samples the solvent is commonly an aqueous buffer. Water will absorb the microwaves, just like in a regular microwave oven, and the sample will heat up. Because microwave dielectric loss is due to molecular motion, which decreases upon freezing, the impact of solvent on resonator Q is much smaller when samples are frozen. To maintain lower temperatures the sample has to be cooled from the outside with a stream of cold gas (nitrogen or helium) which also helps battling the heating up of the sample. The warming up is also minimized by having the sample positioned in the cavity so that the magnetic component is maximal but the electric component that is causing the warming up is minimal. When a sample does have to be measured at RT in aqueous buffer the sample will be measured in a flat cell to further minimize the absorption of the electric field component.

A more important reason to measure at low temperature, however, is the fact that the highest theoretical signal intensities are reached at the lowest possible sample temperature. This is because the energy difference between the two energy levels, the S = -½ level and the S = ½ level involved in the EPR transition is very small and both levels are almost equally occupied with only a small excess in the S = -½ level. Figure 11, shows what the population is in percentage for the *S* = - ½ level (n_0) and the *S* = ½ level (n_1) as a function of the sample temperature. The energy difference between the two energy levels due to the Zeeman splitting is very small, ~0.3 cm^{-1} for X-band EPR. Based on the ***Boltzmann distribution***

$$n_1 = n_0 e^{-\left(\frac{\Delta E}{kT}\right)}, \tag{2}$$

it can be shown that only at low temperatures there will be enough difference in the population of the two levels to create a signal (Fig. 11).

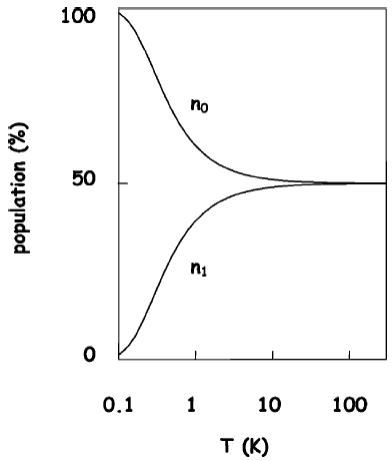

Fig. 11: Boltzmann distribution for the electrons in the *S* = - ½ level (n_0) and the *S* = ½ level (n_1).

This means that in principle we should always measure at the lowest temperature possible. However, there is another property of the sample that has to be taken into consideration: ***spin-lattice relaxation***. Figure 12, Shows how this property is important. The figure gives a representation of the electron distribution in the S = -½ level and the S = ½ level involved in the EPR transition with a small excess in the S = -½ level. The electrons in both levels will absorb energy quanta causing a complete reversal of the electron distribution. We will only continue to observe an absorption signal, however, if the lower energy level has a higher occupancy. Therefore some electrons have to go back to the lower energy level using relaxation before the next set of quanta is absorbed. When this doesn't happen the EPR signal will be lost because the electron distribution between the two levels will be eventually become equal. In addition, the microwave power applied to the sample plays a role. The more power is applied to the sample the higher the chance that an energy quantum is absorbed. When the relaxation of the electron is already limited, an increase in power will speed up the equalization of the electron distribution. Therefore, at lower temperatures EPR signals might not be observable and the chance of that is even higher when high microwave powers are applied, saturating the sample with energy quanta. This effect is therefore described as power saturation of the EPR signal. Note that the relaxation rate is anisotropic and therefore different parts of the spectrum can show different amounts of saturation at different temperatures.

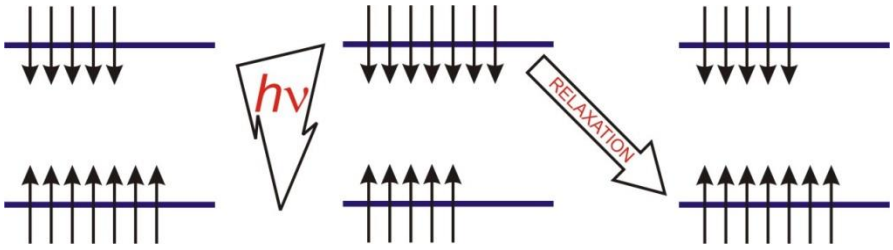

Fig. 12: Change in the electron distributions between the *S* = - ½ level (n_0) and the *S* = ½ level (n_1) during an EPR experiment.

The detection of EPR signals is also affected by the Heisenberg uncertainty principle. Due to the uncertainty principle the EPR spectra will broaden beyond detection at higher temperatures. At lower temperatures the spectra will sharpen up. This sharpening up of the spectrum by cooling the sample is, however, limited by a temperature-independent process: inhomogeneous broadening. The protein or model molecules in dilute frozen solutions are subject to a statistical distribution in conformations, each with slightly different 3D structures and, therefore, slightly different g-values, which manifest themselves as a constant broadening of the EPR line independent of the temperature.

To summarize, the lower the sample temperature the higher the signal intensity will be. At the same time, power saturation might occur at a too low temperature, while temperature broadening might occur at a too high temperature due to the uncertainty principle. As a result of all these conflicting mechanisms there will be a temperature region where the detection of the EPR signal of a particular sample is optimal (Fig. 13). This optimal region, however, will be different for each type of paramagnetic species and has to be determined for each new type of species you will measure.

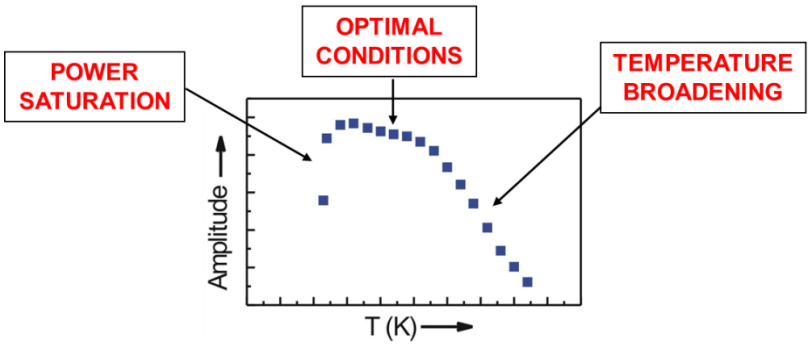

Fig. 13: At low temperatures power saturation will occur while a higher temperatures temperature broadening will occur due to the Heisenberg uncertainty principle, leaving an optimal measuring region somewhere in the middle.

Power plots and Curie plots

With a completely new sample you will not know all the measurement conditions. First of all, you are not sure if you have a signal at all. So one of the first things you have to find out are the optimal measuring temperatures of possible paramagnetic species in your sample. For this you have to scan the sample at different temperatures, for example ***4.5 K, 20 K and 50 K***. At each temperature you make a broad scan in the hope you will see a signal. Preferably, you do this at different powers, ***50 dB, 20 dB and 0 dB***. If you detect a signal, you can zoom in and measure the signal again with a smaller sweep to obtain more detail.

After you have discovered an EPR signal at a certain temperature and microwave power, you have to make sure that the data you obtained is useful: It is important that the signal is not broadened or distorted. The first thing that has to be done is to make sure the signal is measured under non-saturating conditions. There is a method to do this.

The next formula explains the relationship of the amplitude, gain and the power in dB:

$$\left(\frac{amplitude}{gain}\right) \cdot 10^{-dB/20} = \text{constant} \tag{3}$$

The spectrometer is designed such, that ***a non-saturating signal remains constant in amplitude when each change of 1 dB in the microwave power is compensated by 1 step in the gain***. Note that a lower amount of dB means a higher amount of power in mW(atts). If you increase the power you have to decrease the gain. This 'design' also explains why the gain cannot be changed to any value we want but can only have certain values. What this practically means is that we can measure a spectrum, for example at -20 dB. Then we can increase the power to -15 dB, additionally decrease the gain five steps and remeasure the spectrum again. If the signal is not saturating both spectra should have exactly the same amplitude. As an example, the EPR spectra for the Copper Standard at 4.7 K measured at different powers is shown (Fig. 14):

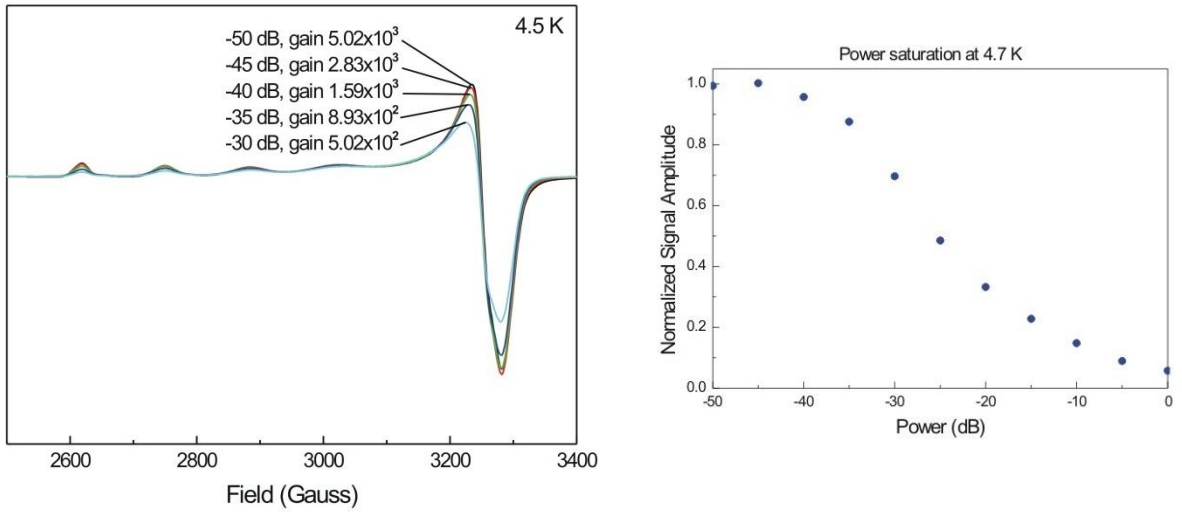

Fig. 14: Power saturation studies. The left panel shows an overlay of spectra obtained for the copper standard at different combinations of microwave power and gain. The right panel shows the signal intensities for each spectra as a function of microwave power (in dB).

What can be seen from Figure 14, left panel, is that from -50 dB to -45 dB the signal amplitude hardly changes, but that the signal amplitude clearly starts to decrease at -40 dB and lower. So if we want to measure the Copper Standard at 4.7 K we should measure with a power of -50 dB. When we measure the copper spectra at different powers going from -50 dB to 0 dB we can make a so-called power plot (Fig. 14, right panel). At the lowest powers (higher dB) you can see there is an area where the curve is horizontal, where the Copper Standard can be measured without saturating the signal. Then starting at -40 dB the signal starts to saturate, the signal broadens and loses amplitude. The Copper Standard has also been measure at 20 K and 50 K (Fig. 15).

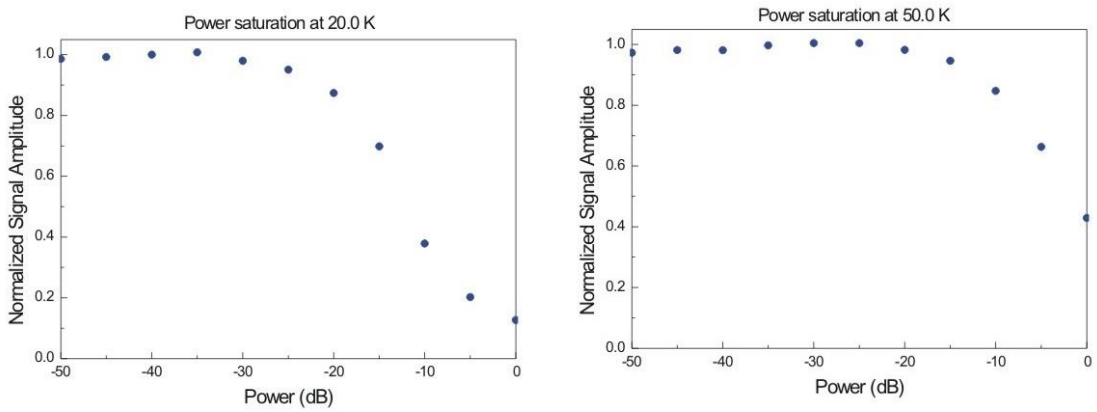

Fig. 15: Power saturation studies for the copper standard at 20 K and 50 K.

The power plots show that at higher temperatures there is a larger power range where the signal can be measured without saturating. At 50 K we can even measure at -20 dB.

It is very important to know the temperature and power behavior of your signal. The lower the temperature you can measure and the higher the power you can use the better the signal-to-noise ratio. The Copper Standard is used because it has the same (corrected) signal intensity at a wide range of temperatures. In general, there will be only a certain small temperature range where your signal can be measured. To get to know this you have to make a so-called Curie plot. Here we plot again the signal amplitude, but now against the temperature. Since the observed signal intensity or amplitude (I_0) will decrease going up in temperature, we will use a normalized intensity or amplitude (I_n), according to the formula:

$$I_n = \frac{\left(I_0 \cdot T \cdot 10^{-dB/20}\right)}{gain} \tag{3}$$

I_n	normalized value for the intensity (normalized double integral)
I_0	observed intensity
T	absolute temperature in K
dB	reading of the attenuator
$gain$	gain

(keeping all other parameters constant)

If we do this for the Copper Standard we get the curve shown in Figure 16. In principle we should get a straight line. Small deviations can be expected dependent on the accuracy and calibration of the heater system. The inhomogeneous broadening will be different at different temperatures which could cause a small slope dependent on the sample being studied. The loss of intensity of the copper signal at 175 K and higher (Fig. 16) is due to a phase change in the sample.

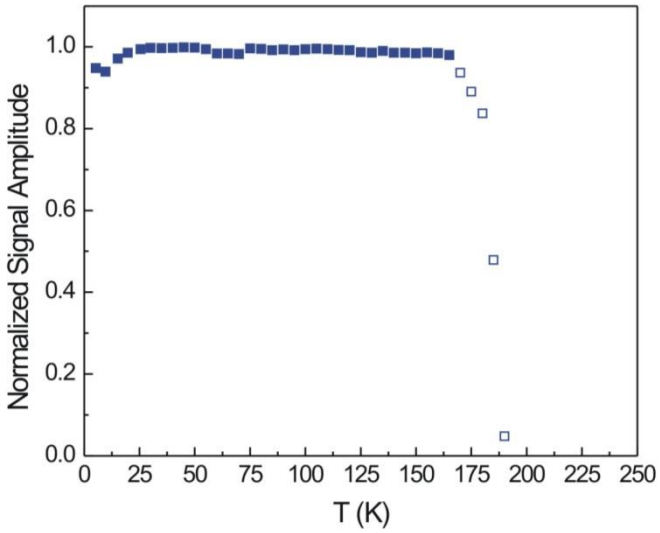

Fig. 16: Curie plot for the copper standard.

For comparison Curie plots for some other samples are shown in Figure 17. The red trace is from the MCRred1-Ni(I) species. This signal can also be detected over a wide temperature range. The signal shows clear saturation, however, below 40 K and shows temperature broadening above 200 K. The black trace is for a standard $[4Fe\text{-}4S]^{1+}$ cluster detected in the enzyme IspH. For 4Fe clusters there is normally only a very small temperature window (10 – 20 K) where the EPR signal can be detected. Like IspG, IspH binds its substrate and a cluster-bound reaction intermediate can be detected in kinetic studies. The curie plot for this species (green trace) is very different. The cluster species can be detected all the way up to 80 K before the temperature broadening sets in.

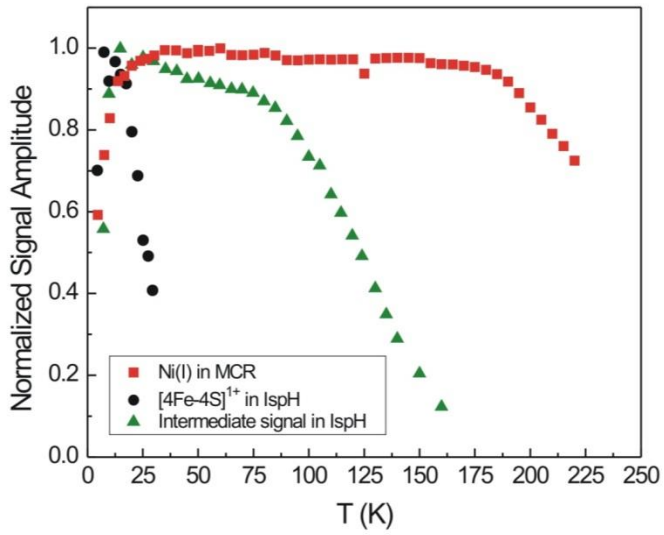

Fig. 17: Curie plots for the MCRred1-Ni(I) species (■), the $[4Fe\text{-}4S]^{1+}$ cluster detected in the IspH enzyme (●), and a cluster-bound reaction intermediate detected in the same IspH enzyme (▲).

2.4 Integration of Signals and Determination of the Signal Intensity

The area under the ***absorption spectrum*** of an EPR signal is, just as in optical spectroscopy, a direct measure for the concentration of unpaired electrons. Unlike electronic absorption spectroscopy, however, there is no 'extinction coefficient' in EPR spectrometry. All S = ½ systems absorb equally well. To correlate the intensity of the EPR signal with a concentration, a standard is needed. Different standards can be used. Here we will use a copper standard, containing 10 mM $CuClO_4$. Made in the proper way, all the copper is 2+ and contributes to the EPR spectrum. So the 'spin concentration' of this standard is also 10 mM. By comparing the spin concentration of the copper standard with the spin concentration of the signal of interest the concentration of that signal can be determined. To be able to make a comparison between the EPR signal of interest and a standard it is important that the spectra to be compared are obtained under exactly the same conditions. If this is not possible it is necessary to scale the signal obtained for the unknown to compare it with the standard. For samples recorded at the same temperature and with the same spin number (e.g., S = ½) the most common parameters that have to be corrected are:

1. Receiver gain. Area scales linearly with gain settings of the detector's amplifier.
2. Microwave power. With the assumption that the spectra are obtained at power levels below saturation. Under these conditions, area scales as the square root of the incident microwave power.
3. *g*-value differences. Area scales as *g*.
4. Field scan width. For first-derivative spectra the scan width correction factor is (1/sweep width)^2.
5. Filling factor of the EPR tube. A wider tube results in a more intense signal. This increase is not linearly due to the sinus wave form of the standing wave and ideally each tube should be calibrated by filling it with the copper standard and measuring the signal intensity.

The following formula put all these correction factors for the parameters together:

$$I_n = \frac{\left(I_0 \cdot d^2 \cdot T \cdot 10^{-dB/20}\right)}{\left(g_p^{av} \cdot f \cdot a\right)} \tag{4}$$

where

I_n	normalized value for the intensity (normalized double integral)
I_0	observed intensity
d	distance between the starting and ending points (in Gauss)
T	absolute temperature in K
dB	reading of the attenuator
f	tube calibration factor
a	gain

and

$$g_p^{av} = \frac{2}{3}\sqrt{\frac{g_x^2+g_y^2+g_z^2}{3}} + \frac{\left(g_x+g_y+g_z\right)}{9} \tag{5}$$

Unfortunately, there are several additional parameters that you might have to correct for which are equipment specific:

6. Modulation amplitude. Area scales linearly with modulation amplitude.
7. When an integrating digitizer is used, the recorded signal area varies with scan time. The signal level increases the longer the integration time (conversion time). Thus, if two spectra of the same sample are obtained will all parameters equal, but one with 10.24 ms conversion time and one with 81.92 ms conversion time, the numerical integral of the digitized spectrum will be eight times larger for the 81.92 ms conversion time. This is often automatically normalized by the software in modern spectrometers.
8. "Signal averaging". The Bruker software that comes with the spectrometer in the Department of Chemistry and Biochemistry does not really average the scans. When more than one scan is measured in one measurement, the scans are just added up and not averaged. Averaging four scans will result in a spectrum with a four times higher signal intensity.
9. Correct for Q differences. When the Q-values are different it is necessary to scale the intensity or double integration results by the ratio of the resonator Q-values that is observed from two samples. Area scales linearly with Q.
10. Bruker spectrometers use a Schottky barrier diode to detect the reflected microwaves. The diode converts the microwave power to an electrical current. At low power levels (less than 1 μW, ~53 dB), the diode current is proportional to the microwave power, and the detector is called a square law detector. At higher power levels (greater than 1 mW, ~23 dB), the diode current is proportional to the square root of the microwave power and the detector is called a linear detector. The transition between the two regions is very gradual. For quantitative signal intensity measurements the diode should operate in the linear region.

Dependent on the type of equipment and software some of these corrections are made automatically. It is important to check what corrections are made by the software. When possible, however, it is important to measure the unknown and the standard under identical conditions like temperature, power, modulation amplitude, conversion time, time constant and total amount of spectra added. Generally, using the same solvent/buffer the Q factor should also be identical.

Using the WINEPR program for integration

The recorded EPR spectra are ***first derivatives*** of the normal absorption spectra. Since an EPR spectrum is a first derivative, we have to integrate twice to obtain the intensity (I_0) (= area under the absorption spectrum). Open the program WINEPR and load the file you want to integrate. Under **WINEPR System** select **1D-processing**. Then under **1D-processing** select **Integrate Region**. The menus will change. Now select **Integration** and **Define Integrals**. Now you can designate the area to be integrated by selecting a point on the left side of the signal and a point on the right side of the signal by moving the mouse and clicking the left mouse button to select the points. Click the right mouse button to confirm your selection. Now you will see the first integral. A good integral will have the Y-values of the start and the end of the curve at the same vertical position (Fig. 18).

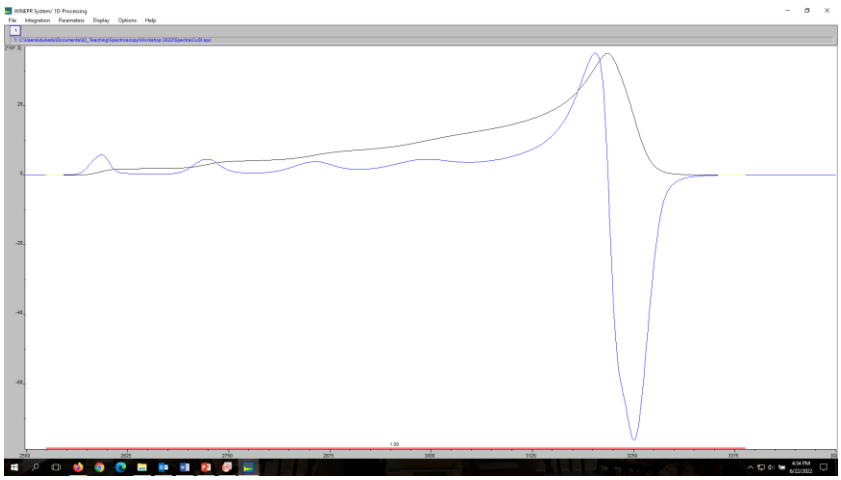

Fig. 18: Screen shot of Integration procedure: integral

Select **Integration**, **Integral type**, **Double**. Now the double integral is shown (Fig. 19). You have the option to change the slope and the bias of the double integral. These might give you a better-looking curve, but doesn't add to the reliability of your integral. You should try to do a baseline correction first. By now selecting **Integration**, **Report** you get an new screen which shows the start position of the integral, the end position of the integral, the double integral (DI) and the normalized double integral (DI/N) (Fig. 19). This last value is the value you need to write down if no additional corrections are needed. Select **Integration**, **Return** if you need to integrate more spectra.

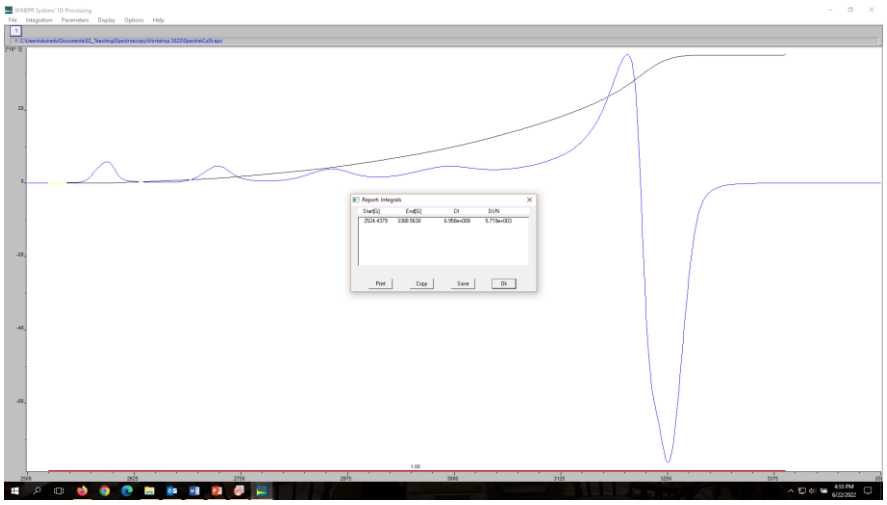

Fig. 19: Screen shot of Integration procedure: double integral and report

By determining the I_n (DI/N) for both your sample and the copper standard you can now determine the concentration of your detectable signal.
The concentration of the unknown (C_u) is now:

$$C_u = \frac{I_{n(u)} \cdot C_{st}}{I_{n(st)}} \quad (6)$$

where

C_u	spin concentration of unknown
C_{st}	spin concentration of standard
$I_{n(u)}$	normalized intensity of unknown
$I_{n(st)}$	normalized intensity of standard

Some spectra are inherently difficult to integrate, because they do not meet the ideal case of isolated peaks with well-defined flat baselines on either side of the EPR spectrum (Fig. 18). If the signal-to-noise is very low, if there is an overlapping spectrum from another species, or the background is large and unavoidable, it may be best to integrate a computer simulated spectrum by fitting the experimental data.

Subtraction of a background spectrum is also an option. This is particularly important when the empty cavity shows an EPR signal due to accumulation of dust and dirt inside the measuring chamber. A background spectrum can be generated by measuring a tube containing the sample solvent/buffer as the unknown. It is important to use a "blank" tube since the quartz walls of the EPR tubes concentrate the field lines in the sample and a slightly different spectrum will be obtained when just the cavity without a sample inside is measured. The main change will be that the cavity is tuned at a different frequency when no sample is present, which causes a shift in the spectrum making it useless for a proper subtraction of the background signal.

Equation 5 only holds if two S = 1/2 spectra are compared. For unequal spin systems the term 1/[S(S+1)] has to be added to the formula of I_n. If possible, however, a standard with the same spin systems should be used.

2.5 Redox Titrations

In section 1.10, it is described how the production of samples in the as-such form, oxidized form, or reduced form can help with the identification of the paramagnetic species present. Some species will only show an EPR signal at a certain oxidation state and detection of this signal can be the first clue on what species is present in the unknown. Dependent on what type of protein you are studying more knowledge about the redox active groups might be needed. The protein could be part of a chain of proteins that transfer electrons and the midpoint potentials of the electron carrier present in the unknown could indicate where it is placed in the chain. Some proteins contain a multitude of redox active groups and determination of the midpoint potential of each group will be needed to establish the electron flow within the protein. This knowledge will also be helpful in finding unique redox potentials where only a small subset (ideally only one) of the redox active groups is paramagnetic and EPR detectable. This will enable the study of these specific species without having no, or only a small set of, other EPR signals present.

Detailed information about the midpoint potential of redox active species can be obtained by performing redox titrations. Different type of detection methods can be used, but when one of the oxidation states is EPR active, and most of the time it is, EPR spectroscopy is the preferred method.

Typically, a titration is performed in both the oxidative and reductive direction. One could start with a fully reduced protein and add small amount of oxidant to slowly increase the redox potential of the protein solution. At specific potentials a sample is withdrawn, placed in an EPR tube and subsequently frozen and stored in liquid nitrogen. When the highest potential is reached reductant can be added and the whole process is repeated in the reductive direction. Sodium dithionite is often used in physiology experiments as a means of lowering a solution's redox potential ($E^{o'}$ ~ -420 mV at pH 7 vs. SHE). Potassium ferricyanide is usually used as an oxidizing chemical in such experiments ($E^{o'}$ ~ 436 mV at pH 7 vs. SHE).

Redox dyes are added to the protein solution before the redox titration is started. Typical dyes are duroquinone (E_m = 86 mV), methylene blue (E_m = 11 mV), indigo-disulphonated (E_m = -125 mV), phenosafranin (E_m = -252 mV), neutral red (E_m = -325 mV), benzyl viologen (E_m = -350 mV), and methyl viologen (E_m = -453 mV). The dyes have two functions. In the first place, they greatly enhance the electronic contact between the protein molecules and the electrode. Secondly, they help buffer the protein solutions, allowing stable potentials outside the range where the protein chromophores accept or donate electrons. Dyes can interfere with the redox titration, however, and caution has to be taken with the selection of the dyes. The 'ideal' combination of dye mediator potentials begins with a dye below the lowest potential data point and extends to a dye above the highest potential data point with no spaces of greater than 60-70 mV between dyes.

The typical redox titration requires about 15 data points. Ideally, the experiment should span a range of 150 mV above and below the midpoint potential of the sample. Normally samples are taken every 20-25 mV depending on the amount of sample and the accuracy desired. Note, ideally the titration should be performed in both the oxidation and reduction directions to verify the **thermodynamic reversibility** of the system. When the potential of the chromophore of the protein under study is not known more points or additional redox titrations will be needed.

Tube Calibration

Since you will be comparing the signal intensity in a series of EPR tubes it is important to know the filling factor of the EPR tubes. Also the thickness of the quartz wall can add to the filling factor. The best way to calibrate tubes is to fill them with a (copper) standard and measure the relative EPR signal intensity for every tube. This has to be done at a stable temperature. The so called liquid nitrogen finger Dewar is perfect since it will work at liquid nitrogen temperature and the stable room pressure. This cannot be obtained with a flow system. In the absence of such a setup the filling factor can be determined by measuring the inner diameter of the tubes (However, the diameter of the top and bottom of an EPR tube can differ slightly.) An alternative is to fill the tube with a set amount of solution and to measure the height of the solution in the tubes.

Of the new batch of tubes, fifty were filled with a copper standard and the signal intensity was measured. The intensities fluctuated ± 5% around an average value. Taking a tube out and putting it back into the cavity also contributes to this deviation (± 3%). So if tubes from the same (new) batch are used no calibration is needed. This, however, is necessary when tubes of different batches are used!

Methyl-coenzyme M reductase: MCRred1 signal

As an example, let us consider the MCRred1 signal again detected in the active forms of methyl-coenzyme M reductase (see Figure 19 in Section 1.7). This protein becomes inactive when the nickel is oxidized. This is an irreversible process. A redox titration was performed to know the midpoint potential of the oxidative inactivation process. Figure 20, left panel, shows some of the spectra obtained during the titration. In this case the signal can be directly double integrated to obtain the signal intensity. The peak all the way at high field is due to radical signals from the redox dyes. If there are overlapping signals in the samples it is also possible to just measure the signal amplitude of an isolated peak. If that is not possible the signal should be simulated and the simulation double integrated. A plot of the signal intensity vs. the potential is shown in Figure 20, right panel. The points have been fitted with a Nernst curve (Fig. 20, right panel, solid line) to obtain the midpoint potential for the oxidative process: E_m = -440 mV. Note that is this case the oxidation is not reversible (solid dots in Fig. 20, right panel).

The curve fitting is based on the Nernst equation:

$$E = E_0 + \frac{RT}{nF} ln\left(\frac{[ox]}{[red]}\right) \tag{7}$$

Using the relationship [ox] + [red] = 1, this can be rewritten as:

$$[red] = \frac{1}{1 + exp\left(n \cdot \frac{F}{RT} \cdot (-E_o + E)\right)} \tag{8}$$

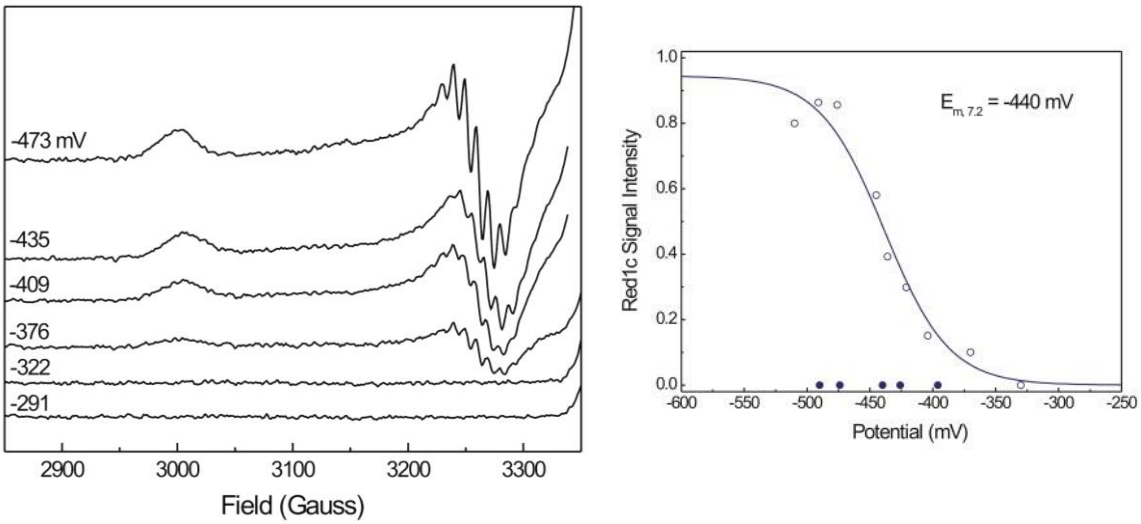

Fig. 20: Redox titration for the MCRred1-Ni(I) species detected in Methyl-coenzyme M reductase. The Left panels shows a selection of the EPR spectra obtained at different redox potentials. The Right panel shows a plot of the signal intensity against the redox potential. The data was fitted with a Nernst Curve with E_m = -440 mV and n = 1.

Equation 8 expresses the detectable amount of the reduced species. For the fitting procedures this is rewritten as:

$$y = I / \left(1 + \exp\left(n \cdot 38.92 \cdot (x - E)\right)\right) \tag{9}$$

where:

- I is the maximal signal intensity
- n is the amount of electrons involved
- E is the midpoint potential
- x are the values in "mV" obtained during the titration
- "38.92" is the value of F/RT (F = 96484.6 C·mol^{-1}, R = 8.31441 J·mol^{-1}·K^{-1}, T = 298.15 K)

A similar equation can be obtained for a signal that is EPR active in the oxidized form:

$$y = I / \left(1 + \exp\left(n \cdot 38.92 \cdot (E - x)\right)\right) \tag{10}$$

Sometimes a species can show more than one redox change, where a signal starts to appear at a certain potential (E_1) and disappear again at a higher potential (E_2). In this case the data should be fitted with a bell-shaped curve, particularly when the two curves that would describe this process are overlapping in such a way that the maximal attainable signal intensity is not reached.

$$y = I / \left(1 + \exp\left(n \cdot 38.92 \cdot (E_1 - x)\right) 1 + \exp\left(n \cdot 38.92 \cdot (x - E_2)\right)\right) \tag{11}$$

2.6 Freeze-quench Experiments

The standard technique to study the pre- and steady state kinetics of enzymatic reaction is stopped-flow. In the most basic setup there are two syringes. One is filled with a solution containing the enzyme and the other is filled with a solution containing the substrate. Other things that are necessary for the reaction to proceed can be added to either of the two syringes. The two syringes are mounted in a setup that allows the two syringes to be emptied simultaneously through a mixing device and into a cuvette. As soon as the liquid is injected into the cuvette, absorption spectra are collected. This can either be the rapid collection of spectra over a longer wavelength range, or the absorption change at a specific set of wavelengths can be monitored. The setup allows the first spectra, or point, to be recorded within a couple of milliseconds.

Different types of detection methods can be used in these types of studies. In some cases, however, the preferred detection method does not allow the continuous detection of changes over time. Instead individual samples have to be prepared at different time intervals. To be able to do that the reaction has to be stopped at a set time. This can for example be achieved by quenching the reaction with a certain chemical. To achieve this, the setup has to be modified. Instead of injecting the sample directly into a cuvette, an aging tube is added that allows the reaction to proceed for a set time. The reaction is stopped by mixing with the quenching agent. This can be present in the collection tube or a third syringe can be added to the setup. The aging of the sample is a function of both the speed which with the syringes are emptied and the length of the aging tube. By changing each of these, samples can be quenched within a couple of milliseconds or longer time intervals.

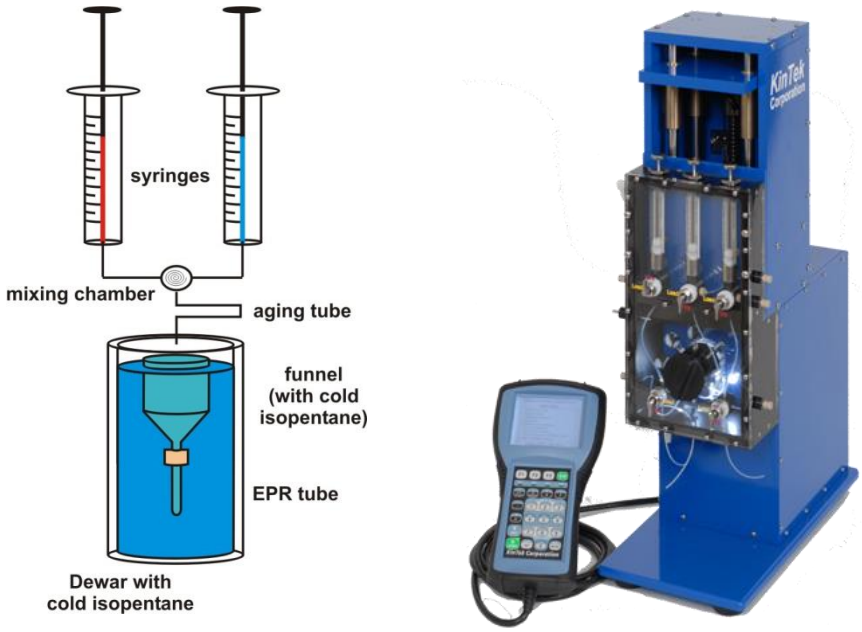

Fig. 21: Schematic overview of the parts which are essential to perform freeze-quench experiments (left panel) and a picture of the commercially available rapid quench-flow instrument from KinTek Corporation (right panel).

Since most biological samples have to be frozen to be studied in EPR spectroscopy, freezing of the enzyme-substrate mixture can be used to quench the reaction. Therefore, this technique is called freeze-quench. The quenching is normally achieved by having the aging tube end just above a cold solution of isopentane (125 K) (Fig. 21, left panel). The enzyme-substrate solution is shot directly into the solution, freezes instantaneously and forms what is called a 'snow'. The snow can now be collected and packed into an EPR tube. The most direct way is to have the aging tube end above a funnel filled with the isopentane that has an EPR tube attached to it allowing the easy packing of the snow into the tube.

Development of paramagnetic reaction intermediates in the enzyme IspG

Again an example from our laboratory: The enzyme IspG ((E)-4-hydroxy-3-methylbut-2-enyl diphosphate synthase) catalyzes the reductive dehydroxylation of the substrate 2-C-methyl-D-erythritol-2,4-cyclodiphosphate (MEcPP) into (E)-4-hydroxy-3-methyl-but-2-enyl diphosphate (HMBPP) (Fig. 22) in the penultimate step of the MEP pathway for isoprene biosynthesis. MEcPP is a cyclic compound and the reaction involves the opening of the ring and removal of the C3 hydroxyl group consuming the total of two electrons. The enzyme contains a single [4Fe-4S] cluster in its active site. Under the assumption that the iron-sulfur cluster is the direct electron donor for this conversion there is the problem that the cluster can only donate one electron at-a-time and it was proposed that some type of radical species is introduced after the first electron is transferred. Since the cluster would have to be re-reduced before it can transfer the second electron there could be a small time window where the intermediate is detectable in EPR spectroscopy.

Fig. 22: Reaction catalyzed by IspG

Since there was high expectation that a radical species should be observable, freeze-quench studies where performed. The results are shown in Figure 23. For this experiment, a solution containing IspG and dithionite was rapidly mixed with a solution containing MEcPP. The reaction was allowed to proceed for a set amount of time after which the reaction was halted by rapid freezing of the reaction mixture. The EPR spectra obtained for the different samples are shown in Figure 23. From 28 ms to 0.5 s the main signal detected was an isotropic EPR signal with g_{iso} = 2.005. At 1.2 s a new, more rhombic EPR signal (designated FeS_A) with g_{xyz} = 2.000, 2.019, and 2.087 started to develop. The intensity of this signal reached a maximum value at 30 s. At 60 s the signal intensity decreased again. The maximal EPR signal intensity of this species ranged from about 0.05 to as high as 0.20 spin in different experiments. The spectra were measured at 77 K. Measurements at other temperatures showed that these are the only paramagnetic species present in these samples. For example, signals with properties typical of $[4Fe\text{-}4S]^{+}$ clusters (perpendicular mode) or of $[3Fe\text{-}4S]^{0}$ clusters (using parallel-mode EPR spectroscopy) were not detected (not shown).

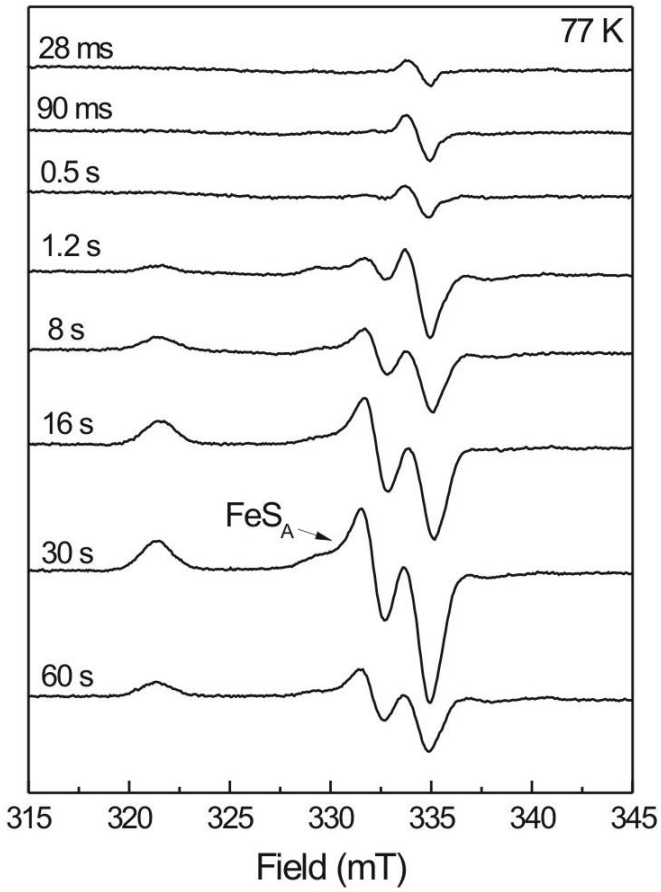

Fig. 23: Electron paramagnetic resonance data for IspG samples obtained with the freeze-quench technique in the presence of dithionite. After mixing each sample contained 0.4 mM IspG, 5.5 mM MEcPP, and 25 mM dithionite in 100 mM TrisHCl, pH 8.0. Samples were mixed and incubated at RT. EPR conditions: microwave frequency, 9.385 GHz; microwave power incident to the cavity, 0.20 mW; field modulation frequency, 100 kHz; microwave amplitude, 0.6 mT; temperature 77 K.

The measurements show that initially a radical-type signal was formed, but it was not clear if that was due to the dithionite that was used in the study. More interestingly a broader signal was detected at a later time (1.2 sec and up). This broader signal was subsequently studied using the ENDOR and HYSCORE techniques discussed in Chapter 1. It turned out that the signal represents a cluster bound reaction intermediate (for the structure see Fig. 41B in Chapter 1). It was proposed that in the reaction mechanism the formation of a radical species is prevented by binding of the substrate to the clusters allowing the transfer of two electrons from the cluster, forming a $[4Fe\text{-}4S]^{3+}$ species. Since this redox state is paramagnetic the species could be detected in our studies.

Rapid freeze-quench can be a very powerful tool in the study of reaction mechanism that involves paramagnetic species. Since these species are transient there detection is dependent on the speed of formation and speed of breakdown. More often than not the energetics of a reaction prohibit the detection of a reaction intermediate, and even when the signal is formed its intensity is generally very low (1-10% of the protein concentration). This makes it difficult to preform freeze quench experiments because a large amount of protein will be needed to make a large set of samples at very

high concentration to be able to see a low intense EPR signal with a decent signal-to-noise ratio. More than one run will be needed to be able to find the optimal set of time intervals and these experiments might have to be followed with runs using labeled substrates.

As discussed in section 2.5 the calibration of the tubes used to make the whole series of EPR samples at different time intervals is very important.

2.7 EPR of Whole Cells and Organelles

Measuring whole cells, or perhaps purified organelles from whole eukaryotic cells, for example mitochondria, goes back to the very first days of bioEPR spectroscopy (Beinert and Lee 1961) and has since then over and over again proven to be useful for the particular purpose of studying respiratory chains, that is, the set of redox enzymes that form the heart of the bioenergetics machinery and that, for this reason, typically occur in high concentration in the cell. An example is the spectrum of whole heart tissue in Figure 24. There are many overlapping spectral components in this spectrum that are reasonably well resolved. The assignment, however, is the result of many years of research on the purified individual enzymes. Typically these types of experiments are done to see what signals are present in a cell and then try to purify the separate enzymes. Alternatively it can be done when all the enzyme are already known but there is a need to see how all the enzymatic components work together in the cell and what signal is detectable under certain specific conditions.

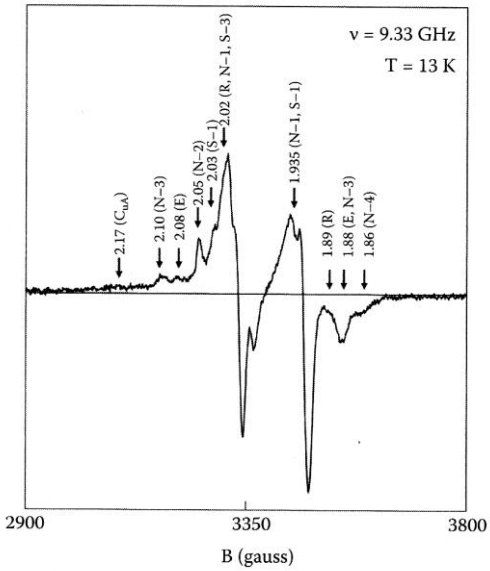

Fig. 24: Whole eukaryotic-cell EPR. A rat heart was frozen in liquid nitrogen and ground to a fine powder. The EPR spectrum shows signals from prosthetic groups in respiratory chain complexes: N1-N4 (iron-sulfur clusters in NADH dehydrogenase); S1, S3 (iron-sulfur clusters in succinate dehydrogenase); R (the Rieske iron-sulfur cluster in the bc_1 complex); Cu_A (the mized-valence copper dimer in cytochrome c oxidase); E (the iron-sulfur cluster in electron-transfer flavoprotein dehydrogenase (Van der Kraaij *et al.* 1989)

Bacterial cells will show less complex EPR spectra. In most cases the energy producing pathways are less complex. Shown in Figure 25 (Right panel) are two spectra taken with whole

Methanothermobacter marburgensis cells, the source of the methyl-coenzyme M reductase which EPR spectra has been discussed throughout this manual.

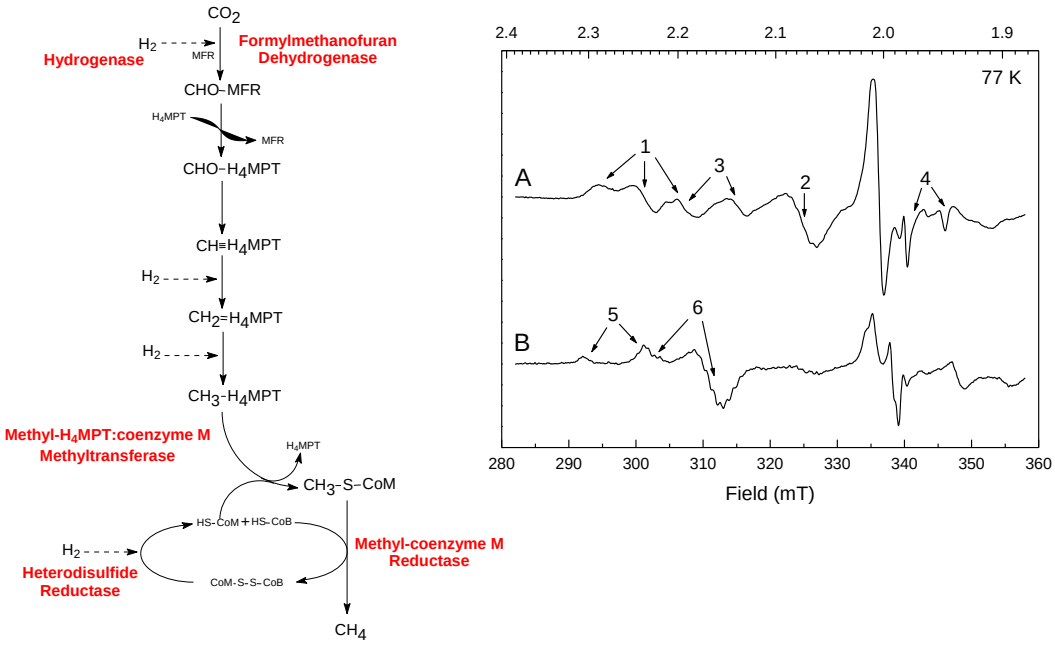

Fig. 25: Metabolic pathway of methanogenesis from CO_2 in *Methanothermobacter marburgensis* (Left panel) and EPR spectra taken of whole cells (Right panel). CHO-MFR, N-formylmethanofuran; CHO-H_4MPT, N^5-formyltetrahydromethanopterin; CH≡H_4MPT^+, N^5,N^{10}-methenyltetrahydromethanopterin; CH_2=H_4MPT, N^5,N^{10}-methylenetetrahydromethanopterin; CH_3-H_4MPT^+, N^5-methyltetrahydromethanopterin; CH_3-S-CoM, methyl-coenzyme M. Trace A in the right panel is a sample taken when the cells are incubated under an atmosphere of 100 % H_2 for 30 min at 65 EC. Trace B is a sample taken when the incubation atmosphere contains 80 % N_2/20 % CO_2. Spectral components: 1) Methyl-coenzyme M reductase in the MCRred2 form; 2) Methyl-coenzyme M reductase in the MCRred1 form, 3) NiFe-Hydrogenase in the Ni-C form, 4) Heterodisulfide reductase; 5) Hydrogenase in the Ni-A form, and 6) Methyl-coenzyme M in the MCRox1 form.

The panel on the left shows the CO_2-reducing pathway of methanogenesis, which uses H_2 and CO_2 as substrates. The reduction of CO_2 to CH_4 proceeds via coenzyme-bound C1-intermediates, methanofuran (MFR), tetrahydromethanopterin (H_4MPT), and coenzyme M (2-mercaptoethanesulfonate, HS-CoM). In the first step CO_2 is reduced to the level of formate: formylmethanofuran. From formylmethanofuran the formyl group is transferred to tetrahydromethanopterin, which serves as the carrier of the C1 unit during its reduction to methylene- and methyltetrahydromethanopterin. The methyl group is then transferred for the fourth and last reduction step in the pathway to a structurally simple substrate, coenzyme M. Methyl-coenzyme M (CH_3-S-CoM) is reduced with coenzyme B (HS-CoB) to methane and CoM-S-S-CoB.

For the reduction steps electrons from the oxidation of H_2 are used. This input is either directly or via coenzyme F_{420}. Hence the most methanogenic bacteria contain two distinct hydrogenases to oxidize H_2: a coenzyme F_{420}-reducing hydrogenase, and a coenzyme F_{420}-non-reducing enzyme. In Figure 25, the five enzymes of this pathway that are metalloenzymes are indicated in red.

H_2 is a reductant for this pathway and exposing the cells to 100% hydrogen in the gas phase results in the detection of the reduced forms for different enzymes in this pathway (Right panel, trace A), MCR, in both the red1 and red2 forms, hydrogenase, in the Ni-C form, and heterodisulfide reductase. Exposure to CO_2 in the absence of H_2 causes the oxidation of these enzymes (Right panel, trace B). MCR is converted into the MCRox1 forms, and the hydrogenase into the Ni-A form. The formylmethanofuran dehydrogenase is not detectable anymore. The individual spectra of each of these enzymes can be found in Appendix C.

A special case of whole cell EPR spectroscopy is when a recombinant paramagnetic protein is overexpressed in a standard host like *Escherichia coli*. The over expressed protein will give an EPR signal, and the background of the host is hardly detectable. This allows the study of the enzyme under more natural conditions without the need for purification when the paramagnetic center or the protein itself are highly unstable.

2.8 Selected Reading

Quantitative EPR

1. *Quantitative EPR* (2010) Eaton, G.R., Eaton, S.S., Barr, D.P., Weber, R.T., Springer, New York

Redox Titrations

2. *Redox potentiometry: Determination of midpoint potentials of oxidation-reduction components of biological electron-transfer systems* (1978) Dutton, P.L., *Meth. Enzymol.* 54, 411-435

3. *Stoichiometric redox titrations of complex metalloenzymes* (2002) Lindahl, P.A., *Meth. Enzymol.* 354, 296-309

Freeze quench

4. *Ribonucleotide reductase: kinetic methods for demonstrating radical transfer pathway in protein R2 of mouse enzyme in generation of tyrosyl free radical* (2002) Gräslund, A., *Meth. Enzymol.* 354, 399-414

Whole cell EPR

5. *Reappraisal of the e.p.r. signals in (post)-ischaemic cardiac tissue* (1989) Van der Kraaij, A.M.M., Koster, J.F., Hagen, W.R., *Biochem. J.*, 264, 687-694

6. *Evidence for a new type of iron containing electron carrier in mitochondria* (1961) Beinert, H., Lee, W., *Biochem. Biophys. Res. Commun.* 5, 40-45

7. *EPR spectroscopy of components of the mitochondrial electron-transfer system* (1978) Beinert, H., *Meth. Enzymol.* 54, 133-150

3. Simulations of EPR Spectra

To gain an understanding of how EPR spectra are built up and how they have to be interpreted, the creation of such spectra via simulations is very instructive.

3.1 Simulation Software

For the simulations we will be using the software package that comes together with the Biomolecular EPR spectroscopy book by Wilfred Hagen (www.bt.tudelft.nl/biomolecularEPRspectroscopy). The minimal system requirements to run these programs are: off-the-shelf PC with Windows XP and a monitor with at least 1280 pixels resolution in the x-dimension. The used file format (input and output) is: bare Ascii files with 1024 amplitude entries (program EPR File Converter can be used to convert from other file formats to this standard).

As a general philosophy this set of eight programs is intended to cover the most common problems in numerical analysis (simulation and manipulation) of CW biomolecular EPR powder spectra. The design of the programs is towards maximization of "ease of use": each program is set up around a standardized single-window user interface that should be intuitive and (nearly) self-explanatory. Choices of mathematical and numerical approaches are automatic and thus completely screened off from the user.

There are eight programs which can be divided into four categories: an introductory, practicing tool, three number crunchers for a variety of anisotropic spectra, two programs to modify experimental and/or simulated spectra, and two programs for the special cases of radicals in solution and for integer-spin systems with strong zero-field interactions.

The program 'Simple Spectrum' is mainly intended as an introductory, hands-on learning tool for those who are inexperienced in EPR spectral simulation.

The program 'Hyperfine Spectrum' expands the options available for the spectral simulation. First of all it allows the simulation of two species at the same time. Each species can have central (metal) hyperfine splittings and also ligand superhyperfine splittings. Also, for each component a 'checkbox' can be ticked for the program to use the natural isotope distribution for one of the elements Cu, Mo, or W.

The program 'GeeStrain-5' can generate sum spectra of up to five different components subject to broadening by *g*-strain. This situation is typically encountered in respiratory-chain complexes and in complex enzymes with multiple electron-transfer prosthetic groups. In a *g*-strained spectrum the linewidth is no longer described by three components W_x, W_y, W_z, along the molecular axes, but by six components of a symmetrical *g*-strain tensor. Each component can be positive or negative. *g*-Strain results in characteristic patterns of skewed and asymmetric features in the powder spectrum. *g*-Strain is a reflection of protein conformational distributions.

The program 'Visual Rhombo' is for half-integer high-spin systems with strong zero-field interaction, which frequently occur in a variety of iron proteins and in high-spin cobalt proteins. It can be used in two ways. Firstly, entering a value for the rhombicity h = E/D will generate a complete set of effective g-values, which may be traced back in experimental spectra. Secondly, spectra (sums of all intradoublet sub spectra) can be generated, where realistic simulation of experimental data frequently requires the rhombicity to be distributed ('D-strain'), and one has to specify the width and the number of digital steps of the simulation.

The program 'EPR File Converter' is a tool to convert experimental data files to the standard (1024 ascii amplitude values) used by the programs in this package. As an extra option 'EPR File Converter' can also produce the first integral (the EPR absorption spectrum) or the second derivative of an experimental or a simulated spectrum.

The program 'EPR Editor' can do several things. When difference spectra have to be produced it is important that the two source spectra have the same frequency. The program normalizes two experimental spectra to the microwave frequency of one of them. The program also provides the numerical value of the second integral of a spectrum (or a difference spectrum) calculated between two limits defined by the user. The second integral is required for quantification (or: spin counting). 'EPR Editor' can also read-out g-values from experimental data which can help with the spectral simulations.

The program 'Isotropic Radicals' is for radicals in solution that tumble so fast as to completely average out any anisotropy in the g- and A-values.

The program 'Single Integer Signal' is for integer spin systems subject to strong zero-field interaction, e.g. Fe(II) complexes, reduced 3Fe-4S clusters or reduced 2Fe oxo clusters, which typically exhibit only a single transition within their highest non-Kramers doublet detectable in parallel-mode EPR and, with increased linewidth and reduced intensity, in normal-mode EPR. 'Single Integer Signal' generates these two spectra simultaneously (parallel-mode in bright red, normal mode in dark red). The shape is a function of three parameters only: an effective g-value and two linewidth parameters that model rhombic D-strain.

Note that the following type of problems are not covered by any of the here provided programs: (i) systems with non-colinear tensors (except for g-strain broadening); (ii) intermediate-field high-spin systems (i.e. systems with electronic Zeeman and zero-field interactions of comparable strength); (iii) data from pulsed techniques. It is not easy to design universally applicable simulators for these problems, whose solution is anyway sufficiently complex as to call for either teaming up with a specialist or, alternatively, to become a specialist oneself and to develop dedicated code for specific cases.

3.2 Simulations

Most EPR spectra from metalloproteins can be satisfactory simulated on basis of only 6 parameters: three *g*-values and three linewidths (W_i in Gauss; Note that it is defined differently in the literature, either as the distance between the inflection points or linewidth at half height, and will therefore have different values). If there is hyperfine interaction, then three additional parameters have to be provided: the hyperfine splitting constants (A_i in Gauss: distance between the hyperfine lines). The cause of the hyperfine interaction, interaction with a nuclear spin of the ion in question (hyperfine interaction) or with the nucleus of a ligand (superhyperfine interaction), is of no concern for the simulation, since they are treated in the same way.

If we are dealing with a single crystal, then there is only one EPR line (all molecules have the same orientation), which might be split up by (super)hyperfine interaction. A single line is also obtained for a radical in solution or for a small metallocomplex in solution (rapid tumbling).

If we are dealing with a powder or with a frozen solution of a paramagnetic species, then it may be somewhat more complicated. The spectrum is then dependent on the symmetry of the magnetic environment of the paramagnet.

For all simulations below, we must choose a 'spectral window': an approximation of the field range that would be required when actually measuring the sample on the EPR spectrometer. We first take a window for the $g = 2$ region and use a microwave frequency of 9500 MHz.

Organic Radicals

A free radical, e.g. an unpaired electron in a π-orbital system of a benzene ring, has no fixed environment. Any local asymmetry experienced by the electron will be average out in time: the electron has a totally symmetric environment and shows an ***isotropic*** spectrum

Open the program **isotropicradicals**. Set the frequency to 9500 MHz, B-min to 3300 gauss, and B-max to 3500 gauss.

1) Take "*g*-Value" = 2 and "Linewidth" = 3 G (so $g_x = g_y = g_z$ and $W_x = W_y = W_z$). Note that in this example there are no (0) interacting nuclei.

Spectrum: _____.dat

2) Now take this radical and put it on a nitrogen atom. The electron is now fixed in position, but we assume a rapid tumbling of the molecule in solution, which likewise results in an 'averaging out' of any asymmetry in the environment of the unpaired spin. Natural nitrogen (^{14}N) has a nuclear spin of 1. Take several values for the hyperfine interaction and make four spectra:

A-value = 25 G	Spectrum: _____.dat
A-value = 15 G	Spectrum: _____.dat
A-value = 5 G (That looks funny. Why?)	Spectrum: _____.dat
A-value = 2 G	Spectrum: _____.dat

3) Now give the radical an interaction with three equivalent protons (nuclear spin ½). Take *A*-value = 40 G for all of them. Explain the result by drawing a 'stick' spectrum'.

Spectrum: _____.dat

4) As (3), but now all protons have been exchanged by deuterons. These have a different nuclear spin (I=1) which is about 0.31 times as strong, so take *A*-value = 12.4 G. This exercise is sometimes useful to predict whether an actual experiment (exchange of H by D in a compound) is worthwhile in order to verify one's interpretation.

Spectrum: _____.dat

5) The radical now interacts with three non-equivalent protons;

For proton 1: *A*-value = 5 G
For proton 2: *A*-value = 10 G
For proton 3: *A*-value = 20 G

Predict the spectrum by making a 'stick spectrum' by hand. Why does the simulated spectrum looks so funny?

Spectrum: _____.dat

6) As discussed in section 2.6 some paramagnetic species, in particular radical species, are only present during a reaction on a very short time scale. Even if you trap the radical at the right time interval it might be unstable enough that it would immediately react. One way to deal with this is to use radical traps that will react with the radical. There is a whole set of these traps available. The challenge is to find one that will react with your radical and form a unique reaction product that also shows a specific EPR signal. The most commonly used spin traps are alpha-phenyl N-tertiary-butyl nitrone (PBN) and 5,5-dimethyl-pyrroline N-oxide (DMPO). The method involves the addition of the product radical to a nitrone spin trap resulting in the formation of a spin adduct, a nitroxide-based persistent radical, that can be detected using EPR. The spin adduct usually yields a distinctive EPR spectrum characteristic of a particular free radical that is trapped. The identity of the radical can be inferred based on the EPR spectral profile of their respective spin adducts such as the *g*-value, but most importantly, the hyperfine-coupling constants of relevant nuclei. Unambiguous assignments of the identity of the trapped radical can often be made by using stable isotope substitution of the radical's parent compound, so that further hyperfine couplings are introduced or altered.

An example of a nitrone is 2,2,6,6-tetramethyl-1-piperidinyloxyl (TEMPO). The expected radical signal is split in three because of the interaction of the unpaired electron with the nitrogen nucleus.

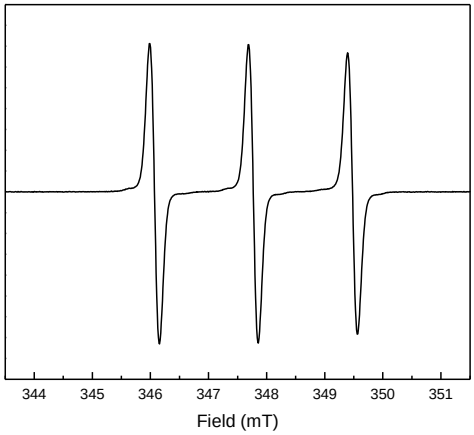

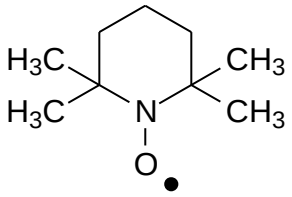

Below is the reaction scheme for the metal-mediated transformation of α-carbonyl diazomethanes into carbene radicals with diazo radicals as key intermediates (Li, F. *et al.* Metal-Diazo Radicals of a-Carbonyl Diazomethanes. *Sci. Rep.* **6**, 22876; doi: 10.1038/srep22876 (2016)). A diazo radical is formed and is stable in the presence of RhCl(cod)2. In this case the blue spectrum (left) is obtained: a quintet EPR signal of an Rh-diazo radical. Upon immediate reaction with DMPO the blue spectrum on the right is obtained: a triplet-of-sextets EPR signal due to the DMPO-trapped diazo radical (DMPO-N•). The diazo radical is unstable and N_2 is released forming a carbene radical. Upon reaction with MNP the purple spectrum is obtained: a doublet-of-triplets EPR signal due to the MNP-trapped carbene radical (MNP-C•). If the carbene radical is trapped with DMPO the green spectrum is obtained: a sextet EPR signal due to a DMPO-trapped carbene radical (DMPO-C•).

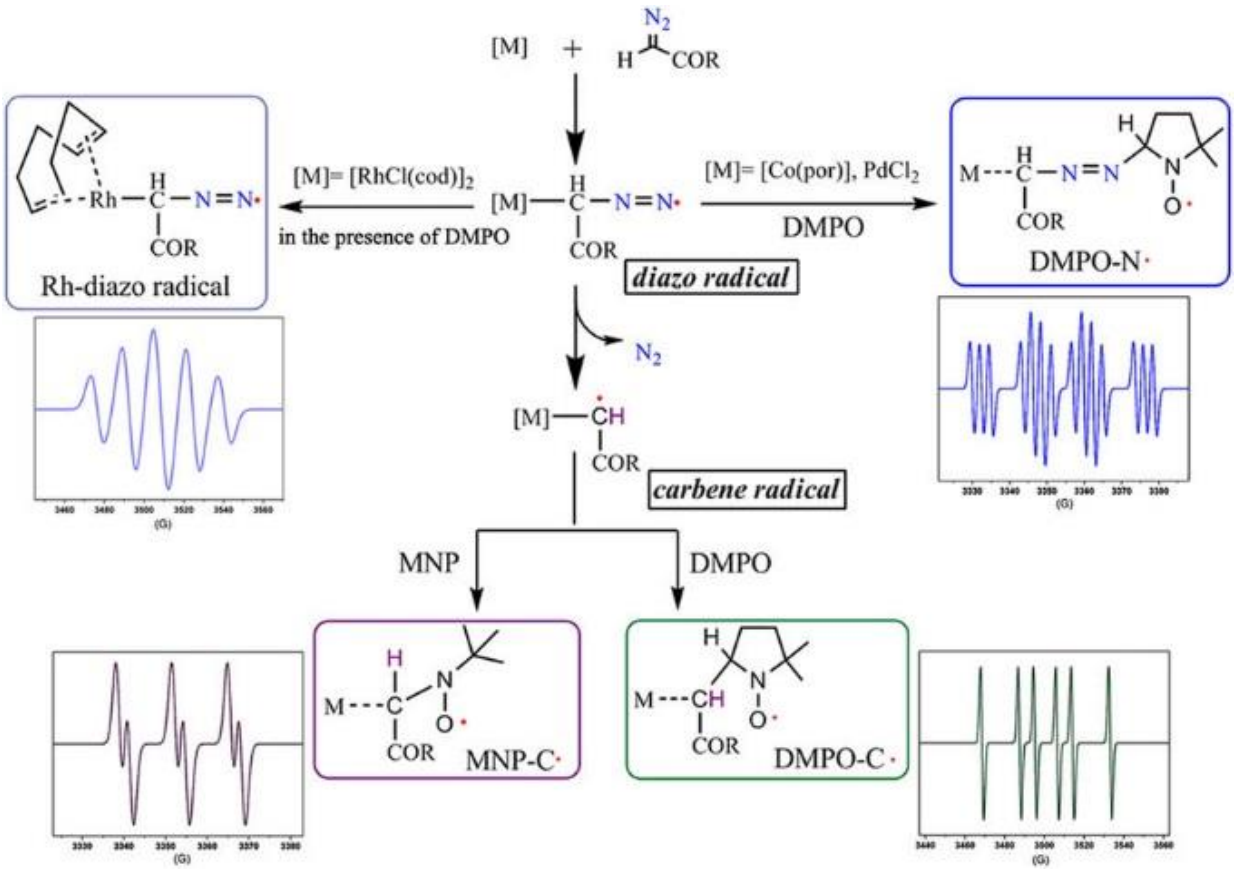

Your task is to reproduce these spectra.

Set the frequency to 9500 MHz, B-min to 3300 gauss, and B-max to 3500 gauss.

Take “g-Value” = 2 and “Linewidth” = 1 G. From the structures shown next to the EPR spectra try to figure out what nuclei are interacting with the unpaired radical shown.

Assignment of Complex Radical Spectra

When multiple nuclei interact with an unpaired electron with different sets of hyperfine couplings, the spectra become very complex and can include hundreds or even thousands of lines. The next set of steps can be taken to help analyze these isotropic EPR spectra and understand the underlying splitting pattern.

i. Make sure the overall spectrum is symmetrical. If this is not the case you are dealing with more than one paramagnetic species. You have to look for measuring conditions that allow the spectra to be measured with different ratios. If that is possible you could try to isolate each species by a series of subtractions. If this is not possible you will have to try to insulate and analyze both spectra separately.

ii. If the structure of the molecule is available, identify all nuclei with a nuclear spin in the α- and β-position relative to the unpaired electron. Use splitting diagrams to reproduce the splitting pattern and use a Pascal triangle to determine the relative intensity of the hyperfine lines for each environment.

iii. To get to the first multiplet (multiplet A), take the distance between the first two lines at the low field (e.g., left side) in the spectrum. Measure out this same distance to detect if there are more lines that belong to this multiplet. Keep in mind that the multiplet might not be symmetrical due to overlap with lines from other multiplets.

For the ethanol radical $HOCH_2CH_2\bullet$ the first step looks like this:

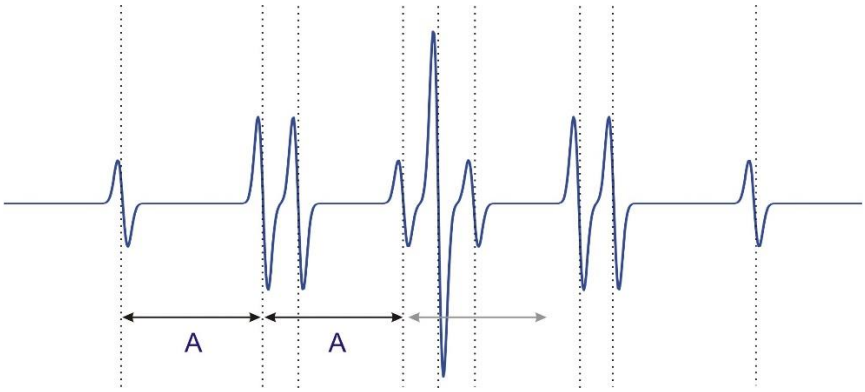

The distance between the first and the second lines indicates the smallest hyperfine constant. A third line at the same distance further upfield completes the first 1:2:1 triplet (multiplet A). If you try to look even further (gray arrow) you will see that there is no peak at this distance.

iv. To find the second multiplet, measure the distance from the outermost line to the first line which does not form part of multiplet A. This distance corresponds to the hyperfine coupling constant of the next multiplet (labelled B). Just as with multiplet A keep on measuring the same distance towards higher field until all the lines of multiplet B have been identified.

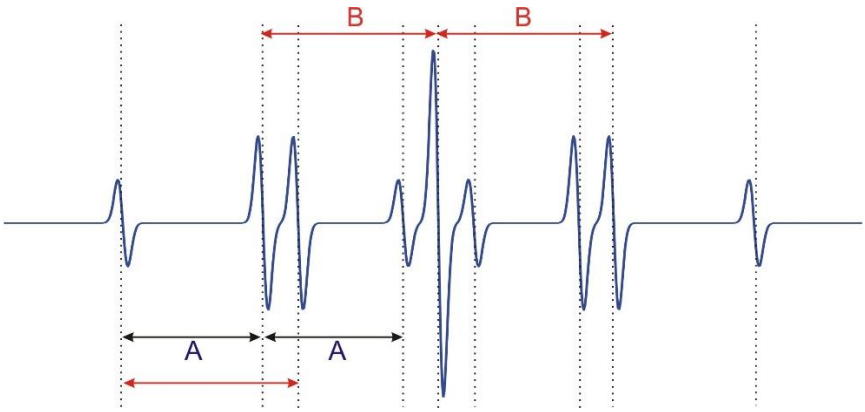

v. Since multiplet B has a larger hyperfine coupling constant A than that of multiplet the hyperfine pattern of multiplet A will be superimposed on each component of multiplet B.

vi. Repeat steps 6-9 until all multiplets have been identified. If you somehow get stuck on the left side also start from the right side and try to get to the middle of the spectrum.

The distance between the outermost line and the first line which is not is part of multiplet A (in this case the third line from the left) is the hyperfine coupling constant for multiplet B (red arrow). The same distance can be measured out one more but not a second time, indicating we also found the complete pattern for multiplet B. The pattern that emerges is that B is the larger constant causing a three-fold split and each B line is split in three with the smaller A value. Multiplet B connect the centers of all the multiplets A. Therefore, the two remaining multiplets can be added to the scheme. In this case we are done with the hyperfine pattern.

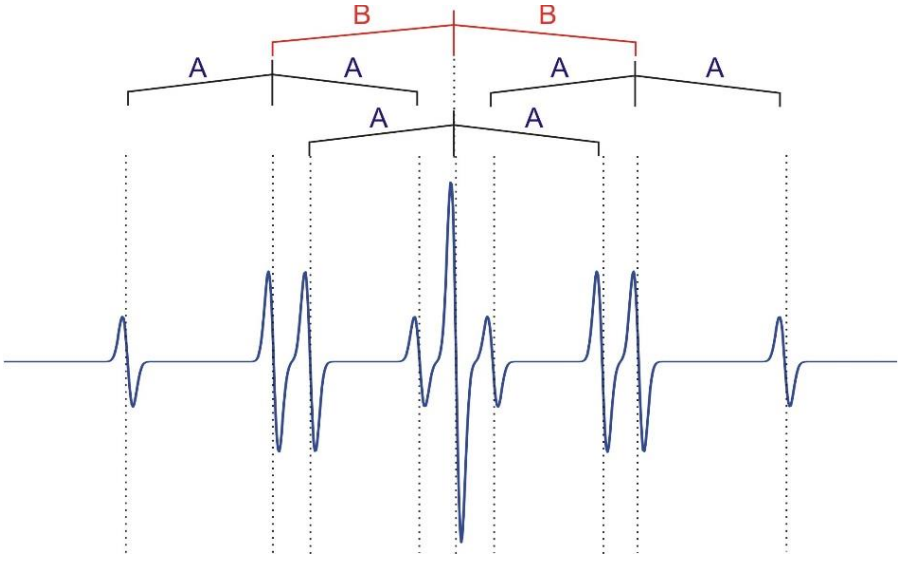

7) Dependent on the reaction conditions it is also possible to generate a different ethanol radical: $CH_3CH\bullet OH$. The EPR spectrum for this species is shown below. For clarity, a simulated spectrum was overlaid (in blue). A worksheet with a larger figure can be found on page 3-17.

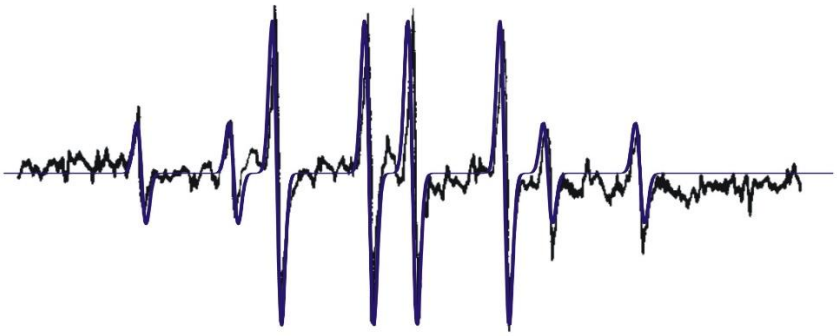

Try to come up with the stick diagram to explain the splitting pattern.

8) Shown are the structure of a radials species and its EPR spectrum. Try to explain the splitting pattern.

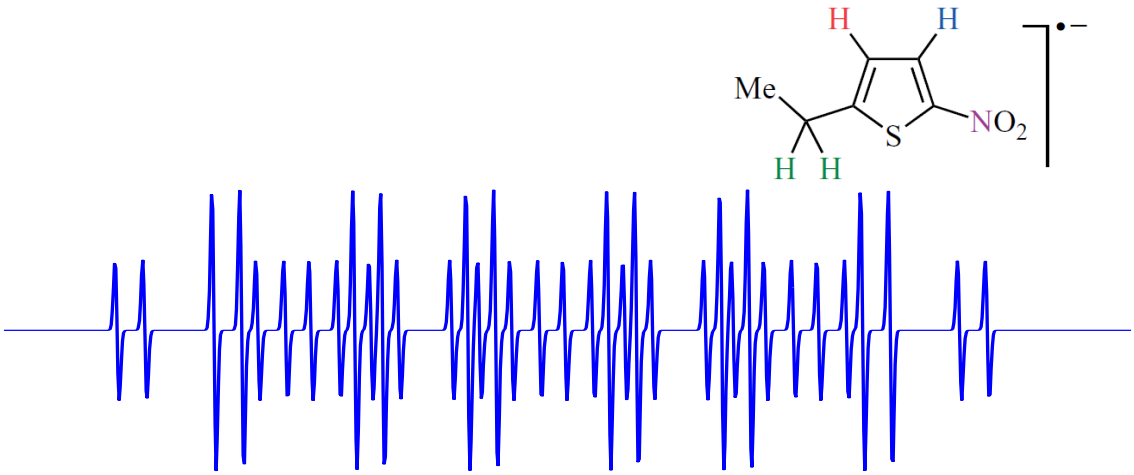

Load the spectrum 'Sim Example 01.txt' into the isotropic radicals program. Use these settings: Frequency = 9500 MHz, B-min = 3370 gauss, and B-max = 3420 gauss. Use a linewidth of 0.1 gauss. A worksheet can be found on page 3-18.

If you have a hard time with this spectrum load 'Sim Example 02.txt' instead. In this sample the interaction with the smallest value of *A* has been removed. A worksheet can be found on page 3-19.

9) Sometimes the hyperfine pattern can be completely deceiving. Here is an example that involves a cobalt radical (I = 7/2) with superhyperfine interactions of 1 N and 3 H nuclei. Take now:

B-min: 3100 gauss
B-max: 3700 gauss.

For Co: A-value = 50 G
For nitrogen: A-value = 20 G
For hydrogen: A-value = 10 G

This spectrum looks misleading! Just try to pinpoint the cobalt splitting!

Spectrum: _____.dat

To understand this, also perform the simulation where the interaction of the nitrogens and hydrogens are removed.

Spectrum: _____.dat

10) Simulation of the dimethyl nitroxyl radical.

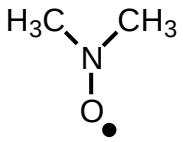

Start by loading the experimental spectrum, "dimethylnitroxyl.dat".
Adjust the parameters:

Frequency:	9766.13 MHz
B-min:	3380 gauss
B-max:	3580 gauss.

This spectrum is different from the other nitrones due to the two methyl groups that are close enough to interact with the unpaired electron. First try to find the central g-value (This should be a position in the middle of the whole spectrum). Then introduce the nitrogen and hydrogen hyperfine splittings. First use an equal value of A for both nuclei and try to match the overall splitting pattern. After that, play around with the A-values.

g = _____, W = _____, A_N = _____, A_H = _____, Spectrum: _____.dat

Powder Spectra

11) *Axial symmetry (so $g_x = g_y \neq g_z$).* Use the program **simplespectrum**.

As an example we take the line shape of an Fe-S cluster.

Frequency:	9500 MHz
B-min:	3000 gauss
B-max:	3800 gauss.
g_{zyx}:	2.054, 1.925, 1.925
W_{zyx}:	10, 16, 16

Now we have to take a finite value for *cos Theta*, since we are no longer dealing with a total symmetric environment. See the discussion in section 1.5 for an in-depth discussion. Playing with the parameter *cos Theta* gives a good impression of how a powder spectrum is actually built up. We therefore take a number of *cos Theta* values (*Phi* is 1 in all cases)

cos Theta:	1	Spectrum: _____.dat
cos Theta:	2	Spectrum: _____.dat
cos Theta:	5	Spectrum: _____.dat
cos Theta:	15	Spectrum: _____.dat
cos Theta:	50	Spectrum: _____.dat
cos Theta:	100	Spectrum: _____.dat
cos Theta:	150	Spectrum: _____.dat

Then make a spectrum with W_{zyx} = 2, 4, 4 and *cos Theta* = 50. Compare this with the previous one with *cos Theta* = 50. What is causing the difference and why?

Spectrum: _____.dat

Compare the spectra with *cos Theta* = 50, 100 and 150 to see when the number of spatial orientations was large enough (i.e. when the powder was 'fine' enough). For this you have to import the spectra in for example Origin and make an overlay plot of the three spectra.

Note: to obtain the best simulation, one always has to increase the number of space orientations until the spectrum doesn't change anymore (infinitely fine powder).

12) *Rhombic symmetry (so $g_x \neq g_y \neq g_z$).*

We take the line shape of a rhombic Fe-S cluster with

Frequency:	9500 MHz
B-min:	3100 gauss
B-max:	3900 gauss.
g_{zyx}:	2.02, 1.91, 1.85
W_{zyx}:	10, 13, 18

Now also *Phi* needs to be larger than 1, since the *x*- and *y*-directions are no longer equivalent. 'Play' again with the parameter *Phi* and see what the effect is. Take:

cos Theta	Phi	
1	1	Spectrum: _____.dat
80	1	Spectrum: _____.dat
80	2	Spectrum: _____.dat
80	5	Spectrum: _____.dat
80	15	Spectrum: _____.dat
150	100	Spectrum: _____.dat

(On older slower computers you might notice a slight increase in computing time. In the last spectrum 15000 first derivative Gaussian lines had to be calculated.)

Spectra of Simple Metalloproteins

13) Simulation of the [2Fe-2S] (S = ½) signal detected in ferredoxin from *Clostridium pasteurianum*. First load the spectrum in 'WinEPR' and read out the *g*-values. Then load the experimental spectrum 'Cp2Fe_spec' into the 'simplespectrum' simulation program. Adjust the parameters:

Frequency:	9630 MHz
B-min:	3005 gauss
B-max:	4005 gauss.

g_{xyz} = _____, _____, and _____
W_{xyz} = _____, _____, and _____
cos Theta = _____, and *Phi* = _____

Spectrum: _____.dat

Overshoot Effect on Cu Spectra

Use the program **hyperfinespectrum**.

Effect of hyperfine interaction on the EPR powder line shape – Hyperfine interactions can have a highly deceiving effect on the appearance of powder-type spectra. This is illustrated here with copper (I = 3/2).

14) To start, we first produce an axial spectrum of a metalloprotein without a nuclear magnetic moment:

Frequency:	9500 MHz
B-min:	1900 gauss
B-max:	3900 gauss
cos Theta:	150
Phi:	1
g_{zyx}:	2.90, 2.07, 2.07
W_{zyx}:	20, 20, 20

Spectrum: _____.dat

It should be easy enough to recognize the parameters in the spectrum.

15) We now include the hyperfine interaction of a copper nucleus as it usually appears in the so-called 'type II' (non-blue) copper proteins:

Metal A_{zyx}: 150, 15, 15

Spectrum: _____.dat

The simulation now takes 4 times as long. This is due to the fact that our unpaired electron in reality 'feels' 4 different magnetic fields. The real spectrum essentially is an overlap of 4 different spectra.

16) We then shift the g_z-value slowly into the direction of the g_{xy}. All other parameters, also the A values, remain unchanged. Make 4 spectra, with:

g_z: 2.4	Spectrum: _____.dat
g_z: 2.3	Spectrum: _____.dat
g_z: 2.2	Spectrum: _____.dat
g_z: 2.1	Spectrum: _____.dat

Note the changes in the *x,y*-direction. The extra line appearing at the high-filed side of the g_{xy}-line is called an ***overshoot*** line. This occurs rather often in *X*-band EPR spectroscopy and not only for Cu proteins. Interpretation of such spectra is often impossible, especially so when we also deal with very rhombic spectra. To analyze such spectra, measurement of the sample at a higher microwave frequency is desired.

Complex Metalloenzyme Spectra

17) In the next example we will simulate a spectrum for the cobalt-containing vitamin B_{12} cofactor that can be found in several different types of enzymes.

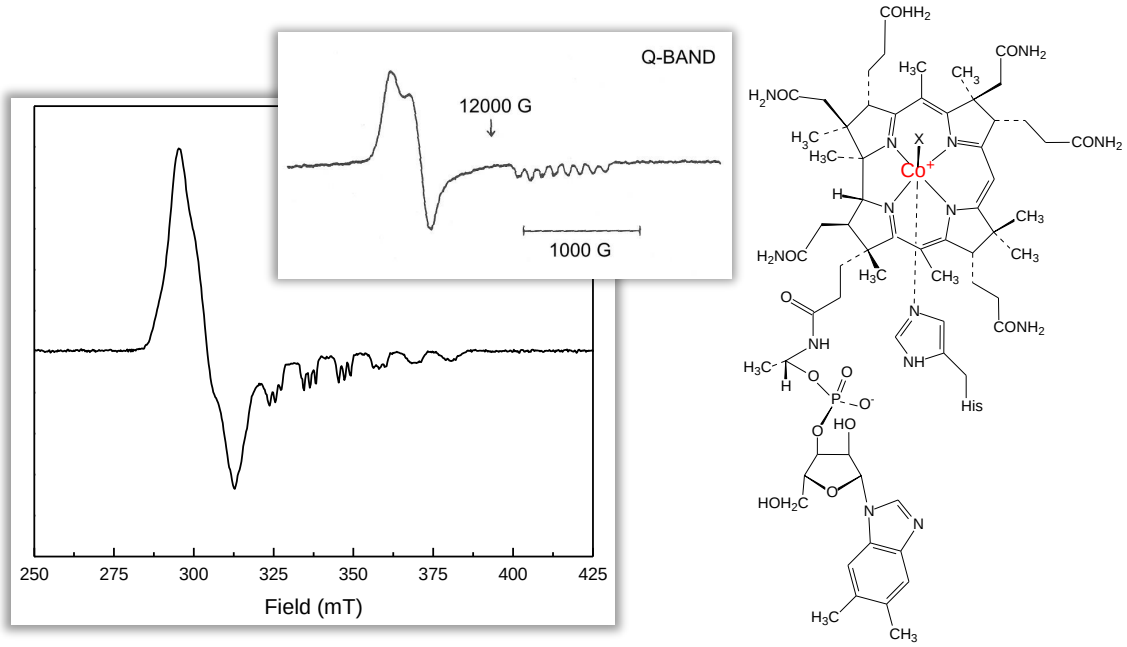

Before we start a small description of the origin of this spectrum is needed. It is due to a Co(II) ion ($3d^7$) with the unpaired electron in the d_{z2} orbital. That means that the electron is not interacting with the four nitrogen ligands in the ring. It is interacting, however, with an axial nitrogen ligand from a histidine residue. The 8 hyperfine lines due to the interaction with the Co nucleus can be easily detected in the *Q*-band spectrum. The low-field lines are more difficult to detect in the *X*-band spectrum. Also note from the Q-band spectrum that the spectrum is not completely axial. For convenience the *g*-values for the simulation are already provided.

Again we will be using the program **hyperfinespectrum** with the spectrum 'Co_spec'.

Hint 1: Use a relative large linewidths for the g_x- and g_y-peaks with a small Co splitting. Assume there is no N splitting for these peaks.

Frequency:	9596.06 MHz	g_{xyz} =	2.275, 2.220, and 2.006
B-min:	2000 gauss	W_{xyz} =	_____, _____, and _____
B-max:	5000 gauss	$A^{Co}{}_{xyz}$ =	_____, _____, and _____
		$A^{N}{}_{xyz}$ =	_____, _____, and _____

Spectrum: _____.dat

Repeat the simulation assuming all N in the sample has been replaced with the ^{15}N isotope (I = ½)

Spectrum: _____.dat

18) The nickel in methyl-coenzyme M reductase is also present in a tetrapyrrole ring. The spectra however are very different. In this case two redox states are accessible: Ni^{3+} ($3d^7$) and Ni^{1+} ($3d^9$). The figure shows the spectra for the MCRox1 form (Ni^{3+}) and the MCRred1 form (Ni^{1+}). In both cases the free electron is in the $d_{x^2-y^2}$ orbital and interacts with all four of the tetrapyrrole nitrogen atoms. Note that this interaction should result in 9 hyperfine lines. Instead 10 hyperfine lines are detected on the g_{xy}-peak of the MCRred1 signal. Since there are no other interactions with the nickel this means that the g_x and g_y have to be slightly different (which was proven by doing measurements at higher frequency, see Chapter 1, Fig. 36). Try to simulate either (or both) of the MCR spectra, 'MCRox1_spec' or 'MCRred1_spec'.

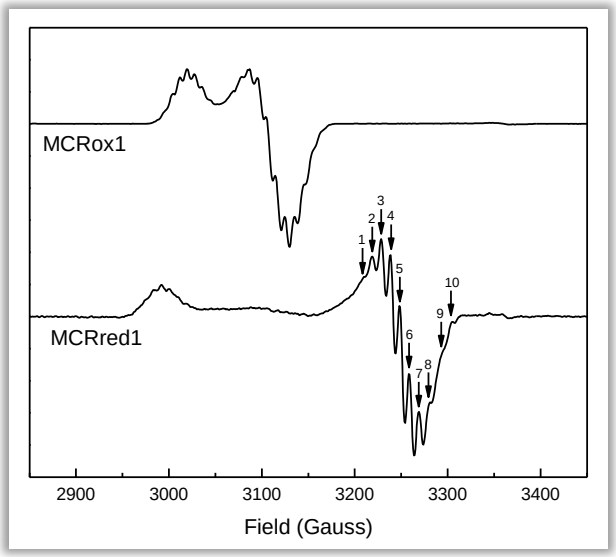

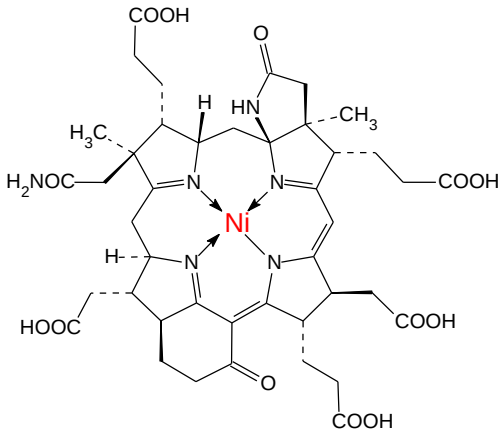

Frequency: 9596.06 MHz (ox1) g_{xyz} = _____, _____, and _____
B-min: 2000 gauss W_{xyz} = _____, _____, and _____
B-max: 5000 gauss A^N_{xyz} = _____, _____, and _____

Spectrum: _____.dat

Frequency: 9431.35 MHz (red1) g_{xyz} = _____, _____, and _____
B-min: 2000 gauss W_{xyz} = _____, _____, and _____
B-max: 5000 gauss A^N_{xyz} = _____, _____, and _____

Spectrum: _____.dat

Integrals and Signal Intensity

19) In this exercise you will determine the ratio of two EPR signals (MCRred1 and MCRox1) present in a mixture of two signals.

Load the two spectra ‘Ox1Red1.spc’ and ‘CuSt.spc’ into WinEPR:

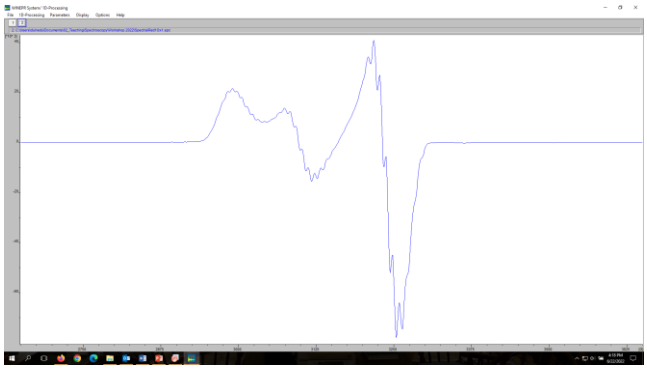

First determine the double integral. Under ***1D-Processing*** select ***Integrate Region***. The menu bar changes. Now under ***Integration*** select ***Define Integrals***. With the left mouse button click on the baseline on both sides of the signal. You can drag the lines that appear if they are not completely on the right spot.

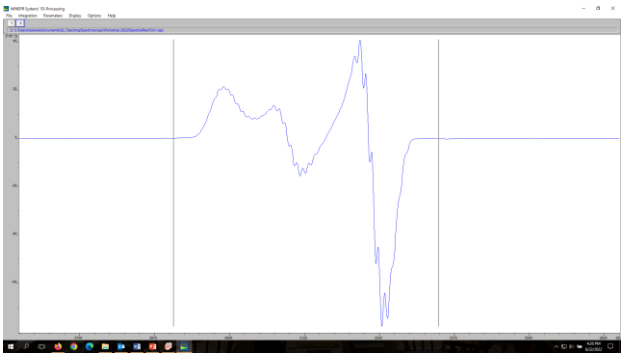

Click the right button and the first derivative appears (the actual absorption signal).

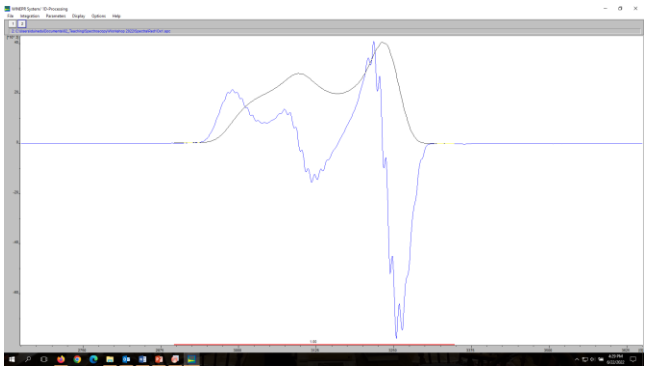

Under ***Integration***, select ***Integral type*** > ***Double***

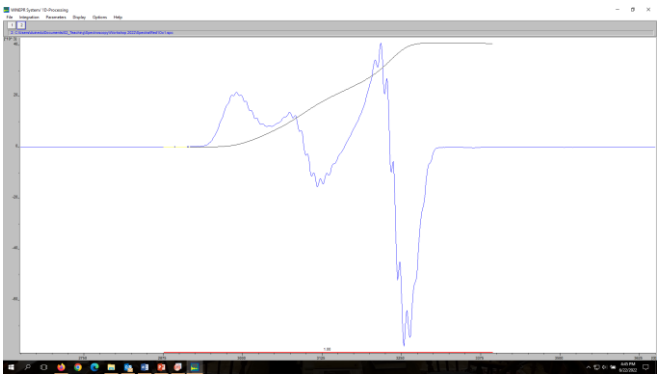

Under ***Integration***, select ***Report***. Write down the number under ***DI/N*** (normalized double integral)

Do this for both Spectra.

To calculate the concentration of the mix use the formula:

$$C_u = \frac{I_{n(u)} \cdot C_{st}}{I_{n(st)}}$$

where

C_u	spin concentration of unknown
C_{st}	spin concentration of standard
$I_{n(u)}$	normalized intensity of unknown
$I_{n(st)}$	normalized intensity of standard

The Copper Standard has a concentration of 10 mM

To be able to calculate the concentration of the individual EPR signals we need to subtract one of the signals and integrate the remaining signal.

For this we will use the program ***Hyperfine Spectrum***. Load the file named Red1Ox1.dat. This is a one column ASCII file. You can make that yourself by saving the Red1Ox1 spectrum as an ASCII file with the WinEPR program. This file will contain 3 columns. You need to use EXCELL or Origin to remove the two extra columns and save the file as a bare bone ASCII file (TAB separated). You still need the parameter settings from the WinEPR program:

Frequency: 9.379902 GHz
Center Field: 3150
Sweep: 1000

In the Hyperfine Spectrum menu you need to enter the parameters. Use MHz instead of GHz and use the beginning of the spectrum and the end values: 2650-3650

You can now use the simulation parameters for Mcr-red1 you determined in exercise 18. NOTE that since the spectra where measured on different machines that values are a bit off due to differences in calibration. Adjust the g values of the simulation to get a good overlay with the mixed spectrum (Shift all peaks with the same value).

Save the simulation.

Now open up EPR Editor. Load both the mixed spectrum (A spectrum) and the simulation (B spectrum). Also add the parameters for both.

With the B-amplitude set to 0 integrate the spectrum. Write this number down.

Now Change the B-amplitude until most of the Red1 signal is gone. The simulation software save the simulation as a normalized file. You need to use a very large B-amplitude value to be able to subtract out the Red1 signal. NOTE that it is very hard to get and accurate fit of the hyperfine and there might be some residual signal left:

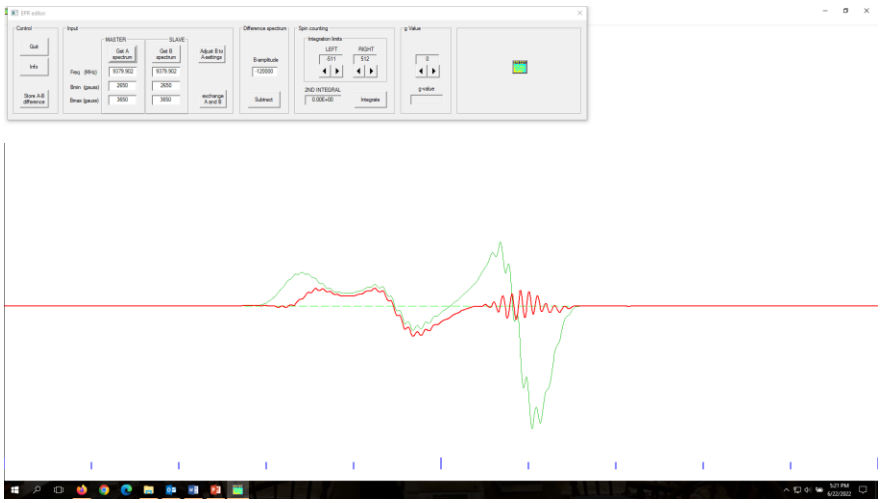

Integrate the remaining signal.

NOTE that the integral values are different than the ones determined with WinEPR. This is because with WinEPR we wrote down the normalized values only.

Use the two integral values for the mixed spectrum and the remaining Ox1 spectrum to determine the ration and/or the concentration of both species in the mixed spectrum.

3.3 Work Sheets

E5

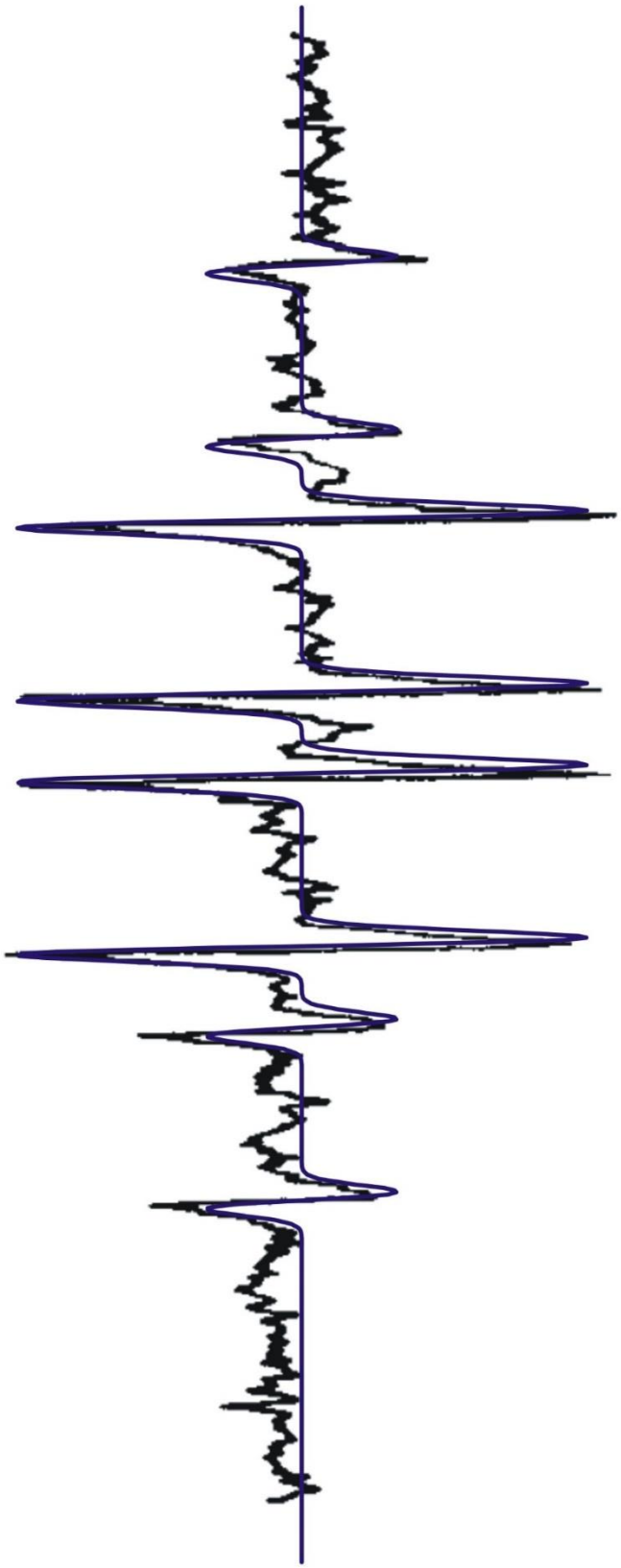

E6

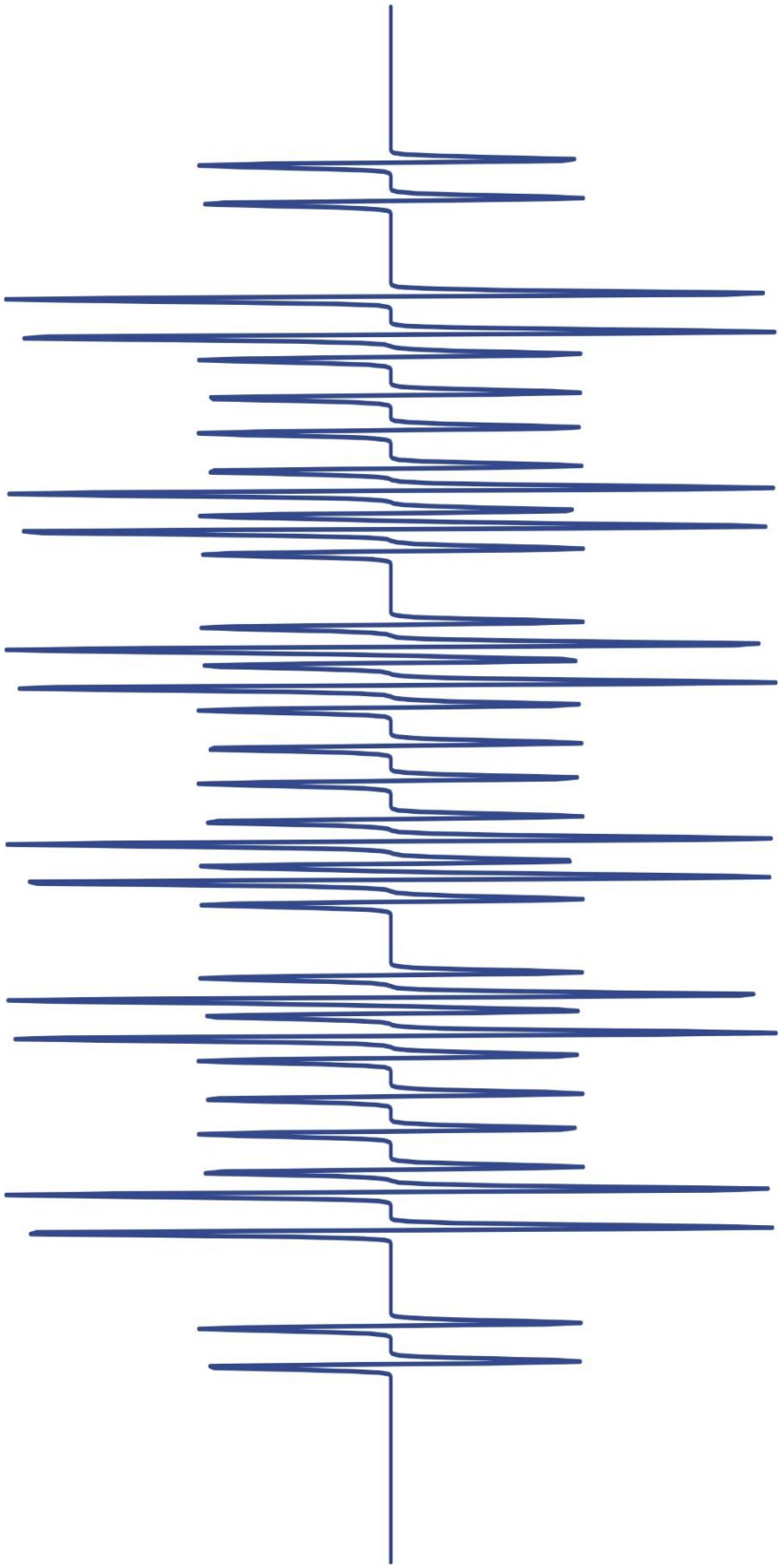

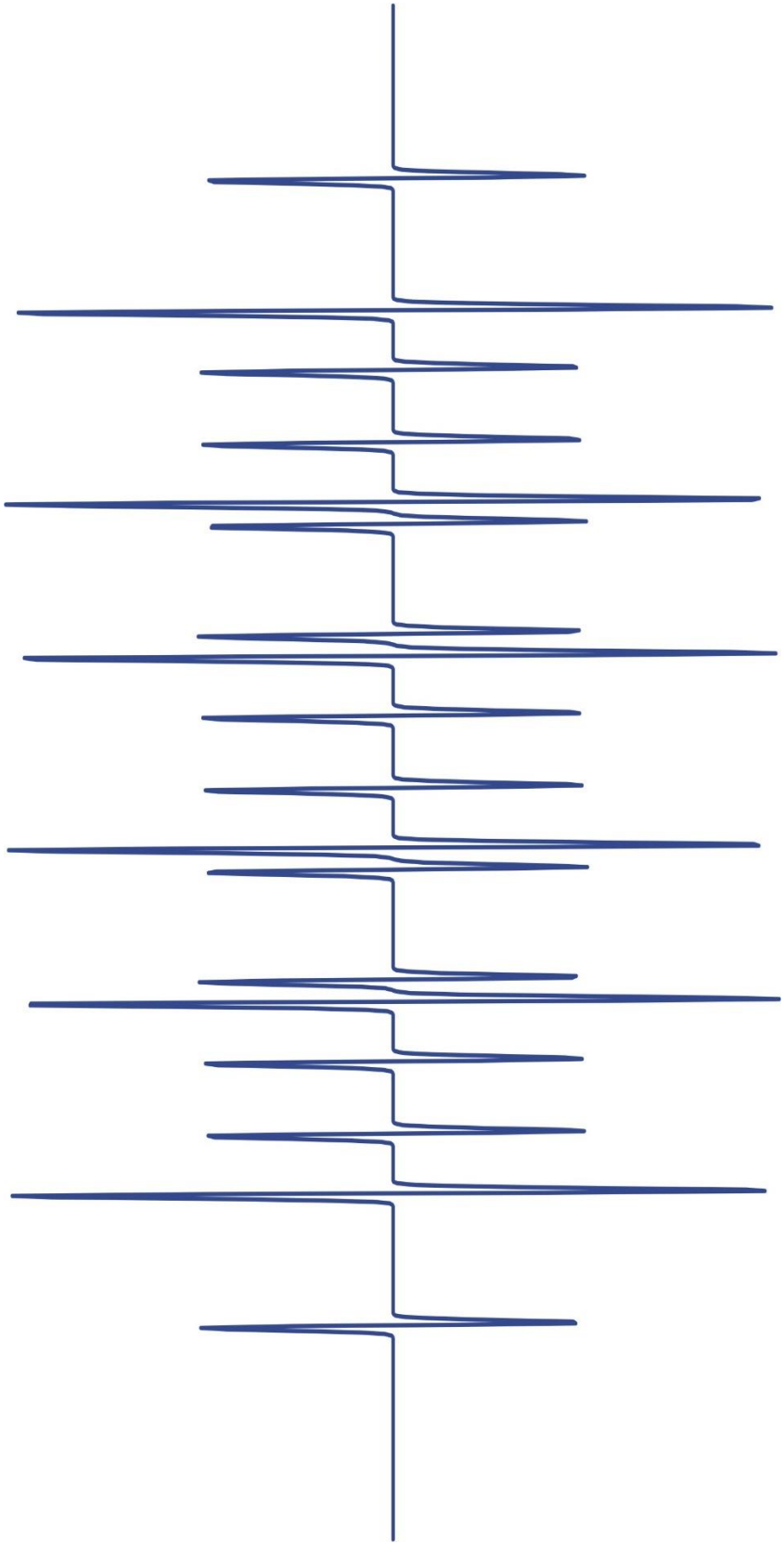

4 Selected samples

4.1 Organic Radicals in Solution

2,2,6,6-tetramethyl-1-piperidinyloxyl (TEMPO)

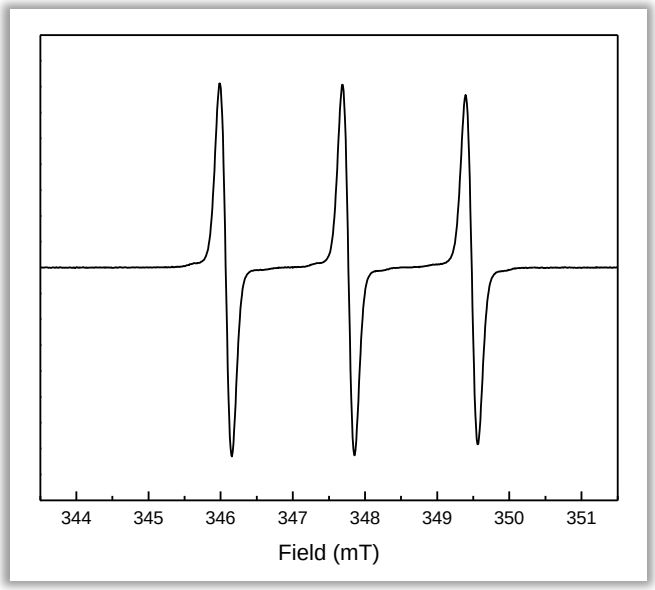

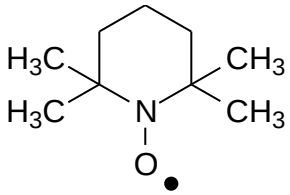

dimethylnitroxyl radical

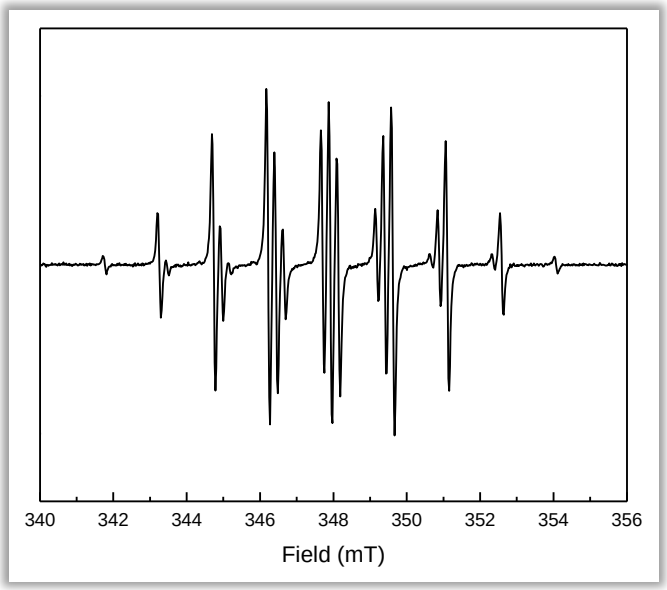

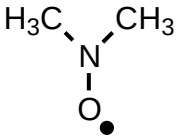

4.2 Single Metal Ions in Proteins

V in chloroperoxidase

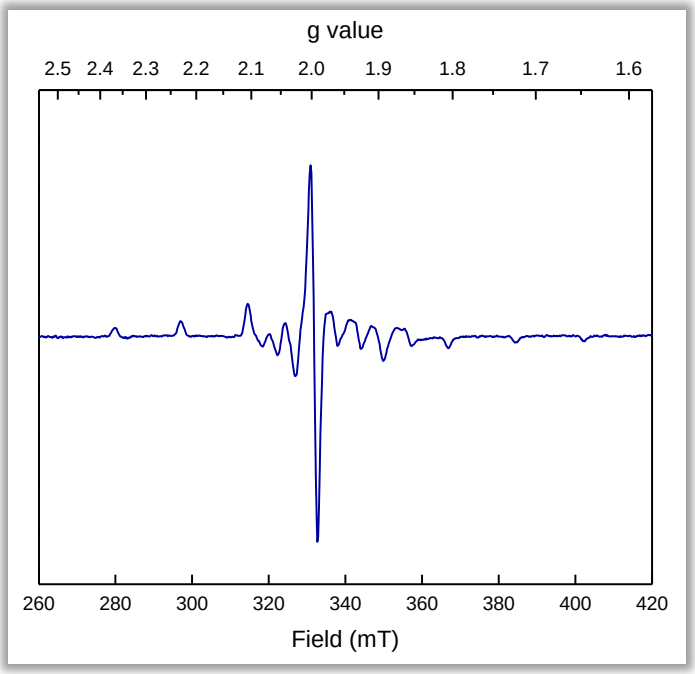

In the reduced form of the enzyme, the spectrum of V^{4+} (d^1) can be observed. Because vanadium has axial symmetry, its powder spectrum consists of two major peaks ($g_\perp$ = 1.95 and $g_{//}$= 1.98). Vanadium possesses one stable isotope ^{51}V with I = 7/2. Therefore each peak will be further split into eight ($2I$ + 1) lines. Due to overlap, not all lines are observed. On top of that the Hyperfine Coupling Constant (A) is very large, causing the hyperfine lines of $g_\perp$ to pass the $g_{//}$ peak, causing an effect termed ***overshoot***. The lines of the $g_\perp$ peak will have a different orientation when they are present on the site of the $g_{//}$ peak opposite to that of the position of the $g_\perp$ peak. The same is true for the hyperfine lines of the $g_{//}$ peak. (See also Fig. 20 in chapter 1)

Fe in Met-Myoglobin with bound CN

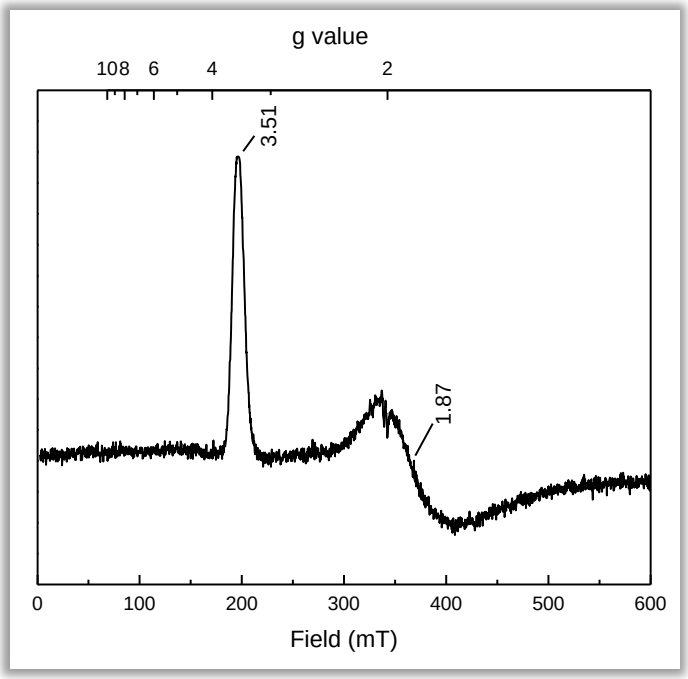

S = ½ (all g-values below 4)

Large spin angular momentum

Degenerate orbitals

High symmetry

HALS-type (highly anisotropic low spin)

$g_x^2 + g_y^2 + g_z^2 = 16$; therefore $g_z = 0.9$

Co in B_{12}

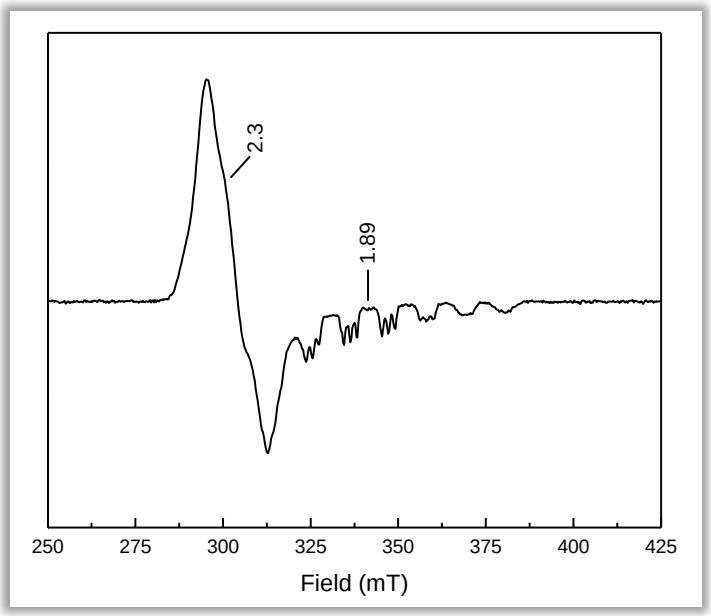

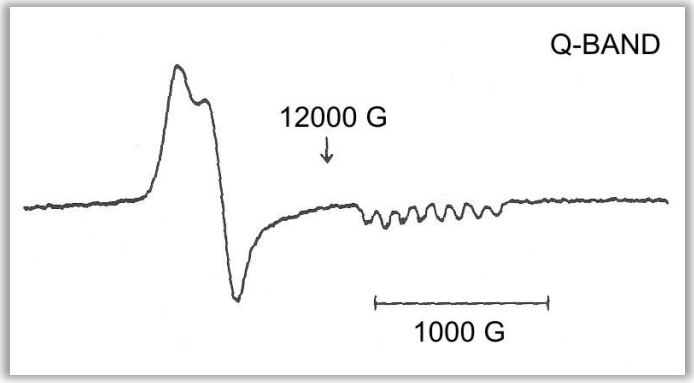

- $S = ½$
- Equally spaced hyperfine: $I = 7/2$; not V ($g_{av} < 2$), but Co^{2+} (d^7)
- Superhyperfine from N
- Vit B_{12}, nitrogen splitting from axial adenosyl

Examples of coupled cob(II)alamin in several different enzyme systems

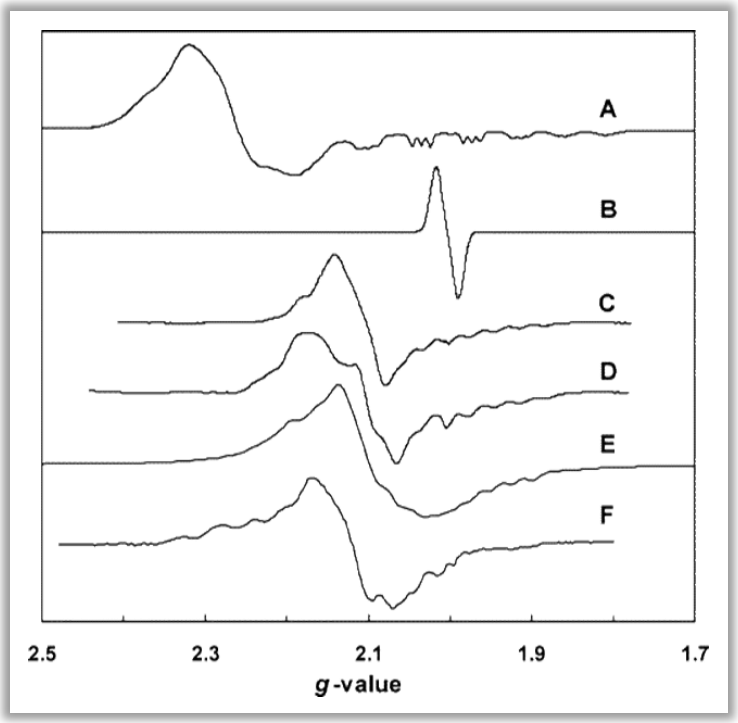

EPR spectra of enzyme bound cob(II)alamins and radicals. (A) Uncoupled cob(II)alamin in methanol:coenzyme M methyltransferase *MtaC* subunit. (B) A simulated malonyl radical. (C) Glutamate mutase and (*S*)-glutamate. (D) 2-Methyleneglutarate mutase and 2-methyleneglutarate. (E) Methylmalonyl-CoA mutase and succinyl-CoA. (F) Ribonucleotide triphosphate reductase, reductant and dGTP. The spectra have been converted to a *g*-value *x* axis to allow better comparison. (Taken from: Pierik et al. (2005) Biochemistry, 44, 10541–10551)

Nickel-containing rubredoxin

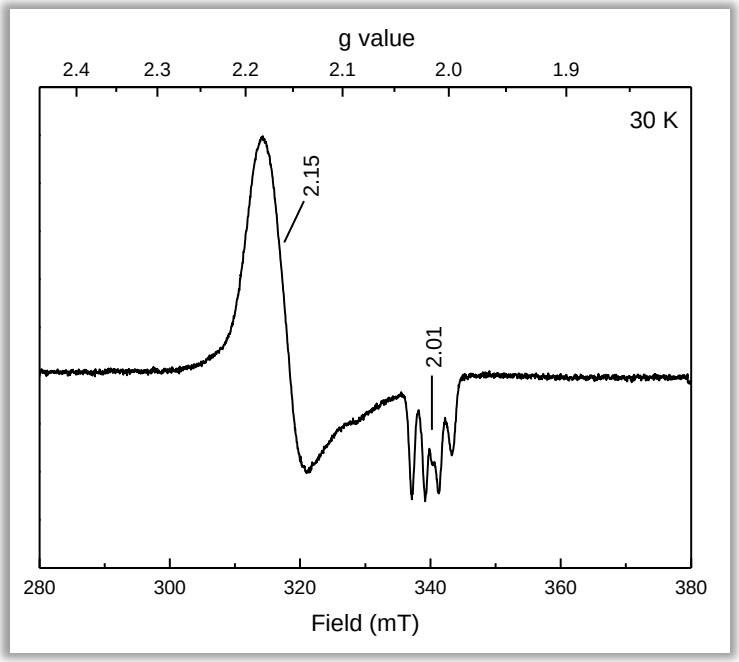

S = ½

Equally spaced hyperfine on g_2 (2.01): I = 3/2, the hyperfine of the $g_\perp$ (2.15) is not resolved

Ni(III) containing rubredoxin with CN^- bound

Sample was enriched in Ni^{61} (I = 3/2)

Mo in sulfite oxidase

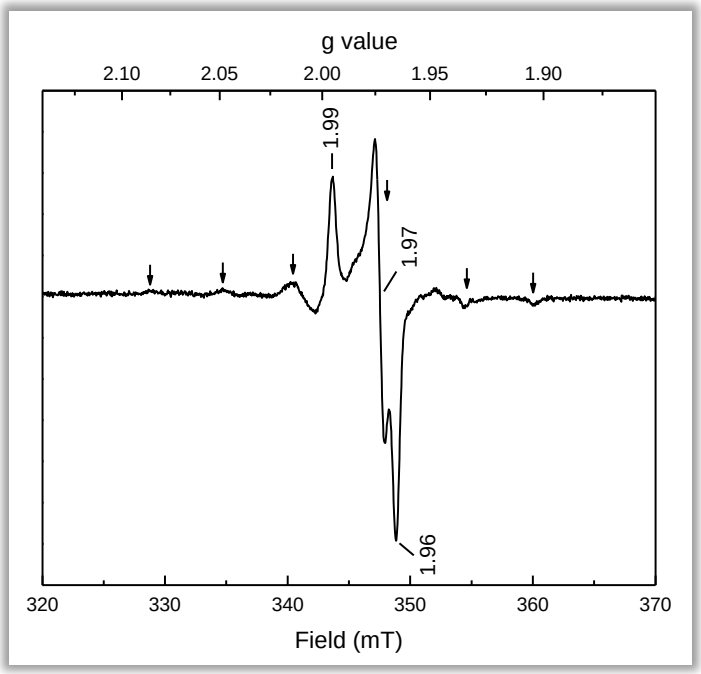

S = ½

$g_{av} < 2$

Mo(V) (d^1)

25% $Mo^{95/97}$ with I = 5/2

75 % Mo with I = 0

Each peak can give different hyperfine

W in aldehyde oxidoreductase

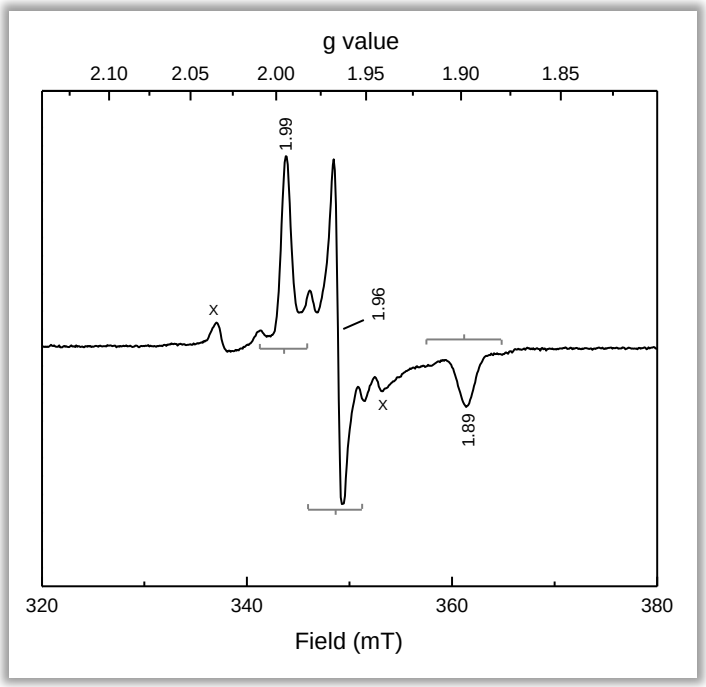

X = ignore
$S = ½$

$g_{av} < 2$

mayor component: $I = 0$

minor component $I = ½$

W: 87 %, $I = 0$; 13 % ^{183}W, $I = 1/2$

4.3 Multi-Metal Systems in Proteins

2-Mn catalase

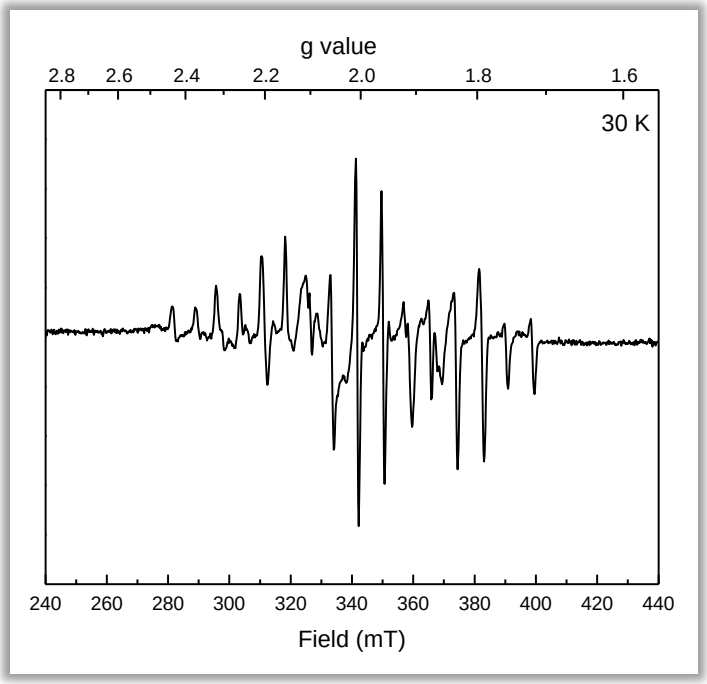

- S = ½
- Isotropic (derivative shapes)
- Hyperfine: equally spaced lines (80 G), only 16 lines
- Mn catalase: $Mn^{3+}Mn^{4+}$; I = 5/2
- Mn^{4+}, S = 2; Mn^{3+}, S = 3/2; AFC give S = ½

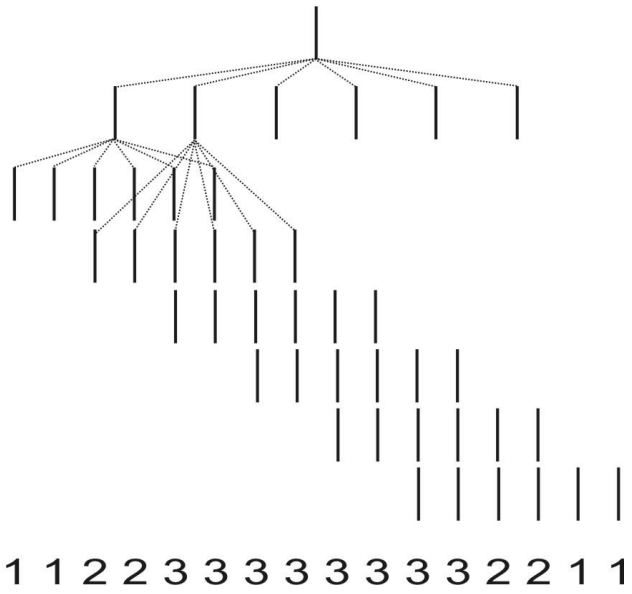

- Mn^{4+} stronger nuclear coupling
- Mn^{3+} : half times Mn^{4+} splitting
- Only 16 lines, could have been 36

4.4 Iron-Sulfur Clusters

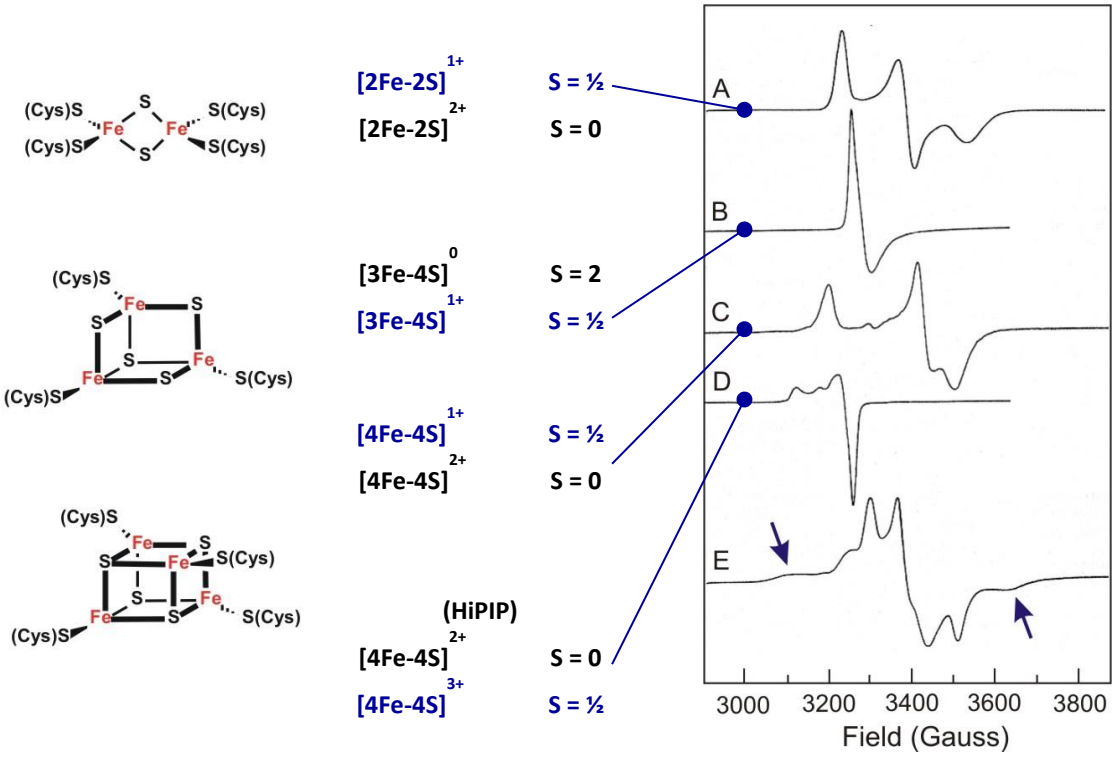

EPR spectra of different types of iron-sulfur clusters. On the left the basic structure of the cluster types is shown. In the middle redox states and their respective spin states are indicated. The panel on the left show the EPR spectra of the iron-sulfur clusters in ferredoxins from *Mastigocladus laminosus* (A), *Desulfovibrio gigas* (B), *Bacillus stearothermophilus* (C), *Chromatium vinosum* high-potential iron-sulfur protein (HiPIP) (D), and *Clostridium pasteurianum* 8Fe ferredoxin (E).

[4Fe-4S]$^{+}$ (S = ½)

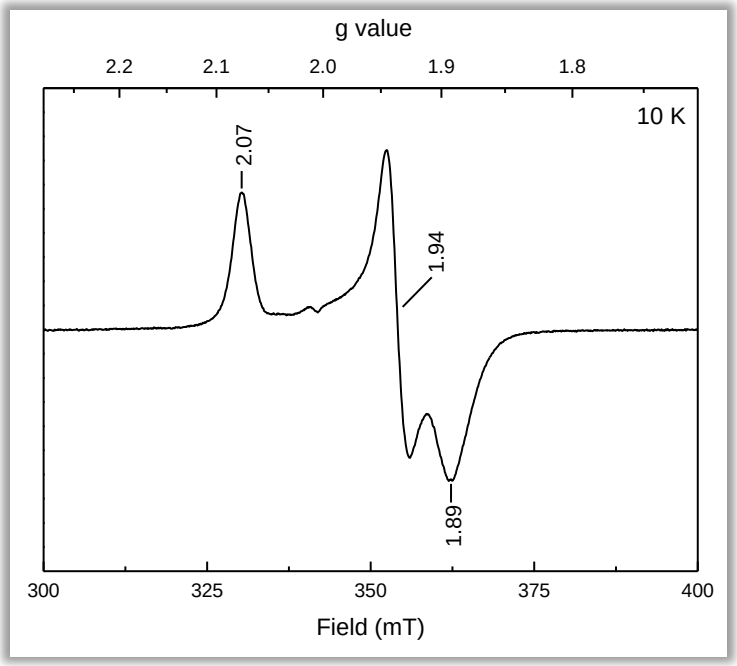

Rhombic *S* = ½

g-values average out close to 2

g-values below 4

Feature at *g* = 2.00 is due to a radical impurity

Signal measured at 10 K, not due to [2Fe-2S]. 4Fe clusters have low-lying excited states causing the signal to show fast relaxation.

Two interacting [4Fe-4S]$^{+}$ (S = ½)

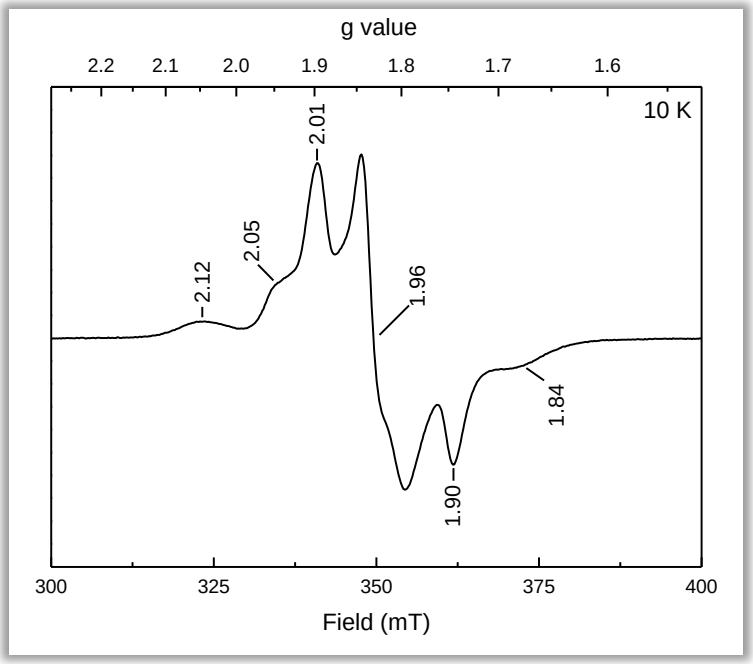

S = 1/2 (g_{av} close to 2)

2 clusters?

Origin: 8Fe ferredoxin containing two [4Fe-4S]$^{+}$ 12 Å apart.

Next step would be to run different temperatures, powers etc.,
to do a simulation of the EPR signal,
to run the same sample at Q or S-band. (If this is an interacting species the *g*-values will change.)

[4Fe-4S]$^{+}$ (S = 3/2)

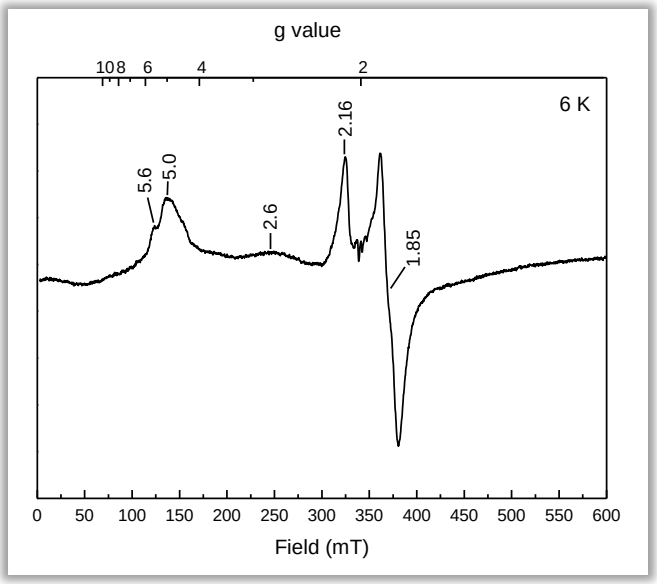

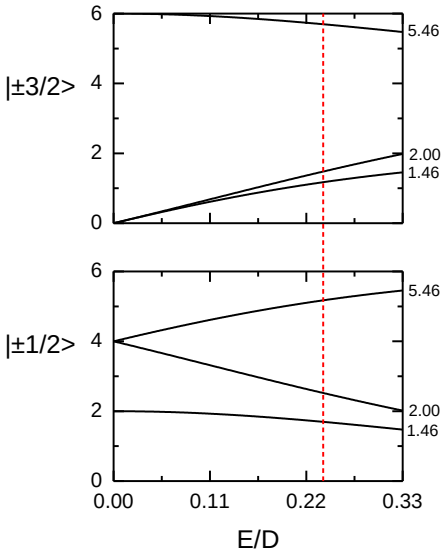

- S = 3/2 (all *g*-values below 6)
  20 % S = ½, 80 % S = 3/2
- S = ½ peaks detectable in the g = 2 region
- E/D ≈ 0.24
- D > 0

[4Fe-4S]$^{3+}$ (S = 1/2)

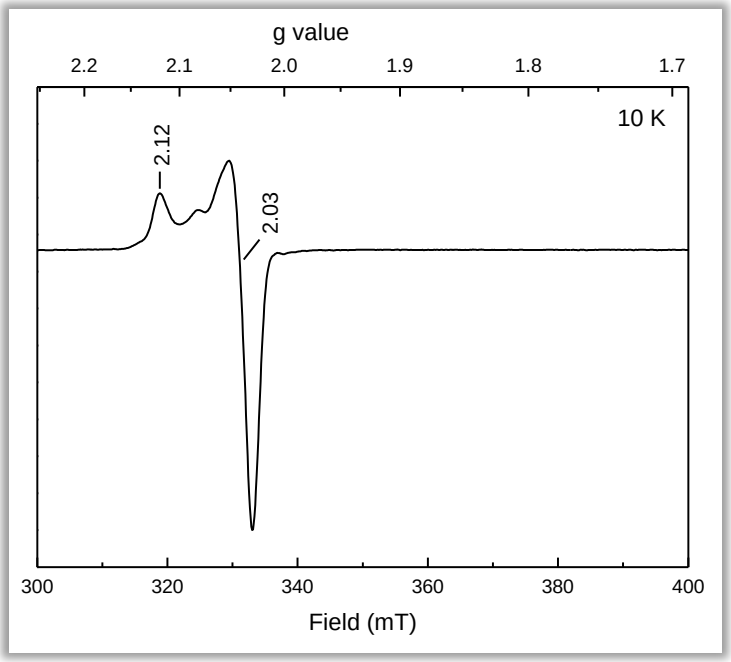

Rhombic S = ½

g-values average out close to 2

g-values below 4

Origin: [4Fe-4S]$^{3+}$ (HiPIP). In general more than on EPR signal associated with one cluster due to valence isomers that consist in this type of cluster

Feature at g = 2.00 is due to a radical impurity

Signal measured at 10 K, not due to [2Fe-2S]. 4Fe clusters have low-lying excited states causing the signal to show fast relaxation.

[Zn-3Fe-4S]$^{+}$ cluster (S = 5/2)

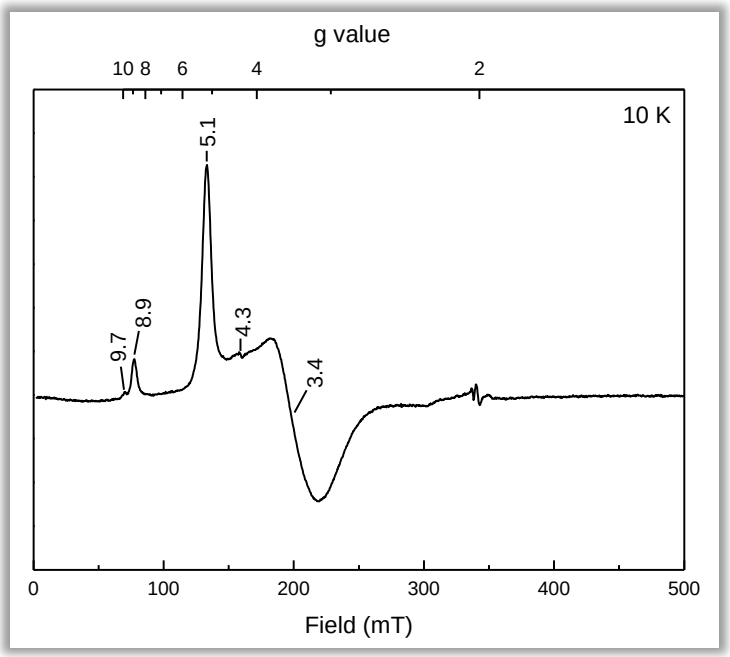

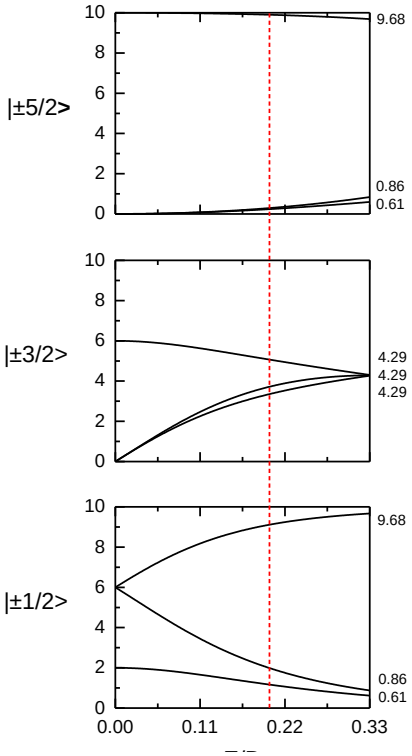

- S = 5/2 (all *g*-values below 10)
- E/D ≈ 0.2 (g = 9.67 is due to a different species)
- D < 0 (determined by temperature studies)

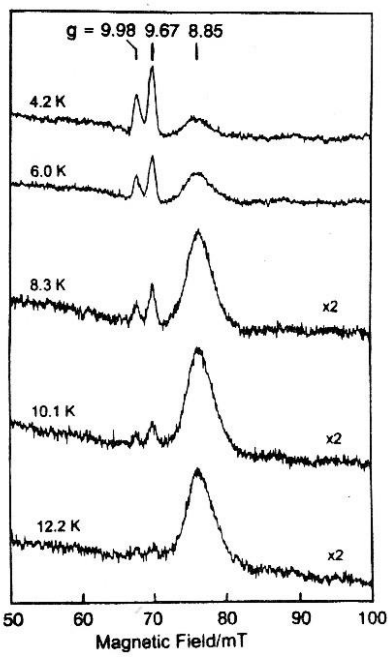

[2Fe-2S]$^{+}$ (S = ½)

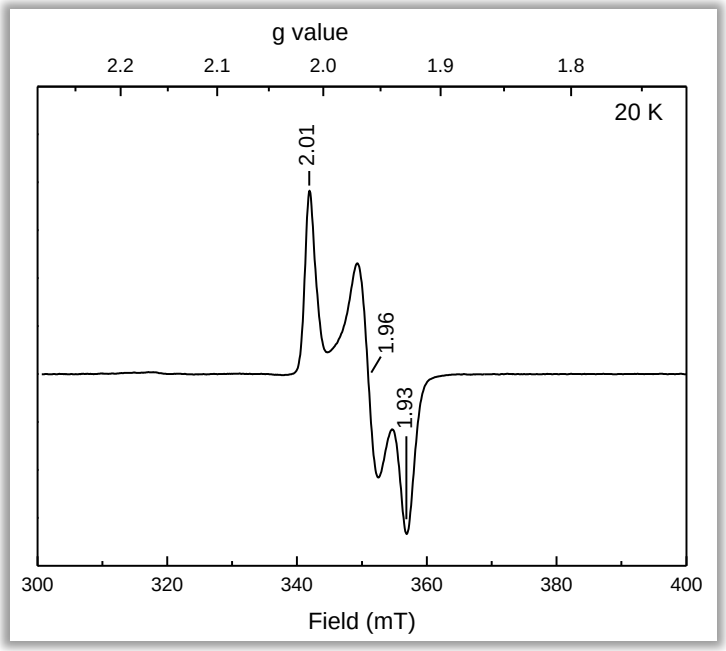

- Rhombic S = 1/2
- *g*-values average out close to 2
- *g*-values below 4

Origin: [2Fe-2S]$^{+}$ (*Clostridium pasteurianum* 2Fe Fd)

- Signal measured at 20 K, not due to [4Fe-4S]. 4Fe clusters have low-lying excited states causing the signal to show fast relaxation.

[2Fe-2S]$^{+}$ (S = 9/2)

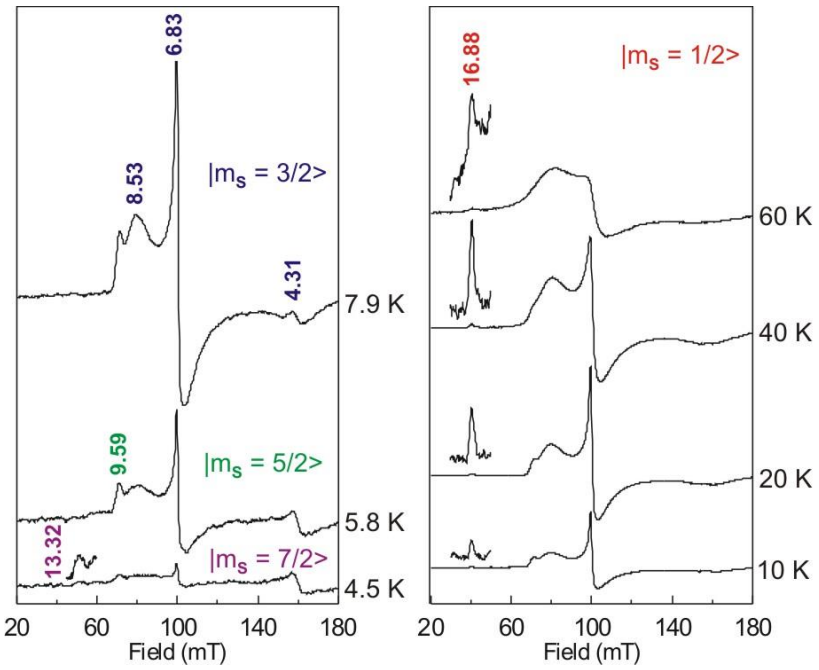

Sample is clearly a species with S > ½. Temperature studies needed to get correct spin state:

Origin [2Fe-2S]$^{+}$ cluster with S = 9/2 (Clostridium pasteurianum 2Fe Fd, C60S mutant)

E/D = 0.17, *g* = 2.00						
| ± 1/2 ⟩	0.35		17.32		0.66	
| ± 3/2 ⟩	3.51	(3.70)	10.05	(10.05)	5.75	(5.92)
| ± 5/2 ⟩	9.00	(9.24)	2.91		3.37	
| ± 7/2 ⟩	13.80		0.19		0.22	
| ± 9/2 ⟩	17.96		0.003		0.003	

D = - 1.4 cm^{-1} (log [$I_{10.05}/I_{9.24}$] versus 1/T)

Rhombogram for S = 9/2

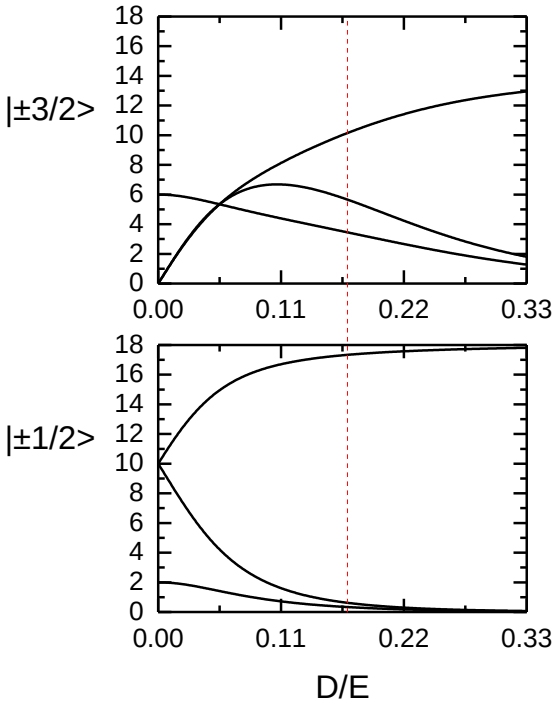

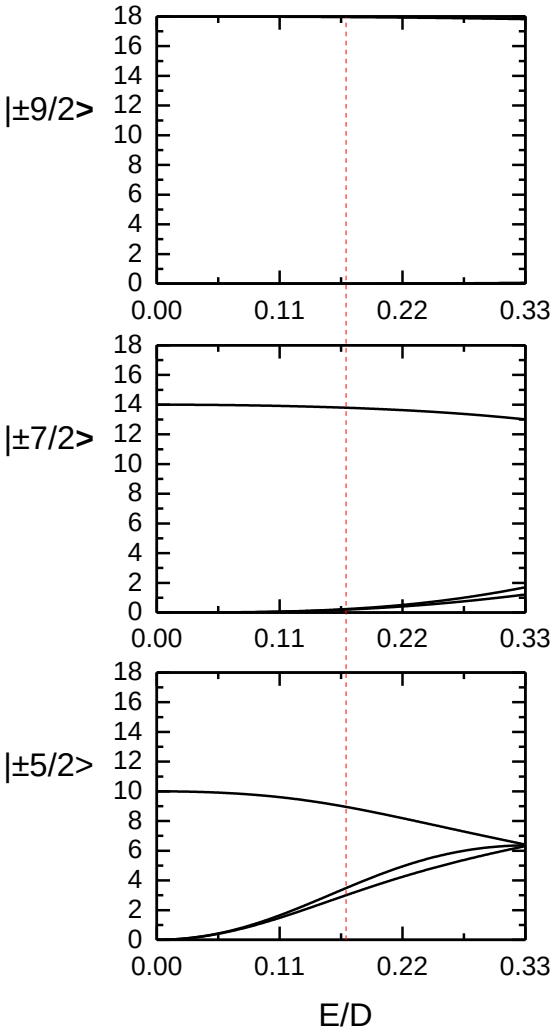

[3Fe-4S]$^{+}$ (S = ½)

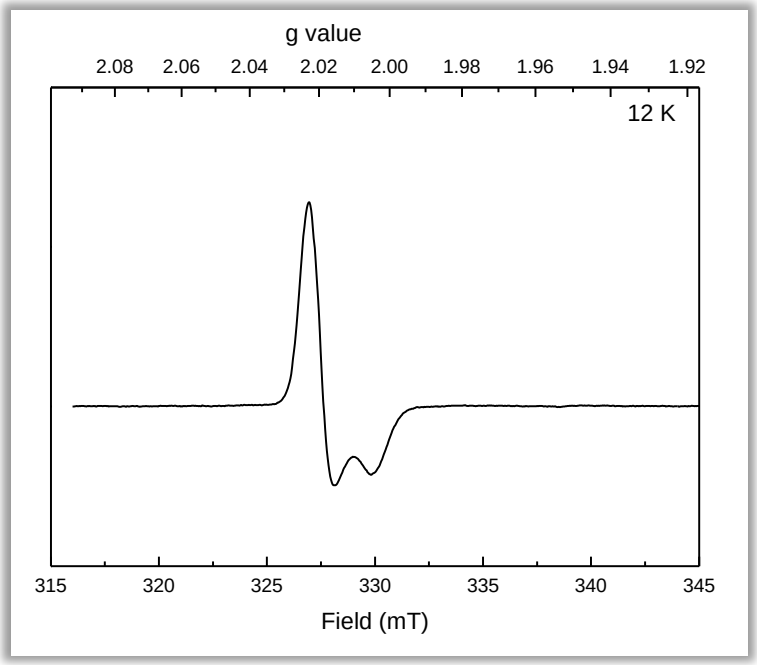

Axial *S* = ½

g-values average out close to 2

g-values below 4

Origin: [3Fe-4S]$^{+}$ (*Allochromatium vinosum* Hydrogenase)

[3Fe-4S]^{0} (S = 2)

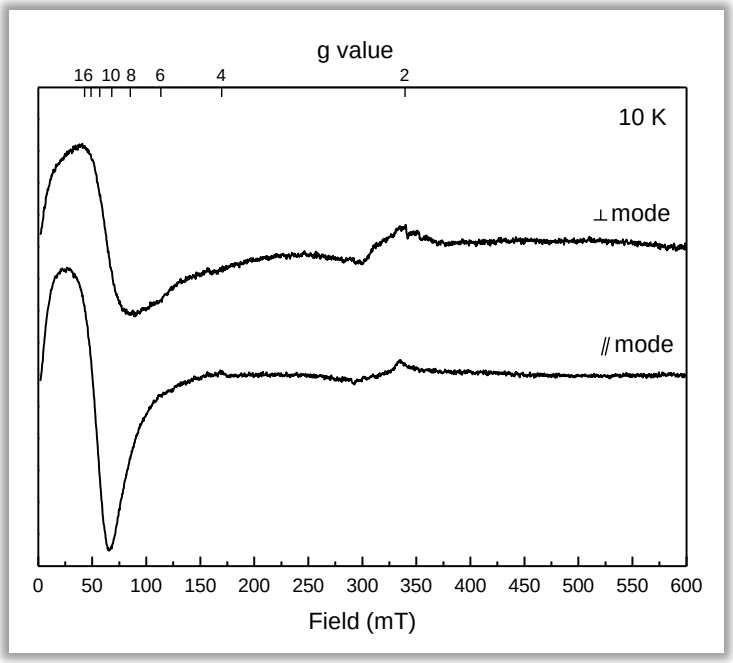

Origin: [3Fe-4S]^{0}, S = 2

[7Fe-9S-Mo-homocitrate] cluster in nitrogenase MoFe protein

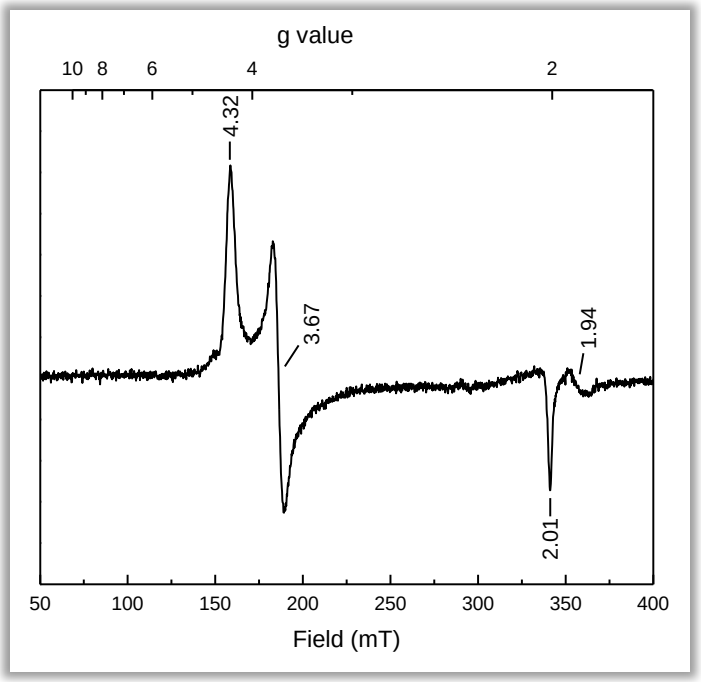

- $S = 3/2$
- E/D = 0.08, D < 0
- $g_{av} < 2$
- regular 4Fe signal present at 1.94
- $g = 6.0$ signal detectable at 20 K
- The nitrogenase MoFe protein contains the active site metallocluster called FeMo-cofactor [7Fe-9S-Mo-homocitrate] that exhibits an $S = 3/2$ EPR signal in the resting state

4.5 Inorganic Complexes

Cu^{2+} in $Cu(ClO_4)$

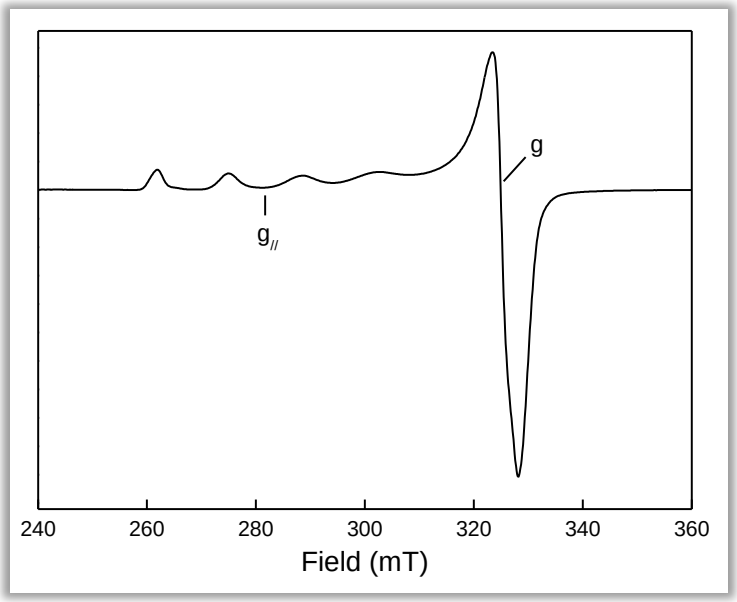

- Cu^{2+} (d^9) typically yields an axial EPR spectrum. The two principal isotopes of copper, ^{63}Cu and ^{65}Cu, both have nuclear spins of 3/2 so that the Zeeman line will be split into four lines (m_I = 3/2, 1/2, -1/2, -3/2). Since the magnetic moments of these two isotopes are very similar, the hyperfine couplings are nearly coincident. The hyperfine coupling along $g_{//}$ for Cu^{2+} is always much greater than that along $g_{\perp}$, resulting in a large splitting of the $g_{//}$ line with only minor (often unobservable) splitting of $g_{\perp}$.

4.6 Solid Particles

Ag/Titania sorbent

- The Ag/Titania sorbent was prepared by the incipient impregnation of the commercial titania extrudate grains (1–2 mm in diameter) by an aqueous solution of $AgNO_3$ to achieve Ag concentration in the sorbent from 0.5 to 17 wt.%, followed by drying at 100 °C, and subsequent calcination in air at 450 °C.
- Several signals can be detected. Trace A shows the ESR spectrum of the Ag/titania sorbent measured at 100 K. Most of the spectrum (>99 %) was assigned to NO trapped in the nanopores of titania, with the ESR simulation shown in Trace D (g_x = 2.002, g_y = 1.999, g_z = 1.930. The presence of NO is consistent with the preparation procedure of the Ag/titania, which involves calcination upon impregnation with AgNO3.
- Trace B shows the spectrum taken at 200 K. Now the NO species is not detectable anymore. The remaining species are mainly Ti based. The peak at 342 mT (g = 1.960), is assigned to the Ti^{3+} ion. The low intensity peaks at 326 and 328 mT are likely due to trace amounts of the paramagnetic Ag^{2+}. Other techniques showed that most of the Ag is present in the 1+ state which is not EPR active.

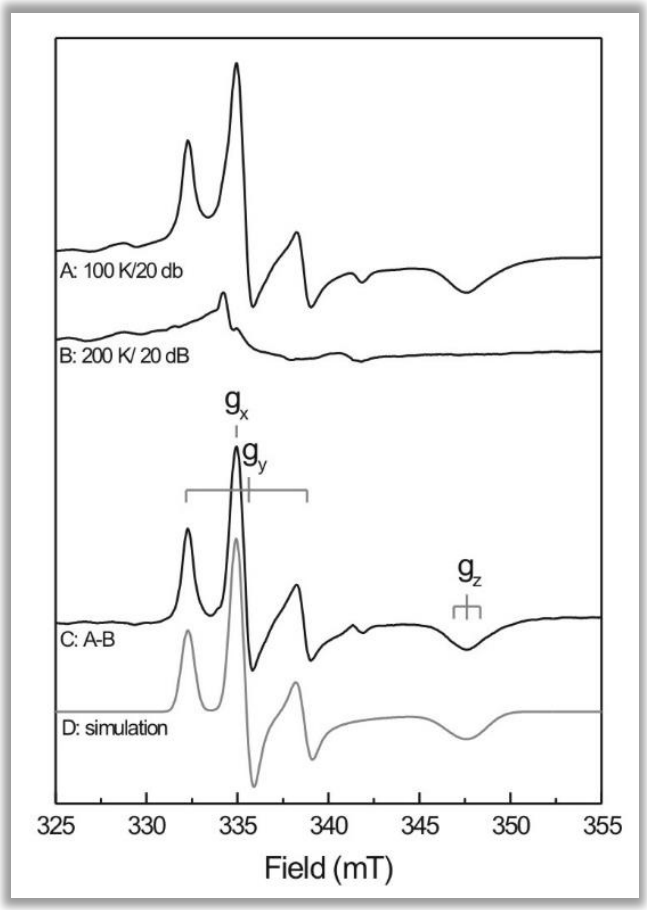

- The Ag^{2+} ion are detectable in a sample that contains 4 % (wt.) of Ag (Trace A). The signal is axial and shows a two-fold split due to the nuclear spin of Ag (I= ½). The simulation is shown in Trace B.

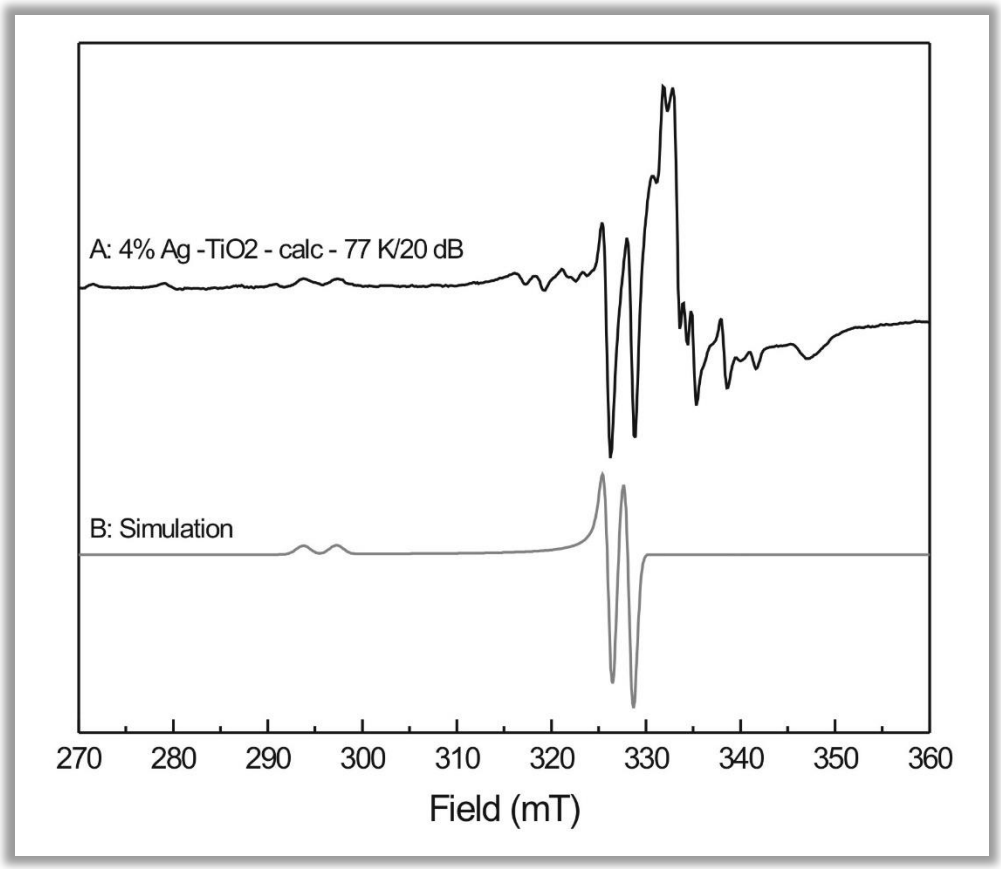

Appendix A

Rhombograms

S = 3/2

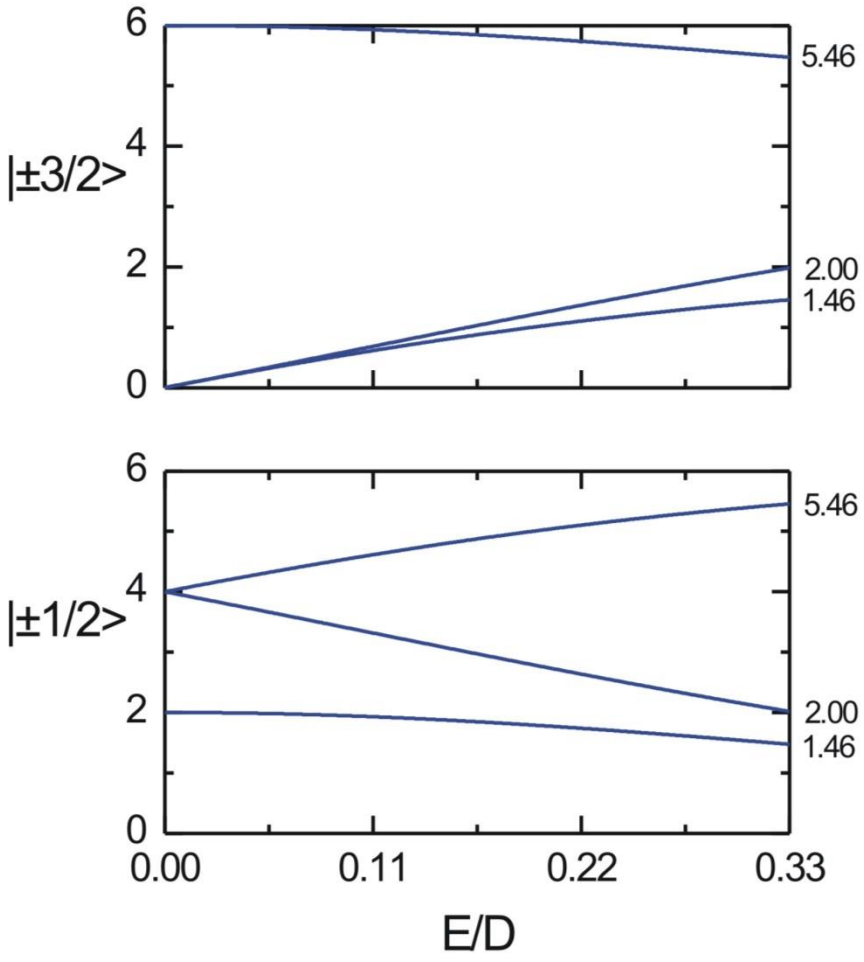

S = 5/2

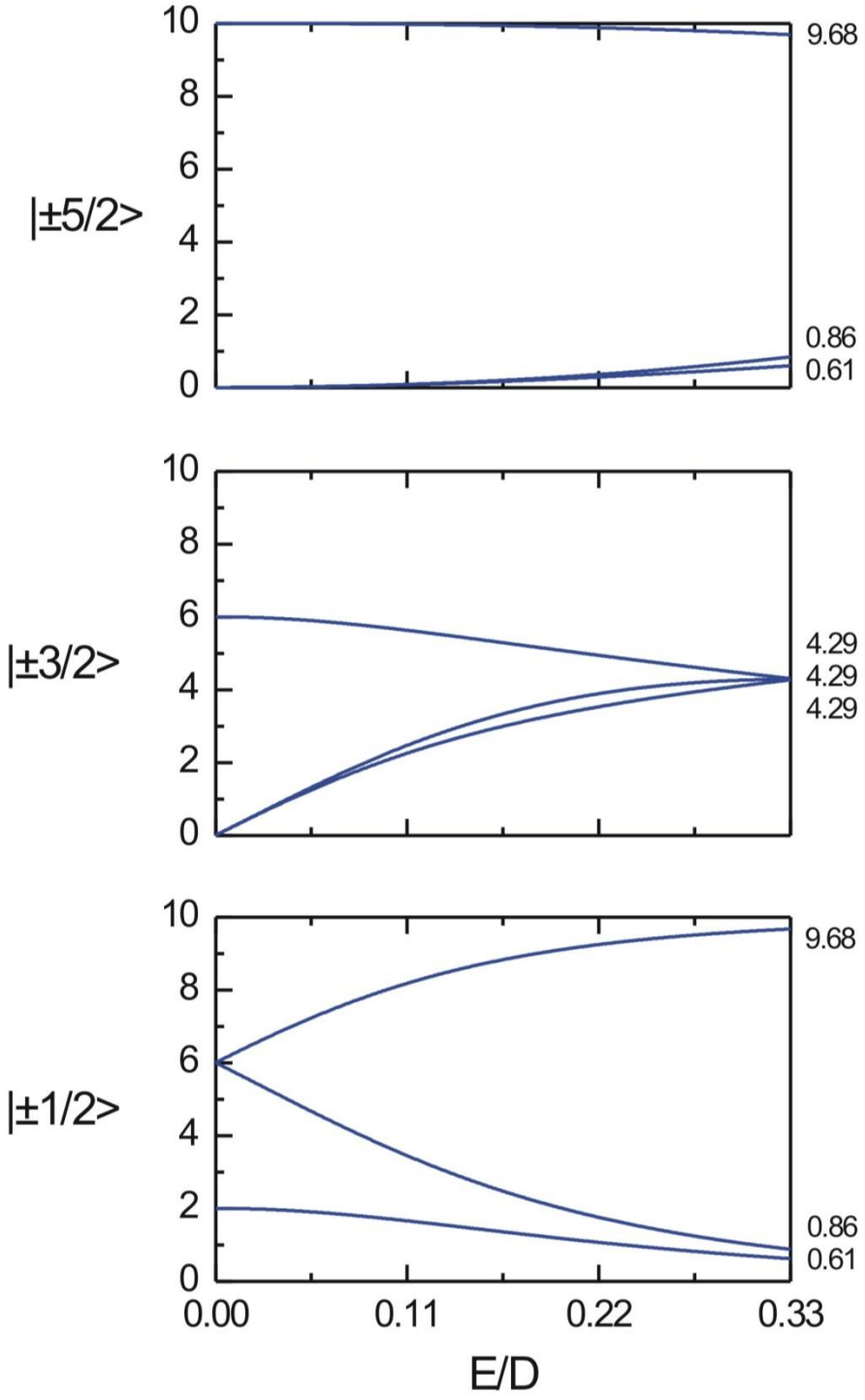

S = 7/2

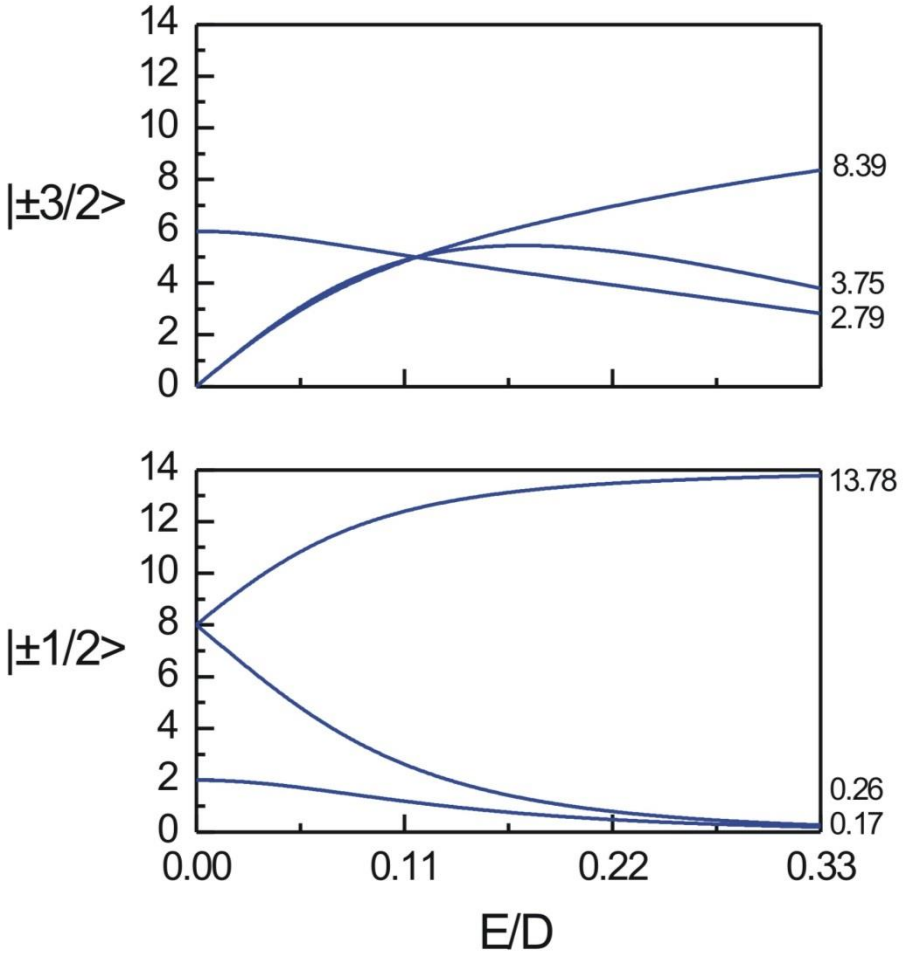
14
12
10
8
6
4
2
0
|±3/2>
8.39
3.75
2.79
14
12
10
8
6
4
2
0
|±1/2>
13.78
0.26
0.17
0.00
0.11
0.22
0.33
E/D

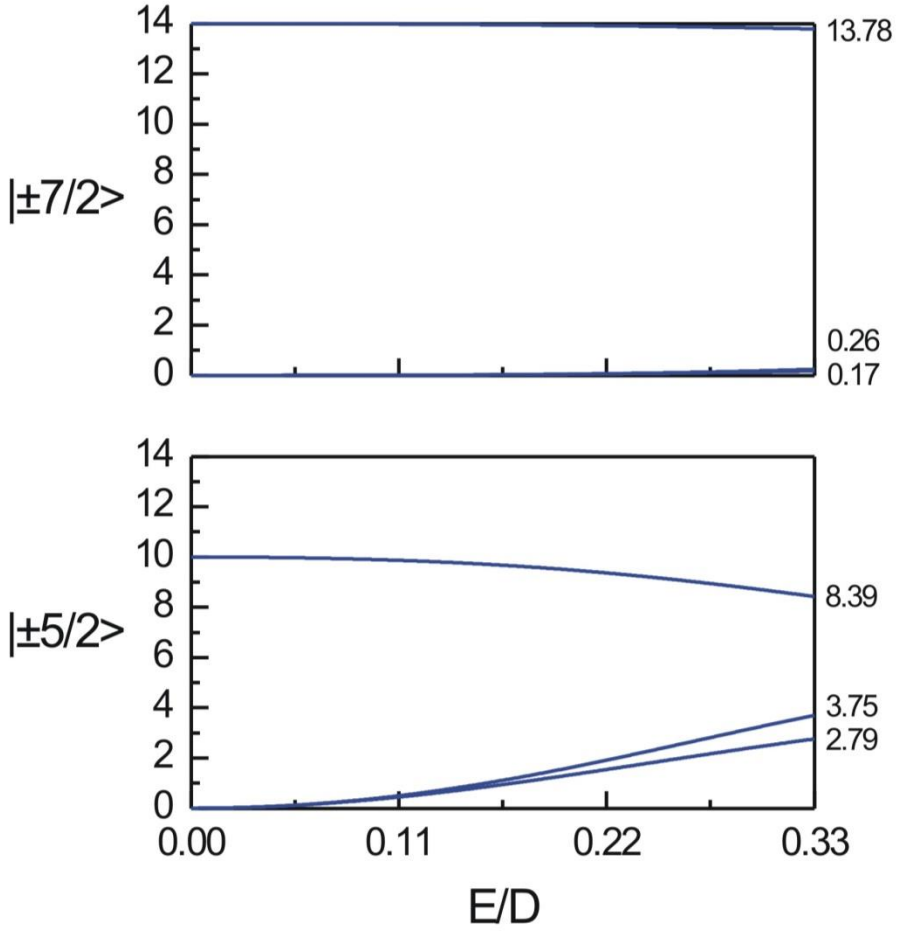
14
12
10
8
6
4
2
0
|±7/2>
13.78
0.26
0.17
14
12
10
8
6
4
2
0
|±5/2>
8.39
3.75
2.79
0.00
0.11
0.22
0.33
E/D

S = 9/2

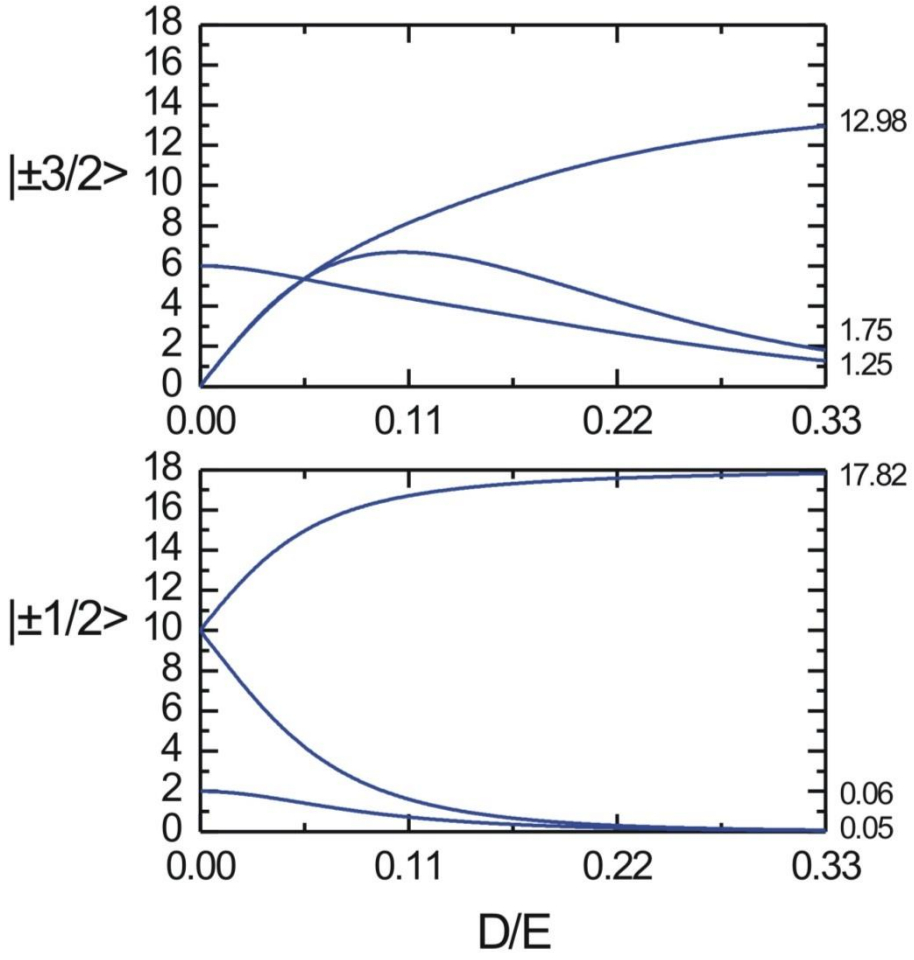

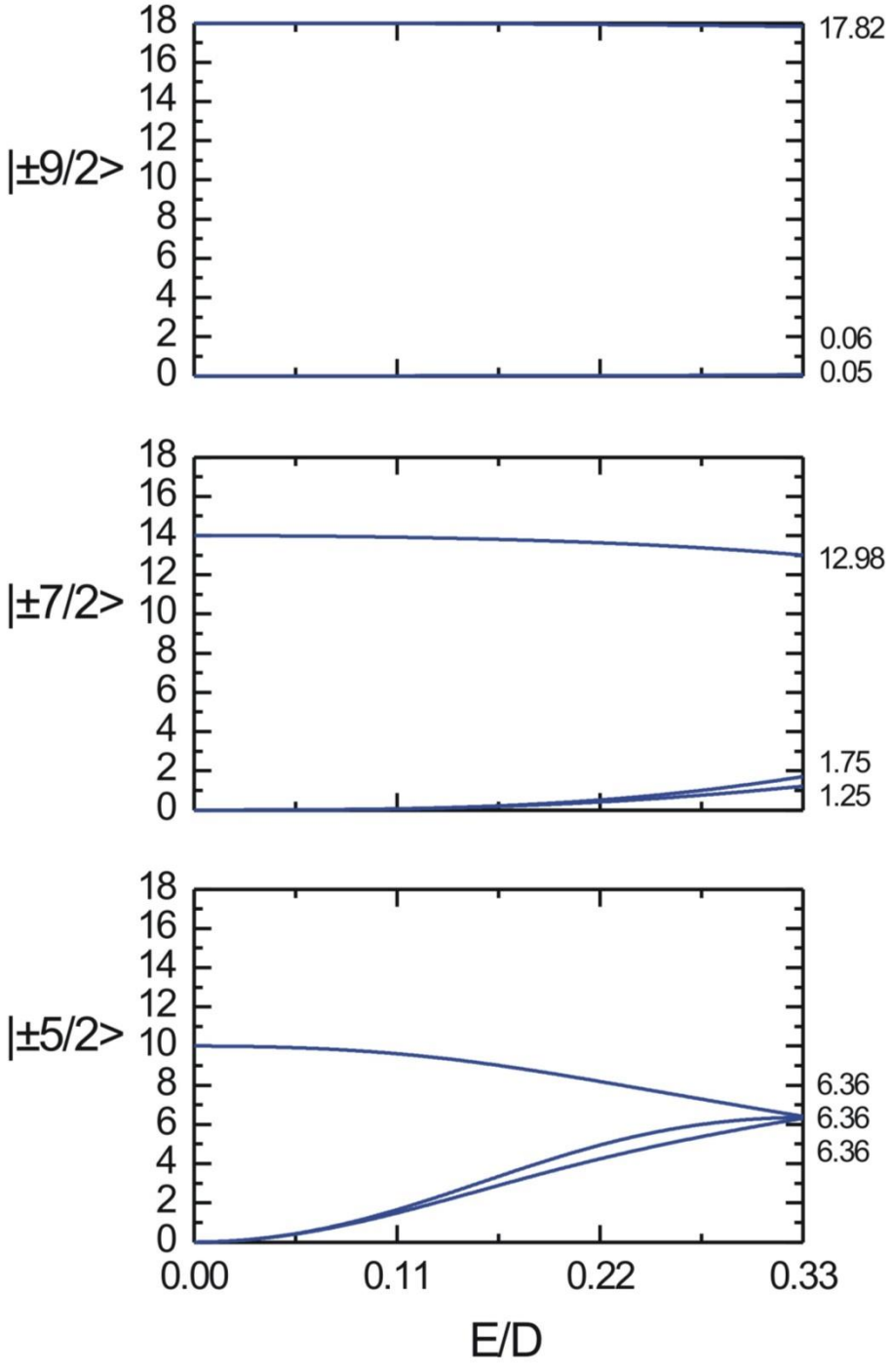
|±9/2>
|±7/2>
|±5/2>
18
16
14
12
10
8
6
4
2
0
17.82
0.06
0.05
12.98
1.75
1.25
6.36
6.36
6.36
0.00
0.11
0.22
0.33
E/D

Appendix B

Metalloenzymes Found in Methanogens

Hydrogenothropic Pathway

Fig. 1 shows the CO_2-reducing pathway of methanogenesis, which uses H_2 and CO_2 as substrates. The reduction of CO_2 to CH_4 proceeds via coenzyme-bound C_1-intermediates, methanofuran (MFR), tetrahydromethanopterin (H_4MPT), and coenzyme M (2-mercaptoethanesulfonate, HS-CoM). In the first step CO_2 is reduced to the level of formate: formylmethanofuran. From formylmethanofuran the formyl group is transferred to tetrahydromethanopterin, which serves as the carrier of the C_1 unit during its reduction to methylene- and methyltetrahydromethanopterin. The methyl group is than transferred for the fourth and last reduction step in the pathway to a structurally simple substrate, coenzyme M. Methyl-coenzyme M (CH_3-S-CoM) is reduced with coenzyme B (HS-CoB) to methane and CoM-S-S-CoB. For the reduction steps electrons from the oxidation of H_2 are used. This input is either directly or via coenzyme F_{420}. Hence the most methanogenic bacteria contain two distinct hydrogenases to oxidize H_2: a coenzyme F_{420}-reducing hydrogenase, and a coenzyme F_{420}-non-reducing enzyme. Five enzymes of this pathway are metalloenzymes and will be discussed in the next section.

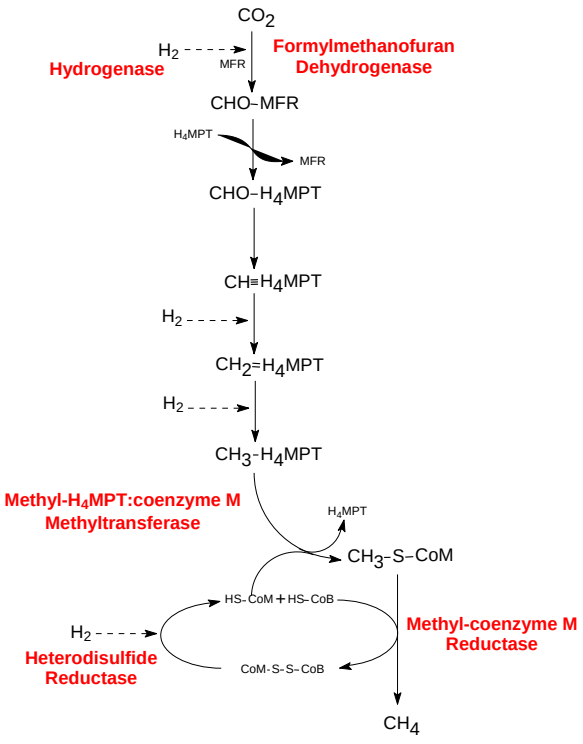

Fig. 1: Metabolic pathway of methanogenesis from CO_2 in *Methanothermobacter marburgensis*. CHO-MFR, N-formylmethanofuran; CHO-H_4MPT, N^5-formyltetrahydromethanopterin; CH≡H_4MPT^+, N^5,N^{10}-methenyltetrahydromethanopterin; CH_2=H_4MPT, N^5,N^{10}-methylenetetrahydromethanopterin; CH_3-H_4MPT^+, N^5-methyltetrahydromethanopterin; CH_3-S-CoM, methyl-coenzyme M.

Formylmethanofuran Dehydrogenase

The enzyme (Fdh) catalyzes the reversible reduction of CO_2 plus methanofuran (MFR) to *N*-formylmethanofuran (CHO-MFR). Fdh contains molybdenum, a molybdopterin dinucleotide, and iron-sulfur clusters.

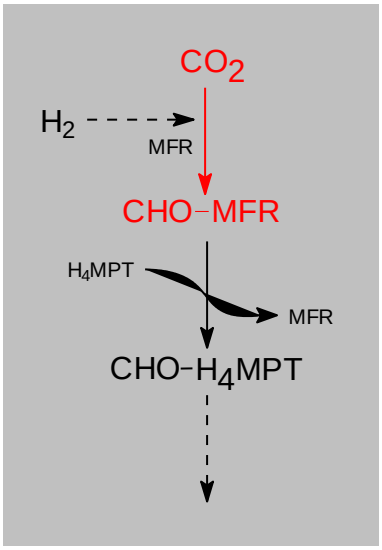

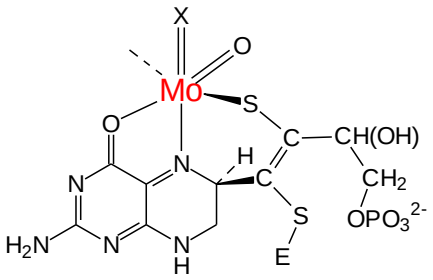

E = H, CH_3 or protein

Fig. 2: Structure of the molybdopterin cofactor

Methanobacterium wolfei contains two active Fdh enzymes I and II. Fdh I predominated in cells growing in the presence of molybdate and Fdh II in cells grown in the presence of tungstate. *M. wolfei* differs from other methanogens in that it can use tungstate as well as molybdate for growth.

The EPR spectrum of active Fdh I is depicted in Fig. 3 (trace A). The spectrum of a preparation, which has lost most of its activity due to the loss of Mo is shown in Fig.4 (trace B). This signal is probably due to a [2Fe-2S] cluster because it is detectable at 60 K. (At lower temperature, 15 K, additional signals could be detected due to [4Fe-4S] clusters.) Fig.4 (trace C) is the difference spectrum of traces A and B, showing the Mo spectrum. Fig. 4 (trace D) shows the spectrum of Fdh I purified from cells grown in the presence of ^{97}Mo-molybdate, which has a nuclear spin of I = 5/2.

The EPR spectrum C is composed of two overlapping rhombic signals with only slightly different *g*-values (signal I: g_{xyz} = 2.003, 1.989, 1.955; Signal II: g_{xyz} = 2.00, 19.84, 1.941). It has the characteristics of EPR signals due to Mo^{5+} (d^1). This is particularly demonstrated by the spectrum of the ^{97}Mo-containing enzyme (Fig. 4, trace D). The two overlapping signals are now split.

When *M. wolfei* cells are grown on tungstate, Fdh II is expressed. In addition it was found that Fdh I was still expressed, but contained W instead of Mo. Fig. 4 (trace A) shows the spectrum of the tungsten-substituted molybdenum Fdh I; W^{5+} (d^1) with g_{xyz} = 2.0488, 2.0122, 1.9635. Fig. 4 (trace B) shows a simulation of the spectrum. Fig.4 (Trace B) is a summation of a calculated rhombic S = 1/2 signal without a nuclear hyperfine interaction and the same rhombic signal interacting with a nuclear spin of I = 1/2. The relative intensity of both spectra in the final simulation, 85.6 to 14.4 respectively, was based on the natural abundance of the tungsten isotopes: I = 0: ^{180}W, 0.14%; ^{182}W, 26.4%; ^{184}W, 28.4% and I = 1/2: ^{183}W, 14.4%.

Note that the tungsten EPR signal displayed two *g*-values above 2.0 which is rather unexpected. It has been shown, however, that this is possible for a tungsten(V) complex with a low energy charge transfer exited state.

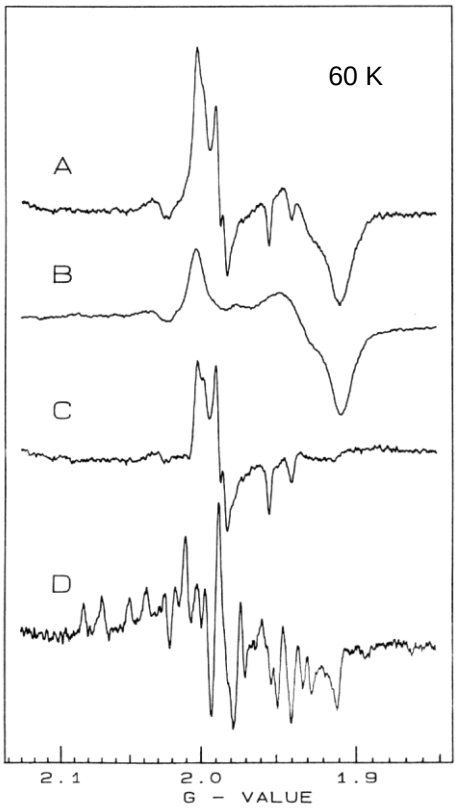

Fig.3: EPR spectra of formylmethanofuran dehydrogenase I from *M. wolfei.*

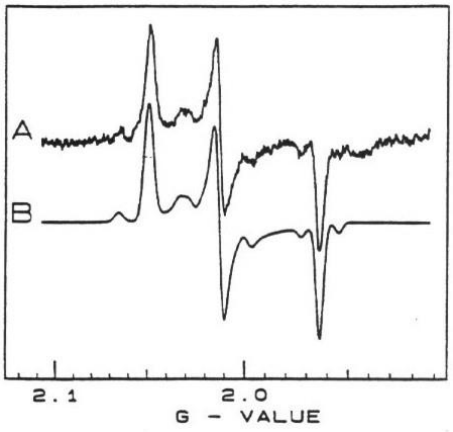

Fig. 4: EPR spectrum of the tungsten-substituted molybdenum formylmethanofuran dehydrogenase I from *M. wolfei*.

References:

Schmitz, R.A., Albracht, S.P.J., Thauer, R.K. (1992) Eur. J. Biochem. 209, 1013-1018.

Schmitz, R.A., Albracht, S.P.J., Thauer, R.K. (1992) FEBS Lett. 309, 78-81.

Hydrogenase

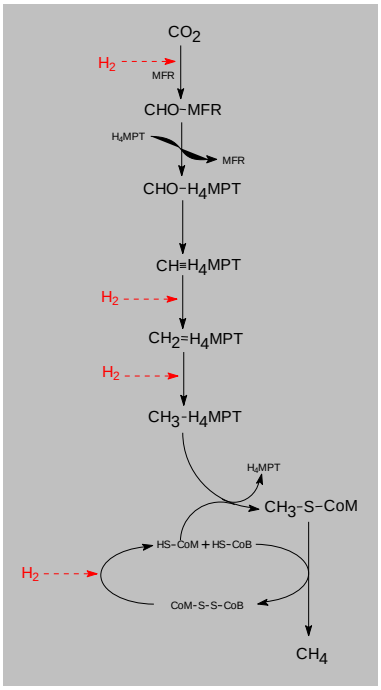

Hydrogenases catalyze the simple yet important reversible reaction:

$$H_2 \leftrightarrow 2H^+ + 2e^-$$

Through this basic reaction molecular hydrogen is connected to a whole series of metabolic routes. The assimilation of H_2 provides organisms with a supply of reductant which can also be used for energy generation. Alternatively, some organisms dispose of excess reductant in the absence of electron acceptors other than protons by producing H_2.

The input of electrons in methanogenesis by oxidation of H_2 is shown in red in the reaction pathway.

Due to the diverse roles of hydrogenases in organisms the enzyme can be either found alone but more often as a part of a larger enzyme complex. The F_{420}-non-reducing hydrogenase from *Methanobacterium marburgensis*, for example, forms a complex with heterodisulfide reductase. The basic unit, however, needed for hydrogenase activity seems to contain two [4Fe-4S] clusters and a dinuclear Ni-Fe center, the place where H_2 binds.

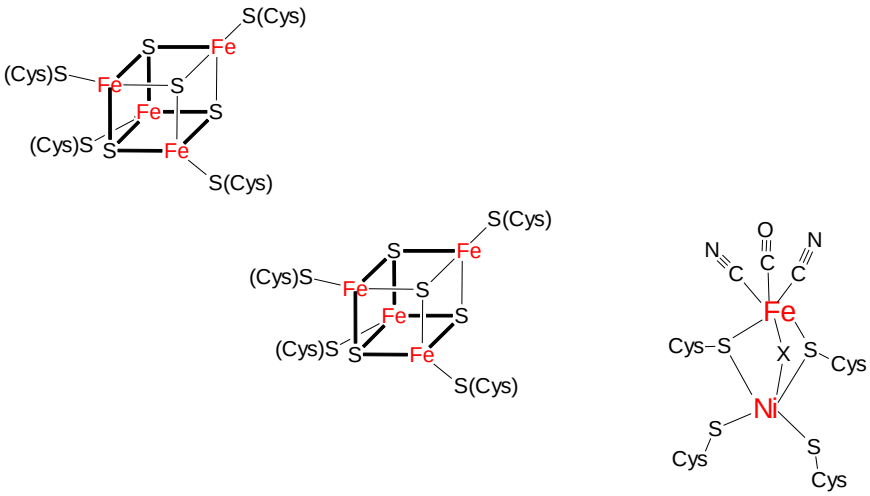

Fig.5: Prosthetic groups found in the minimal hydrogenase unit

It was early realized that hydrogenases might contain nickel, since it was required for the biosynthesis of the enzyme. The actual proof came by showing hyperfine splitting of the EPR signal by using the isotope ^{61}Ni (I = 3/2) (Fig. 6). The discovery that the active site contained iron in addition to the nickel was made when the crystal structure was solved. Since the iron stays in the low-spin 2+ state it is not detectable in EPR spectroscopy.

Fig. 7 shows the different nickel EPR signals found for hydrogenases. In the literature there are two systems for naming the different EPR signals. One is based on redox titrations and involves 3+ (d^7), 2+ (d^8), 1+ (d^9) and 0 (d^{10}) redox states. Since, however, X-ray absorption spectroscopic measurements showed that the electron density on the nickel hardly changes going from 3+ to 1+ the different states are also named A (unready), B (ready), SI (for silent - EPR silent), C (active), and R (for reduced - active and EPR silent). The EPR signal of the C form is light sensitive and the form after illumination is called L. A hydrogen species is expected to bind to the active site at the position of the X in Fig. 5 in the Ni-C state. Upon illumination the bond between this species and the nickel is broken. This was concluded from experiments in D_2O where the illumination reaction is 6 times slower. The origin of the hydrogen species is still not known. Note for example that the nickel EPR signal is not split by the nuclear spin of a H atom (I = 1/2).

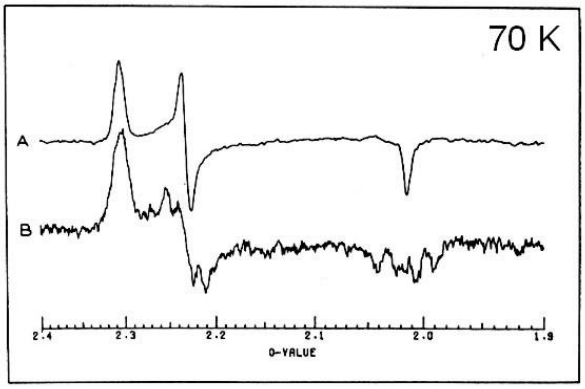

Fig. 6: Comparison of the EPR spectra of hydrogenase from *M. marburgensis* grown on different isotope mixtures: (**A**) growth was performed with natural Ni (natural abundance of ^{61}Ni is 1.19%); (**B**) growth in the presence of ^{61}Ni.

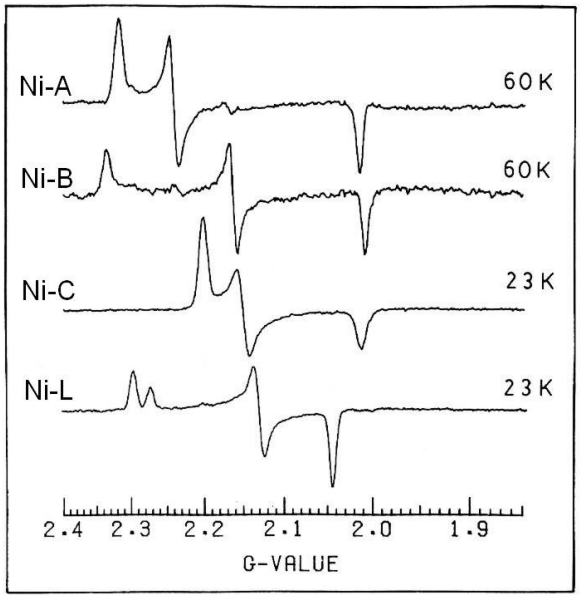

Fig. 7: Different EPR detectable states for hydrogenase from *Chromatium vinosum*.

Reference:

Albracht, S.P.J., Graf, E.-G., Thauer, R.K. (1982) FEBS Lett. 140, 311-313.

Methyl-H_4MPT:coenzyme M methyltransferase

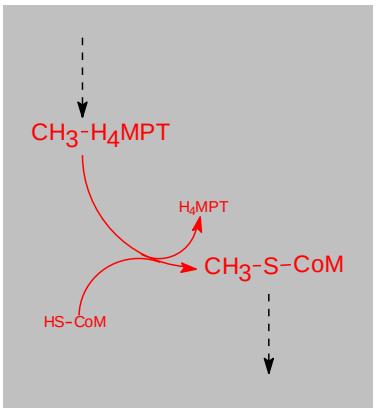

N^5-Methyltetrahydromethanopterin:coenzyme M methyltransferase (Mtr) from *M. marburgensis* is a membrane-associated enzyme complex, composed of eight different subunits, MtrA-H. MtrA harbors as prosthetic group 5'-hydroxybenzimidazolyl-cobamide:

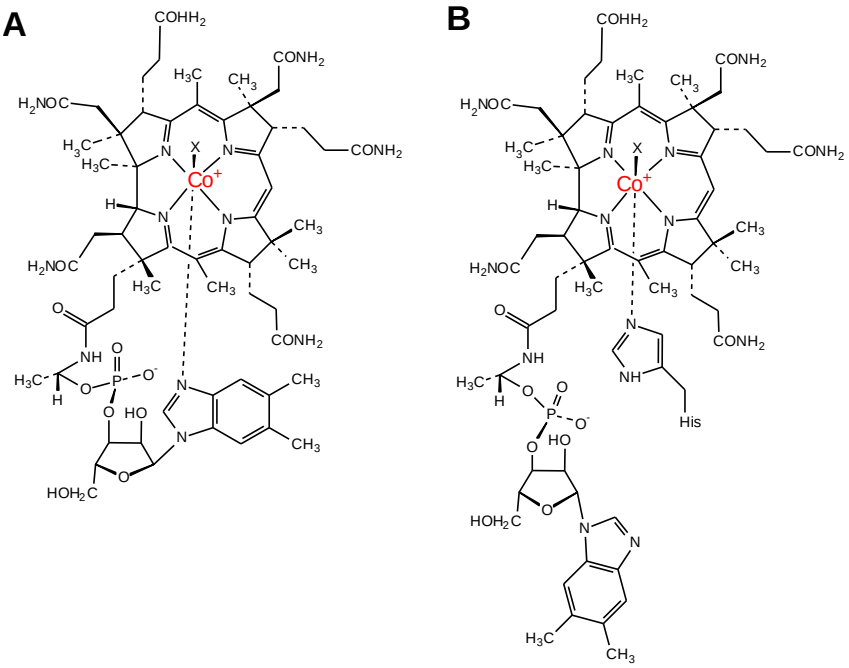

Fig. 8: 5'-hydroxybenzimidazolyl-cobamide in the free, base-on form (**A**) and the protein-bound, base-off form (**B**).

In its super reduced cob(I)amide state this cofactor was shown to accept the methyl group from CH_3-H_4MPT yielding enzyme-bound methyl-cob(III)amide:

$$CH_3\text{-}H_4MPT + E\text{:}CoB(I) \rightarrow H_4MPT + E\text{:}CH_3\text{-}Cob(III)$$

In a second reaction, the methyl group is further transferred to HS-CoM regenerating the enzyme-bound cob(I)amide:

$$E\text{:}CH_3\text{-}CoB(III) + HS\text{-}CoM \rightarrow CH_3\text{-}S\text{-}CoM + E\text{:}CoB(I)$$

Fig. 9 (trace A) shows the EPR spectra of the purified enzyme. Trace B shows a simulation of the spectrum. Characteristics of the Co^{2+} (d^7) spectrum are its *g*-values, g_{xyz} = 2.2591, 2.2530, 2.00659, and the hyperfine splitting of the g_z signal into eight equally spaced lines due to the interaction of the electron with the cobalt nucleus (I = 7/2). The eight lines are further split into triplets, which indicates an interaction of the electron with a ^{14}N-containing axial ligand.

Fig. 10 shows the EPR spectra of the MtrA subunit heterologously overexpressed in *Escherichia coli*. The overexpressed subunit did not contain its corrinoid prosthetic group. Unfolding and refolding in the presence of cobalamin resulted in correctly folded enzyme containing cob(II)alamin. The EPR spectra of the enzyme differentially labeled with ^{14}N (I = 1) and ^{15}N (I = 1/2) revealed that the corrinoid is bound to MtrA in the base-off form and that the Co(II) of the prosthetic group is coordinated by a histidine residue of the apoprotein. Fig. 10, trace B, shows that when the cells were grown on $^{15}NH_4Cl$ the eight lines were split in doublets, proving the axial N ligand came from the enzyme and not from the cofactor itself.

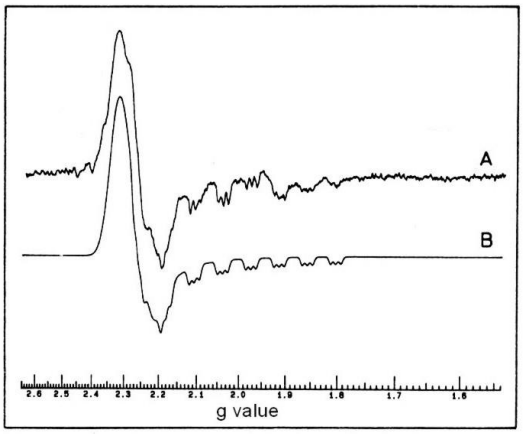

Fig. 9: EPR spectrum of the methyltransferase from *M. marburgensis*. (**A**) Protein as isolated. (**B**) Computer simulation.

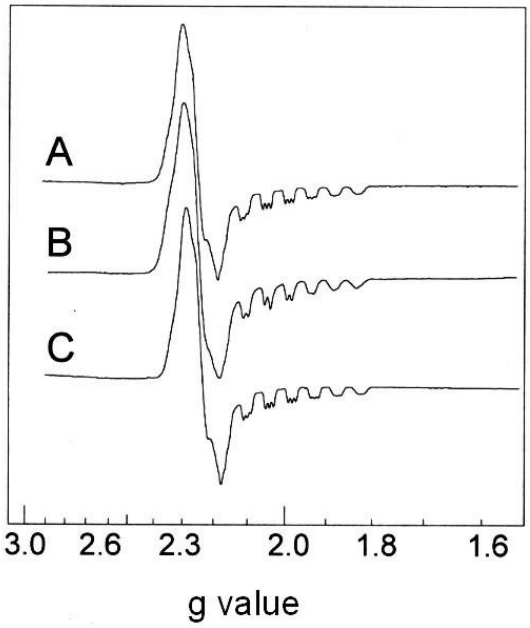

Fig. 10: EPR spectrum of reconstituted MtrA holoprotein in the cob(II)amide oxidation state. (**A**) Holoprotein reconstituted from apoprotein from *E. coli* cells grown on $^{14}NH_4Cl$ containing medium. (**B**) Holoprotein reconstituted from apoprotein from *E. coli* cells grown on $^{15}NH_4Cl$ containing medium. (**C**) Holoprotein reconstituted from apoprotein from *E. coli* cells grown on $^{15}NH_4Cl$ plus [^{14}N]-histidine-containing medium.

References:

Schulz, H., Albracht, S.P.J., Coremans, J.M.C.C. and Fuchs, G. (1988) Eur. J. Biochem. 171, 589-597.

Gartner, P., Weiss, D.S., Harms, U. and Thauer, R.K. (1994) Eur. J. Biochem. 226, 465-472.

Harms, U. and Thauer, R.K. (1996) Eur. J. Biochem. 241, 149-154.

Methyl-coenzyme M reductase

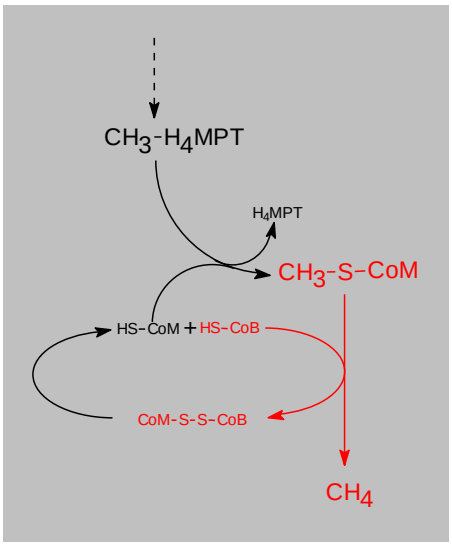

Methyl coenzyme M reductase (Mcr) catalyzes the actual production of methane from methyl coenzyme M (CH_3-S-CoM). MCR contains F_{430} as prosthetic group which is a nickel porphinoid:

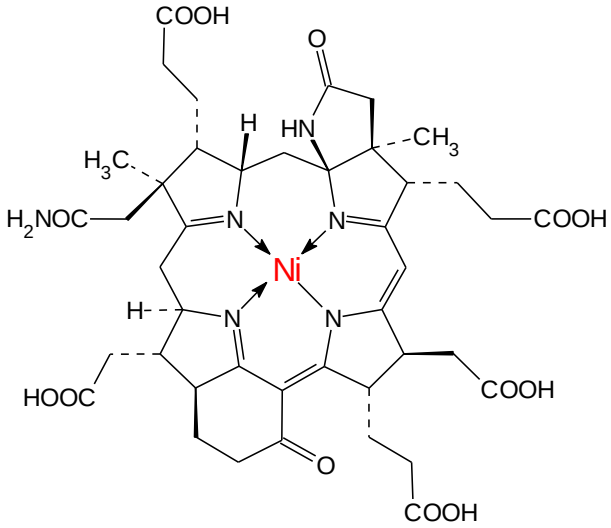

Fig. 11: Structure of F_{430}.

The four nitrogen atoms from the tetrapyrrole coordinate the nickel atom. As a result syperhyperfine structure due to the nuclear spin of the N atom (I = 1) can be detected, dependent on the orbital the free electron is in.

For the free cofactor three redox states can be obtained, 1+ (d^9), 2+ (d^8) and 3+ (d^7). Only the 1+ and 3+ states are EPR active (Fig. 12). In the 3+ state the unpaired electron is in the d_{z2} orbital that points to the loosely bound axial ligands, in this example one molecule of propionitrile. This also contains a nitrogen atom, which coordinates to the nickel causing the superhyperfine structure detectable on the g_z peak. In the 1+ state the unpaired electron is in the d_{x2-y2} orbital that point towards the nitrogen ligands of F_{430}. If you look carefully you will see some hyperfine structure. The hyperfine splitting is of the same magnitude as the line width of the signal. Hyperfine structure can only be detected when the hyperfine splitting is bigger than the line width. If the hyperfine splitting is smaller it might still broaden the signal but is not be recognizable as hyperfine anymore. In that case we call it unresolved hyperfine. By looking at spectra with different EPR frequencies one will be able to determine if this is the case for a particular signal.

For Mcr different signals can be found (Fig. 12). From comparison of the EPR spectra and other spectroscopical data is was concluded that the nickel in the silent state is 2+. The red1 forms show high spectroscopic similarities with those of F_{430} in the 1+ state. Therefore it is generally accepted that the nickel in the red1 form is in the 1+ state too. Note that there are two red1 forms, one with highly resolved superhyperfine structure (Red1m) and one with less resolved superhyperfine structure (Red1c). The EPR spectrum of the so-called Ox1 form is less well understood. The position of the *g*-values cannot be explained based on what is known about nickel complexes. The nickel can either be 1+ or 3+. X-ray absorption data indicated that a large part of the electron density might be on a sulfur ligand bound to

the nickel, which could explain the *g*-values. With the Red2 spectrum we have the same problem. In this case it is also proposed that the rhombic EPR spectrum is due to sharing of the unpaired electron with an axial ligand bound to the nickel.

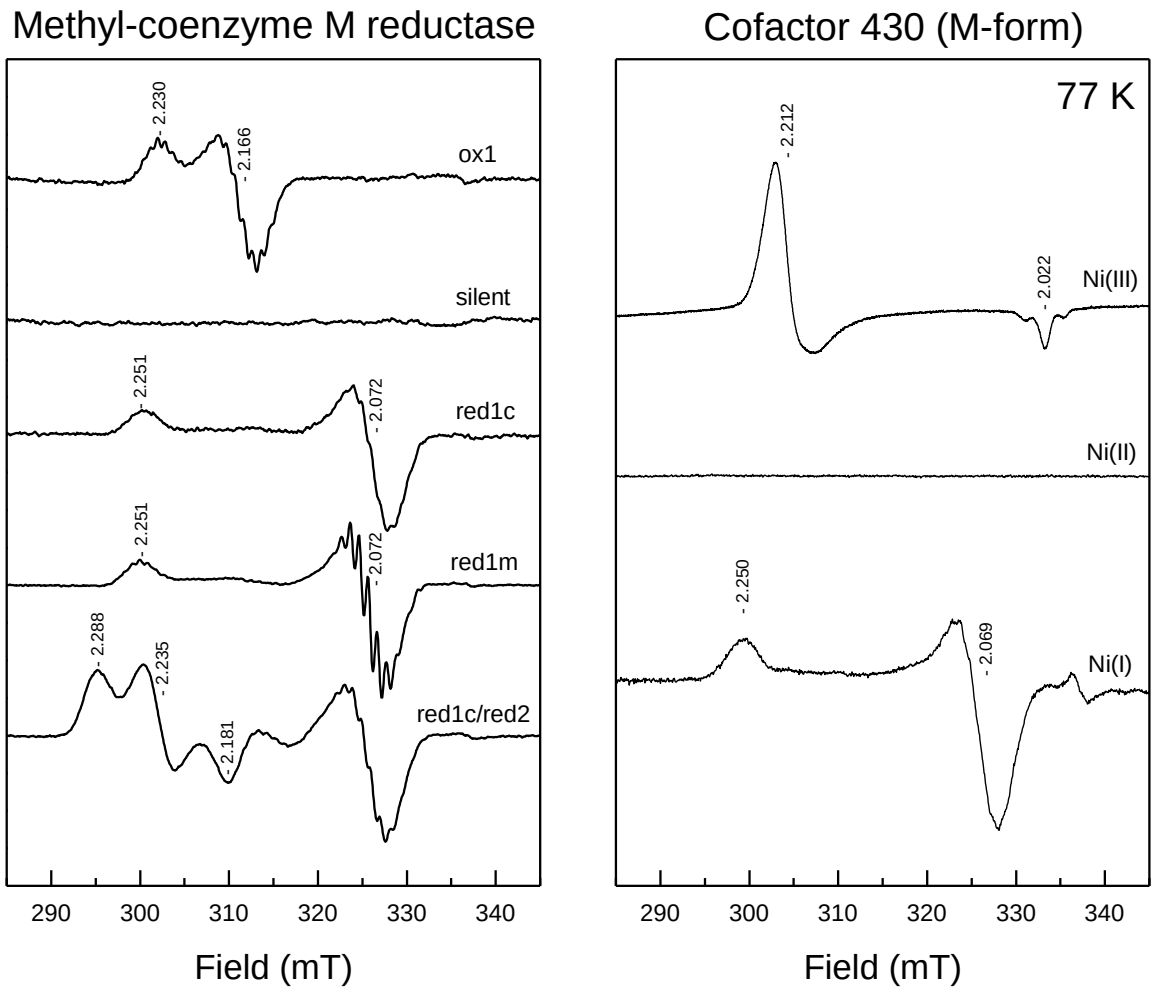

Fig. 12: EPR spectra of different forms of methyl-coenzyme M reductase from *M. marburgensis* and the free cofactor 430.

Heterodisulfide Reductase

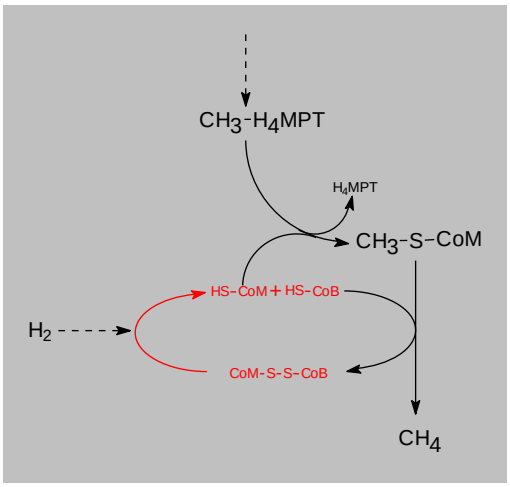

Heterodisulfide reductase (Hdr) from *M. marburgensis* is an iron-sulfur-flavin protein that catalyzes the reversible reduction of the heterodisulfide (CoM-S-S-CoB) of the thiol-coenzymes, coenzyme M (HS-CoM) and coenzyme B (HS-CoB).

Hdr is composed of three subunits, HdrA, HdrB and HdrC. HdrA contains a typical FAD binding motif and four binding motifs for $[4Fe\text{-}4S]^{1+/2+}$ clusters. HdrC contains two additional binding motifs for $[4Fe\text{-}4S]^{1+/2+}$ clusters while HdrB contains a special motif that binds a $[4Fe\text{-}4S]^{2+/3+}$ cluster that is directly involved in the catalytic reaction.

EPR spectroscopic studies indicated the presence of unique paramagnetic species that were formed upon reaction of the oxidized enzyme with HS-CoM, HS-CoB and CoM-S-S-CoB (Fig. 13). By growing cells on ^{57}Fe (I = 1/2) it was shown that the signals were iron based and probably due to iron-sulfur clusters. This can be seen in Fig. 14 where the two spectra obtained for the HS-CoM induced signal are shown. The black spectrum is the signal obtained for enzyme purified from cells grown on natural abundance iron. The red spectrum is for enzyme from cells grown on ^{57}Fe. It can clearly be detected that the ^{57}Fe signal is much broader due to unresolved hyperfine splitting due to interaction of the electron with the four iron nuclei.

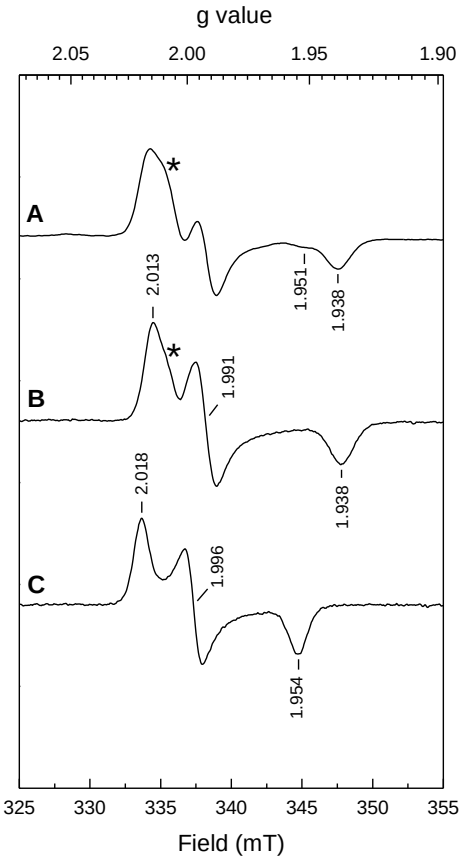

Fig. 13: EPR spectra of heterodisulfide reductase from *M. marburgensis*, (**A**) after incubation with CoM-S-S-CoB, (**B**) after incubation with HS-CoM, (**C**) after incubation with HS-CoB.

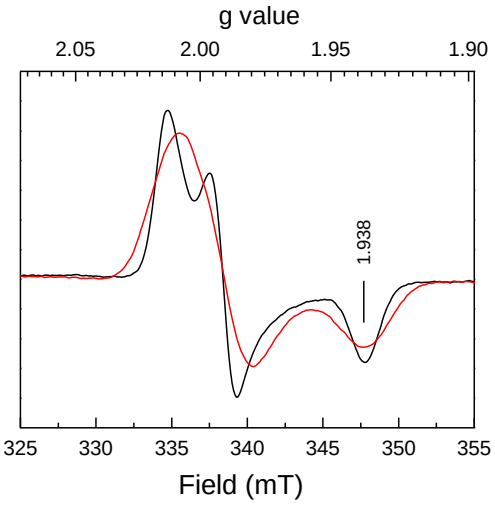

Fig. 14: EPR spectra of heterodisulfide reductase from *M. marburgensis* after incubation with HS-CoM (—) Enzyme from cells grown on natural abundance Fe. (—) Enzyme from cells grown on ^{57}Fe.

Due to the unique EPR spectra it was not clear what type of cluster was present in the active site. Magnetic circular dichroism investigations of oxidized HDR in the presence of HS-CoM or HS-CoB, however, confirmed that HDR contains a 4Fe-type cluster in its active site that is involved in disulfide reduction.

There are two models to explain the EPR signals. In the first model (Fig. 15, A) there is also an active disulfide in the active site present. The substrate, in this case HS-CoM, reacts with this disulfide and one of the disulfide sulfurs coordinates to the cluster as a way to delocalize electron density on this sulfur. In a second model (Fig. 15, B) the substrate binds directly to the cluster.

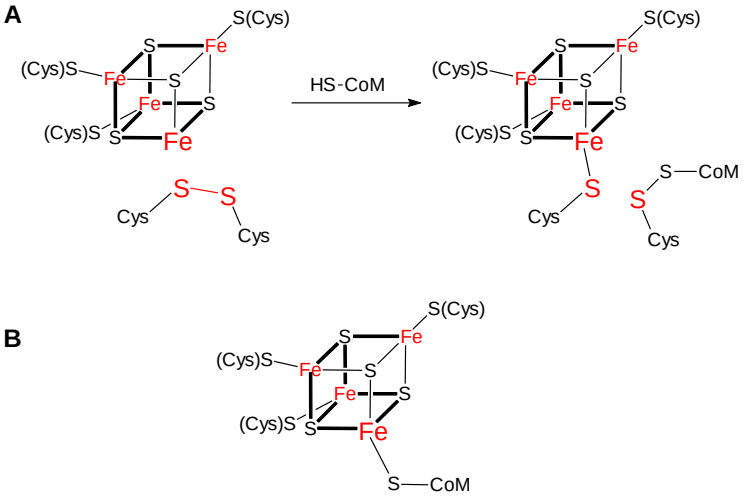

Fig. 15: Possible structures for the reaction intermediate in the active site of heterodisulfide reductase from *M. marburgensis* upon incubation with HS-CoM.

Reference:

Madadi Kahkesh, S., Duin, E.C., Heim, S., Albracht, S.P.J., Johnson, M.K., and Hedderich, R. (2001) *Eur. J. Biochem.*, 268, 2566-2577.

EPR signals in whole cells

Some of the enzymes in *M. marburgensis* are highly abundant. For example it has been estimated that the methyl-coenzyme M reductase enzyme constitutes about 10% of the total protein present in the cell. Therefore cells of these species and also cell extracts can be used to study the behavior of some of these proteins. Fig. 16 shows two EPR spectra of whole cells which have been gassed with 100% H_2 (Fig. 16, trace A) or with 80% N_2/20% CO_2 (Fig. 16, trace B). Can you recognize the different methanogenic metalloenzymes?

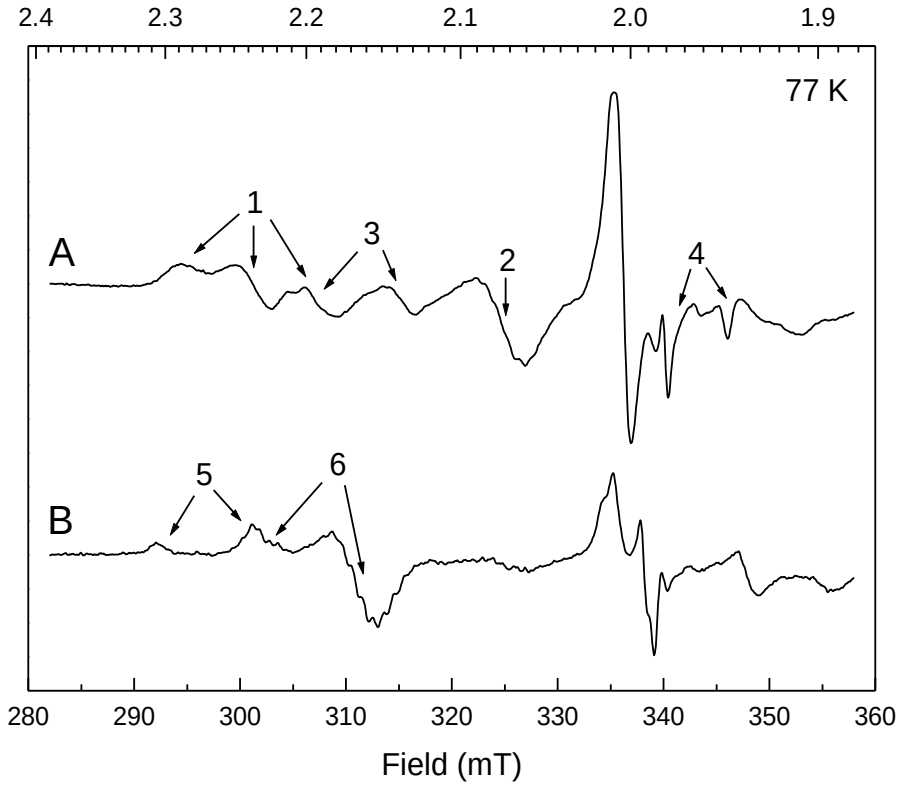

Fig. 16: EPR spectra of cells *from M. marburgensis*. (A) Cells after 30 min gassing with 100% H_2. (B) Cells after 30 min gassing with 80% N_2/20% CO_2.

Solution:

1: Methyl-coenzyme M reductase, red2 form.
2: Methyl-coenzyme M reductase, red1 c form (g_y and g_x).
3: Hydrogenase, Ni-C form (g_x and g_y).
4: Hetrodisulfide Reductases.
5: Hydrogenase, Ni-A form (g_x and g_y).
6: Methyl-coenzyme M reductase, ox1 form.

Solutions for Chapter 4

1) Frequency = 9500 MHz, B-min = 3300 Gauss, and B-max = 3500 Gauss.
   g = 2, W = 3, A = 0

2) I-spin = 2/2, A-value = 25 Gauss
   A-value = 15 Gauss
   A-value = 5 Gauss
   A-value = 2 Gauss

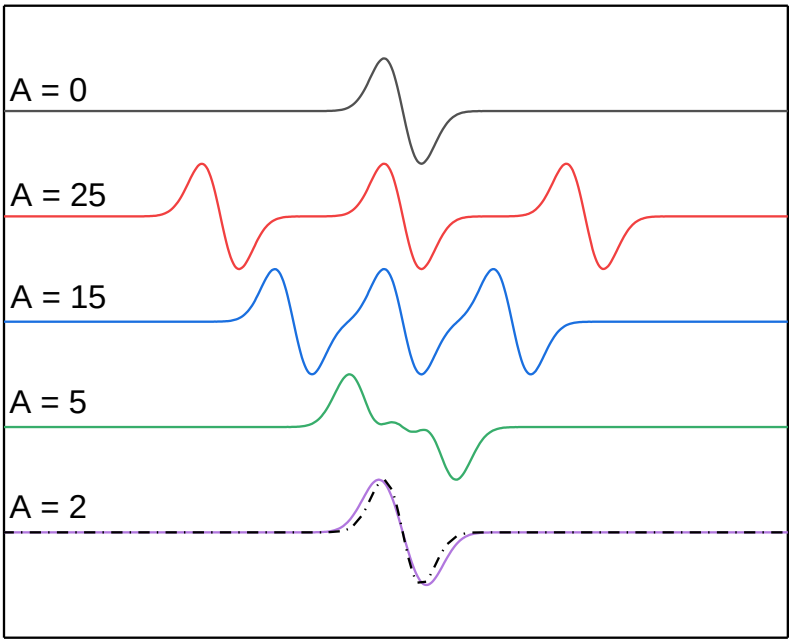

As the value of A come close to the line width of the signal, the hyperfine lines start to cancel each other (A = 5, green line) or only a small broadening of the signal is detectable which is called unresolved hyperfine splitting (A = 2, purple line). The A = 0 spectrum is overlain (dash/dot) for comparison.

3) Three protons with A = 40 G

4) Three deuterium with A = 12.4 G.

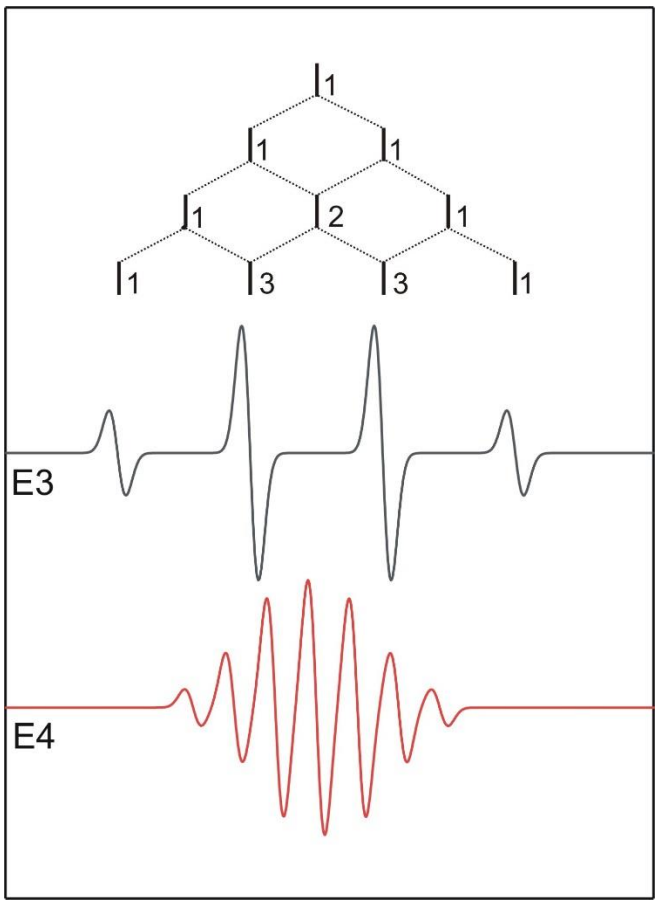

5) Proton 1: A = 20 G
Proton 2: A = 10 G
Proton 3: A = 5 G

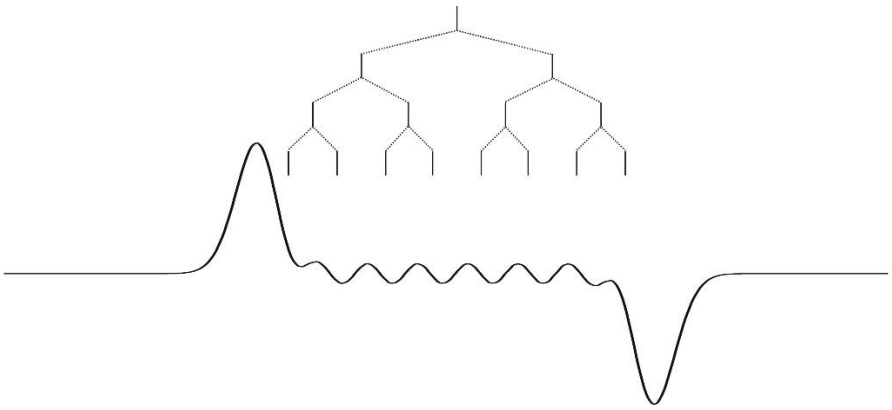

Just as in exercise 2, the splitting between the lines is very close to the line width. (You can try a much smaller line width (like 1 or 0.5 Gauss) to show the complete hyperfine pattern

6) Frequency, 9500 MHz; B-min, 3300 Gauss; B-max, 3500 Gauss.

Rh-diazo radical: Two N interactions with identical *A*.
For nitrogen 1: *A*-value = 10 G
For nitrogen 2: *A*-value = 10 G

MNP-C•: Interaction with 1 N (large A) and 1 H (smaller *A*)
For nitrogen: *A*-value = 15 G
For hydrogen: *A*-value = 4 G

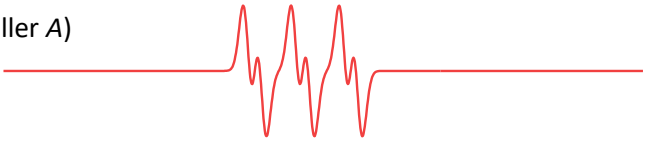

DMPO-C•: Interaction with 1 H (large *A*) and 1 N (smaller *A*)
For nitrogen: *A*-value = 30 G
For hydrogen: *A*-value = 40 G

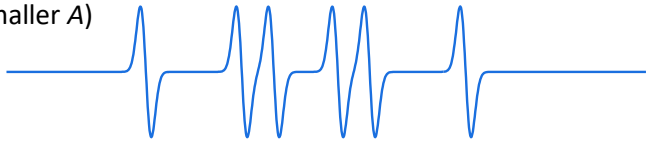

DMPO-N•: Similar interaction with 1 H (large *A*),
1 N (smaller *A*) and 1 N (even smaller *A*)
For hydrogen: *A*-value = 50 G
For nitrogen 1: *A*-value = 40 G
For nitrogen 2: *A*-value = 10 G

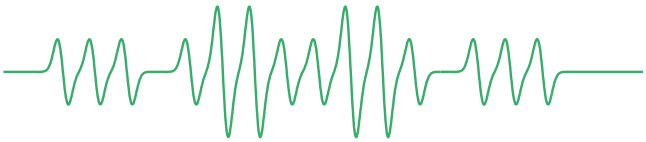

7)

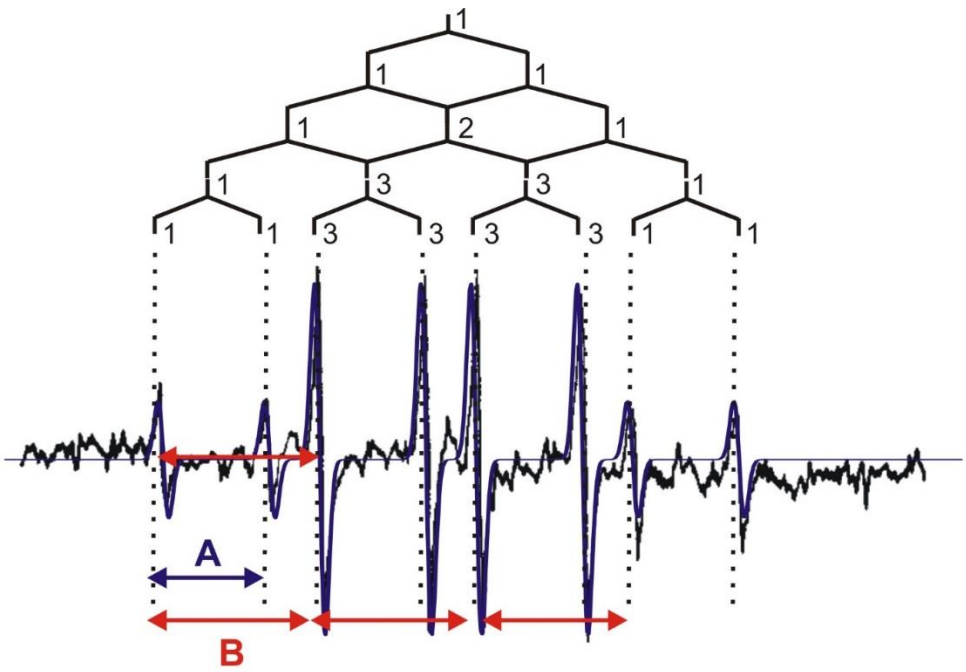

Signal is split into four due to the three Hβ. There is an additional split into two due to the single Hα.

8)

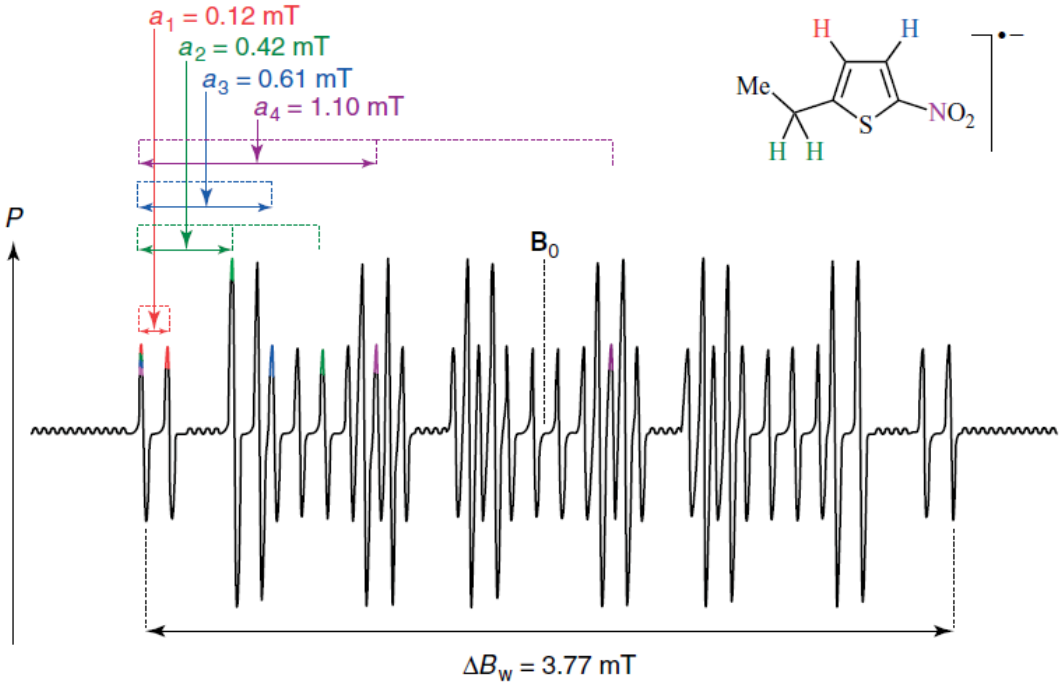

The first multiplet (A) induces a small two-fold split due to one I = ½ nucleus
The second (B) is a triplet due to two equal I = ½ nucleus
The third (C) is again a two-fold split due to one I = ½ nucleus
The fourth (D) is a triplet due to a I = 1 nucleus

9) B-min: 3100 gauss, B-max: 3700 gauss.
For Co: *A*-value = 50 G, for nitrogen: *A*-value = 20 G, for hydrogen: *A*-value = 10 G

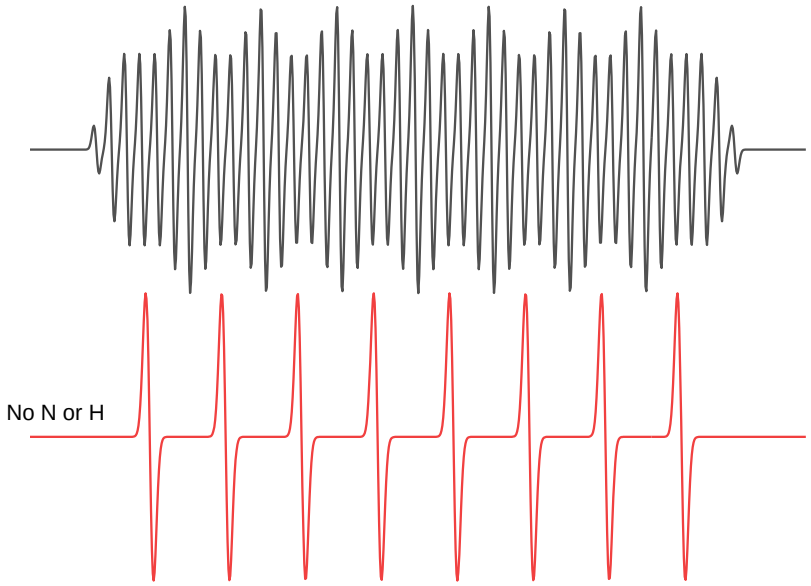

10) Simulation of the dimethyl nitroxyl radical.

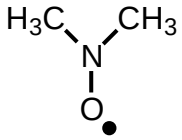

Frequency = 9766.13 MHz, B-min = 3380 gauss, B-max = 3580 gauss.
g = 2.005, W = 0.7, A_N = 17.0 (1x), A_H = 14.8 (6x)
To get the pattern right A_N needs to be just a bit larger than A_H

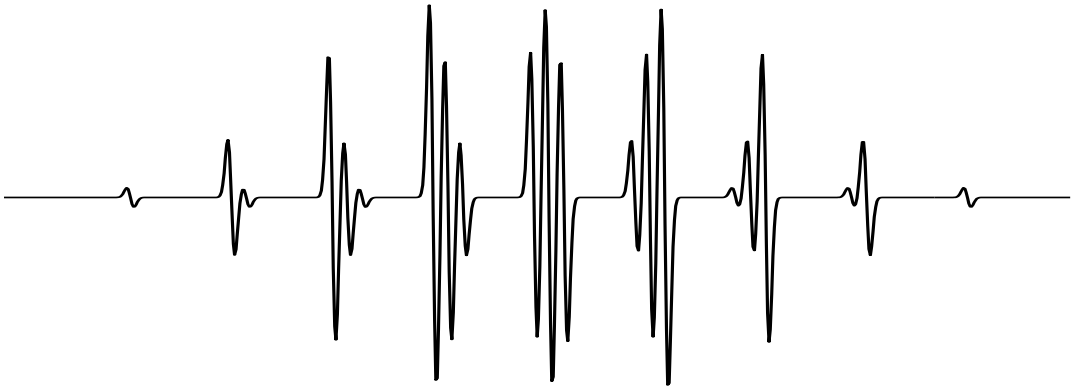

11) *Axial symmetry (so $g_x = g_y \neq g_z$).* Use the program **simplespectrum**.

Frequency = 9500 MHz, B-min = 3000 gauss, B-max = 3800 gauss.
g_{zyx} = 2.054, 1.925, 1.925, W_{zyx} = 10, 16, 16, Phi = 1

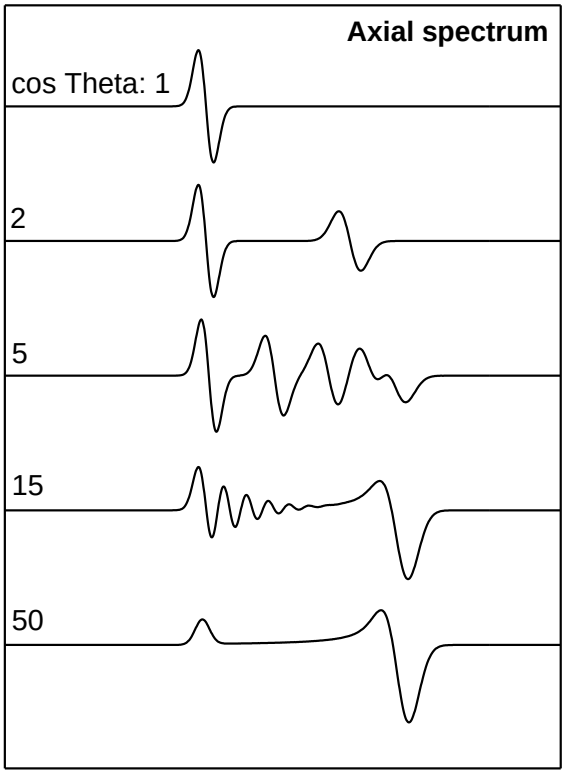

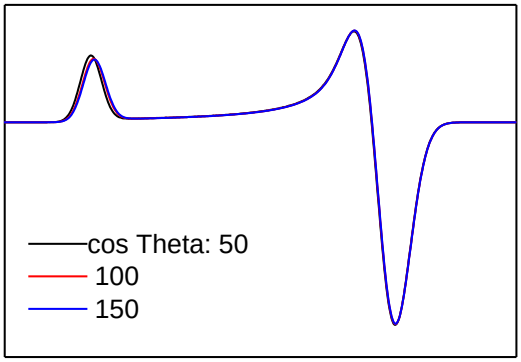

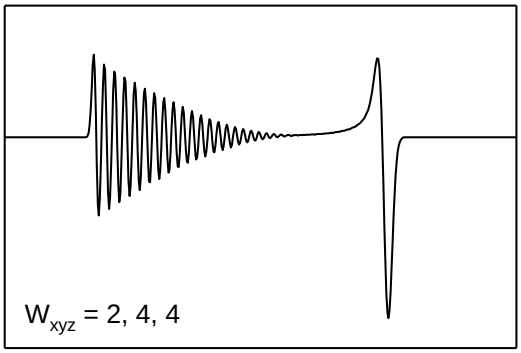

12) Frequency: 9500 MHz
B-min: 3100 Gauss
B-max: 3900 Gauss.
g_{zyx}: 2.02, 1.91, 1.85
W_{zyx}: 10, 13, 18

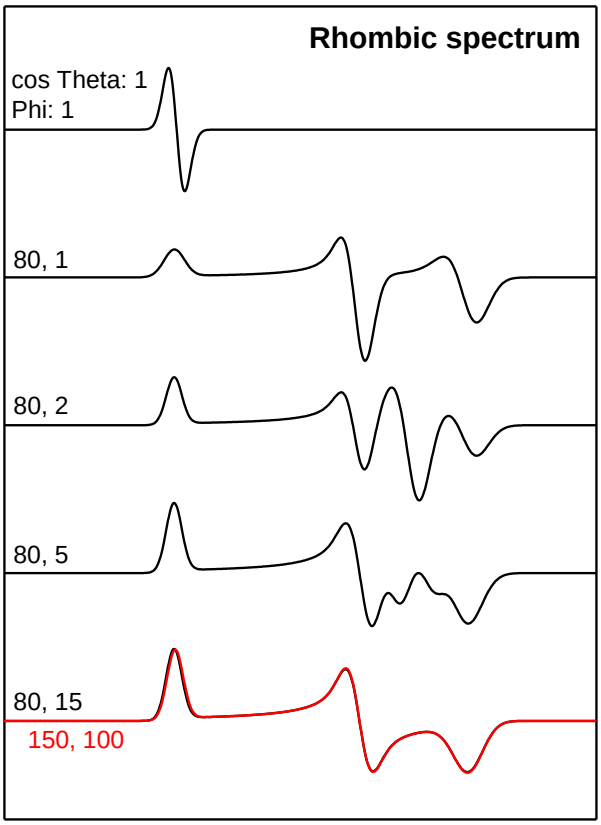

13) Frequency = 9630 MHz, B-min = 3005 Gauss, B-max = 4005 Gauss.

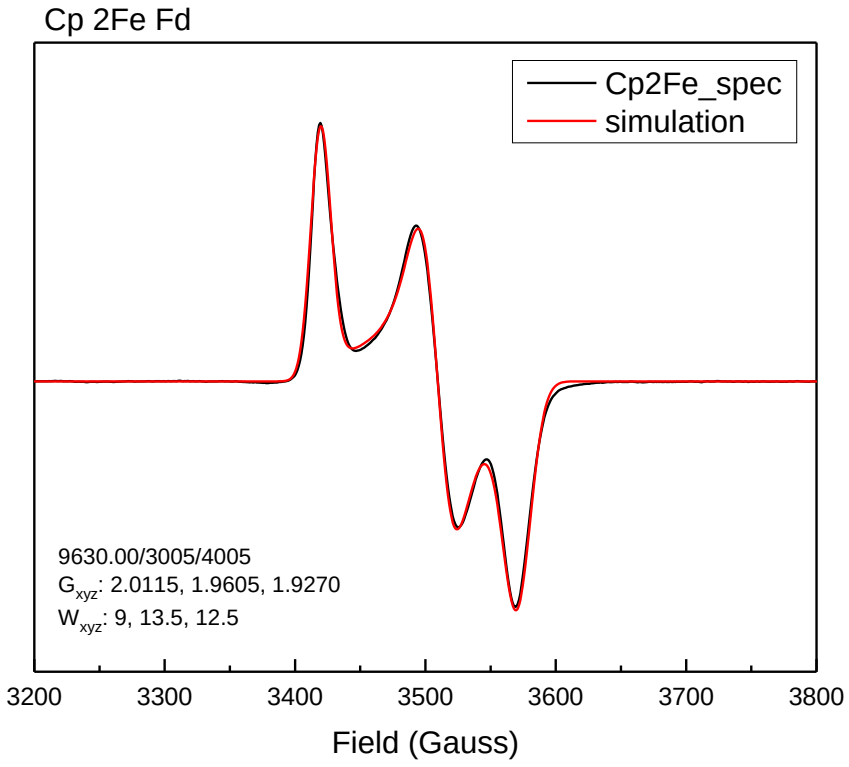

14) Frequency = 9500 MHz, B-min = 1900 Gauss, B-max = 3900 gauss
cos Theta = 150, Phi = 1
g_{zyx}: = 2.90, 2.07, 2.07; W_{zyx}: = 20, 20, 20

15) Metal A_{zyx}: 150, 15, 15

16) g_z = 2.4; g_z = 2.3; g_z = 2.2; g_z = 2.1

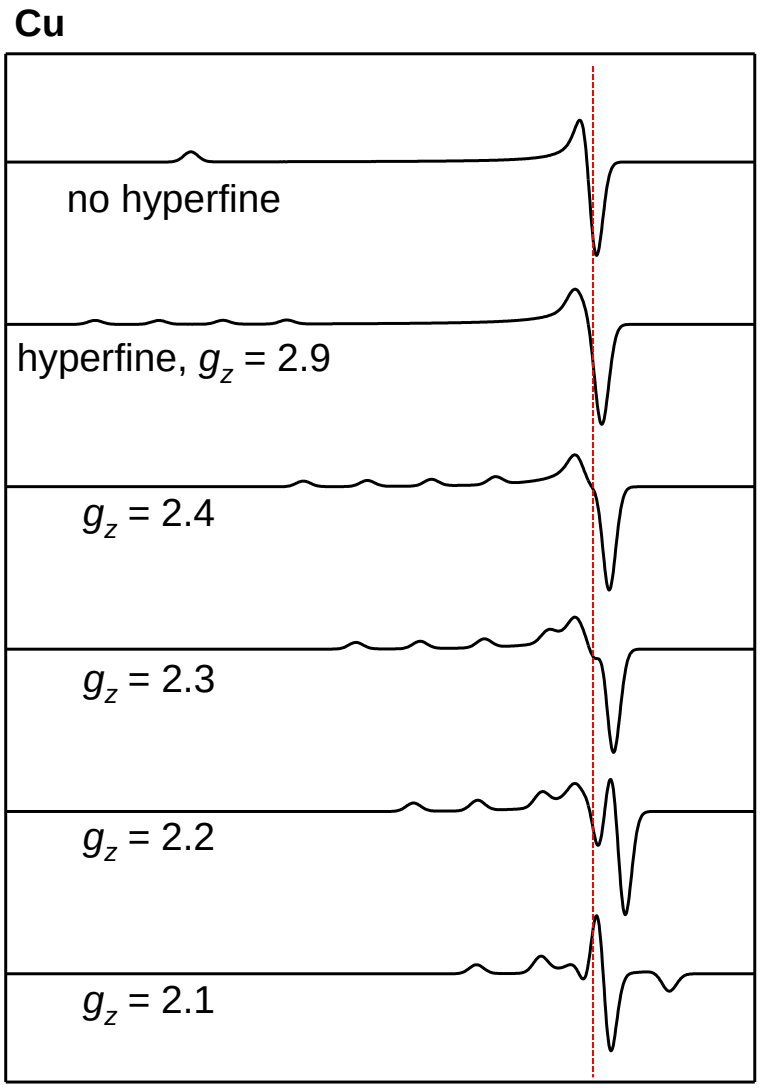

The red dashed line indicate the position of the g_{xy}. Due to the overshoot this position is hard to recognize in the spectra where g_z is closer to the g_{xy} value.

17) Frequency = 9596.06 MHz, B-min = 2000 gauss, B-max = 5000 gauss
g_{xyz} = 2.275, 2.220, and 2.006; W_{xyz} = 25, 25, and 7; $A^{Co}{}_{xyz}$ = 11, 11, and 111; $A^{N}{}_{xyz}$ = 18, 18, and 18

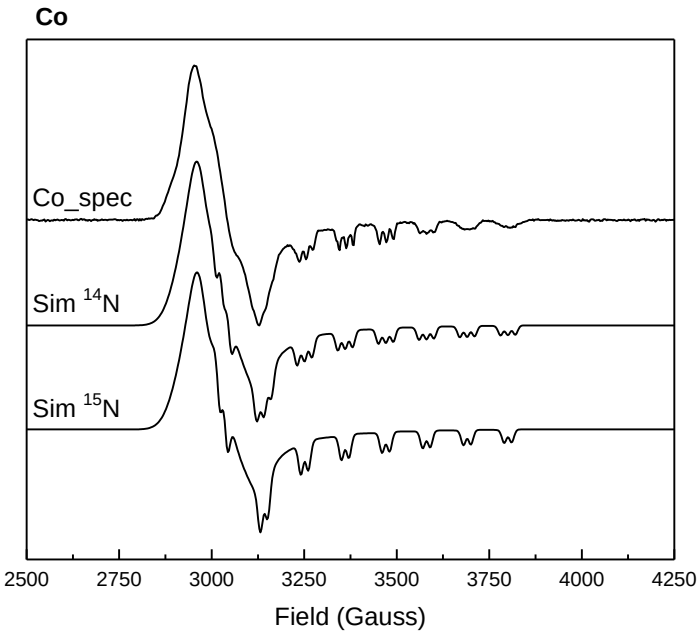

18) MCRox1: Frequency = 9596.06 MHz; B-min = 2000 Gauss; B-max = 5000 Gauss
g_{xyz} = 2.2305, 2.1665, and 2.1530; W_{xyz} = 3.5, 4.0, and 4.0; $A^{N}{}_{xyz}$ = 8.0, 9.7, and 9.7

MCRred1: Frequency = 9431.35 MHz; B-min = 2000 Gauss; B-max = 5000 Gauss
g_{xyz} = 2.2495, 2.0720, and 2.0625; W_{xyz} = 4.5, 3.5, and 5.0; $A^{N}{}_{xyz}$ = 8.8, 9.9, and 9.9

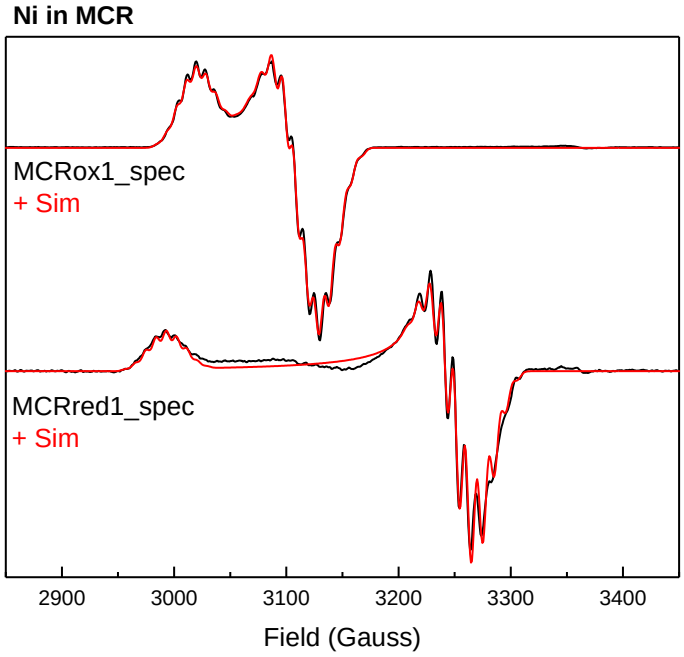

19)

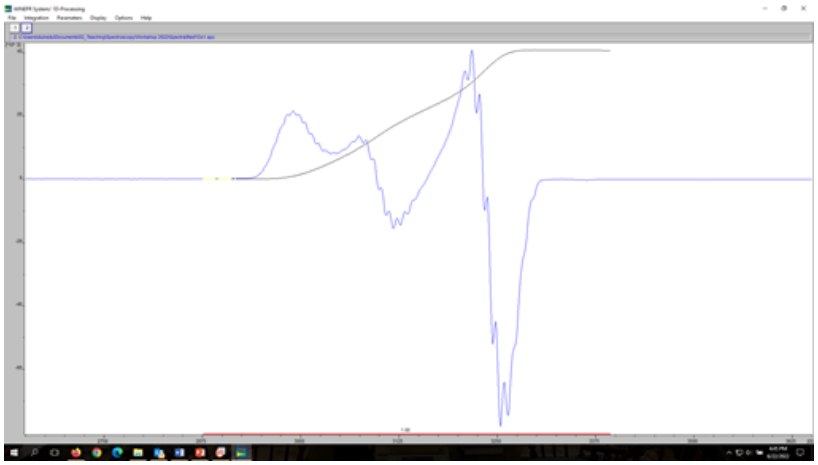

DI/N for mix: 1.350e2
DI/N for CuSt: 5.716e3 (= 10 mM)

$$C_u = \frac{I_{n(u)} \cdot C_{st}}{I_{n(st)}}$$

Mix is 0.236 mM

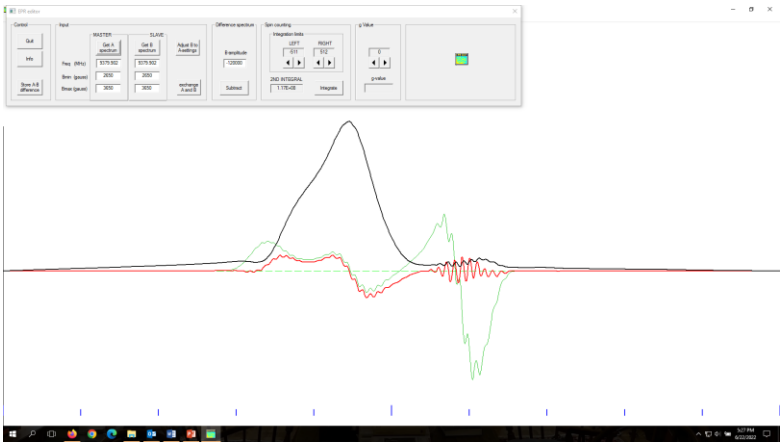

There is some residual Red1 signal, but the first integral shows the main absorption to be due to Ox1.

Ox1red1: 4.90e8

Ox1: 1.17e8 = 23%

Red1 = 77%